# Power system stability and frequency control for transient performance improvement

Xi, Kaihua

**DOI**
10.4233/uuid:6ae2a876-310b-4401-84b7-da9e1ed49079

**Publication date**
2018

**Document Version**
Final published version

**Citation (APA)**
Xi, K. (2018). *Power system stability and frequency control for transient performance improvement*. [Dissertation (TU Delft), Delft University of Technology]. https://doi.org/10.4233/uuid:6ae2a876-310b-4401-84b7-da9e1ed49079

**Important note**
To cite this publication, please use the final published version (if applicable).
Please check the document version above.

# Power system stability and frequency control for transient performance improvement

# Power system stability and frequency control for transient performance improvement

## Proefschrift

ter verkrijging van de graad van doctor
aan de Technische Universiteit Delft,
op gezag van de Rector Magnificus Prof.dr.ir. T. H. J. J. van der Hagen
voorzitter van het College voor Promoties,
in het openbaar te verdedigen op
woensdag 20 juni 2018 om 12:30 uur

door


## Kaihua XI

Master of Science in Computational Mathematics,
Shandong University, China
geboren te Shandong, China

Dit proefschrift is goedgekeurd door de promotoren en de copromotor.

Samenstelling promotiecommissie:

| | |
|---|---|
| Rector Magnificus, | voorzitter |
| Prof. dr. ir. H. X. Lin, | Technische Universiteit Delft, promotor |
| Prof. dr. ir. J. H. van Schuppen, | Technische Universiteit Delft, promotor |
| Dr. J. L. A. Dubbeldam, | Technische Universiteit Delft, copromotor |
| | |
| *Onafhankelijke leden:* | |
| Prof. dr. ir. M. Loccufier | Universiteit Gent, België |
| Prof. dr. Y. Liu | Shandong University, China |
| Prof. dr. ir. R. K. Boel | Universiteit Gent, België |
| Prof. ir. L. van der Sluis | Technische Universiteit Delft |
| Prof. dr. ir. C. W. Oosterlee | Technische Universiteit Delft, reservelid |



This research was funded by the China Scholarship Council (CSC).

*Keywords:* load frequency control, economic power dispatch, transient performance, centralized control, distributed control, multi-level control, transient stability, energy barrier, equilibria



ISBN 978-94-6186-931-9



An electronic version of this dissertation is available at
http://repository.tudelft.nl/.

*Science is a wonderful thing*
*if one does not have to earn one's living at it.*

Albert Einstein

# CONTENTS

# SUMMARY

The electrical power grid is a fundamental infrastructure in today's society. The synchronization of the frequency to nominal frequency over all the network is essential for the proper functioning of the power grid. The current transition to a more distributed generation by weather dependent renewable power sources, which are inherently more prone to fluctuations, poses great challenges to the functioning of the power grid. Among these fluctuations, the frequency fluctuations negatively affect the power supply and stability of the power grid. In this thesis, we focus on load frequency control laws that can effectively suppress the frequency fluctuations, and methods that can improve the synchronization stability.

The load frequency control consists of a three-level control, primary control which synchronizes the frequency, secondary frequency control which restores the nominal frequency and tertiary control which guarantees the security and economic optimality of the power system. Large frequency fluctuations are usually caused by power-imbalance which is the imbalance between power supply and demand. The traditional secondary frequency control restores the nominal frequency by steering area control error to zero. Existing control laws are usually of integral control type, which suffer from either a slow convergence to the steady state or an overshoot problem. In order to effectively suppress the frequency fluctuations, a faster reaction of the control input to the power imbalance is critical. To accelerate this convergence, we propose a centralized control law, namely *Power-Imbalance Allocation Control* (PIAC), for the secondary frequency control to restore the nominal frequency with a minimized control cost. In PIAC, a central coordinator collects from local nodes frequency deviations and then calculates the control inputs for these local nodes by solving an economic power dispatch problem. By including a proportional control input into the secondary frequency control, the total control inputs converges to the power-imbalance exponentially with a speed determined by a control parameter. Thus the overshoot and slow convergence are avoided. When implemented in a non-cooperative multi-area control, PIAC decouples the control actions of the areas such that the controllers of an area is independent on the disturbances from its neighboring areas. Lyapunov stability analysis shows that PIAC is locally asymptotic stable for strictly convex cost functions of the economic power dispatch problem. Case studies indicate that PIAC can effectively accelerate the convergence of the system to its steady state. Thus the large frequency fluctuations can be effectively suppressed by PIAC.

Because of the overhead for communications and for extensive computations, the centralized control law, PIAC, is still not practical for large-scale power systems. Distributed control can eliminate these drawbacks, which however generally suffers from a slow convergence to the optimal steady state. With the idea of PIAC on suppressing the frequency fluctuations, we propose a multi-level control law, called *Multi-level Power-Imbalance Allocation Control* (MLPIAC), for large-scale power system with several cooperative areas, where there is a coordinator in each area. In MLPIAC, a centralized control law named *Gather-*

*broadcast Power-Imbalance Allocation Control* (GBPIAC) is implemented in each area and a distributed one named *Distributed Power-Imbalance Allocation Control* (DPIAC) is implemented over the areas. As in PIAC, the total control input in MLPIAC also converges to the power-imbalance exponentially with a speed determined by a control parameter. Thus the frequency fluctuation can be effectively suppressed. In addition, because the number of nodes in each area is smaller than that of the network, the overhead communications and the complexity of the computations for the coordinator of each area can be greatly decreased. Because the number of areas is smaller than that of nodes, MLPIAC can obtain the optimal steady state more efficiently than the pure distributed control law. Hence, the common drawback of centralized control and that of distributed control can be well balanced in MLPIAC. Lyapunov stability analysis shows that if a sufficient condition for the control parameters is satisfied, MLPIAC is locally asymptotic stable. Case studies demonstrate that MLPIAC can also effectively accelerate the convergence to the optimal state of the system.

For the proposed control laws, PIAC, DPIAC and GBPIAC, we further investigate the influences of the control parameters on the transient performance of the power system. We model the disturbance at power loads as Gaussian white noise and measure the transient performance of the frequency deviation and control cost by the $\mathscr{H}_2$ norm. Though it is hard for general power systems, the $\mathscr{H}_2$ norms are calculated for specific power systems with homogeneous parameters, which provides useful insights on the influences of the control parameters. It is shown that a trade-off between the frequency deviation and control cost is established. This trade-off is determined by the control parameters, which is demonstrated by both analysis and case studies. Furthermore, it is found that with the same control cost, PIAC is more efficient on suppressing the frequency than GBPIAC and by increasing a control parameter, the transient performance of DPIAC converges to that of GBPIAC.

With respect to the synchronization stability of power systems, we investigate the synchronous states and their stability of networks with a ring topology. The number of stable equilibria is calculated and the synchronization stability of the equilibria is investigated. The energy barrier is used to measure the synchronization stability, which is the potential energy difference between the type-1 saddles and the stable equilibrium. We find from the analytical calculation that when the generators and loads are evenly distributed in an alternating way, the energy barrier decreases to a constant as the size of the ring approaches infinity. Numerical simulation shows that for a heterogeneous distribution of generators and loads, the energy barrier decreases with the size of the ring. In addition, it shows that the more heterogeneous is the distribution of the generators and loads, the smaller is the energy barrier. So the energy barrier can be increased either by adding small rings to the network or decreasing the heterogeneity of the distribution of the generators and loads. In addition, by comparing the energy barrier of a ring network and a tree network, we find that a line connecting two nodes in a ring network is more robust than the one in a tree network when they are transmitting the same amount of power. The smaller the ring network, the larger is the energy barrier difference. Thus if the same robustness is expected, the line in a ring network can transmit more power than a corresponding one in a tree network. Because the synchronization stability of a network is usually limited by the lines that are less robust, the security constraint should be more strict on the lines with tree connections than that on the ones with ring connections.

# SAMENVATTING

Het elektriciteitsnetwerk is een fundament van de infrastruktuur van de hedendaagse maatschappij. De gebruikers van het netwerk vereisen dat de frequentie van het netwerk die wordt aangeboden overall gelijk is en niet veel afwijkt van de nominale frequentie. De huidige ontwikkelingen naar een elektriciteitsnetwerk met meer gedistribueerde opwekking van energie geeft aanleiding tot nieuwe en grote uitdagingen voor de regeling van het netwerk. Vanwege de vele variaties in de energieopwekking is er het gevaar dat de energieopwekking uitvalt of dat de stabiliteit van het elektrische netwerk verloren gaat. In dit proefschrift worden regelwetten en methodes voorgesteld die de frequentie van het elektriciteitsnetwerk regelen zodanig dat variaties van de energieopwekking en van netwerkinstabiliteiten worden onderdrukt.

De frequentieregeling wordt in het algemeen onderscheiden naar drie onderdelen: de eerste frequentieregeling die bij elke energieopwekker de lokale frequentie rond de nominale frequentie houdt; de tweede frequentieregeling die de frequentie in het gehele netwerk terugbrengt naar de nominale frequentie; en de derde frequentieregeling die ervoor zorgt dat de kosten van energieopwekking en -distributie geminimaliseerd worden en de veiligheid gewaarborgd is bij de gewenste nominale frequentie. Grote fluctuaties in de frequentie worden meestal veroorzaakt doordat de energieopwekking en het energieverbruik niet in evenwicht zijn, bij een frequentieonevenwichtigheid. De meest gebruikte tweede frequentieregeling brengt de afwijking in de frequentie van de nominale waarde naar nul, welke afwijking de gemiddelde netwerkfout wordt genoemd. De bestaande regelwetten voor de tweede frequentieregeling zijn gebaseerd op het principe van geïntegreerde afwijkingen die als nadeel hebben dat of de frequentie zeer langzaam teruggaat naar de nominale waarde of de frequentie de nominale waarde voorbij schiet en pas na enkele fluctaties naar de nominale waarde convergeert. Voor een goede tweede frequentieregeling is het van groot belang dat de frequentie zeer snel wordt teruggebracht naar de nominale waarde. Om een goede tweede frequentieregeling te bereiken wordt in dit proefschrift een centrale regeling voorgesteld die *power imbalance allocation control* (PIAC) wordt genoemd, (in het Nederlands een *toewijzingsregeling voor elektrisch vermogen*). Het bijbehorende regeldoel is de kosten van de energieopwekking in alle vermogensbronnen te minimaliseren. De regelwet functioneert als volgt: als eerste ontvangst de centrale regelaar van alle andere knooppunten informatie over de lokale frequenties; als tweede rekent, op basis van deze informatie en een kostenfunctie, de centrale regelaar uit wat de nieuwe ingangssignalen zijn van de energieopwekkers gedurende de komende korte periode; en als laatste worden elke ingangswaarde toegezonden aan de corresponderende vermogensopwekker. Doordat de regelwet gebaseerd is op proportionele en geïntegreerde frequentieafwijkingen convergeert het ingangssignaal op een exponentiële wijze naar de evenwichtswaarde met een snelheid die een parameter is van de regelwet. Op deze wijze wordt het voorbijschieten van de nominale frequentie en langzame convergentie voorkomen. Voor een elektriciteitsnetwerk met niet-samenwerkende deelnetwerken, ontkoppelt de regelwet PIAC de ingangssignalen van

elk beschouwd deelnetwerk van alle andere buurdeelnetwerken. Op deze wijze is de regeling van een deelnetwerk onafhankelijke van de frequentieafwijkingen van de andere deelnetwerken. Een stabiliteitsstelling toont aan dat het geregelde elektriciteitsnetwerk lokaal asymptotisch stabiel is als een strikt convexe kostenfunktie wordt gebruikt. Een illustratie van een elektriciteitsnetwork dat geregeld wordt met PIAC toont aan dat de frequentie, na een opzettelijk aangebrachte verstoring, snel wordt teruggebracht naar de nominale frequentie. De regelwet PIAC kan dus afwijkingen van de frequentie van de nominale waarde, snel terugbrengen naar nul.

Voor een grootschalig elektriciteitsnetwork is de PIAC regelwet niet praktisch vanwege de vele uitwisseling van informatie en vanwege de vereiste berekeningen van het ingangssignaal. Een gedistribueerde implementatie van de regeling kan deze bezwaren ondervangen maar ten koste van een langzame convergentie naar de stabiele evenwichtstoestand. Daarom wordt voorgesteld de *multilevel power-imbalance allocation control* (MLPIC) (in het Nederlands, *meer-niveau toewijzingsregeling voor elektrisch vermogen*). Hierbij wordt het elektriciteitsnetwerk opgedeeld in vele samenwerkende deelnetwerken met in ieder deelnetwerk een regelaar. MLPIAC bestaat uit twee onderdelen: (1) *gather-broadcast power-imbalance allocation control* (GBPIAC) (in het Nederlands *verzamel-en-verzend-toewijzingsregeling voor elektrische vermogen*) die geïmplementeerd wordt in elk deelnetwerk; en (2) *distributed power-imbalance allocation control* (DPIAC) (in het Nederlands *gedistribueerde toewijzingsregeling voor elektrische vermogen*) die geïmplementeerd wordt op een hoger niveau en dus de regelaars van elk deelnetwerk aanstuurt. In een elektrisch netwerk dat geregeld wordt door MLPIAC convergeert de som van alle ingangssignalen exponentieel naar de som van de afwijkingen van het vermogen met een snelheid die bepaald wordt door parameters van de regelwet. De frequentieafwijkingen van een grootschalig elektriciteitsnetwwerk kunnen dus effektief worden onderdrukt. Omdat het aantal knooppunten van een deelnetwerk veel lager is dan dat van het gehele netwerk zijn in MLPIAC de communicatielast en de berekeningslast voor regeling veel lager. Omdat het aantal deelnetwerken kleiner is dan het aantal knooppunten kan de MLPIAC regelwet het gehele netwerk efficiënter regelen dan een puur gedistribueerde regelwet. Daarom is MLPIAC een goed alternatief voor zowel een centrale regelwet als een puur gedistribueerde regelwet. Een elektriciteitsnetwerk dat geregeld wordt door MLPIAC is lokaal asymptotisch stabiel zoals blijkt uit een Lyapunov stabiliteitsanalyse met een voorwaarde op de parameters van de regelwet. Berekeningen voor een specifiek netwerk tonen aan dat MLPIAC de frequentieafwijkingen naar nul kan regelen met elke gewenste snelheid.

Het effekt van de parameters van de regelwet op het transiente gedrag van het elektriciteitsnetwerk is nader onderzocht voor de regelwetten PIAC, DPIAC en GBPIAC. Hiervoor wordt het model uitgebreid met een Gaussische witte ruis signaal voor de vermogensbelastingen van alle knooppunten met belastingen Verder worden bepaald de resulterende varianties van de frequentieafwijkingen en van de ingangssignalen in termen van een $H_2$ norm. In het algemeen is het een moeilijk probleem om de variantie te berekenen. Door vereenvoudigingen is het mogelijk om een schatting te verkrijgen van deze varianties die nuttig zijn voor een analyse van het effekt van de regeling. Er is een afweging mogelijk tussen de variantie van de frequentieafwijkingen en die van de ingangssignalen. Door keuzes te maken voor de waarden van de parameters van de regelwet kan een gewenste optimale keuzes tussen deze varianties worden bepaald. De resultaten worden gepresenteerd in ana-

lytische vorm en in de vorm van simulaties van het geregelde elektrische netwerk. Hieruit blijkt dat bij gelijke kosten PIAC een lagere variantie bereikt bij gelijke variantie van het ingangssignaal dan GBPIAC en dat het transiënte gedrag van DPIAC convergeert naar dat van GBPIAC.

De stabiliteit van een geregeld elektriciteitsnetwerk is onderzocht door de bepaling van synchrone toestanden en hun stabiliteit. Dit onderzoek is alleen verricht voor een ringnetwerk met aanvullende eigenschappen. Het aantal synchrone toestanden is berekend en er is bepaald welke van die toestanden stabiel zijn. Een maat voor de stabiliteit van de stabiele synchrone toestanden is de energiebarrière die gedefinieerd is als het verschil in energiewaarde tussen de stabiele synchrone evenwichtstoetand en die van het minimum van alle nabije evenwichtstoestanden met één instabiele eigenwaarde, in feite dus zadelpunten. Er is bewezen dat als de knooppunten in het netwerk afwisselend of energieopwekker of energiegebruiker zijn die gelijkmatig over de ring zijn gespreid dat dan de energiebarrière naar een constante waarde convergeert als de straal van de ring naar oneindig gaat. Door simulatie is aangetoond dat voor een niet-homogene verdeling van energieopwekkers en -gebruikers, de energiebarrière daalt met de straal van de ring. Bovendien is aangetoond dat de energiebarrière kleiner wordt als de verdeling van de opwekkers en gebruikers heterogener wordt. De energiebarrière kan dus worden verhoogd of door toevoeging van kleine ringen of door de verdeling van de energieopwekkers en -gebruikers minder heterogeen te maken. Door vergelijking van een ringnetwerk en een boomnetwerk is bepaald dat een transmissielijn die in een ringnetwerk twee knooppunten met elkaar verbind een meer robuust effect heeft op het gedrag van het systeem dan een lijn in een boomnetwerk in het geval dat beide lijnen dezelfde hoeveelheid vermogen overbrengen. De hoogte van de energiebarrière neemt af als het ringnetwerk een grotere straal heeft. Als dezelfde mate van robuustheid is vereist dan transporteert een lijn in een ring netwerk meer vermogen dan één in een boomnetwerk. Omdat de stabiliteit van een netwerk meestal wordt bepaald door de lijnen die minder robuust zijn moeten de veiligheidsvoorwaarden in een boomnetwerk meer stringent zijn dan in een ringnetwerk.

# 1

# INTRODUCTION

*Today, to fight the climate change and move to more sustainable energy generations, increasing more renewable energy such as wind turbines and solar Photo-Voltaic (PV) system are installed for power generation. It is known that wind turbines and solar PV system are weather dependent. The weather cannot be controlled or even accurately predicted by humans. A challenge brought by this transition to renewable power generation is frequency fluctuation that negatively affects the power supply and stability of the power system. For large-scale power systems, we investigate how to effectively suppress the fluctuation and increase the capability of keeping frequency synchronization from the perspective of control theory and stability theory of power systems respectively. In this chapter, we give a brief overview of the development trends of power systems and present the research problem and corresponding research questions of this thesis.*

1

This chapter is organized as follows. First, the development trends of power systems are described in Section 1.1. We then formulate the research problem and corresponding research questions of this thesis in Section 1.2 and finally describe the thesis outline in Section 1.3.

## 1.1. POWER SYSTEMS

Power system is one of the most complex man-made system ever which plays an important role in human's life since the late 19th century when it was first built. The power system consists of three parts, namely power generation, transmission and distribution to consumers as shown in Fig. 1.1. In traditional power system, power is generated by various kind of power plants, such as coal plant, hydraulic plant, nuclear plant, oil plant and gas plant, then it is transmitted by the transmission lines and distributed to the consumers. The power generation is controlled to meet the power loads by steering the frequency to its nominal value, e.g., 50 Hz in Europe and China or 60 Hz in North America.

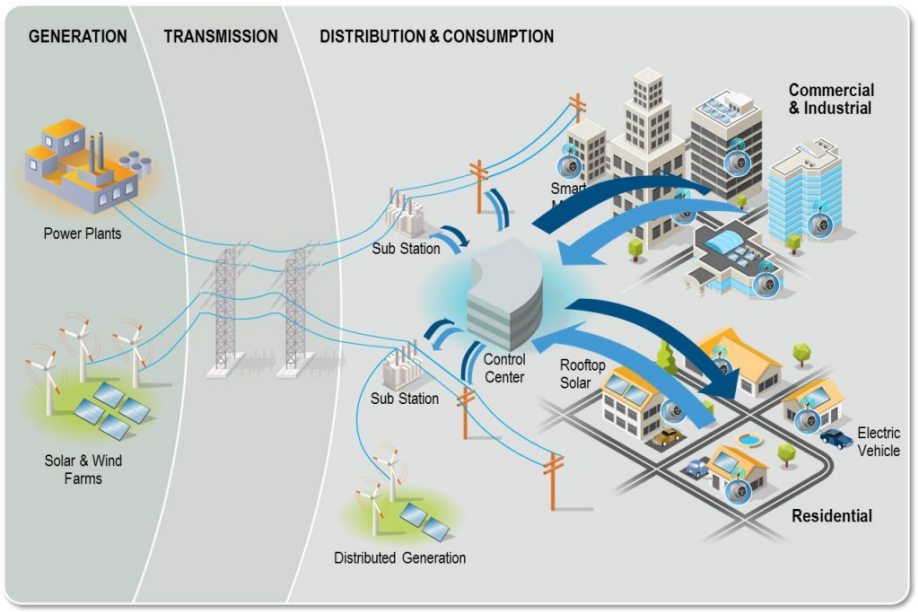


Figure 1.1: Future smart grid. From https://trilliant.com/home/smart-grid.

In the past decade, three factors have driven the development of power systems, i.e., the rapid establishment of renewable energy on the generation side, small and widely-distributed power sources, e.g., rooftop Photo-Voltaic (PV) systems, biomass generators, on the load side and smart digital electronics, such as smart meters and infrastructures for communication. In order to decrease the $CO_2$ emissions from the traditional fossil fuel power plants, there are more and more wind farms and solar PV farms established on the generation side and rooftop solar PV system installed on the load side almost all over the world. Fig. 1.2 shows the penetration rate of wind energy in the 28 states in EU (EU-28)

in 2016. It can be observed that the wind energy penetration of the three highest countries, Denmark, Ireland and Portugal, have reached more than 25% and the average penetration of the EU-28 also is more than 10%. The wind power penetration of these countries are still increasing, e.g., it is expected that 50% of the electricity generation in Denmark will be covered by wind energy by 2020 [1]. Fig. 1.3 shows the share of solar energy in the total power consumption in EU-28 in 2016. It can be seen that the solar PV accounted nearly 4% of the power demand in the EU-28 and more than 7% in Italy and Germany. It is estimated that the solar capacity can easily supply more than 15% of the power demand by 2030 if Europe would build on its solar experience and utilize the low cost solar energy[2]. Parts of this solar energy will be provided by solar farms and the other parts will be provided by the distributed rooftop PV systems at the load side as shown in Fig. 1.1. The development of digital electronics such as smart meters, Phase Measure Units, efficient communication networks and large capacity batteries, drives the development of the power grid to a future smart grid, in which the control center is able to monitor the power system accurately by bi-direction communication with the consumers and control it effectively and automatically [3].

The rapid increase of the weather dependent power energy, which is also called variable renewable energy, brings several challenges to the power system. It is well known that these renewable power generation depends on the weather which cannot be controlled or even accurately predicted. In this case, unlike the traditional power system where the uncertainties usually come from the load side only, the uncertainties now come from both the generation and load side and thus will be harder to manage. *These fluctuations do not only deteriorate the quality of power supply but decrease the power system stability* [4]. Furthermore, the distributed power sources, such as the weather dependent rooftop PV systems, also inject power into the power grid when good weather generates more energy than usual. Control efforts are required to be extended to the load side [5]. *This obviously increases the burden of the already busy control center of the large-scaled power system considered.* In order to keep the power supply despite many disturbances and to guarantee the stability and the security operation of the large-scale power system, these challenges should be well addressed, which is the focus of this thesis.

## 1.2. RESEARCH PROBLEM & RESEARCH QUESTIONS

Since power systems rely on the synchronous machines for power generation, a requirement for normal system operation is that all the synchronous machines remain in synchronization. The ability of a power system to maintain the synchronization when subjected to severe transient disturbance such as short-circuit of transmission lines, loss of generation, is called *transient stability* [6], which we will also refer to as *synchronization stability* in this thesis. This stability depends on both the initial operating state of the system and the severity of the disturbance. In order to prevent losing synchronization, the transmitted power by transmission lines at the initial operating state cannot be too large, otherwise, the system may easily lose the synchronization after a small disturbance, which may cause serious blackouts. For a power system with a complex topology, the transmitted power of the transmission lines at the operating state does not only depend on the power generation and loads but also on the network topology.

As described in Section 1.1, the characteristics of the renewable energy such as wind

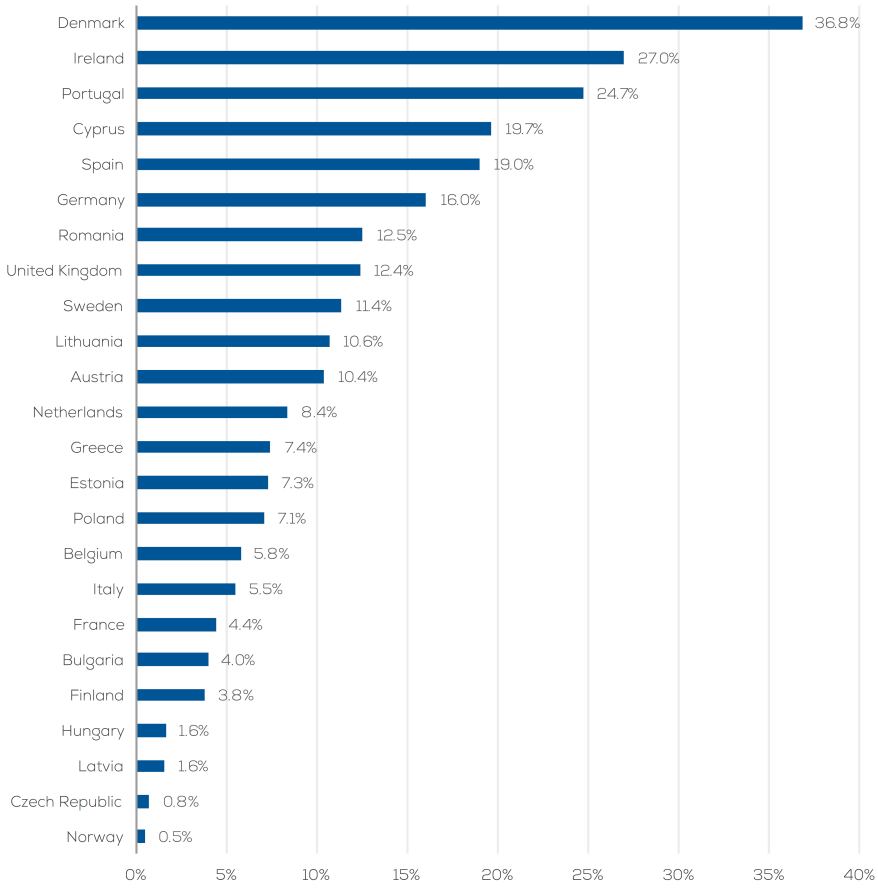


Figure 1.2: Wind power penetration in EU-28 countries in 2016. From [1].

power and solar power is the uncertainty from the weather, which causes the frequency fluctuations of the large-scale power system. These continuous fluctuations of the frequency may further lead the system to losing the synchronization. With respect to the frequency fluctuations and the synchronization stability, we focus on the following *Research Problem* (RP) in this thesis.

*Research Problem (RP): How to effectively suppress the frequency fluctuations and increase the synchronization stability of the systems for the large-scale power systems integrated with a large amount of weather dependent and distributed renewable energy and with advanced infrastructure of communication network and sensor devices?*

This research problem actually consists of the following two sub-problems.

*Sub-Research Problem 1 (Sub-RP1): For the large-scale power systems with advanced infrastructure of communication networks, how to effectively suppress the frequency fluctuations from the uncertainties of weather dependent renewable energy?*

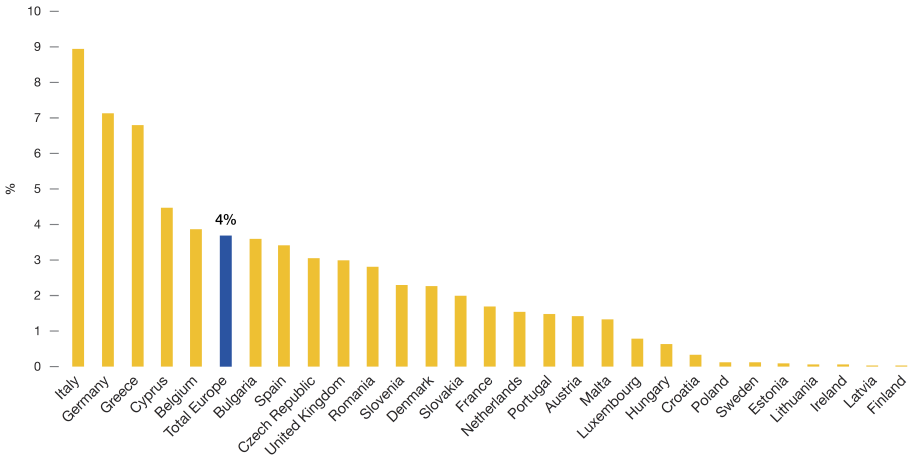


Figure 1.3: Solar power penetration in EU-28 countries in 2016. From [2].

*Sub-Research Problem 2 (Sub-RP2): For the large-scale power systems, how to increase the synchronization stability to avoid losing frequency synchronization caused by various disturbances which may mainly come from the weather dependent power energy?*

We consider Sub-RP1 from the perspective of control theory and Sub-RP2 from the perspective of stability theory of power systems in this thesis.

Regarding to Sub-RP1, the traditional control laws to control the frequency to the desired range usually focus on the steady state only without considering the transient performance. However, the power system is never at a real steady state because of the continuously fluctuations of the power loads and the generation of the weather dependent renewable energy. So beside the steady state for theoretical analysis, we also focus on the transient performance of the power system after a disturbance. With advanced communication infrastructures, state monitor systems and control actuators, we aim to design effective control algorithms to address the large fluctuation problem of the frequency by answering the following three *Research Questions* (RQs).

*RQ 1. Does a stable control law exist that is able to effectively suppress large fluctuations of the power system integrated with a large amount of weather dependent renewable energy?*

*RQ 2. Could the proposed control law be used in a large-scale power system? If not, how could it be reformulated for the large-scale power systems? Whether is the reformulated control law for the large-scale power system still stable?*

*RQ 3. In the proposed control laws, how the control parameters influence the transient performance of power system?*

With respect to Sub-RP2, we study the influence of the topology and the distribution of power generation and loads on the synchronization stability. The topology usually consists of ring connections and tree connections. In this thesis, we also mention a ring as a cycle.

The tree connection in the power system plays a similar role on the synchronization stability as a single line. So we analyze the role of rings on the synchronization as formulated in the following question.

*RQ 4. How do the rings of the power network influence the synchronization stability? How to increase the synchronization stability by controlling power generation and loads?*

## 1.3. THESIS OUTLINE

This thesis is organized as follows.

(1) In Chapter 2, the mathematical model, traditional hierarchical control laws and stability theory of power systems and the control architectures of network systems are introduced. With these preliminaries, we next review existing control laws of the power system and then mathematically explain the RP and its corresponding RQs. We finally present the possibilities to solve the RP and to answer the RQs.

(2) In Chapter 3, for RQ 1, we propose a stable centralized control law to improve the transient performance of the power system and compare it with the traditional control laws by case studies.

(3) In Chapter 4, for RQ 2, based on centralized control and distributed control, we present a multi-level control law that can be implemented in large-scale power systems with improved transient performance. Asymptotic stability analysis and numerical simulations are provided to show the performance of the proposed control law.

(4) In Chapter 5, RQ 3 is answered. We analyse the influence of the control parameters on the transient performance of power system using the $\mathscr{H}^2$ norm. We compare the performance of the proposed centralized, distributed control laws in Chapter 3 and Chapter 4.

(5) In Chapter 6, we focus on RQ 4. With cyclic power grids, we investigate how the rings in the topology and the distribution of power generation and loads of the power system influence the synchronization stability against disturbances.

(6) In Chapter 7, we conclude this thesis and introduce the research outlook on the control and stability improvement of future smart grids.

The definitions, theorems and lemmas and so on, in the following chapters, are numbered consecutively per section.

# 2

# PROBLEM FORMULATION

*In this chapter, we introduce the network model of power systems and the preliminaries of load frequency control, transient stability of the power systems. Regarding load frequency control, we first describe the traditional hierarchical control of power systems and control architectures of network systems. We then review the existing secondary frequency control approaches and formulate the problems that need to be solved to answer RQ 1-RQ 3 of Chapter 1. Regarding the transient stability concerned in RQ 4, the energy barrier is introduced to measure the stability. The connection between the setting of parameters in the power flow optimization and the transient stability are explained. The ideas to answer the four RQs are finally explained in this chapter.*

This chapter is organized as follows. The model and load frequency control of power systems are introduced in Section 2.1 and 2.2 respectively. We then introduce the control architectures of network systems in Section 2.3 followed by the description of economic power dispatch problem in secondary frequency control and corresponding control approaches in Section 2.4. The transient stability and its measurement using energy barrier, are introduced in Section 2.5. We finally formulate the problems that need to be solved in the RQs and describe the ideas to answer these questions in Section 2.6.



## 2.1. POWER SYSTEMS-A NETWORK MODEL

There are three main components in power systems, namely power generators, transmission network, and loads. We consider the power system described by a graph $\mathcal{G} = (\mathcal{V}, \mathcal{E})$ with nodes $\mathcal{V}$ and edges $\mathcal{E} \subseteq \mathcal{V} \times \mathcal{V}$ where a node represents a bus and edge $(i, j)$ represents the direct transmission line connection between node $i$ and node $j$. The buses connect to power generators and loads.

Each bus has associate variables of voltage phasor, active and reactive power injections. The voltage phasor at bus $i$ is denoted by $\mathbf{V}_i = V_i e^{\mathbf{j}\theta_i} = V_i \angle\theta$ where $\mathbf{j}^2 = -1$, $V_i > 0$ is voltage magnitude and $\theta_i$ is phase angle. The apparent power at bus $i$ is denoted by $\mathbf{S}_{ei} = P_{ei} + \mathbf{j}Q_{ei}$ where $P_{ei}$, $Q_{ei}$ are the active and reactive power respectively.

The transmission lines can be modeled by so-called $\pi$-equivalent circuits [6, chapter 6]. The network admittance matrix is denoted by $\mathbf{Y} = \hat{G} + \mathbf{j}\hat{B}$ where $\mathbf{Y}_{ij} = \hat{G}_{ij} + \mathbf{j}\hat{B}_{ij}$ is the mutual admittance and equals the negative of the transfer admittance between bus $i$ and $j$; $\mathbf{Y}_{ii} = \hat{G}_{ii} + \mathbf{j}\hat{B}_{ii}$ is the self-admittance of bus $i$ which includes all the admittance terminating on bus $i$ and any shunt admittance to ground $\mathbf{Y}_{i0}$, and the matrices $\hat{G}$ and $\hat{B}$ denote the real and imaginary parts of the admittance matrix respectively.

In this thesis, we focus on the transmission network of power systems and assume the transmission lines are lossless such that $\hat{G}_{ij} = 0$ for all $(i, j)$. Denote the current at bus $i$ by $\mathbf{I}_i$ with its complex conjugate denoted by $\bar{\mathbf{I}}_i$, we obtain the apparent power based on the Ohm's law as

$$\mathbf{S}_{ei} = \mathbf{V}_i \bar{\mathbf{I}}_i,\ \mathbf{I}_i = \sum_{j \in \mathcal{V}} \mathbf{Y}_{ij} \mathbf{V}_j,$$

which yields the *power flow equations*

$$P_{ei} = \sum_{j \in \mathcal{V}} \hat{B}_{ij} V_i V_j \sin(\theta_i - \theta_j), \tag{2.1a}$$

$$Q_{ei} = -\sum_{j \in \mathcal{V}} \hat{B}_{ij} V_i V_j \cos(\theta_i - \theta_j). \tag{2.1b}$$

Since the control of the voltage and of the frequency can be decoupled when the transmission lines are lossless [7], we do not model the dynamics of the voltages and assume the voltage of each bus is a constant which can be derived from power flow calculation [8].

We consider two types of generators, i.e., synchronous generators and frequency dependent power generators such as power inverters of renewable energy, where the inertias are small and are neglected[9, 10]. The dynamics of the synchronous generator at bus $i$ is

modeled by the classical swing equations [11, chapter 3],

$$\begin{aligned}\dot{\theta}_i &= \hat{\omega}_i - \omega_R,\\ M_i\dot{\hat{\omega}}_i &= P_i - D_i(\hat{\omega}_i - \omega_R) - P_{ei} + u_i,\end{aligned}$$

where $\omega_R$ is the nominal frequency, i.e., $\omega_R = 50$ or 60 Hz, $M_i > 0$ is the moment inertia of the machine, $P_i$ is the injected mechanical power, $D_i > 0$ is the droop control coefficient including damping of the machine, $P_{ei}$ is the transmitted power as defined in (2.1a), $u_i$ is the secondary frequency control input. Here, we have used $\theta_i$ to denote the rotor angle of the machine since it is rigidly coherent with the bus phase angle when the voltage of the system is constant [11, chapter 3]. The dynamics of the frequency dependent power generator at bus $i$ is specified by the differential algebraic equations,

$$\begin{aligned}\dot{\theta}_i &= \hat{\omega}_i - \omega_R,\\ 0 &= P_i - D_i(\hat{\omega}_i - \omega_R) - P_{ei} + u_i,\end{aligned}$$

where $P_i$ is the operating point of power injection, $D_i > 0$ is the droop control coefficient, $P_{ei}$ and $u_i$ are the transmitted power and secondary frequency control input respectively. This model can be used for the frequency dependent power loads when $P_i < 0$ and inverters of wind farms when $P_i > 0$. The bus connected to a passive power load is modeled as

$$P_i - P_{ei} = 0,$$

where $P_i$ is the consumed power at bus $i$. Note that in secondary frequency control, the transmitted power $P_{ei}$ may need to be measured, which depends on the control objectives and constraints, e.g., congestion elimination [12].

Denote the set of buses of the synchronous machines, frequency dependent power sources, passive loads by $\mathcal{V}_M, \mathcal{V}_F, \mathcal{V}_P$ respectively, thus $\mathcal{V} = \mathcal{V}_M \cup \mathcal{V}_F \cup \mathcal{V}_P$. We replace $\hat{\omega}_i - \omega_R$ by $\omega_i$ as the frequency deviation at the buses of synchronous machines and frequency dependent power sources. The formula of $P_{ei}$ will not change because it only depends on the phase angle differences $(\theta_i - \theta_j)$, which is not changed by the replacement of $\omega_i$. Adding secondary frequency control inputs to the nodes of synchronous machines and frequency dependent power sources, we derive the dynamics of the power system described by the following *Differential Algebraic Equations* (DAEs),

$$\dot{\theta}_i = \omega_i,\ i \in \mathcal{V}_M \cup \mathcal{V}_F, \tag{2.4a}$$

$$M_i\dot{\omega}_i = P_i - D_i\omega_i - \sum_{j\in\mathcal{V}} B_{ij}\sin(\theta_i - \theta_j) + u_i,\ i \in \mathcal{V}_M, \tag{2.4b}$$

$$0 = P_i - D_i\omega_i - \sum_{j\in\mathcal{V}} B_{ij}\sin(\theta_i - \theta_j) + u_i,\ i \in \mathcal{V}_F, \tag{2.4c}$$

$$0 = P_i - \sum_{j\in\mathcal{V}} B_{ij}\sin(\theta_i - \theta_j),\ i \in \mathcal{V}_P, \tag{2.4d}$$

where $u_i$ is the secondary frequency control input at node $i$, and $B_{ij} = \hat{B}_{ij}V_iV_j$. We assume that the nodes participating in secondary frequency control are equipped with a primary controller. Denote the set of nodes equipped with the secondary controllers by $\mathcal{V}_K$, thus $\mathcal{V}_K \subseteq \mathcal{V}_M \cup \mathcal{V}_F$.

This model and the ones with linearized sine function are widely studied, e.g.,[9, 10, 12–16], in which the frequency dependent nodes are usually used to model the renewable power inverters. It has been demonstrated in [17, 18] that frequency droop controlled Micro-Grids which have some sort of energy storage and lossless transmission lines can also be modeled by second-order swing equations (2.4a-2.4b).



## 2.2. LOAD FREQUENCY CONTROL

In this section, we introduce the hierarchical frequency control of power systems, i.e., primary, secondary and tertiary frequency control. In general, frequency control is implemented at three different levels distinguished from fast to slow timescales [8, 11]. On a short time scale, the power grid is stabilized by decentralized droop control, which is called *primary control*. While successfully balancing the power supply and demand, and synchronizing the power frequency, the primary control induces frequency deviations from the nominal frequency, e.g., 50 or 60 Hz. The *secondary frequency control* regulates the frequency back to its nominal frequency in a slower time scale than the primary control. On top of the primary and secondary control, the *tertiary control* is concerned with global economic power dispatch over the networks in a large time scale. Consequently it depends on the energy prices and markets.

### 2.2.1. PRIMARY FREQUENCY CONTROL

Primary control is commonly known as frequency response. It balances the power demand and supply quickly and synchronizes the frequencies of the power generators in a short time-scale. The most fundamental, front-line control of the frequency is the action of generator governors which lets the generators maintain a constant stable system frequency.

In system (2.4), the control input of primary control is proportional to the frequency deviation which is represented by the term $-D_i\omega_i$ in (2.4b) and (2.4c). With the proportional control input $-D_i\omega_i$, system (2.4) synchronizes at an equilibrium state, called the *synchronous state* as in the Kuramoto-model [19] as follows.

**Definition 2.2.1** *Define a* steady state *of the power system (2.4) with constant power loads (generation) such that,*

$$\omega_i = \omega_{syn},\ i \in \mathcal{V}_M \cup \mathcal{V}_F \tag{2.5a}$$
$$\dot{\omega}_i = 0,\ i \in \mathcal{V}_M \cup \mathcal{V}_F, \tag{2.5b}$$
$$\theta_i = \omega_{syn} t + \theta_i^*,\ i \in \mathcal{V}, \tag{2.5c}$$
$$\dot{\theta}_i = \omega_{syn}, \tag{2.5d}$$

*in which $\theta_i^*$ is the rotor angle of bus $i$ at the steady state, $\omega_{syn} \in \mathbb{R}$ is the synchronized frequency deviation.*

Without the secondary frequency control input, i.e., $\{u_i = 0,\ i \in \mathcal{V}_K\}$, substituting (2.5) into system (2.4), we derive the explicit formula of the synchronized frequency deviation

$$\omega_{syn} = \frac{\sum_{i\in\mathcal{V}} P_i}{\sum_{i\in\mathcal{V}_M\cup\mathcal{V}_F} D_i}, \tag{2.6}$$

which indicates that the frequency deviation is proportional to the *power-imbalance*

$$P_s = \sum_{i \in \mathcal{V}} P_i. \tag{2.7}$$



The reference for primary control at node $i$ is $P_{ref} = P_i$ and the primary control input is $\{\Delta P_i = -D_i \omega_{syn},\ i \in \mathcal{V}_M \cup \mathcal{V}_F\}$, which are illustrated in Fig. (2.1a). We derive from (2.6) that at the steady state it yields

$$-\omega_{syn} \sum_{i \in \mathcal{V}_M \cup \mathcal{V}_F} D_i + P_s = 0.$$

which indicates that the power supply and demand are balanced. Here, the power demand includes the power losses on the damping of the machines. In addition, the allocation of the power imbalance is only determined by $\{D_i,\ i \in \mathcal{V}_M \cup \mathcal{V}_F\}$. However, if the power imbalance $P_s$ is nonzero, the frequency deviation will also be nonzero, which raises the necessity of secondary frequency control.

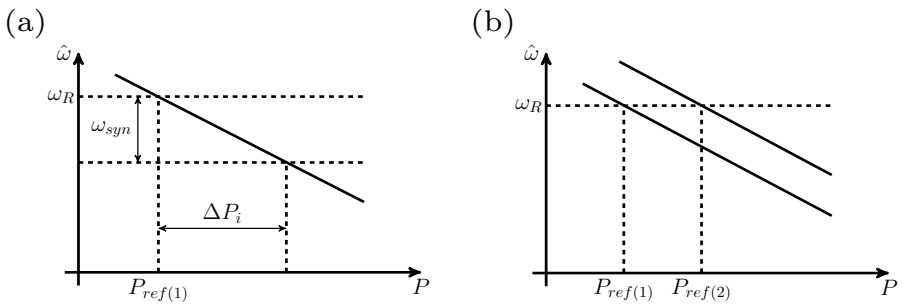


Figure 2.1: Primary and Secondary frequency response. The slop of the lines are $-D_i$. (a). Primary frequency response. (b) Secondary frequency response.

### 2.2.2. SECONDARY FREQUENCY CONTROL

Secondary frequency control is used to restore frequency to its nominal value, e.g., 50 or 60 Hz, following a disturbance. It calculates the generation references for primary control in a slower time-scale than in primary control and maintains power allocation among the power units in accordance with area dispatching needs.

For system (2.4) with secondary frequency control inputs, substituting (2.5) into system (2.4), we derive the explicit formula of $\omega_{syn}$ as

$$\omega_{syn} = \frac{\sum_{i \in \mathcal{V}} P_i + \sum_{i \in \mathcal{V}_K} u_i}{\sum_{i \in \mathcal{V}_M \cup \mathcal{V}_F} D_i}, \tag{2.8}$$

The necessary condition to recover the nominal frequency such that $\omega_{syn} = 0$ is

$$P_s + \sum_{i \in \mathcal{V}_K} u_i = 0,$$

which can be satisfied by determining the appropriate values of $\{u_i,\ i \in \mathcal{V}_K\}$ with a control law.

With the control input $u_i$, the power generation references for primary control becomes $P_{ref} = P_i + u_i$. The movement of the reference controlled by secondary frequency control is illustrated in Fig. (2.1b).



An economic power dispatch problem is often involved into secondary frequency control law, which will be further discussed in Section 2.4.

### 2.2.3. TERTIARY CONTROL

Tertiary control calculates the operating point for primary and secondary control on the slowest time-scale [20, chapter 9]. This control depends on the structure of the network and the role that the power plant plays in the network. The operating point for individual power plants are set based on economic power dispatch or more generally *Optimal Power Flow* (OPF), which minimizes the control cost or maximizes the social welfare. The operating point is such that the power demand is satisfied and the power interchange between areas is scheduled under security constraints.

The operating point of the reactive power generation for voltage control is also calculated by tertiary control. With the prediction of the power loads (or generation of weather dependent power sources) or scheduled power generation, a typical OPF model can be represented using the following security constrained optimization problem [21, chapter 8], [22, chapter 6],

$$\min_{P_g} \ F(P_g) = \min_{P_g} \sum_i F_i(P_{ig}), \tag{2.9a}$$

$$\text{s.t.} \quad f(\theta, V, P, Q) = 0, \tag{2.9b}$$

$$P_{g\min} \le P_g \le P_{g\max}, \tag{2.9c}$$

$$Q_{g\min} \le Q_g \le Q_{g\max}, \tag{2.9d}$$

$$V_{\min} \le V \le V_{\max}. \tag{2.9e}$$

$$|P_{ij}(\theta, V)| \le P_{ijmax},\ (i,j) \in \mathcal{E}, \tag{2.9f}$$

where $P_g,\ \theta,\ V,\ P,\ Q_g,\ P_{g\min}, P_{g\max}, Q_{g\min}, Q_{g\max}, V_{\max}, V_{\min}$ are vectors, $P_{ij}(\theta, V)$ and $P_{ijmax}$ are scalars, $P_g$ denotes the active power generation, $Q_g$ denotes the reactive power generation, $F(P_g)$ is a specified objective function for generation cost of the power system, $f(\theta, V, P, Q)$ are the power flow equations, $P_{\max}$ and $P_{\min}$ are the specified upper and lower limits for the active power generation (or loads), $Q_{\min}$ and $Q_{\max}$ are the upper and lower bound for the reactive power generation, $V_{\max}$ and $V_{\min}$ are the upper and lower limits of the voltage. $P_{ij}(\theta, V)$ denotes the power flows through a line, which is limited by $P_{ijmax}$ concerning system security. The power flow equations $f(\theta, V, P, Q)$ may include the losses on the transmission lines, which are different from the ones in (2.1). In this optimization problem, power load shedding is allowed if the objective function contains the benefits from the loads [22, chapter 6], which becomes the social benefits.

In practical implementation, a number of other optimization objectives and security management functions, such as transmission losses and stability margins are included, for which we refer to [21, 22].

Because the power flow equations are satisfied, the power supply and demand are balanced which leads to $\omega_{syn} = 0$. The solution of the optimization problem (2.9) is the operating point of primary and secondary control which is denoted by $(\hat{\theta}, \hat{V}, \hat{P}, \hat{Q})$. Note that to solve the OPF problem, a prediction of the power demand has to be available.



**Remark 2.2.2** *After the tertiary control actions, the generation $P_g$ of traditional power plants such as coal plant and nuclear plant can be set to their operating points $\hat{P}_g$, while the weather dependent renewable generation and power loads usually deviate from their operating points due to the uncertainties of the weather and the behaviors of power consumers. This leads to a nonzero power-imbalance $P_s$ in (2.7), which further results in a nonzero frequency deviation. As increasingly more and more renewable power sources are integrated into the power system, the power-imbalance $P_s$ may fluctuate severely leading to frequency fluctuations.*

**Remark 2.2.3** *The parameters $P_{ij\max}$ for all lines are usually specified off-line concerning the frequency and voltage stability. If the voltage is well controlled, the power flow in a line is mainly determined by the phase angle difference between the two terminal buses. A smaller $P_{ij\max}$ leads to a larger security margin for the synchronization stability. This will be further explained in Section 2.5. From the perspective of the synchronization stability, the phase angle differences should not be too large, otherwise the machines lose synchronization easily after a disturbance, which could result in complete frequency collapse [23]. This requires a small parameter $P_{ij\max}$ to limit the phase angle difference. On the other side, if $P_{ij\max}$ is too small, only a small amount of power can be transmitted, which limits the economic efficiency of the transmission line. Furthermore, the feasible solution of the optimization problem (2.9) may not exist for too small $P_{ij\max}$.*

## 2.3. CONTROL ARCHITECTURE OF NETWORK SYSTEMS

In this section, we introduce the different control architectures of network systems, i.e., centralized, distributed, decentralized control and multi-level control. The power system is a good example of network systems, where each node represents a subsystem coupled with its neighbors by transmission lines.

The *centralized control* of network systems is defined as follows.

**Definition 2.3.1** *Consider a network system with all the subsystems connected to a central controller by a communication network. In* centralized control*, the central controller gathers the state information from all the subsystems to compute the control commands and then sends control commands to each subsystem via the communication network.*

The diagram in Fig. (2.2) describes the centralized control architecture, where each subsystem is represented by a box. In the centralized control architecture, the central controller has to collect the state information and computes the control inputs for all the subsystems. An advantage is the high control efficiency for achieving a control objective. The main disadvantages are the overhead communications and computations for large-scale network systems.

In contrast, in the *distributed control architecture*, the control inputs are computed locally by the subsystems, which is defined as follows.

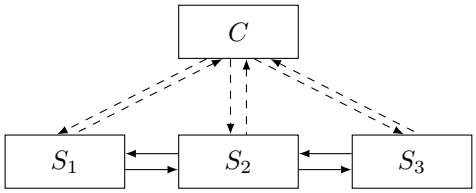


Figure 2.2: Diagram for centralized control. The dashed lines denote communications and the solid lines denote the coupling of the subsystems. The controller $C$ collects the state information from the subsystem $S_1, S_2, S_3$ and then computes the control inputs and finally sends them to the subsystems.

**Definition 2.3.2** *Consider a network system with all subsystems equipped with local controllers, and there is a communication network connecting all the local controllers. In* distributed control *with communication between controllers, the local controller computes the control input with the local state information and the information obtained from its neighbors.*

The diagram in Fig. (2.3) describes the distributed control architecture where the subsystems and the controllers are represented in two separated boxes. The advantage of this control architecture is that it reduces the complexity of the computations and communications compared with the centralized control. The disadvantage is that for a large-scale network system, the control efficiency for achieving a control objective is usually lower than centralized control.

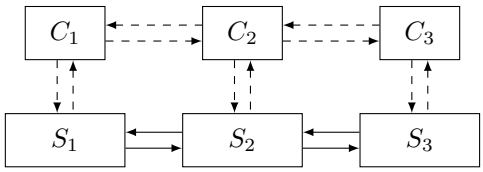


Figure 2.3: Diagram for distributed control. The dashed lines denote communications and the solid lines denote the coupling of the subsystems. The controller $C_i$ calculates the control input for $S_i$ with the local state information and control information from its neighbors.

Without communications between the controllers, the distributed control reduces to the *decentralized control* which is described in Fig. (2.4). The primary frequency control of the power system actually is a decentralized control.

We use the term "multi-level" control to describe the control of the system with several levels over the network in this thesis to distinguish from the hierarchical control over time,. The power system has a multi-level architecture. For example, the systems at the level of communities are subsystems of the systems at the level of provinces, which are further subsystems at a higher level of the states. For a network with multi-level architecture, the *multi-level control architecture* is defined as follows.

**Definition 2.3.3** *Consider a network system with a multi-level architecture, where the con-*

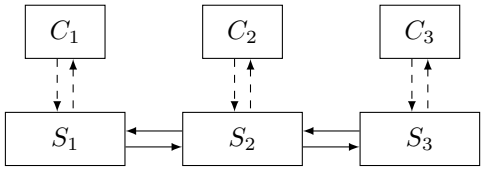




Figure 2.4: Diagram for decentralized control. The dahsed lines denote communications and the solid lines denote the coupling of the subsystems. The controller $C_i$ calculates the control input for $S_i$ with its local state information. There are no communications between the controllers.

*trollers at different levels are connected via a communication network. In* multi-level control*, the control input of the system is computed by controllers at different levels with various control objectives. The controllers at the highest level calculates the control input in a centralized or distributed way with the information from its subsystems. The controllers at the other levels calculate the control input either with the local state information at the level only or with both the local state information and the control information from other controllers at one level higher than this level.*

We remark that this definition may have not included all kinds of multi-level control laws. The essential aspect of the multi-level control is that the control input of the system is calculated at different levels with various objectives. For the power system, for example, the primary, secondary and tertiary control can also be seen as a three-level control where the primary control balances the power supply and demand quickly with the local frequency deviation, the secondary control recovers the nominal frequency with the local frequency deviation, which may communicate with other controllers, and the tertiary control calculates the input with the predicted power demand of the network at different nodes.

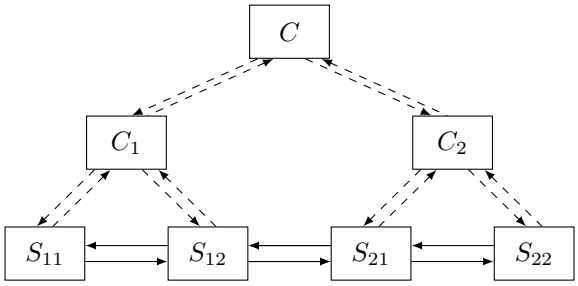


Figure 2.5: Diagram of a two-level control. The dahsed lines denote communications and the solid lines denote the coupling of the subsystems. The control $C_i$ calculates the control input with the local state information of $S_{11}, S_{12}$ and the control command from $C$ at the top level.

The multi-level control may consist of centralized, distributed and decentralized control. With a well designed multi-level control, the overhead communication and complicated computations in the centralized control and the control efficiency in the distributed control for a large-scale system can be well addressed.

The selection of the control architecture depends on the scale of the system, the established communication network and the desired performance.

## 2.4. SECONDARY FREQUENCY CONTROL WITH ECONOMIC POWER DISPATCH

In this section, we introduce the secondary frequency control related to an economic power dispatch problem and review the existing control laws for it.

### 2.4.1. ECONOMIC POWER DISPATCH

We consider the system (2.4) in this thesis, where the voltage is constant and the transmission lines are lossless.

As explained in Subsection 2.2.2 and 2.2.3, the power generation and loads usually deviate from their operating point which leads to a nonzero power-imbalance and subsequently a nonzero frequency deviation from the nominal frequency. Secondary frequency control restores the nominal frequency, for which we consider the following problem.

**Problem 2.4.1** *Design a control law with the inputs* $\{u_i,\ i \in \mathcal{V}_K\}$ *for the system (2.4) such that, after a disturbance,*

*(i) the state converges to a synchronous state as in (2.5) with* $\omega_{syn} = 0$*,*

*(ii) the control cost is minimized at the synchronous state.*

In order to minimize the control cost at the synchronous state with $\omega_{syn} = 0$, the following economic power dispatch problem is considered [11, chapter 13], [21, chapter 3].

$$\min_{\{u_i \in \mathbb{R}, i \in \mathcal{V}_K\}} \sum_{i \in \mathcal{V}_K} J_i(u_i), \tag{2.10a}$$

$$s.t.\ \ P_s + \sum_{i \in \mathcal{V}_K} u_i = 0, \tag{2.10b}$$

$$\underline{u}_i \le u_i \le \overline{u}_i, \tag{2.10c}$$

where the control costs $J_i(u_i),\ i \in \mathcal{V}_K$, of the controllers are different for various reasons such as different device maintenance prices.

**Remark 2.4.2** *If the congestion problem in the transmission lines is considered in secondary frequency control, the constraints of (2.10) are replaced by*

$$P_i - \sum_{j \in \mathcal{V}} B_{ij} \sin\theta_{ij} + u_i = 0,\ i \in \mathcal{V}_M \cup \mathcal{V}_F, \tag{2.11a}$$

$$P_i - \sum_{j \in \mathcal{V}} B_{ij} \sin\theta_{ij} = 0,\ i \in \mathcal{V}_P, \tag{2.11b}$$

$$|\theta_{ij}| \le \gamma_{ij} \le \frac{\pi}{2},\ (i,j) \in \mathcal{E},$$

$$\underline{u}_i \le u_i \le \overline{u}_i,\ i \in \mathcal{V}_K,$$

*where the power flow equations (2.11a) and (2.11b) determine the phase angle differences $\theta_{ij}$. We neglect the congestion constraints in the secondary frequency control in this thesis, which can be guaranteed by tertiary control. In fact, as the power generation and loads $P_i$ do not deviate significantly from their operating points calculated from the tertiary control, the congestion will not be triggered.*



To simplify the problem, The following assumptions are made for the economic power dispatch problem (2.10).

**Assumption 2.4.3** *For Problem (2.4.1), assume that*

*(i) the power-imbalance $P_s$ defined in (2.7) is a constant,*

*(ii) the power imbalance can be compensated by the control inputs such that*

$$-P_s \in \big[ \sum_{i\in\mathcal{V}_K} \underline{u}_i, \sum_{i\in\mathcal{V}_K} \overline{u}_i \big],$$

As explained in Remark (2.4.2),Assumption (2.4.3) is also realistic.

We integrate the constraint $u_i \in [\underline{u}_i, \overline{u}_i]$ into the cost function $J_i(u_i)$, e.g., by barrier functions [24, chapter 13]. The *Lagrangian function* of the economic power dispatch problem is

$$L(u,\lambda) = \sum_{i\in\mathcal{V}_K} J_i(u_i) - \lambda(P_s + \sum_{i\in\mathcal{V}_K} u_i),$$

where $u = \mathrm{col}(u_i)$ is a vector consisting of $u_i,\ i \in \mathcal{V}_K$, and $\lambda \in \mathbb{R}$ is a dual variable. The necessary *Karush-Kuhn-Tucker* (KKT) optimality conditions require that [24]

$$\frac{\partial L(u,\lambda)}{\partial u} = 0,$$

which leads to a necessary condition for solving the economic dispatch problem (2.10)

$$J'_i(u_i) = J'_j(u_j) = \lambda, \forall\ i,j \in \mathcal{V}_K, \tag{2.12}$$

where $J'_i(u_i) = \frac{dJ_i(u_i)}{du_i}$ is the *marginal cost* of node $i$ for all $i \in \mathcal{V}_K$ and $\lambda$ is the *nodal price*.

Note that if the power imbalance $P_s$ is known, the optimization problem (2.10) can be solved analytically with the necessary condition (2.12). However, $P_s$ is unknown in practice since the loads cannot be predicted precisely on a short timescale.

After a disturbance, the state of the power system experiences two phases: a transient phase and a steady phase. However, the optimization problem (2.10) focuses on the steady state only, e.g., [10, 13, 14, 16, 25, 26].

### 2.4.2. REVIEW OF EXISTING APPROACHES

In this subsection, we briefly outline existing secondary frequency control methods and discuss their relevance for finding a solution to Problem (2.4.1).

*ACE based AGC[11]:* The *Area Control Error* (ACE) of an area is defined as

$$ACE(t) = B\omega(t) + P_{ex}(t) - P^*_{ex},$$

where $B$ is a positive constant, $\omega$ is the frequency deviation of the area, $P_{ex}$ is the net power export, and $P_{ex}^*$ is the nominal value of $P_{ex}$. The adjustment of the power injection of the area is given as follows

$$\dot{u} = -k \cdot ACE(t)$$



where $k$ is a positive control gain coefficient. In the traditional *Automatic Generation Control* (AGC) method, the frequency deviation is measured at a local node and communicated by a coordinator as the ACE to the controllers in the system, which calculate their control inputs according to their participation factors. When the interconnected system is considered as a single area, the AGC has the form [10]

$$\dot{\lambda}(t) = -k\omega_{i^*}(t),\ i \in \mathcal{V}, \quad u_i(t) = J_i'^{-1}(\lambda(t)), \tag{2.13}$$

where $k$ is a control gain coefficient, $\omega_{i^*}$ is the measured frequency deviation at a selected node $i^*$. Note that $\lambda$ can be seen as the nodal price which converges to the market clearing price $\lambda^*$ as the power supply and demand is balanced. Note that the participation factor is involved in the derivative of the cost function, $J_i'(u_i)$. The frequency deviation of the area is not well reflected in (2.13) since it is measured at only one node. Furthermore, the communication network is not used efficiently because it only communicates the nodal price $\lambda$ from the coordinator to the controllers.

*Gather-Broadcast (GB) Control [10]:* In order to accurately reflect the frequency deviation of the area and use the communication network efficiently, the GB method measures the frequency deviations at all the nodes connected by the communication network. It has the form

$$\dot{\lambda}(t) = -k \sum_{i \in \mathcal{V}} C_i \omega_i(t),\ i \in \mathcal{V}, \quad u_i(t) = J_i'^{-1}(\lambda(t)), \tag{2.14}$$

where $k$ is a control gain coefficient and $C_i \in [0,1]$ is a set of convex weighting coefficients with $\sum_{i \in \mathcal{V}} C_i = 1$. As in the ACE based AGC method, a coordinator in the network also broadcasts the nodal price to the controllers and the controllers compute the control inputs according to their own cost functions.

*Distributed Averaging Integral control (DAI):* Unlike the ACE based AGC method and GB method which are implemented in a centralized way, DAI is implemented in a distributed way based on the consensus control principle [26]. In the DAI method, there are no coordinators and each controller computes its own nodal price and communicates to its neighbors. A local node in the system calculates its control input according to the local frequency deviation and the nodal prices received from its neighbors. As the state of the interconnected system reaches a new steady state, the nodal prices of all the nodes achieve consensus at the market clearing price, thus Problem (2.4.1) is solved. It has the form [27]

$$\dot{\lambda}_i(t) = -k_i\omega_i(t) + \sum_{j \in \mathcal{V}} w_{ij}(\lambda_j(t) - \lambda_i(t)),\ u_i(t) = J_i'^{-1}(\lambda_i(t)), \tag{2.15}$$

where $k_i$ is a gain coefficient for the controller $i$ and $w_{ij}$ denotes the undirected weighted communication network. When $w_{ij} = 0$ for all the lines of the communication network, the DAI control law reduces to a *Decentralized Integral* (DecI) control law. The DAI control

has been widely studied on both traditional power grids and Micro-Grids, e.g., [25, 28]. Note that, $\omega_i$ is the frequency deviation from the nominal frequency at node $i$, which should be known for all nodes in $\mathcal{V}_K$. Wu *et.al.* [29] proposed a distributed secondary control method where it is not necessary to know the nominal frequency for all the nodes in $\mathcal{V}_K$.



When a steady state exists for the nonlinear system (2.4), all the approaches above can restore the nominal frequency with an optimized control cost. However, it can be easily observed that the control approaches, e.g., (2.13) and (2.14), are in the form of integral control where the control inputs are actually the integral of the frequency deviation. A common drawback of integral control is that *the control input suffers from an overshoot problem with a large gain coefficient or slow convergence speed with a small one, which causes extra oscillation or slow convergence of the frequency* [30–32].

The methods that we discussed above are related to controlling the nonlinear system (2.4) based on passivity methods. However, the linearized version of the evolution equations (2.4) was also addressed based on primal-dual method in the literature.

Li *et al.* proposed an Economic AGC (EAGC) approach for the multi-area frequency control [16]. In this method each controller exchanges control signals that are used to successfully steer the state of the system to a steady state with optimized dispatch, by a partial primal-dual gradient algorithm [33]. Unfortunately, transient performance was not considered in the method. A potentially very promising method to the control of the linear system was recently proposed by Zhao *et al.* In [12] a novel framework for primary and secondary control, which is called Unified Control (UC), was developed. The advantage of UC is that it automatically takes care of the congestions that may occur in the transmission lines. Numerical simulations results show that the UC can effectively reduce the harmful large transient oscillations in the frequency. However, so far a theoretical analysis on how the UC improves the transient performance is lacking. Other recently reported studies are by Liu *et al.* in [34] and by Z. Wang *et al.* in [35]. They investigated distributed real-time optimal power flow control, while at the same time they provide a stability analysis. These methods both optimize control costs and manage power flow congestion using the principle of consensus control, but cannot prevent large frequency deviations at short times. For more details of distributed frequency control, we refer to the survey paper [36].

Finally, we mention here control methods whose underlying principle is neither based on integral control nor on primal-dual method. A robust approach is based on the concept of the Active Disturbance Rejection Control (ADRC) [37]. It was pursued by Dong *et al.* [38]. The method is robust against model uncertainties, parameter variations and large perturbations. It was employed to construct a decentralized load frequency approach for interconnected systems. However, the decentralized control employed in this method prevents a solution to the economic power dispatch. Frequency control treated by optimal control [39, 40] as introduced in Appendix A.2, concerns primarily the transient performance. In that optimal control framework, the control objective is to minimize the control cost and frequency deviation over a short horizon. However, the solution of the optimal secondary frequency control cannot be solved directly since an exact forecast of the fluctuating loads is needed, which is impossible in practice.

Problem (2.4.1) focuses on the steady state only and the transient performance of the corresponding control methods is poor, as extra frequency oscillations are caused by the overshoot of controllers. The traditional method to eliminate the overshoot is to calculate

the control gain coefficients by analyzing the eigenvalue of the linearized systems [41, 42]. However, the improvement of the transient performance obtained by the eigenvalue analysis is still poor because of the dependence of the eigenvalues on the control law structure, and the large scale, complex topology and heterogeneous power generation and loads of the power system.

There are also other control laws have been proposed to address the slow convergence problem, e.g., sliding mode based control laws [43, 44], and $\mathscr{H}_2/\mathscr{H}_\infty$ control based control laws [45, Chapter 5] and [46] *et al*, and fuzzy PI control law [47], which are able to shorten the transient phase while avoiding the overshoots and large frequency deviations. However, they focus on the linearized system and did not consider the economic power dispatch problem (2.10) at the steady state.

As explained in Remark (2.2.2), the fluctuations in the power supply become faster and larger as more and more renewable power sources are integrated into the power system. There is a need to design a control law that has a good transient performance without the overshoot problem and with a high convergence speed.

## 2.5. STABILITY OF POWER SYSTEMS

In this section, we introduce the synchronization stability of power systems.

A large excursion of the state variables of the power system, such as the voltage and the phase angle, usually occur after a disturbance. *Transient stability* is defined as the ability of a power system to remain the synchronization when subjected to various disturbances [6]. This stability is influenced by the nonlinearity of the power system. The *basin of attraction* (also called the *stability region*) of a nonlinear system is defined as the set of the starting points of the trajectories which converge to the equilibrium as the time goes to infinity. For a nonlinear system with a small basin of attraction, the trajectory usually has a small escape time from the region when subjected to disturbances. The stability region of power systems, has been analyzed by Chiang [48] and Zaborszky *et al* [49, 50]. However, because of the large-scale and complexity of the power network, the basin of attraction which is related to the transient stability is still hard to be well estimated.

In order to investigate the stability, basin stability [51, 52] has been proposed to measure the transient stability, which however is hard to be analytically calculated due to the nonlinearity. In this thesis, inspired by the *direct method* to estimate whether the power system is stable after a disturbance [53–56], we use the *energy barrier* to measure the transient stability which is explained through the following *Single Machine Infinite Bus* (SMIB) system as shown in Fig. 2.6(a).

The SMIB model is described by the following equations.

$$\begin{aligned} \dot{\delta} &= \omega, \\ M\dot{\omega} &= P - D\omega - B\sin\delta, \end{aligned}$$

which can be directly derived from (2.4). Here $P$ and $B$ are the transmitted power and the capacity of the line respectively, the voltages are also assumed as constants, $\delta$ is the angle difference between the synchronous machine and the infinite bus, which should be in a small range in order keep the synchronization. This requires $\omega = 0$ and $P = B\sin\delta$ at the

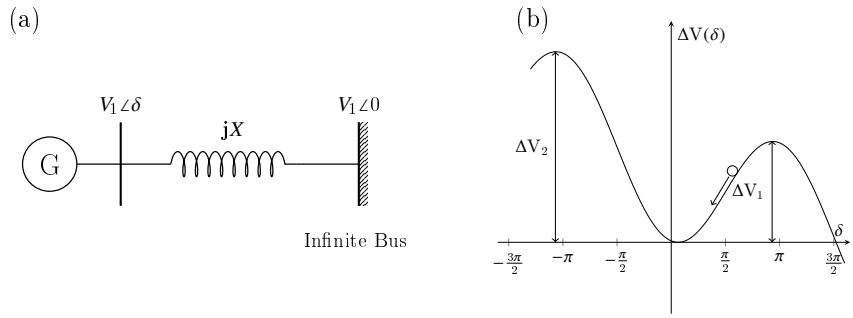


Figure 2.6: (a) The SMIB model. (b) The potential energy landscape of the SMIB system.

synchronized state. The potential energy of this system is

$$\mathrm{V}(\delta) = -B\cos\delta - P\delta.$$

Fig. 2.6(b) plots the potential energy difference $\mathrm{V}(\delta) - \mathrm{V}(\delta_0)$ where $\delta_0 = \arcsin\frac{P}{B}$ is the phase angle difference at the steady state. In the figure, the position and the moving speed of the circle are $\delta$ and $\omega$ respectively. The potential energy possesses three extreme points in the range $(-\frac{3\pi}{2}, \frac{3\pi}{2})$, which include two unstable equilibria and one stable equilibrium. It can be observed that the trajectory will converge to the minimum of $\mathrm{V}(\delta)$ if its kinetic energy is smaller than the potential energy $\Delta\mathrm{V}_1$ and $\Delta\mathrm{V}_2$. If obtaining enough energy from a disturbance to overcome the potential energy, the trajectory will go out of the valley and thus leads to a desynchronization. Hence, the energy barrier $\Delta\mathrm{V}_1$ and $\Delta\mathrm{V}_2$ which are the potential energy differences between the two unstable equilibria and the stable equilibrium, can be used to measure the synchronization stability, which have the following formula [53]

$$\Delta\mathrm{V}_1 = P(-\pi + 2\arcsin\frac{P}{B}) + 2\sqrt{B^2 - P^2}, \tag{2.17a}$$

$$\Delta\mathrm{V}_2 = P(\pi + 2\arcsin\frac{P}{B}) + 2\sqrt{B^2 - P^2}. \tag{2.17b}$$

It can be obtained from the above equations that $\Delta\mathrm{V}_1$ decreases while $\Delta\mathrm{V}_2$ increases as the transmitted power $P$ increases. As shown in Fig. 2.6(b), it is much easier for the trajectory to overcome $\Delta\mathrm{V}_1$ to escape from the valley. So $\Delta\mathrm{V}_1$ provides a conservative approximation of the basin of attraction and can be used to measure the transient stability.

## 2.6. PROBLEM FORMULATION

In this section, regarding to the power system (2.4), we formulate the problems that need to be solved to answer the RQs introduced in Chapter 1 and describe the ideas to answer them.

Regarding to the fluctuation suppression problem in Sub-RP1, as described in Subsection 2.4.2, it is critical to accelerate the convergence speed of the control input and avoid the overshoot problem for the frequency. Based on the framework of PI control, this thesis focuses on the transient performance and aims to design secondary frequency control methods that remedies the drawbacks mentioned above of the existing methods. To this end, we consider the following problem concerning the transient performance of the power system (2.4) after a disturbance.

**Problem 2.6.1** *For the power system (2.4) with primary and secondary controllers, design a secondary frequency control law which computes inputs $\{u_i,\ i \in \mathcal{V}_K\}$ to the mechanical power so as to eliminate the extra fluctuations of the frequency caused by the controllers, thus improving the transient performance of the system after a disturbance through an accelerated convergence of the control inputs.*

The control laws for Problem (2.6.1) can be of different control architectures as introduced in Section 2.3. Each of them has their own advantages and disadvantages.

Centralized control can achieve a control objective with high efficiency, such as minimizing control cost while recovering the nominal frequency of a power system. However, the centralized control is usually limited by the overhead of communications and computational complexity and is applicable only for relatively small-scale power system. The distributed control architecture can effectively reduce the communications and computations, which however has a lower efficiency on achieving the control objective than the centralized control. So for large-scale power systems, we resort to multi-level control architecture to balance the advantages and disadvantages of centralized and distributed control.

The primary objective of Problem (2.6.1) is to improve the transient performance of the systems after a disturbance. For the power system controlled by the designed centralized, multi-level control laws, we analyze how to improve the transient performance by tuning the control parameters. The ideas to answer RQ1-RQ3 are summarized as follows.

(i) To answer RQ 1, we design a centralized control law so as to solve Problem (2.4.1) and Problem (2.6.1) for the power system (2.4). This is accomplished in Chapter 3.

(ii) To answer RQ 2, we design a distributed control law and further a multi-level control law so as to solve Problem (2.4.1) and Problem (2.6.1) for the large-scale power system (2.4). This is accomplished in Chapter 4.

(iii) To answer RQ 3, we investigate the relationships between the control parameters of the proposed centralized, distributed and multi-level control laws and the transient performance of the corresponding closed-system. This is accomplished in Chapter 5.

With respect to the enhancement of the synchronization stability in Sub-RP2, the problem is to find a suitable measurement for the transient stability. We select the energy barrier as defined in Section 2.5 to measure this stability in this thesis.

In the following, we connect the parameter setting in the optimal power flow calculation and the synchronization stability. To increase the synchronization stability, the transmitted power by the lines should be small, which is considered as a constraint in (2.9). As described in Remark (2.2.3), when the voltage is well controlled such that each bus voltage

is close to its nominal value, the power flows are mainly determined by the phase angle differences, which should not be too large in order to keep the frequency synchronization of the generators. The parameters ($\gamma_{ij}$) constrain the phase angle differences. It is actually not necessary to set the parameters ($\gamma_{ij}$) identical for all lines. This is because for the synchronization stability, the effect of the various transmission line are different because of the complex topology of the network, e.g., a line with a large phase angle difference may have small threat to the synchronization while the one with a small angle difference may destroy the synchronization easily. The lines which have small influences on the synchronization stability should transmit more power, and the parameter $\gamma_{ij}$ for this line should be larger. It can be observed from the power flow equations that at a steady state, the phase angle differences depend on the topology of the power network and the distribution of the power generators and loads.

The topology of a power network is complex due to various locations of power generation and demand. It usually consists of cycles and single tree branches. A transmission line of the power network is either a single branch or in a cycle. The energy barriers for a tree power network can be calculated analytically as in (2.17), which however is hard to be calculated for general networks. In this thesis, we focus on the synchronization stability of cyclic power grids, for which the energy barrier can be calculated analytically and numerically. The idea to answer RQ 4 is summarized as follows

(iv) To answer RQ 4, we calculate analytically and numerically the energy barrier of cyclic power grids and investigate the influence of the size and the distribution of power generation (loads) on the synchronization stability.

# 3

# POWER-IMBALANCE ALLOCATION CONTROL

*The traditional secondary frequency control of power systems restores nominal frequency by steering* Area Control Errors *(ACEs) to zero. Existing methods are a form of integral control with the characteristic that large control gain coefficients introduce an overshoot and small ones result in a slow convergence to a steady state. In order to deal with the large frequency deviation problem, which is the main concern of the power system integrated with a large number of renewable energy, a faster convergence is critical. In this chapter, we propose a secondary frequency control method named* Power-Imbalance Allocation Control *(PIAC) to restore the nominal frequency with a minimized control cost, in which a coordinator estimates the power imbalance and dispatches the control inputs to the controllers after solving an economic power dispatch problem. The power imbalance estimation converges exponentially in PIAC, both overshoots and large frequency deviations are avoided. In addition, when PIAC is implemented in a multi-area controlled network, the controllers of an area are independent of the disturbance of the neighbor areas. A Lyapunov stability analysis shows that PIAC is locally asymptotically stable. For a power system with time-varying power-imbalance, a bound is derived for the synchronized frequency. Simulation results demonstrate that PIAC can effectively suppress the frequency fluctuations.*

---

Parts of this chapter have been published in:
K. Xi, J. L. A. Dubbeldam, H.X.Lin and J. H. van Schuppen. Power-imbalance allocation control of power systems-Secondary frequency control. *Automatica*, 92: 72-85, (2018).
K. Xi, J. L. A. Dubbeldam, H. X. Lin and J. H. van Schuppen. Power-imbalance allocation control of secondary frequency control of power systems. In *proceedings of the 20th IFAC World Congress*, Toulouse, France. 4382-4387 (2017).
K. Xi, H. X. Lin and J. H. van Schuppen. Power-imbalance allocation control of power systems-A Frequency bound for time-varying loads. In *proceedings of the 36th Chinese Control Conference*, Dalian, China. 10528-10533 (2017).

## 3.1. INTRODUCTION

The secondary frequency control is the focus of this chapter. An interconnected electric power system can be described as a collection of subsystems, each of which is called a control area. The secondary control in a single area is regulated by *Automatic Generation Control* (AGC), which is driven by *Area Control Error* (ACE). The ACE of an area is calculated from the local frequency deviations within the area and power transfers between the area and its neighbor areas. The AGC controls the power injections to force the ACE to zero, thus restores the nominal frequency. Due to the availability of a communication network, other secondary frequency control approaches have recently been developed which minimize the control cost on-line [9], e.g., the Distributed Average Integral Method (DAI) [27], the Gather-Broadcast (GB) method [10], economic AGC (EAGC) method [16], and distributed real time power optimal power control method [34]. These methods suffer from a common drawback, namely that they exhibit overshoot for large gain coefficients and slow convergence for small gain coefficients. This is due to the fact that they rely on the integral control which is well-known to give rise to the two phenomena mentioned above. Note that the slow convergence speed results in a large frequency deviation which is the main concern of low inertia power systems.

The presence of fluctuations is expected to increase in the near future, due to the presence of generators with low inertia, such as solar and wind energy. These renewable power sources often cause serious frequency fluctuations and deviation from the nominal frequency due to the uncertainty of the weather. This demonstrates the necessity of good secondary frequency control methods whose transient performance is enhanced with respect to the traditional methods. We have recently derived such a method called *Power Imbalance Allocation Method* (PIAC) in [57], which can eliminate the drawback of the integral control based approach. This chapter is the extended version of the conference paper [57] with additional stability analysis and the extension of PIAC to multi-area control.

We consider the power system (2.4) with lossless transmission lines, which comprise traditional synchronous machines, frequency dependent devices (e.g., power inverters of renewable energy or freqeuncy dependent loads) and passive loads. We assume the system to be equipped with the primary controllers and propose the PIAC method in the framework of Proportional-Integral (PI) control, which first estimates the power imbalance of the system via the measured frequency deviations of the nodes of the synchronous machines and frequency dependent power sources, next dispatches the control inputs of the distributed controllers after solving the economic power dispatch problem. Since the estimated power imbalance converges exponentially at a rate that can be accelerated by increasing the control gain coefficient, the overshoot problem and the large frequency deviation problem is avoided. Hence the drawback of the traditional ACE method is eliminated. Furthermore, the control gain coefficient is independent to the parameters of the power system but only relies on the response time of the control devices. Consequently the transient performance is greatly enhanced by improving the performance of the control devices in PIAC. When implemented in a multi-area power network, PIAC makes the control actions of the areas independent, while the controllers of each area handles the power imbalance of the local area only.

The chapter is organized as follows. We present the secondary frequency control approach for the system (2.4), *Power-Imbalance Allocation Control* (PIAC), based on esti-

mated power imbalance in Section 3.2, then analyze its stability invoking the Lyapunov/LaSalle stability criterion in Section 3.3 and present a bound of the synchronized frequency of the power system with time-varying loads in Section 3.4. Finally, we evaluate the performance of PIAC by simulations on the IEEE-39 New England test power system in Section 3.5 and 3.6. Section 3.7 concludes with remarks.

## 3.2. POWER IMBALANCE ALLOCATION CONTROL



The aim of this chapter is to design a centralized control law which solves Problem (2.4.1) and (2.6.1) for system (2.4).

After integration of the constraint (2.10c) into the cost function, e.g., in the form of barrier functions as in [24], the economic power dispatch problem (2.10) can be rewritten as

$$\min_{\{u_i\in\mathbb{R}, i\in\mathcal{V}_K\}} \sum_{i\in\mathcal{V}_K} J_i(u_i), \tag{3.1a}$$

$$s.t.\ \ P_s + \sum_{i\in\mathcal{V}_K} u_i = 0, \tag{3.1b}$$

With respect to the existence of the solution of the economic power dispatch problem (3.1), we make the following assumption.

**Assumption 3.2.1** *The cost functions $J_i : \mathbb{R} \to \mathbb{R},\ i \in \mathcal{V}_K$ are twice continuously differentiable and strictly convex such that $J''(u_i) > 0$ where $J''(u_i)$ is the second order derivative of $J(u_i)$ with respect to $u_i$.*

Assumption (3.2.1) is realistic because the constraint $u_i \in [\underline{u}_i, \overline{u}_i]$ can be incorporated in the objective function $J_i(u_i)$ for $i \in \mathcal{V}_K$ in a smooth way. Since in practice the power imbalance is uncertain with respect to the fluctuating power loads, the economic power dispatch problem (3.1) cannot be solved directly.

The communication network is necessary for solving Problem (2.4.1), for which we make the following assumption.

**Assumption 3.2.2** *All the buses in $\mathcal{V}_M \cup \mathcal{V}_F$ can communicate with a coordinator at a central location via a communication network. The frequency deviations $\omega_i,\ i \in \mathcal{V}_M \cup \mathcal{V}_F$, can be measured and subsequently communicated to the coordinator. For $i \in \mathcal{V}_K$, the control input $u_i$ can be computed by the coordinator and dispatched to the controller at node $i$ via the communication network.*

In Assumption (3.2.2), the local nodes need to provide the coordinator the local frequency deviation which are the differences between the measured frequencies by meters and the nominal frequency. We remark that there usually are time-delay in the measurement and communications which are neglected in this thesis.

In the following, we first define an abstract frequency deviation of the power system, for which we design a control law to eliminate the overshoot of the control input, then introduce the PIAC method for the power system controlled as a single area and followed by a multi-area approach in subsection (3.2.2) and (3.2.3) respectively.

### 3.2.1. ABSTRACT FREQUENCY DEVIATION

With Assumption (3.2.2), the power system can be viewed as a machine, in which all the state information can be collected and all the disturbances can be estimated accurately via the state information. For the power system, we define *abstract frequency deviation* as follows.

**Definition 3.2.3** *For the power system (2.4), define an abstract frequency deviation $\omega_s$ such that*

$$M_s\dot{\omega}_s = P_s - D_s\omega_s + u_s, \tag{3.2}$$

*where $M_s = \sum_{i\in\mathcal{V}_M} M_i$, $P_s = \sum_{i\in\mathcal{V}} P_i$, $D_s = \sum_{i\in\mathcal{V}} D_i$, and $u_s = \sum_{i\in\mathcal{V}_K} u_i$.*

Note that $\omega_s(t)$ is a *virtual global frequency deviation*, which neither equals to $\omega_i(t)$ nor $\omega_{syn}(t)$ in general. However, if the frequencies $\{\omega_i,\ i \in \mathcal{V}_M \cup \mathcal{V}_F\}$ synchronize quickly, the differences between $\omega_i(t)$ and $\omega_s(t)$ are negligible, i.e., $\omega_i(t) = \omega_s(t)$, by summing all the equations of (2.4), (3.2) is derived.

At the steady state of (3.2), we have $\omega_s^* = (P_s + u_s)/D_s$ which leads to $\omega_s^* = \omega_{syn}^*$ by (2.8). Then the objective of the secondary frequency control that restores the nominal frequency of the system (2.4) is equivalent to controlling $\omega_s$ of (3.2) to zero, i.e., $\lim_{t\to\infty}\omega_s(t) = 0$.

Since the frequencies $\{\omega_i,\ i \in \mathcal{V}_M \cup \mathcal{V}_F\}$ of system (2.4) with primary controllers synchronize quickly, the extra oscillations of $\omega_i$ are actually introduced by the overshoot of the total amount of control inputs $u_s$ in the traditional control approach (2.13). This is because it is in the form of integral control. It will be explained in an extreme case where system (2.4) is well controlled by primary controllers such that $\omega_i = \omega_s$ for all $i \in \mathcal{V}$. It can then be obtained easily for (2.13) by substituting $\omega_i$ by $\omega_s$ that the total amount of control inputs, $u_s$, is calculated as follows,

$$\dot{\lambda}_s = \omega_s, \tag{3.3a}$$
$$u_s = -k\lambda_s, \tag{3.3b}$$

which is in the form of integral control. Note that (3.3) can also be obtained similarly for the GB method (2.14) and for the DAI method (2.15) with a special setting of control gain coefficients $k_i$ and communication weight $w_{ij}$ e.g., $\{k_i,\ i \in \mathcal{V}_k\}$ are all identical and $w_{ij}$ forms a Laplacian matrix, $L = (w_{ij})$, such that $\sum_{i=1}^{n_K} w_{ij} = 0$ for all $j = 1, \cdots, n_K$( $n_K$ is the number of nodes in $\mathcal{V}_K$).

In order to eliminate the extra oscillations of the frequency, the overshoot of $u_s$ should be avoided. Similar to the PI cruise control of a car [58], for $\omega_s$ in (3.2), we introduce the following control law to eliminate the overshoot,

$$\dot{\eta}_s = D_s\omega_s, \tag{3.4a}$$
$$u_s = -kM_s\omega_s - k\eta_s, \tag{3.4b}$$

where $k \in (0, +\infty)$ is a parameter to be chosen by engineers. Details on the setting of this parameter will be further discussed after introducing the PIAC method in this section. From (3.4) and (3.2), we obtain

$$\dot{u}_s(t) = -k\big(P_s + u_s(t)\big), \tag{3.5}$$

which indicates that $u_s$ is an estimate of $-P_s$ and converges to the power imbalance $-P_s$ exponentially. Hence, the overshoot of $u_s$ is eliminated. With the value of $u_s$ obtained from (3.4), the control input $u_i$ for node $i \in \mathcal{V}_K$ is computed by solving the following economic power dispatch problem,

$$\begin{aligned} &\min_{\{u_i \in \mathbb{R}, i \in \mathcal{V}_K\}} \sum_{i \in \mathcal{V}_K} J_i(u_i), \\ &s.t. \ -u_s(t) + \sum_{i \in \mathcal{V}_K} u_i(t) = 0. \end{aligned} \tag{3.6}$$



However, $u_s$ cannot be calculated as in (3.4) since $\omega_s$ is a virtual frequency deviation which cannot be measured in practice. In the following, we introduce the PIAC method where $u_s$ also converges to $-P_s$ exponentially as in (3.5).

### 3.2.2. SINGLE-AREA IMPLEMENTATION OF PIAC

We consider the power system controlled as a single area without any power export (or import). The PIAC method is defined as follows.

**Definition 3.2.4** *Consider the power system described by (2.4) with assumption (2.4.3), (3.2.1) and (3.2.2), the PIAC control law is defined as the dynamic controller,*

$$\dot{\eta}(t) = \sum_{i \in \mathcal{V}_M \cup \mathcal{V}_F} D_i \omega_i(t), \tag{3.7a}$$

$$u_s(t) = -k\Big(\eta(t) + \sum_{j \in \mathcal{V}_M} M_j \omega_j(t)\Big), \tag{3.7b}$$

$$0 = -u_s(t) + \sum_i J_i'^{-1}(\lambda(t)), \tag{3.7c}$$

$$u_i(t) = J_i'^{-1}(\lambda(t)), \ i \in \mathcal{V}_K, \tag{3.7d}$$

*where $k \in (0, \infty)$ is a parameter of the control law, $\eta$ is a state variable introduced for the integral term as $\eta_s$ in (3.4a), and $\lambda$ is an algebraic variable for solving the optimization problem (3.6).*

For the special case with quadratic cost function $J_i(u_i) = \frac{1}{2}\alpha_i u_i^2$ for node $i$, the control law becomes

$$\begin{aligned} \dot{\eta} &= \sum_{i \in \mathcal{V}_M \cup \mathcal{V}_F} D_i \omega_i, \\ u_s &= -k\Big(\sum_{i \in \mathcal{V}_M} M_i \omega_i + \eta_s\Big), \\ u_i &= \frac{\alpha_s}{\alpha_i} u_s, \ i \in \mathcal{V}_K, \\ \frac{1}{\alpha_s} &= \sum_{i \in \mathcal{V}_K} \frac{1}{\alpha_i}, \end{aligned}$$

where $\alpha_i \in \mathbb{R}$ is the control price of node $i$.

The control law is based on the design principle of coordination. The local nodes in $\mathcal{V}_M \cup \mathcal{V}_F$ send the measured frequency deviations to the coordinator. The coordinator computes the control inputs $\{u_i, i \in \mathcal{V}_K\}$ or marginal cost $\lambda$ using the local measurements and sends them to all local controllers of the nodes indexed by $\mathcal{V}_K$. The procedure is similar to the Gather-Broadcast control which gathers the locally measured frequency deviation from the nodes and broadcasts the nodal price to the controllers. The control procedure and properties of PIAC are summarized in the following procedure and theorem respectively.



**Procedure 3.2.5** *If the assumptions (2.4.3),(3.2.1) and (3.2.2) hold, then the secondary frequency control approach of the power system (2.4), PIAC, is implemented as follows.*

*(i) Collect the measured frequency deviations*

$$\{\omega_i, i \in \mathcal{V}_M \cup \mathcal{V}_F\},$$

*(ii) Calculate the total amount $u_s(t)$ of control inputs by (3.7b),*

*(iii) Solve the optimization problem (3.6) by (3.7c,3.7d),*

*(iv) Allocate the power compensation $\{u_i, i \in \mathcal{V}_K\}$ to the controllers.*

**Theorem 3.2.6** *Consider the power system (2.4) and the PIAC control law, the controller has the following properties,*

*(a) at any time, $t \in T$, $u_s(t)$ satisfies (3.5). Thus it is an estimate of the power imbalance $-P_s$;*

*(b) at any time, $t \in T$, the input values $\{u_i(t), i \in \mathcal{V}_K\}$ are computed by solving the optimization problem (3.6). So the total amount of control inputs, $u_s(t)$, are dispatched to the local nodes of $\mathcal{V}_K$ economically;*

*(c) at the steady state, $\omega_i^* = 0$ for all $i \in \mathcal{V}_M \cup \mathcal{V}_F$ and the power-imbalance $P_s$ is optimally compensated by the local controllers. Hence Problem (2.4.1) is solved;*

*Proof:* (a). From (2.4) it follows,

$$\sum_{i\in\mathcal{V}_M} M_i\dot{\omega}_i = \sum_{i\in\mathcal{V}} P_i - \sum_{i\in\mathcal{V}_M\cup\mathcal{V}_F} D_i\omega_i + \sum_{i\in\mathcal{V}} u_i. \tag{3.9}$$

It follows from (3.7a,3.7b) that,

$$\begin{aligned}
\dot{u}_s(t) &= -k\Big(\sum_{i\in\mathcal{V}_M\cup\mathcal{V}_F} D_i\omega_i(t) + \sum_{j\in\mathcal{V}_M} M_j\dot{\omega}_i(t)\Big) \\
&\text{by (3.9)}, \\
&= -k\Big(\sum_{i\in\mathcal{V}_K} u_i(t) + \sum_{j\in\mathcal{V}} P_i\Big) \\
&\text{by (3.7d)}, \\
&= -k\Big(\sum_{i\in\mathcal{V}_K} J_i'^{-1}(\lambda) + \sum_{j\in\mathcal{V}} P_i\Big) \\
&\text{by (3.7c)}, \\
&= -k\Big(u_s(t) + P_s\Big),
\end{aligned}$$

Thus (3.5) is obtained which indicates that $u_s(t)$ is an estimate of $-P_s$ with $k \in (0,\infty)$, i.e., $u_s(t)$ converges to $-P_s$ exponentially with a speed determined by $k$.

(b). According to the definition of the PIAC control law that at any time, $t \in T$,

$$J_i'(u_i(t)) = J_j'(u_j(t)) = \lambda(t),\ \forall\ i, j \in \mathcal{V}_K.$$

Thus the necessary condition (2.12) for economic dispatch of $u_s(t)$ to all the local nodes is satisfied and at any time $t \in T$, the control inputs $\{u_i,\ i \in \mathcal{V}_K\}$ solve the optimization problem (3.6). Hence, $\{u_i(t), i \in \mathcal{V}\}$ achieve minimal cost.

(c). It follows from (3.5) that $u_s^* = -\sum_{i\in\mathcal{V}} P_i$ at the steady state, which yields $\omega_{syn} = 0$ by (2.8). Thus $\omega_i^* = 0$ for all $i \in \mathcal{V}_M \cup \mathcal{V}_F$ by (2.5). It follows from (b) that the control inputs $\{u_i, i \in \mathcal{V}\}$ achieve minimal cost at the steady state. So the optimization problem (3.1) is solved at the steady state. Hence, Problem (2.4.1) is solved. ■

Note that in Theorem (3.2.6c), we have assumed that the steady state exists which will be further described in Assumption (3.3.1) in Section 3.3. Because

$$u_s(t) = -k \sum_{i\in\mathcal{V}_M} M_i\omega_i - k\int_0^t \sum_{j\in\mathcal{V}_M\cup\mathcal{V}_F} D_j\omega_j dt,$$

the PIAC control law is of proportional-integral type.

With the abstract frequency deviation $\omega_s$ and control inputs $u_s$, we decompose the dynamic process of the power system (2.4) into three sub-processes,

(i) the convergence process of $u_s$ to $-P_s$ as in (3.5) with a speed determined by $k$.

(ii) the convergence process of $\omega_s$ to zero as in (3.2) with a speed determined by $u_s$ and $D_s$.

(iii) and the synchronization process of $\{\omega_i,\ i \in \mathcal{V}_M \cup \mathcal{V}_F\}$ to $\omega_s$ described by (2.4) and with the synchronization speed mainly determined by $\{D_i,\ i \in \mathcal{V}_M \cup \mathcal{V}_F\}$.

The transient performance of the power system can be improved by tuning the corresponding control gain coefficients for the sub-processes. PIAC focuses on the first two sub-processes only in which the transient behaviors of $u_s$ and $\omega_s$ can be improved by increasing the parameter $k$, and the primary control focuses on the synchronization of $\{\omega_i,\ i \in \mathcal{V}_M \cup \mathcal{V}_F\}$ which can be improved by tuning the coefficient $\{D_i, i \in \mathcal{V}_M \cup \mathcal{V}_F\}$ as in [9, 59]. As $u_s$ converges to $-P_s$ exponentially, the control inputs $\{u_i,\ i \in \mathcal{V}_K\}$ in (3.7d) also converge to the desired optimal values in an exponential way without any overshoots and their convergence speed increase with a large $k$. Thus the extra oscillation caused by the overshoot of $u_s$ is avoided and Problem (2.6.1) is solved by PIAC.

With the process decomposition, the improvement in the transient performance by the UC control law [12] can be explained, and the control gain coefficients of the primal-dual based control laws, e.g. [35], without triggered constraints of line flows, which also estimate the power disturbance, can be tuned to improve the transient performance.

In the following, we introduce the properties of PIAC in the implementation for the power system controlled as a single area.

On the communications in PIAC, note that the communicated data include dynamic data and static data. The dynamic data are the frequency deviations $\{\omega_i,\ i \in \mathcal{V}_M \cup \mathcal{V}_F\}$ and

the control inputs $\{u_i\ i \in \mathcal{V}_K\}$, both should be communicated frequently. The static data are the moment inertia $\{M_i,\ i \in \mathcal{V}_i\}$, the droop control coefficients $\{D_i,\ i \in \mathcal{V}_M \cup \mathcal{V}_F\}$ and the cost functions $\{J_i(u_i), i \in \mathcal{V}_K\}$, which are constant in a short time as in Assumption (2.4.3) and are not necessary to communicate as frequently as the dynamic data.

In the computing of the control inputs $\{u_i,\ i \in \mathcal{V}_K\}$, solving the optimization problem (3.6) is equivalent to solving the equations (3.7c) and (3.7d). So the computation includes calculating the integral of frequency deviation in (3.7a) and solving the algebraic equation (3.7c,3.7d). For quadratic cost functions $J_i(u_i) = u_i^2/\alpha_i$, the computation requires approximately $4n_M + n_F$ arithmetic operations that are $\times$, $+$, $-$ etc. For non-quadratic and nonlinear cost functions, an iteration method is used to solve the one dimension nonlinear algebraic equation (3.7c) for $\lambda$, which needs more computing than for the quadratic cost functions.

**Remark 3.2.7** *PIAC is a centralized control where the communications and computations increase as the scale of the power systems increases. In a large-scale power system, a large number of devices communicate to the coordinator simultaneously. In that case, the time-delay due to the communications and computing is not negligible, in such a situation further investgation for the transient performance and stability of the nonlinear system is needed.*

On the dynamics of $u_s$, it can be observed from (3.5) that $u_s$ converges exponentially with a speed that can be accelerated by increasing the control gain coefficient $k$ which does not depend on any parameters of the power system and the cost functions. Hence, when the dynamics of the voltages are considered which does not influence the dynamics of $u_s$ in (3.5), the power supply and demand can also be balanced.

On the control gain coefficient $k$, we remark that it does neither depend on the parameters of the system nor on the economic power dispatch problem, and can be set very large from the perspective of theoretical analysis. However, it relies on how sensitive the control devices are to the fluctuation of power imbalance. In this case, it can be tuned according to the response time of the control devices and the desired range of the frequency deviation. The control actuators of traditional hydraulic and steam turbines are their governor systems. For details of the model of the governor system and its response time, we refer to [6, chapter 9,11]

By Assumption (3.2.2), the PIAC method requires that all the nodes in $\mathcal{V}_M \cup \mathcal{V}_F$ can communicate with the coordinator. However, our initial numerical experiments show that PIAC can still restore the nominal frequency even without all the frequency deviation collected, where the estimated power imbalance converges to the actual power imbalance although not exponentially. This is because PIAC includes the integral control which drives the synchronized frequency deviation to zero.

In PIAC, the frequency dependent nodes are allowed to participate in secondary frequency control, which releases the control burden of the tradition power generators on frequency oscillation suppression.

**Remark 3.2.8** *In practice, the state of the power system is never at a true equilibrium state, because of the fluctuating of the power imbalance caused by the power loads. Furthermore, the fluctuating becomes even more serious when a large amount of renewable power sources are integrated into the power system. In this case, it is more practical to*

*model the power imbalance as a time-varying function. For the power system with time-varying power imbalance, analysis and numerical simulations show that PIAC is also able to effectively control the synchronized frequency to any desired range by increasing the control gain coefficient k [60].*

### 3.2.3. MULTI-AREA IMPLEMENTATION OF PIAC

When a power system is partitioned into several control areas, each area has either an export or an import of power. After a disturbance occurred, the power export or the power import of an area must be restored to the nominal value calculated by tertiary control. In this subsection, we introduce the implementation of PIAC for multi-area control where each area has power export (or import).



Denote the set of the nodes in the area $A_r$ by $\mathcal{V}_{A_r}$, the set of the boundary lines between area $A_r$ and all the other areas by $\mathcal{E}_{A_r}$. Denote $\mathcal{V}_{M_r} = \mathcal{V}_M \cap \mathcal{V}_{A_r}$ and $\mathcal{V}_{F_r} = \mathcal{V}_F \cap \mathcal{V}_{A_r}$. The multi-area control of PIAC in the area $A_r$ is defined as follows.

**Definition 3.2.9** *Consider the power system (2.4) controlled as several areas with Assumption (2.4.3), (3.2.1) and (3.2.2), the multi-area implementation of PIAC for area $A_r$ is defined as the dynamic controllers,*

$$\dot{\eta}_r(t) = \sum_{i\in\mathcal{V}_{M_r}\cup\mathcal{V}_{F_r}} D_i\omega_i(t) + P_{ex}(t) - P_{ex}^*, \tag{3.11a}$$

$$u_r(t) = -k_r\Big(\sum_{i\in\mathcal{V}_{M_r}} M_i\omega_i(t) + \eta_r(t)\Big), \tag{3.11b}$$

$$0 = -u_r + \sum_{i\in\mathcal{V}_K} {J'_i}^{-1}(\lambda_r), \tag{3.11c}$$

$$u_i = {J'_i}^{-1}(\lambda_r),\ i \in \mathcal{V}_{M_r}\cup\mathcal{V}_{F_r}. \tag{3.11d}$$

*where $P_{ex} = \sum_{i\in\mathcal{V}_{A_r},(i,j)\in\mathcal{E}_{A_r}} B_{ij}\sin(\theta_{ij})$ is the export power of area $A_r$, $P_{ex}^*$ is the nominal value of $P_{ex}$, which is also the desired value at the steady state, $k_r \in (0,\infty)$ is a control gain coefficient, $\eta_r$ is a state variable for the integral term as $\eta_s$ in (3.4a) and $\lambda_r$ is an algebraic variable for the controller.*

It can be observed from (3.11) that the control law for the coordinator in area $A_r$ is similar to Procedure 3.2.5 but the power export deviation, $P_{ex} - P_{ex}^*$, should be measured. This measurement can be done either via Phase Measurement Units or active power measurement unit. If there are more than one transmission line between two areas, all the transmitted power should be measured. In that case, the total amount of power exchange between the two areas can converge to its setpoint at the steady state. However, the transmitted power of a line may deviate from its setpoint at the steady state, which will be further illustrated in the case study in Subsection 3.5.2.

The sum of the three terms in the right hand side of (3.11a) is actually the ACE of the area [61]. PIAC has the proportional control input included in secondary frequency control, which is consistent with the PI based secondary frequency control [20, Chapter 9] and [45, Chapter 4]. In PIAC, the weights of the frequency deviation of node $i$ are specified as the inertia $M_i$ and the droop coefficient $D_i$ for the proportional input and integral input respectively. The proportional input is used to estimate the power stored in the inertia at the

transient phase, which is usually neglected in the traditional ACE method. The control gain coefficient $k_r$ can be different for each area, which can be tuned according to the sensitivity of the control devices in the area. By (3.11a), as the synchronous frequency deviation is steered to zero, $P_{ex}$ also converges to the nominal value $P_{ex}^*$. Similar as the derivation of (3.5) for PIAC (3.7), we derive for (3.11) that

$$\dot{u}_r(t) = -k_r\Big(\sum_{i\in\mathcal{V}_{A_r}} P_i + P_{ex}^* + u_r(t)\Big)$$



which indicates that the controllers in area $A_r$ only respond to the power imbalance $\sum_{i\in\mathcal{V}_{A_r}} P_i$. Hence, in the network, the control actions of all the areas can be done in *an asynchronous way where each area can balance the local power supply-demand at any time according to the availability of the devices*.

In particular, PIAC becomes a decentralized control method if each node is seen as a single area and $\mathcal{V}_P = \emptyset$, $\mathcal{V}_K = \mathcal{V}_M \cup \mathcal{V}_F$, i.e., for all $i \in \mathcal{V}_M \cup \mathcal{V}_F$,

$$\begin{aligned}\dot{\eta}_i &= D_i\omega_i + \sum_{j\in\mathcal{V}} B_{ij}\sin(\theta_{ij}) - \sum_{j\in\mathcal{V}} B_{ij}\sin(\theta_{ij}^*),\\ u_i &= -k_i(M_i\omega + \eta_i),\end{aligned}$$

where $\{\theta_i^*,\ i \in \mathcal{V}\}$ are the steady state calculated by tertiary control. Since $u_i$ is tracking $-P_i + \sum_{j\in\mathcal{V}} B_{ij}\sin(\theta_{ij}^*)$, each node compensates the power imbalance locally and the control actions of the nodes are irrelevant to each other. However, the control cost is not optimized by the decentralized control method.

## 3.3. ASYMPTOTIC STABILITY OF PIAC

In this section, we analyze the stability of PIAC with the Lyapunov-LaSalle approach as in [13, 14]. The stability proof makes use of Theorem (A.1.3) stated in the Appendix A.

We first prove the stability of PIAC implemented in a single-area network. Extension to multi-area control networks then follows immediately. With the control law (3.7), the closed-loop system of PIAC is

$$\dot{\theta}_i = \omega_i,\ i \in \mathcal{V}_M \cup \mathcal{V}_F, \tag{3.13a}$$

$$M_i\dot{\omega}_i = P_i - D_i\omega_i - \sum_{j\in\mathcal{V}} B_{ij}\sin(\theta_{ij}) + J_i'^{-1}(\lambda),\ i \in \mathcal{V}_M, \tag{3.13b}$$

$$0 = P_i - D_i\omega_i - \sum_{j\in\mathcal{V}} B_{ij}\sin(\theta_{ij}) + J_i'^{-1}(\lambda),\ i \in \mathcal{V}_F, \tag{3.13c}$$

$$0 = P_i - \sum_{j\in\mathcal{V}} B_{ij}\sin(\theta_{ij}),\ i \in \mathcal{V}_P, \tag{3.13d}$$

$$\dot{\eta} = \sum_{i\in\mathcal{V}_M\cup\mathcal{V}_F} D_i\omega_i, \tag{3.13e}$$

$$0 = \sum_{i\in\mathcal{V}_K} J_i'^{-1}(\lambda) + k(\sum_{i\in\mathcal{V}_M} M_i\omega_i + \eta), \tag{3.13f}$$

$$0 = J_i'^{-1}(\lambda), i \notin \mathcal{V}_K. \tag{3.13g}$$

where $\theta_{ij} = \theta_i - \theta_j$ is the phase angle differences between the nodes connected by a transmission line.

We denote the angles in the sets $\mathcal{V}_M, \mathcal{V}_F, \mathcal{V}_P$ by vectors $\theta_M, \theta_F, \theta_P$, the frequency deviations by vectors $\omega_M, \omega_F, \omega_P$, the angles in $\mathcal{V}$ by $\theta = (\theta_M^T, \theta_F^T, \theta_P^T)^T$, and the frequency deviations by $\omega = (\omega_M^T, \omega_F^T, \omega_P^T)^T$.

Note that the closed-loop system may not have a synchronous state if the power injections $\{P_i, i \in \mathcal{V}\}$ are much larger than the line capacity $B_{ij}$. For more details on the synchronous state of the power system, we refer to [62, 63]. Therefore, we make Assumption (3.3.1).



**Assumption 3.3.1** *For the closed-loop system (3.13), there exists a synchronous state* $(\theta^*, \omega^*, \eta^*, \lambda^*) \in \mathbb{R}^n \times \mathbb{R}^n \times \mathbb{R} \times \mathbb{R}$ *with* $\omega_i^* = \omega_{syn}$ *and*

$$\theta^*(t) \in \Theta = \{\theta \in \mathbb{R}^n || \theta_i - \theta_j | < \frac{\pi}{2},\ \forall (i,j) \in \mathcal{E}\}.$$

The condition $\theta^* \in \Theta$ is commonly referred to as a security constraint [14] in power system analysis. It can be satisfied by reserving some margin of power flow when calculating the operating point in tertiary control [11].

Since the power flows $\{B_{ij} \sin(\theta_i - \theta_j),\ (i,j) \in \mathcal{E}\}$ only depend on the angle differences and the angles can be expressed relative to a reference node, we choose a reference angle, i.e., $\theta_1$, in $\mathcal{V}_M$ and introduce the new variables

$$\varphi_i = \theta_i - \theta_1,\ i = 1, 2, \cdots, n$$

which yields $\dot{\varphi}_i = \omega_i - \omega_1$. Note that $\theta_1$ is selected as a reference angle for the stability analysis only, which can be the angle of any node in $\mathcal{V}_M$. It can be easily obtained that $\varphi_1 = 0, \dot{\varphi}_1 = 0$ for all $t > 0$. With $\omega_i = \dot{\varphi}_i + \omega_1$ for $i \in \mathcal{V}_F$, the closed loop system (3.13) can be written in the DAE form as (A.1) in the Appendix,

$$\dot{\varphi}_i = \omega_i - \omega_1,\ i \in \mathcal{V}_M \tag{3.14a}$$

$$M_i \dot{\omega}_i = P_i - D_i \omega_i - \sum_{j \in \mathcal{V}} B_{ij} \sin(\varphi_{ij}) + J_i'^{-1}(\lambda), i \in \mathcal{V}_M, \tag{3.14b}$$

$$D_i \dot{\varphi}_i = P_i - D_i \omega_1 - \sum_{j \in \mathcal{V}} B_{ij} \sin(\varphi_{ij}) + J_i'^{-1}(\lambda), i \in \mathcal{V}_F, \tag{3.14c}$$

$$0 = P_i - \sum_{j \in \mathcal{V}} B_{ij} \sin(\varphi_{ij}), i \in \mathcal{V}_P, \tag{3.14d}$$

$$\dot{\eta} = \sum_{i \in \mathcal{V}_M \cup \mathcal{V}_F} D_i \omega_i, \tag{3.14e}$$

$$0 = \sum_{i \in \mathcal{V}_K} J_i'^{-1}(\lambda) + k(\sum_{i \in \mathcal{V}_M} M_i \omega_i + \eta), \tag{3.14f}$$

where $\varphi_{ij} = \varphi_i - \varphi_j$, and the equations (3.14a-3.14d) are from the power system and (3.14e-3.14f) from the controllers. We next recast the system (3.14) into the form of the DAE system (A.1), the state variables are $x = (\varphi_M, \varphi_F, \omega_M, \eta) \in \mathbb{R}^{n_M - 1} \times \mathbb{R}^{n_F} \times \mathbb{R}^{n_M} \times \mathbb{R}$, the algebraic variables are $y = (\varphi_P, \lambda) \in \mathbb{R}^{n_P} \times \mathbb{R}$, the differential equations are (3.14a-3.14c,3.14e) and the algebraic equations are (3.14d, 3.14f). Here $\varphi_M$ is with the components $\{\varphi_i, i \in \mathcal{V}_M\}$

besides $\varphi_1$ which is a constant, $\varphi_F$ with components $\{\varphi_i, i \in \mathcal{V}_F\}$, and $\varphi_P$ with components $\{\varphi_i, i \in \mathcal{V}_P\}$. Note that the variables $\{\omega_i, i \in \mathcal{V}_F\}$ are not included into the state variable or algebraic variables since the terms $\{D_i\omega_i, i \in \mathcal{V}_F\}$ in (3.14e) can be replaced by $\{P_i - \sum_{j\in\mathcal{V}} B_{ij}\sin(\varphi_{ij}) + J_i'^{-1}(\lambda), i \in \mathcal{V}_F\}$ . (3.13g) is neglected since it is irrelevant to the following stability analysis.

When mapping $\theta$ to the coordinate of $\varphi$, Assumption (3.3.1) yields

$$\varphi \in \Phi = \{\varphi \in \mathbb{R}^n || \varphi_i - \varphi_j| < \frac{\pi}{2},\ \forall (i,j) \in \mathcal{E},\ \text{and}\ \varphi_1 = 0\}.$$



We remark that each equilibrium state of (3.14) corresponds to a synchronous state of (3.13). In the new coordinate, we have the following theorem for the stability of system (3.14).

**Theorem 3.3.2** *If the assumptions (2.4.3), (3.2.1), (3.2.2) and (3.3.1) hold, for the system (3.14), then*

*(a) there exists an unique equilibrium state* $z^* = (\varphi^*, \omega_M^*, \eta^*, \lambda^*) \in \Psi$ *where* $\Psi = \Phi \times \mathbb{R}^{n_M} \times \mathbb{R} \times \mathbb{R}$.

*(b) there exists a domain* $\Psi^d \subset \Psi$ *such that for any initial state* $z^0 \in \Psi^d$ *that satisfies the algebraic equations (3.14d) and (3.14f), the state trajectory converges to the unique equilibrium state* $z^* \in \Psi$.

Note that the cost functions are not required to be scaled for the local asymptotically stable of PIAC as assumed in [10], and the size of the attraction domain of the equilibrium state $z^*$ is not determined in Theorem (3.3.2) which states the stability of the PIAC method. The proof of Theorem (3.3.2) is based on the Lyapunov/LaSalle stability criterion as in Theorem (A.1.3). In the following, we first present the verification of the Assumption (A.1.1) and (A.1.2) in the Appendix for the DAE system (3.14), then prove the stability of (3.14) by designing a Lyapunov function as $V(x, y)$ in Theorem (A.1.3). Lemma (3.3.3) states that (3.14) possesses an equilibrium state, which verifies Assumption (A.1.1), and Lemma (3.3.4) claims the regularity of the algebraic equation (3.14d, 3.14f), which verifies Assumption (A.1.2).

**Lemma 3.3.3** *There exists at most one equilibrium state* $z^* = (\varphi^*, \omega_M^*, \eta^*, \lambda^*)$ *of the system (3.14) such that* $z^* \in \Psi$ *and*

$$\omega_i^* = 0,\ i \in \mathcal{V}_M, \tag{3.15a}$$

$$\sum_{i\in\mathcal{V}} P_i + \sum_{i\in\mathcal{V}_K} J_i'^{-1}(\lambda^*) = 0. \tag{3.15b}$$

$$\sum_{i\in\mathcal{V}} P_i - k\eta^* = 0. \tag{3.15c}$$

*Proof:* At the synchronous state, from (3.5) and (3.7b) it follows that

$$k(\sum_{i\in\mathcal{V}_M} M_i\omega_i^* + \eta^*) = \sum_{i\in\mathcal{V}} P_i. \tag{3.16}$$

Substitution into the algebraic equation (3.14f) yields (3.15b). Substitution of (3.15b) into (2.8) with $u_i = J_i'^{-1}(\lambda^*)$, we obtain $\omega_{syn} = 0$ which yields $\{\omega_i^* = 0, i \in \mathcal{V}_M\}$. Hence this and (3.16) yield

$$\sum_{i \in \mathcal{V}_K} J_i'^{-1}(\lambda^*) + k\eta^* = 0.$$

which leads to (3.15c). It follows from [64, 65] that the system (3.13) has at most one power flow solution such that $\theta \in \Theta$. Hence there exists at most one equilibrium for the system (3.14) that satisfies $\varphi \in \Phi$. ■

With respect to the regularity of the algebraic equations (3.14d, 3.14f), we derive the following lemma.

**Lemma 3.3.4** *For any $\varphi \in \Phi$ and strictly convex functions of $\{J_i(u_i), i \in \mathcal{V}_K\}$ in the optimization problem (3.1), the algebraic equations (3.14d, 3.14f) are regular.*

*Proof:* Since (3.14d) and (3.14f) are independent algebraic equations with respect to $\varphi_P$ and $\lambda$ respectively, the regularity of each of them is proven separately.

First, we prove the regularity of (3.14d) by showing that its Jacobian is a principle minor of the Laplacian matrix of a weighted network. In the coordination of $\theta$, we define function

$$\overline{U}(\theta) = \sum_{(i,j) \in \mathcal{E}} B_{ij}(1 - \cos(\theta_i - \theta_j)).$$

The Hessian matrix of $\overline{U}(\theta)$ is

$$\overline{L} = \begin{pmatrix} \overline{B}_{11} & -B_{12}\cos(\theta_{12}) & \dots & -B_{1n}\cos(\theta_{1n}) \\ -B_{21}\cos(\theta_{12}) & \overline{B}_{22} & \dots & -B_{2n}\cos(\theta_{2n}) \\ \vdots & \vdots & \ddots & \vdots \\ -B_{n1}\cos(\theta_{n1}) & -B_{n2}\cos(\theta_{n2}) & \dots & \overline{B}_{nn} \end{pmatrix},$$

where $\overline{B}_{ii} = \sum_{j \in \mathcal{V}} B_{ij}\cos(\theta_{ij})$ and $\theta_{ij} = \theta_i - \theta_j$. $\overline{L}$ is the Laplacian of the undirected graph $\mathcal{G}$ defined in Section 2.1 of chapter 2 with positive line weights $B_{ij}\cos(\theta_i - \theta_j)$. Hence $\overline{L}$ is semi-positive definite and all its principle minors are nonsingular[66, Theorem 9.6.1]. In the coordination of $\varphi$, we define function

$$U(\varphi) = \sum_{(i,j) \in \mathcal{E}} B_{ij}(1 - \cos(\varphi_i - \varphi_j)), \tag{3.17}$$

with Hessian matrix

$$L = \begin{pmatrix} B_{22} & -B_{23}\cos(\varphi_{23}) & \dots & -B_{2n}\cos(\varphi_{2n}) \\ -B_{32}\cos(\varphi_{32}) & B_{33} & \dots & -B_{3n}\cos(\varphi_{3n}) \\ \vdots & \vdots & \ddots & \vdots \\ -B_{n2}\cos(\varphi_{n2}) & -B_{n2}\cos(\varphi_{n3}) & \dots & B_{nn} \end{pmatrix} \tag{3.18}$$

where $B_{ii} = \sum_{j \in \mathcal{V}} B_{ij}\cos(\varphi_{ij})$, $\varphi_{ij} = \varphi_i - \varphi_j$, and $\varphi_1 = 0$. Because $B_{ij}\cos\varphi_{ij} = B_{ij}\cos\theta_{ij}$, $L$ is a principle minor of $\overline{L}$ and is nonsingular. Hence the Jacobian of (3.14d) with respect to $\varphi_P$, which is a principle minor of $L$, is nonsingular.

Second, because $J_i$ is strictly convex by Assumption (3.2.1) such that $J_i'' > 0$, we obtain $(J'^{-1}_i)' = \frac{1}{J_i''} > 0$ which yields $\left(\sum_{i\in\mathcal{V}_K} J'^{-1}_i(\lambda)\right)' > 0$. Hence (3.14f) is nonsingular. ■

What follows is the proof of Theorem (3.3.2) with the Lyapunov/LaSalle stability criterion.

*Proof of Theorem (3.3.2):* Lemma (3.3.3) and Assumption (3.3.1) states that the equilibrium state $z^* = (\varphi^*, \omega_M^*, \eta^*, \lambda^*) \in \Psi$ is unique. The proof of the statement (b) in Theorem (3.3.2) is based on Theorem (A.1.3). Consider an incremental Lyapunov function candidate,

$$V(\varphi, \omega_M, \eta, \lambda) = V_1 + \alpha V_2 + V_3. \tag{3.19}$$

where $V_1$ is the classical energy-based function [14],

$$V_1(\varphi, \omega_M) = U(\varphi) - U(\varphi^*) - \nabla_\varphi U(\varphi^*)(\varphi - \varphi^*) + \frac{1}{2}\omega_M^T M_M \omega_M,$$

and $V_2, V_3$ are positive definite functions

$$\begin{aligned} V_2(\lambda) &= \frac{1}{2}\Big(\sum_{i\in\mathcal{V}_K} J'^{-1}_i(\lambda) - \sum_{i\in\mathcal{V}_K} J'^{-1}_i(\lambda^*)\Big)^2, \\ V_3(\omega_M, \eta) &= \frac{k^2}{2}\Big(\sum_{i\in\mathcal{V}_M} M_i\omega_i + \eta - \eta^*\Big)^2. \end{aligned}$$

Note that the definition of $U(\varphi)$ is in (3.17) and $V_2 = V_3$ by (3.14f). $V_3$ is introduced to involve the state variable $\eta$ into the Lyapunov function.

First, we prove that $\dot{V} \le 0$. From the dynamic system (3.14) and the definition of $V_1$, it yields that

$$\dot{V}_1 = -\sum_{i\in\mathcal{V}_M\cup\mathcal{V}_F} D_i\omega_i^2 + \sum_{i\in\mathcal{V}_K} \omega^T (J'^{-1}_i(\lambda) - J'^{-1}_i(\lambda^*)), \tag{3.20}$$

by (3.14f), we derive

$$\begin{aligned} \dot{V}_2 &= -k\Big[\sum_{i\in\mathcal{V}_K} J'^{-1}_i(\lambda) - \sum_{i\in\mathcal{V}_K} J'^{-1}_i(\lambda^*)\Big]\Big[\sum_{i\in\mathcal{V}_M} M_i\dot{\omega}_i + \dot{\eta}\Big] \\ &\quad \text{by summing (3.14b-3.14e)} \\ &= -k\Big[\sum_{i\in\mathcal{V}_K} J'^{-1}_i(\lambda) - \sum_{i\in\mathcal{V}_K} J'^{-1}_i(\lambda^*)\Big]\Big[\sum_{i\in\mathcal{V}} P_i + \sum_{i\in\mathcal{V}_K} J'^{-1}_i(\lambda)\Big] \\ &\quad \text{by (3.15b)} \\ &= -k\Big[\sum_{i\in\mathcal{V}_K} J'^{-1}_i(\lambda) - \sum_{i\in\mathcal{V}_K} J'^{-1}_i(\lambda^*)\Big]^2, \qquad (3.21a) \\ &\quad \text{by expanding the quadratic} \\ &= -k\sum_{i\in\mathcal{V}_K}\big[J'^{-1}_i(\lambda) - J'^{-1}_i(\lambda^*)\big]^2 - 2k\sum_{i\neq j, i,j\in\mathcal{V}_K}\Big[J'^{-1}_i(\lambda) - J'^{-1}_i(\lambda^*)\Big]\Big[J'^{-1}_j(\lambda) - J'^{-1}_j(\lambda^*)\Big] \\ &\quad \text{by Newton-Leibniz formula} \\ &= -k\sum_{i\in\mathcal{V}_K}\big[J'^{-1}_i(\lambda) - J'^{-1}_i(\lambda^*)\big]^2 - 2k\sum_{i\neq j, i,j\in\mathcal{V}_K}\Big[\int_{\lambda^*}^{\lambda}(J'^{-1}_i)'ds\Big]\Big[\int_{\lambda^*}^{\lambda}(J'^{-1}_j)'ds\Big]. \qquad (3.21b) \end{aligned}$$

and by $V_3 = V_2$ and (3.21a), we obtain

$$\dot{V}_3 = -k\Big[\sum_{i\in\mathcal{V}_K}(J_i'^{-1}(\lambda) - J_i'^{-1}(\lambda^*))\Big]^2. \tag{3.22}$$

Hence, with (3.20,3.21b,3.22), we derive

$$\begin{aligned}
\dot{V} =& -\sum_{i\in\mathcal{V}_M\cup\mathcal{V}_F} D_i\omega_i^2 + \sum_{i\in\mathcal{V}_K}\omega^T[J_i'^{-1}(\lambda) - J_i'^{-1}(\lambda^*)] - k\alpha\sum_{i\in\mathcal{V}_K}[J_i'^{-1}(\lambda) - J_i'^{-1}(\lambda^*)]^2\\
&- k\alpha\sum_{i\neq j,i,j\in\mathcal{V}_K}\Big[\int_{\lambda^*}^{\lambda}(J_i'^{-1})'ds\Big]\Big[\int_{\lambda^*}^{\lambda}(J_j'^{-1})'ds\Big] - k\Big[\sum_{i\in\mathcal{V}_K}J_i'^{-1}(\lambda) - \sum_{i\in\mathcal{V}_K}J_i'^{-1}(\lambda^*)\Big]^2\\
=& -\sum_{i\in\mathcal{V}_K}\frac{D_i}{2}\omega_i^2 - \sum_{i\in\mathcal{V}_K}\frac{D_i}{2}\Big[\omega_i - \frac{J_i'^{-1}(\lambda) - J_i'^{-1}(\lambda^*)}{D_i}\Big]^2 - \sum_{i\in\mathcal{V}_K}\big[k\alpha - \frac{1}{2D_i}\big][J_i'^{-1}(\lambda) - J_i'^{-1}(\lambda^*)]^2\\
&- 2k\alpha\sum_{i\neq j,i,j\in\mathcal{V}_K}\Big[\int_{\lambda^*}^{\lambda}(J_i'^{-1})'ds\Big]\Big[\int_{\lambda^*}^{\lambda}(J_j'^{-1})'ds\Big]\\
&- k\Big[\sum_{i\in\mathcal{V}_K}J_i'^{-1}(\lambda) - \sum_{i\in\mathcal{V}_K}J_i'^{-1}(\lambda^*)\Big]^2 - \sum_{i\in\mathcal{V}_M\cup\mathcal{V}_F/\mathcal{V}_K}D_i\omega_i^2
\end{aligned}$$

where the equation

$$\sum_{i\in\mathcal{V}_M\cup\mathcal{V}_F}D_i\omega_i^2 = \sum_{i\in\mathcal{V}_K}D_i\omega_i^2 + \sum_{i\in\mathcal{V}_M\cup\mathcal{V}_F\setminus\mathcal{V}_K}D_i\omega_i^2$$

is used due to the fact that $\mathcal{V}_K \subseteq \mathcal{V}_M\cup\mathcal{V}_F$. Since $J_i(u_i)$ is strictly convex and $(J_i'^{-1})' = \frac{1}{J_i''} > 0$, we derive

$$k\alpha\sum_{i\neq j,i,j\in\mathcal{V}_K}\Big[\int_{\lambda^*}^{\lambda}(J_i'^{-1})'ds\Big]\Big[\int_{\lambda^*}^{\lambda}(J_j'^{-1})'ds\Big] > 0,$$

Thus by setting $\alpha > \frac{1}{kD_i}$, we obtain $\dot{V} \le 0$.

Second, we prove that $z^* = (\varphi^*, \omega_M^*, \eta^*, \lambda^*)$ is a strict minimum of $V(\varphi, \omega_M, \eta, \lambda)$ such that $\nabla V|_{z^*} = 0$ and $\nabla^2 V|_{z^*} > 0$. It can be easily verified that $V|_{z^*} = 0$ and

$$\nabla V|_{z^*} = \mathrm{col}(\nabla_\varphi V, \nabla_{\omega_M} V, \nabla_\eta V, \nabla_\lambda V)|_{z^*} = 0 \in \mathbb{R}^{n+n_M+1}$$

where

$$\begin{aligned}
&\nabla_\varphi V = \nabla_\varphi U - \nabla_\varphi U^*,\\
&\nabla_{\omega_M} V = M\omega_M + M\Big(k^2(\sum_{i\in\mathcal{V}_M}M_i\omega_i + \eta - \eta^*))1_{n_M}\Big),\\
&\nabla_\eta V = k^2(\sum_{i\in\mathcal{V}_M}M_i\omega_i + \eta - \eta^*)),\\
&\nabla_\lambda V = \alpha\Big(\sum_{i\in\mathcal{V}_K}J_i'^{-1}(\lambda) - \sum_{i\in\mathcal{V}_K}J_i'^{-1}(\lambda^*)\Big)\Big(\sum_{i\in\mathcal{V}_K}J_i'^{-1}(\lambda)\Big)'.
\end{aligned}$$

Here $k^2(\sum_{i\in\mathcal{V}_M}M_i\omega_i + \eta - \eta^*)1_{n_M}$ is a vector with all components equal to $k^2(\sum_{i\in\mathcal{V}_M}M_i\omega_i + \eta - \eta^*))$. The Hessian matrix of $V$ is

$$\nabla^2 V|_{z^*} = \mathrm{blkdiag}(L, H, \Lambda),$$

which is a block diagonal matrix with block matrices $L$,$H$, and $\Lambda$. $L$ is positive definite by (3.18),

$$\Lambda = \alpha\Big(\big(\sum_{i\in\mathcal{V}_K} J_i'^{-1}(\lambda^*)\big)'\Big)^2 > 0$$

which is a scalar value, and $H$ is the Hessian matrix of the function

$$\overline{V} = \frac{1}{2}\omega_M^T M_M \omega_M + \frac{k^2}{2}\Big(\sum_{i\in\mathcal{V}_M} M_i\omega_i + \eta - \eta^*\Big)^2$$



which is positive definite for any $(\omega_M, \eta - \eta^*)$, thus $H$ is positive definite. Hence, we have proven that $z^*$ is a strict minimum of $V$.

Finally, we prove that the invariant set

$$\Big\{(\varphi,\omega_M,\eta,\lambda)|\dot{V}((\varphi,\omega_M,\eta,\lambda) = 0\Big\}$$

contains only the equilibrium point. $\dot{V} = 0$ implies that $\{\omega_i = 0, i \in \mathcal{V}_M \cup \mathcal{V}_F\}$. Hence $\{\varphi_i, i \in \mathcal{V}\}$ are constants. By lemma (3.3.3), there is at most one equilibrium with $\varphi \in \Phi$. In this case, $z^*$ is the only one equilibrium in the neighborhood of $z^*$ , i.e., $\Psi^d = \{(\varphi,\omega_M,\eta,\lambda)|V(\varphi,\omega_M,\eta,\lambda) \le c, \varphi \in \Phi\}$ for some $c > 0$. Hence with any initial state $z^0$ that satisfies the algebraic equations (3.14d) and (3.14f), the trajectory converges to the equilibrium state $z^*$. ■

For the multi-area implementation of PIAC, we choose a Lyapunov candidate function

$$V(\varphi,\omega_M,\eta,\lambda) = V_1 + \sum_{A_r}(\alpha V_{2r} + V_{3r}),$$

where $\lambda = \mathrm{col}(\lambda_r)$ is a column vector consisting of the components $\lambda_r$, $V_1$ is defined as in (3.19) and $V_{2r}$ and $V_{3r}$ are defined for area $A_r$ as

$$V_{2r} = \frac{1}{2}\Big(\sum_{i\in\mathcal{V}_{K_r}} J_i'^{-1}(\lambda_r) - \sum_{i\in\mathcal{V}_{K_r}} J_i'^{-1}(\lambda_r^*)\Big),$$

$$V_{3r} = \frac{k^2}{2}\Big(\sum_{i\in\mathcal{V}_{M_r}} M_i\omega_i + \eta_r - \eta_r^*\Big)^2.$$

Following the proof of Theorem (3.3.2), we can obtain the locally asymptotic stability of PIAC implemented in multi-area control.

**Remark 3.3.5** *The assumptions (2.4.3), (3.2.1), (3.2.2) and (3.3.1) are realistic at the same time. Assumption (2.4.3) and (3.2.2) are necessary for the implementation of PIAC to solve Problem (2.4.1). Assumption (3.2.1) and (3.3.1) are general sufficient conditions for the stability of the nonlinear systems (2.4) controlled by PIAC. Assumption (2.4.3) and (3.3.1) can be guaranteed by tertiary control and Assumption (3.2.2) by an effective communication infrastructure. Assumption (3.2.1) usually holds for frequently used convex cost functions, e.g., quadratic cost function, where the requirement of scale cost functions in [10, Assumption 1] is not needed.*

## 3.4. A FREQUENCY BOUND FOR TIME-VARYING LOADS

As mentioned in Remark (3.2.8), the power system is never at a true equilibrium state in practice because of the fluctuating of power loads and unexpected equipment failures. Furthermore, as more renewable power sources are integrated into the power grid, the power imbalance becomes more fluctuating with more ramping. Even through the imbalance can be predicted, a prediction bias can still exist, which causes a time-varying power imbalance. Note that if the power imbalance is unknown and time-varying, it is almost impossible to design a control law with $u_i$ such that $\omega_{syn} = 0$. In this case, it is practical to balance the power supply and demand such that the frequency deviation $\omega_i$ is within a prespecified range. In this section, we describe time-varying loads and generation as time-varying power imbalance. Because the frequencies of the nodes in the system usually synchronize quickly, it is practical to neglect the differences between the frequency deviations at all the nodes and make the following assumption for the time-varying power imbalance.



**Assumption 3.4.1** *The power-imbalance $P_s(t) = \sum_{i\in\mathcal{V}} P_i(t)$ changes relative slowly such that the frequencies of all the nodes in $\mathcal{V}_M \cup \mathcal{V}_F$ are in a synchronized state, i.e., $\omega_i - \omega_s = 0$. Furthermore, assume $P(t)$ is Lipschitz-continuous, i.e., there exists a constant $L \in [0, +\infty)$ such that $|P(t_1) - P(t_2)| \le L|t_1 - t_2|$ for all $t_1 > 0, t_2 > 0$.*

For the system (2.4) with a time-varying power imbalance $P_s(t)$, the objective of the secondary frequency control is to design a control law $u(t)$ to control the frequency deviation $\omega_i$ to a prespecified range, i.e., $|\omega_i| \le \overline{\omega}$ for all $i \in \mathcal{V}_M \cup \mathcal{V}_F$. With Assumption (3.4.1), the following problem for the time-varying power imbalance needs to be solved as an alternative of Problem (2.4.1).

**Problem 3.4.2** *For the system (3.2) with a slowly changing time-varying power imbalance as in Assumption (3.4.1), determine the input $u_s(t)$ at time $t > 0$ so as to achieve: (i) the control objective of a balance of power supply and demand in terms of $|\omega_s| < \overline{\omega}$ where $\overline{\omega} > 0$ gives a prespecified range of $\omega_s$, and (ii) the control cost is minimized at every time $t > 0$, equivalently, the following economic dispatch problem (3.25) is solved at every time $t$,*

$$\min_{u_j\in\mathbb{R}, j\in\mathcal{V}_K} \sum_{i\in\mathcal{V}_K} J_i(u_i) \tag{3.25a}$$

$$s.t. - u_s(t) + \sum_{i\in\mathcal{V}_K} u_i(t) = 0, \tag{3.25b}$$

*where $J_i(u_i)$ is as defined in (3.1).*

In Problem (3.4.2), $u_s(t)$ is determined first for (3.2) such that $|\omega_s(t)| < \overline{\omega}$ and $\{u_i(t), i \in \mathcal{V}_K\}$ are calculated by solving optimization problem (3.25) then. Note that Problem (3.4.2) focuses on the transient phase while Problem (2.4.1) focuses on the steady state of the power system only.

We remark that when $\omega_i$ is not synchronized at $\omega_{syn}$ at a $t > 0$, $\omega_i$ is considered as a local frequency deviation and $\omega_{syn}$ as a global frequency deviation which is a virtual frequency and can be used to measure the power imbalance. In this case, Problem (3.4.2) still focuses on the global frequency deviation.

To guarantee the stability of the system, we make the following assumption

**Assumption 3.4.3** *The power imbalance is relatively small such that there is no congestion occurring in the lines during the transient, i.e., for all* $t > 0$, $|\theta_i(t) - \theta_j(t)| < \gamma_{ij} < \frac{\pi}{2}$ *for all the lines in* $\mathcal{E}$*, where* $\gamma_{ij}$ *is a positive value derived from the flow limit of the line connecting node* $i$ *and node* $j$.

Assumption (3.4.3) is commonly referred to as a security constraint [14] in power system analysis. It can be satisfied by reserving of a margin of power flow when calculating the operating point in the tertiary control [11].



It follows from Theorem (3.2.6) that $u_s(t)$ estimates the time-varying imbalance $-P(t)$. Define the estimation error as

$$e(t) = -P(t) - u_s(t).$$

The following theorem states the bound of the estimation error $e(t)$ and of the frequency deviation $\omega_s$.

**Theorem 3.4.4** *If assumptions (2.4.3), (3.4.1), (3.4.3), (3.3.1) hold, then for the power system (2.4) under control of PIAC, the error*

$$|e(t)| \leq \frac{L}{k} + o(e^{-kt}), \tag{3.26}$$

*where* $k$ *is the control gain coefficient. Hence the synchronized frequency deviation*

$$|\omega_{syn}| \leq \frac{L}{kD} + o(e^{-kt}). \tag{3.27}$$

**Proof:** Since the set of continuous and differentiable functions is dense in the set of Lipschitz functions, it only needs to be proven that, when $P_s(t)$ is a continuous and differentiable function such that $|P_s'(t)| < L$, the inequality (3.26) holds. From the definition of $e(t)$ and (3.5), it yields

$$\dot{e}(t) = P'(t) - \dot{u}_s(t) = P'(t) - ke(t)$$

Define $w(t)$ such that $\dot{w}(t) = L - kw(t)$ and $w(0) = e(0)$ which is the initial value of $e(t)$, then

$$\dot{e}(t) - \dot{w}(t) = P'(t) - L - k(e(t) - w(t)) \leq -k(e(t) - w(t))$$

which yields $e(t) - w(t) \leq (e(0) - w(0))e^{-kt} = 0$ by Gronwall inequality. Hence $e(t) \leq w(t) = \frac{L}{k} + (e_0 - \frac{L}{k})e^{-kt}$. The lower bound of $e(t)$ is derived similarly with $e(t) \geq -\frac{L}{k} + (e_0 + \frac{L}{k})e^{-kt}$. Then

$$|e(t) - e_0 e^{-kt}| \leq \frac{L}{k}(1 - e^{-kt})$$

which yields

$$|e(t)| \leq \frac{L}{k}(1 - e^{-kt}) + |e_0|e^{-kt}.$$

By plugging $e(t)$ into (3.2) with the term $o(e^{-kt})$ neglected, the bound of $\omega_{syn}$ can be derived similarly. ■

From Theorem (3.4.4), by neglecting the term $o(e^{-kt})$, the control gain coefficient $k$ can be tuned such that $k > \frac{L}{D\overline{\omega}}$, which yields $|\omega_{syn}| < \overline{\omega}$. By (3.7b, 3.7c,3.7d), the optimization problem (3.25) is solved. Hence Problem (3.4.2) is solved subsequently.

Note that $k$ depends on the power imbalance function, the acceptable range of the frequency deviation, and the droop control coefficients $\{D_i, i \in \mathcal{V}_M \cup \mathcal{V}_F\}$. In practice, it also depends on how sensitive the control devices are to the power imbalance. Theorem (3.4.4) confirms that if there are sufficient communication lines and the control devices are sensitive enough, the synchronized frequency can be steered to any desired range. Therefore, the larger and faster fluctuations from the renewable power sources can be addressed by improving the communication network and the sensitivity of control devices using PIAC. When the global frequency deviation is steered to a desired range, the local frequency deviation $\omega_i$ can also be steered to a desired range by the primary control which is independent on the secondary frequency control of PIAC.



## 3.5. CASE STUDY-1

In this section, we evaluate the performance of the PIAC method and compare it with with those of the GB (2.14), DAI (2.15) and DecI control laws on the IEEE New England power grid shown in Fig. 3.1, where DecI is a special case of DAI without communications between the controllers. The data are obtained from [67]. In the test system, there are 10 generators, and 39 buses and it serves a total load of about 6 GW. The voltage at each bus is a constant which is obtained by power flow calculation with the *Power System Analysis Toolbox* (PSAT) [22]. In the network, there actually are 49 nodes, i.e., 10 nodes for the generators, 39 nodes for the buses. Each synchronous machine is connected to a bus and its phase angle is rigidly tied to the rotor angle of the bus if the voltages of the system are constants, e.g., the classical model of synchronous machines [11]. We simplify the test system to a system of 39 nodes by considering the generator and the bus as one node. This is reasonable because the angles of the synchronous machine and the bus have the same dynamics. The 10 generators are in the set $\mathcal{V}_M = \{30, 31, 32, 33, 34, 35, 36, 37, 38, 39\}$ and the other buses are in the set $\mathcal{V}_F$ which are assumed to be frequency dependent loads. The nodes participating in secondary frequency control are the 10 generators, thus $\mathcal{V}_K = \mathcal{V}_M$. In order to compare the result of [10, 27], the frequency dependent nodes do not participate in the secondary frequency control even though they can help release the control burden in PIAC. The inertias of the generators as stated in [67] are all divided by 100 in order to obtain the desired frequency response as in [10, 27]. This makes the comparison of PIAC with GB, DAI and DecI on the frequency response more explicit. The buses in $\mathcal{V}_M \cup \mathcal{V}_F$ and controllers in $\mathcal{V}_K$ are connected by a communication network.

As in [10, 27], we set the droop control coefficient $D_i = 1$ (p.u. power/p.u. frequency deviation) for $i \in \mathcal{V}_F \cup \mathcal{V}_M$ under the power base of 100 MVA and frequency base of 60 Hz with the nominal frequency $f^* = 60$ Hz, and we choose the quadratic cost function $J_i(u_i) = \frac{u_i^2}{2a_i}$, $i \in \mathcal{V}_K$. The economic dispatch coefficients $a_i$ are generated randomly with a uniform distribution on $(0, 1)$. It can be easily verified that the quadratic cost functions are all strictly convex.

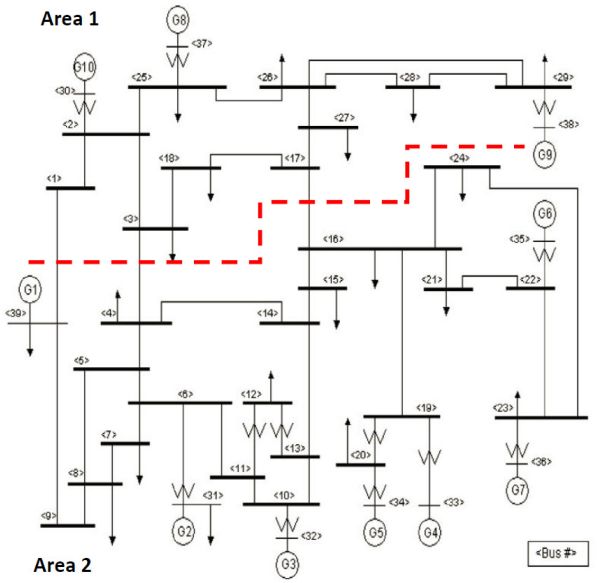


Figure 3.1: IEEE New England test power system.

In the simulations, the system is initially at a supply-demand balanced state with nominal frequency denoted by $f^* = 60$ Hz. At time $t = 0.5$ second, a step-wise increase of 33 MW of the loads at each of the buses 4, 12, and 20, amounting to a total power imbalance of 99 MW, causes the frequency to drop below the nominal frequency. The loads at the other nodes do not change.

Table 1. The control parameters

| PIAC | GB | | DAI | | DecI |
|---|---|---|---|---|---|
| $k$ | $k_{GB}$ | $C_i$ | $k_i$ | $w_{ij}$ | $k_i$ |
| 5 | 60 | $\frac{1}{39}$ | 50 | -20 | 50 |

We conduct the simulations with the open source software PSAT and use the Euler-Forward method to discretize the ordinary differential equations and the Newton-Raphson method to solve the nonlinear system. We first evaluate the performance of PIAC on the network which is assumed as a single area. We compare the PIAC method with the GB, DAI and DecI control laws. For illustrations of the overshoot phenomena of other control laws, we refer to the simulation results of the literature published recently, e.g., [13, 16]. Then we implement the PIAC method in the network separated into two areas and show that the control actions of the areas are totally decoupled by PIAC as described in the subsection 3.2.3. Finally, we verify the analysis in Theorem (3.4.4) on the bound of the synchronized frequency when the loads of the system are time-varying in subsection 3.5.3.

### 3.5.1. SINGLE-AREA IMPLEMENTATION OF PIAC

In this subsection, the network is seen as a single area. The parameters for PIAC, GB, DAI and DecI are listed in Table 1. For DAI, the communication network is a weighted network as shown in Fig. 3.1 by the black dotted lines. The weight $w_{ij}$ for line $(i, j)$ is set as in Table 1 and $w_{ii} = -\sum_{(i,j)} w_{ij}$. The settings of these gain coefficients are chosen for a fair comparison in such a way that the slopes of the total control inputs, which reflect the required response time of the actuators, show close similarity (see Fig. 3.2$d_1$-3.2$d_4$).

Fig. 3.2 shows the comparison of the performances between the four control laws. Fig. 3.2a-3.2d show the responses of frequencies $\overline{\omega}_i = \omega_i + f^*$ for all $i \in \mathcal{V}_M$, virtual *standard frequency* $\overline{\omega}_s = \omega_s + f^*$, relative frequency $\{\omega_i - \omega_s,\ i \in \mathcal{V}_M\}$ and control input $u_s$ respectively. The latter three illustrate the three-subprocesses decomposed from the dynamics of the system (2.4). Here, the responses of $\omega_s$ are obtained from (3.2) with $u_s$ as the total amount of control inputs of the PIAC and GB method respectively. It can be observed from Fig. 3.2$a_1$ and 3.2$a_4$ that both all the control laws can restore the nominal frequency. However, the frequency deviation under the PIAC method is much smaller than under the other three control laws which introduces extra oscillations to the frequency. This is because the sum of control inputs of the GB, DAI and DecI method overshoots the desired value as Fig. 3.2$d_2$ shows, while the one of the PIAC method converges exponentially as Fig. 3.2$d_1$ shows. Because of the overshoot, the GB, DAI and DecI control laws require a maximum mechanical power input of about 140 MW from the 10 generators after the disturbance while the PIAC method only requires 99 MW in this simulation. This scenario is also well reflected in the response of the virtual frequency $\overline{\omega}_s$ as shown in Fig. 3.2$b_1$ and Fig. 3.2$b_4$. Note that the convergences of the relative frequencies $\{\omega_i - \omega_s,\ i \in \mathcal{V}_M\}$ to zero as shown in Fig. 3.2$c_1$ and 3.2$c_4$ are the main concern of primary frequency control [9, 59]. Since the economic power dispatch is solved on-line, it can be observed in Fig. 3.2$e_1$ and 3.2$e_2$ that the marginal costs of all the controllers are the same during the transient phase under the control of PIAC. This is the same as for the control of the GB method. In contrast with PIAC and GB, the marginal costs of DAI are not identical during the transient phase even though they achieve a consensus at the steady state. Because there are no control coordinations between the controllers in DecI, the marginal costs are not identical even at the steady state as shown in Fig. 3.2$e_4$. Since $u_i = \alpha_i \lambda$, the control inputs of the PIAC method and the GB method have similar dynamics as those of their marginal costs as shown in Fig. 3.2$f_1$-3.2$f_2$. Note that as shown in Fig. 3.2$f_4$, the control inputs of DecI are very close to each other because of the identical setting of $k_i$ and the small differences between the frequency deviations. As shown in Fig. 3.2$f_1$-Fig. 3.2$f_3$, the control inputs of some generators in the PIAC, GB and DAI control laws are small due to the high control prices.

We remark that the larger the gain of the GB method the larger are the oscillations of frequency deviations even though the frequencies converge to the nominal frequency faster. However, the control inputs of the PIAC method converge to the power imbalance faster under larger control gain $k$, which leads to smaller frequency deviations. As shown in Fig. 3.2$a_1$, the frequency drops about 0.4 Hz which can be even smaller when $k$ is larger. However, $k$ is related to the response time of the control devices and cannot be infinitely large. If the step-wise increase of the loads is too big and the gain coefficient $k$ is not large enough, i.e., the controllers cannot response quickly enough, the frequency might become so low that they damage the synchronous machines.

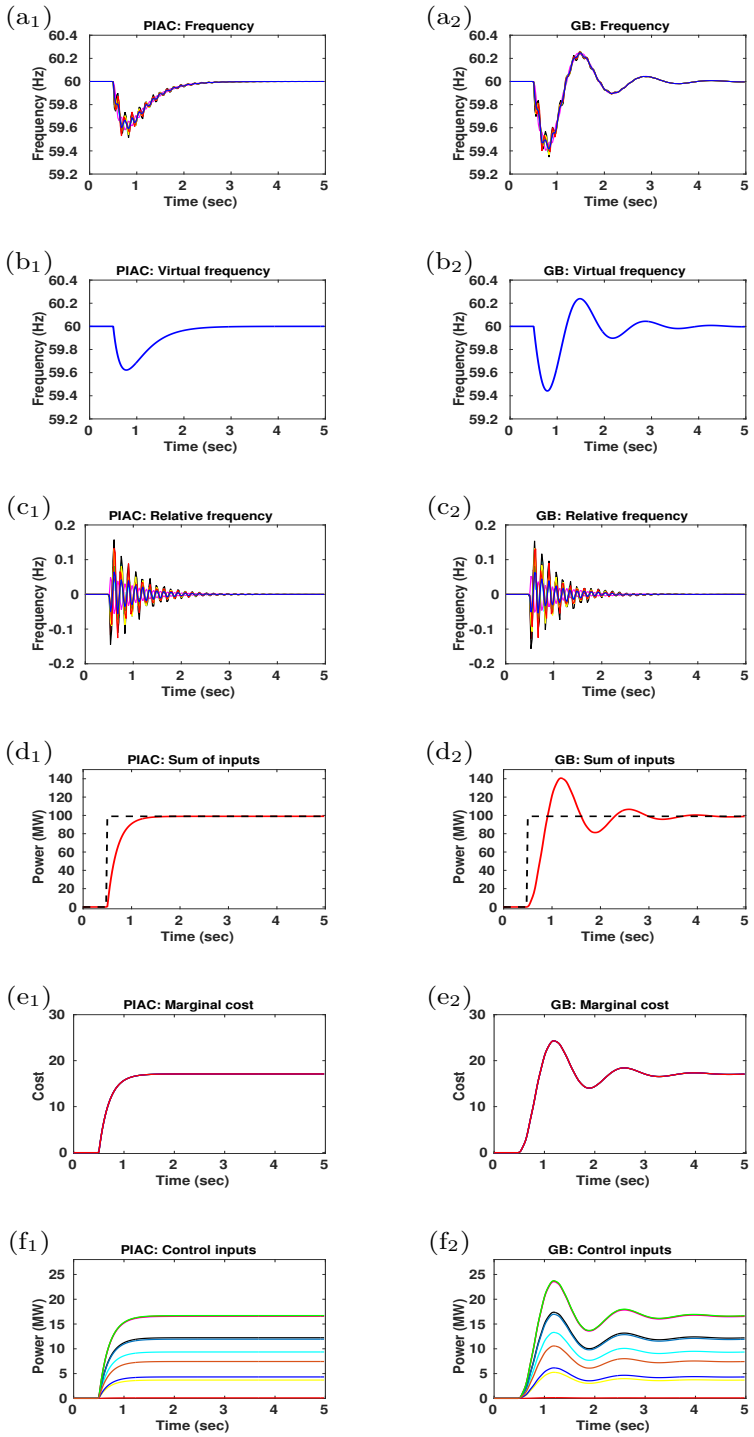


Figure 3.2: Part1: Comparison of PIAC and GB method (single area implementation). In ($d_1$-$d_2$), the black dashed lines denote the power imbalance of the network. In these simulations, the inertias $\{M_i,\ i \in \mathcal{V}_M\}$ obtained from [67] are all divided by 100.

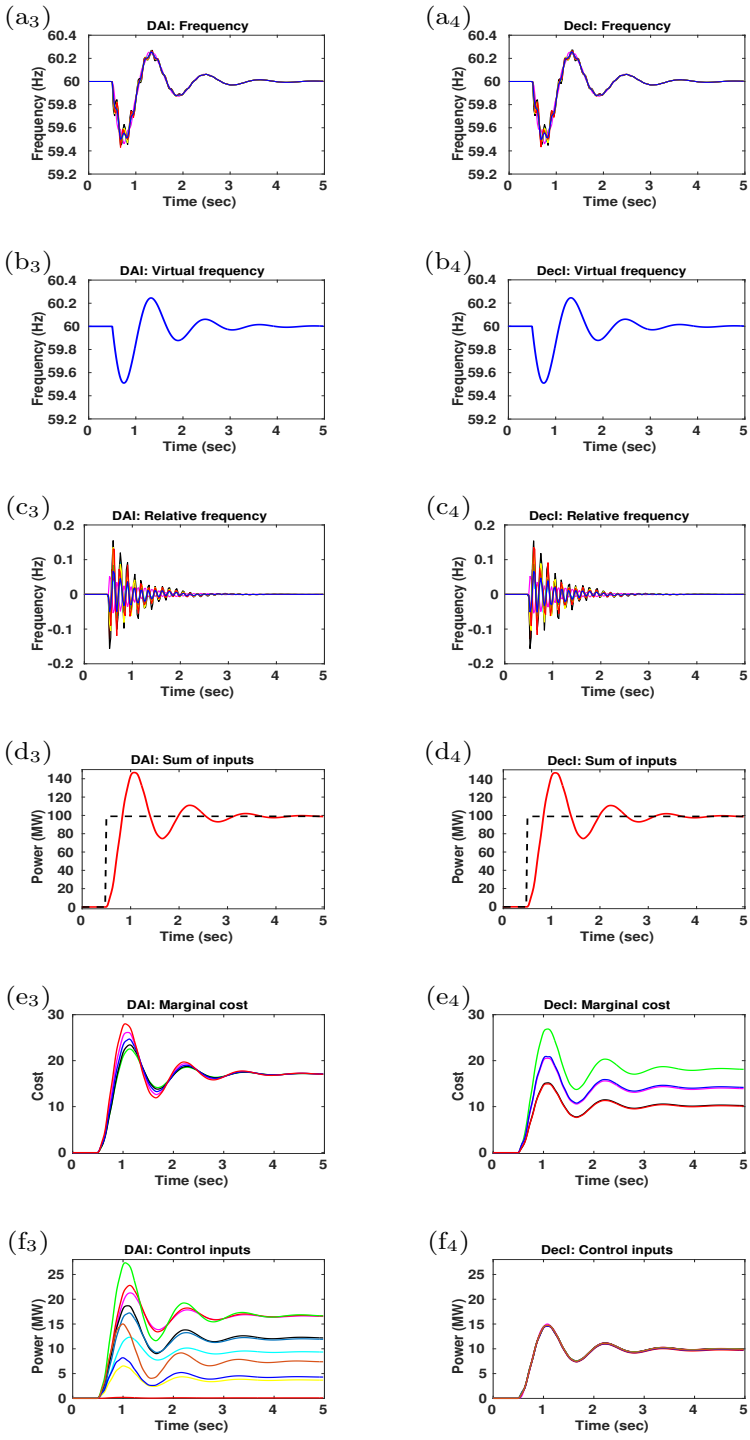


Figure 3.2: Part 2: Comparison of the DAI and DecI method (single area implementation). In ($d_3$-$d_4$), the black dashed lines denote the power imbalance of the network. In these simulations, the inertias $\{M_i,\ i \in \mathcal{V}_M\}$ obtained from [67] are all divided by 100.

### 3.5.2. MULTI-AREA IMPLEMENTATION OF PIAC

In this subsection, the network is separated into two areas by the red dashed line with the purpose of illustrating the properties of PIAC on decoupling the control actions of the areas. This separation is done such that there are controllers in both the two areas, which only react to the disturbances of their own area. All the parameters of the controllers are the same to the ones in the single-area implementation. There are 3 generators in area $A_1$ and 7 generators in the area $A_2$ i.e., $\mathcal{V}_{M_1} = \{30,37,38\}, \mathcal{V}_{M_2} = \{31,32,33,34,35,36,39\}$. The boundary lines of area $A_1$ are in $\mathcal{E}_{A_1} = \{(1,39),(3,4),(17,16)\}$. As in subsection 3.5.1, the secondary frequency controllers are installed at the nodes of the generators. After the step-wise increase of the loads at buses 4, 12 and 20 with the total amount of 99 MW in the area $A_2$, the multi-area implementation of PIAC recovers the nominal frequency as shown in Fig. 3.3a and the power export deviation of area $A_1$ converges to zero as shown by the black dashed lines in Fig. 3.3b. Fig. 3.3b also shows that as the system converges to a new state, the power flows in the three line in $\mathcal{E}_{A_1}$ are different from the ones before the step-wise increase of the loads in area $A_2$. A characteristic of PIAC is that it decouples the control actions of the areas, which can be observed in Fig. 3.3c. Since the step-wise increase of the power loads at the buses 4, 12 and 20 happen in area $A_2$, the control inputs of area $A_1$ are zero and the power is balanced by the controllers in the area $A_2$. This shows that with the PIAC method, the power can be balanced locally in an area without influencing to its neighbours. *This characteristic of PIAC is attractive for such a non-cooperative multi-area control of a power system that different areas might have different amount of renewable energy. It is fair for the area with a large amount of renewable energy to respond to the disturbance in its own area. As mentioned in subsection 4.2, this characteristic allows the controllers in different areas control the system in an asynchronous way at any time according to the power imbalance within the area.*

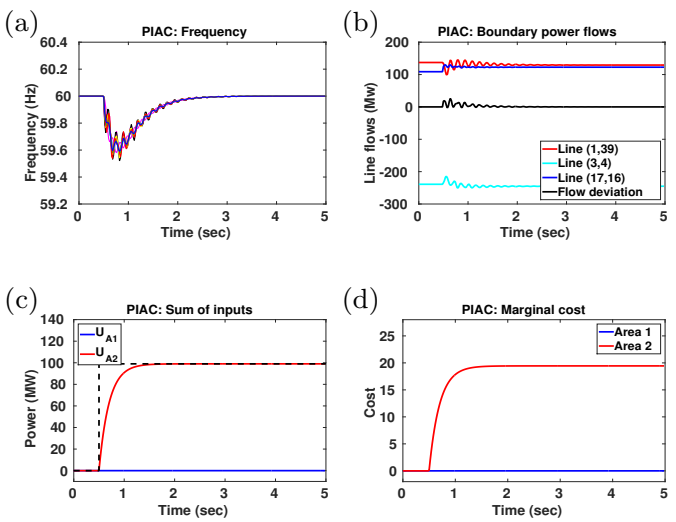


Figure 3.3: Multi-area control implementation of PIAC. The inertias $\{M_i,\ i \in \mathcal{V}_M\}$ obtained from [67] are all divided by 100.

### 3.5.3. THE BOUND OF THE SYNCHRONIZED FREQUENCY

In this subsection, we still focus on the IEEE New England test system. But now the power imbalance is a time-varying function instead of a constant as in the previous subsections. The system is initially at a supply-demand balanced state with 60 Hz frequency. The loads at bus {4,12,20} deviate from their nominal loads at $t = 0.5$ with time-varying functions $P_4(t) = 0.33\sin(t-0.5)$, $P_{12}(t) = 0.33\sin(2t-1)$, $P_{20} = 0.33\sin(3t-1.5)$. The load deviations lead to $P(t) = -0.33\big(\sin(t-0.5)+\sin(2t-1)+\sin(3t-1.5)\big)$ with $|P'(t)| \le 1.98$, which yields the Lipschitz coefficient $L = 1.98$ in Eq. (3.26). We compare our result with the Gather-Broadcast control method. We set the control gain $k = 10$ for the PIAC method and $k_{GB} = 5$ for the Gather-Broadcast control method (2.14) respectively. We choose $k_{GB}$ that leads to the fastest convergence without overshoot above the nominal frequency 60 Hz.

Fig. 3.4 shows the performance of PIAC. Under PIAC, it can be seen that the control input $u$ is closely tracking $P(t)$ in Fig. 3.4a. In contrast, the control input of the GB method is not tracking the power imbalance and the primary control has to be used to balance the power supply and demand. Fig. 3.4b shows the frequency response to the power imbalance. We remark that all the synchronous machines are close to a synchronous state, i.e., $\omega_i \approx \omega_j$, under the PIAC method, Gather-Broadcast control and open-loop system respectively. So we only plot the frequency at bus 34 to evaluate the performance of the PIAC and Gather-Broadcast control methods. We do not plot the marginal costs of the controllers since they are the same and are with the same shape of control input $u$ in Fig. 3.4a.

Under PIAC, the bound derived by Theorem (3.4.4) for the frequency deviation is $|\omega_{syn}| \le L/kD = 0.0051$. Converting it to the bound of the real frequency whose nominal frequency is 60 Hz, we obtain the upper bound $\omega^+ = 60(1 + L/kD) = 60.3$ and the lower bound $\omega_- = 60(1 - L/kD) = 59.7$ of the frequency. Both the upper bound and the lower bound are plotted by dotted horizontal lines in Fig. 3.4b, by which the frequency is bounded under PIAC. However, compared to the frequency deviation of the open-loop system, the frequency deviation is not suppressed so much by the GB method. We remark that the GB method can also effectively suppress the frequency deviation with a large control gain coefficient for the system with time-varying power imbalance, but extra oscillations are introduced when disturbances happen and the bound of the frequency deviation has not been obtained as in Theorem (3.4.4).

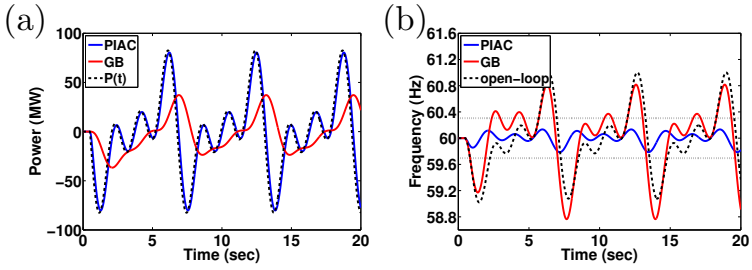


Figure 3.4: (a). The control input $u$ of PIAC and Gather-Broadcast control, and the power imbalance $P(t)$. (b). The response of the frequency at bus 34 under PIAC, Gather-Broadcast control and open-loop system. In this simulation, the inertias $\{M_i,\ i \in \mathcal{V}_M\}$ obtained from [67] are all divided by 100.

## 3.6. CASE STUDY-2

In Section 3.5, the inertia $M_i$ for the generators in the IEEE 39-bus system obtained from [67] are all divided by 100 in order to compare the results with those in the literature [10, 27]. In this section, we compare the performance of PIAC, GB, DAI and DecI using the original data of $M_i$. As in Section 3.5, the 10 generators are in the set $\mathcal{V}_M = \{30,31,32,33,34,35,36,37,38,39\}$, the other buses are in the set $\mathcal{V}_F$ which are assumed to be frequency dependent loads. The nodes participating in secondary frequency control are the 10 generators, thus $\mathcal{V}_K = \mathcal{V}_M$. The buses in $\mathcal{V}_M \cup \mathcal{V}_F$ are connected by a communication network.



We set the droop control coefficient $D_i = 70$ (p.u. power/p.u. frequency deviation) for $i \in \mathcal{V}_M$ and $D_i = 1$ (p.u. power/p.u. frequency deviation) for $i \in \mathcal{V}_F$ under the power base of 100 MVA and frequency base of 60 Hz with the nominal frequency $f^* = 60$ Hz. The droop coefficients are set in such a way that the *frequency response factor* of this system is $\beta = -1.2$ p.u./0.1 Hz, which equals to that of the Quebec power grids of Canada which connects to this system via bus 1 [61]. Here, the unit p.u./0.1Hz is commonly used in load frequency control [61]. The frequency response factor is calculated in the following way.

$$\beta = -\sum_{i \in \mathcal{V}_M \cup \mathcal{V}_F} D_i = -729,$$

with unit (p.u power base /p.u. frequency base). Transferring the unit of $\beta$ into (p.u. power base/0.1 Hz), we derive $\beta = -729 \times 0.1/f^* = -1.2$ (p.u. power base/0.1 Hz). This setting of $D_i$ is more realistic than in the case study in Section 3.5.

We choose the quadratic cost function $J_i(u_i) = \frac{u_i^2}{2a_i}$, $i \in \mathcal{V}_K$. The economic dispatch coefficients $a_i$ are generated randomly with a uniform distribution on $(0,1)$. It can be easily verified that the quadratic cost functions are all strictly convex.

In the simulations, the system is initially at a supply-demand balanced state with the nominal frequency. At time $t = 5$ second, a step-wise increase of 66 MW of the loads at each of the buses 4, 12, and 20, amounting to a total power imbalance of 198 MW, causes the frequency to drop below the nominal frequency. We show the simulation results in the following two subsections.

### 3.6.1. SINGLE-AREA IMPLEMENTATION OF PIAC

Table 2. The control parameters

| PIAC | GB | | DAI | | DecI |
|---|---|---|---|---|---|
| $k$ | $k_{GB}$ | $C_i$ | $k_i$ | $w_{ij}$ | $k_i$ |
| 0.4 | 0.6 | $D_i$ | $0.6D_i$ | -1 | $0.6D_i$ |

In this subsection, the network is seen as a single area. The parameters for PIAC, GB, DAI and DecI are listed in Table 2. For the DAI method, the communication network is a weighted network as shown in Fig. 5.2 by the black dotted lines. The weight $w_{ij}$ for line $(i,j)$ is set as in Table 2 and $w_{ii} = -\sum_{(i,j)} w_{ij}$. As in Subsection 3.5.1, the settings of these gain coefficients are chosen for a fair comparison in such a way that the slopes of the total control inputs, which reflect the required response time of the actuators, show close similarity (see Fig. 3.5d$_1$-3.5d$_4$).

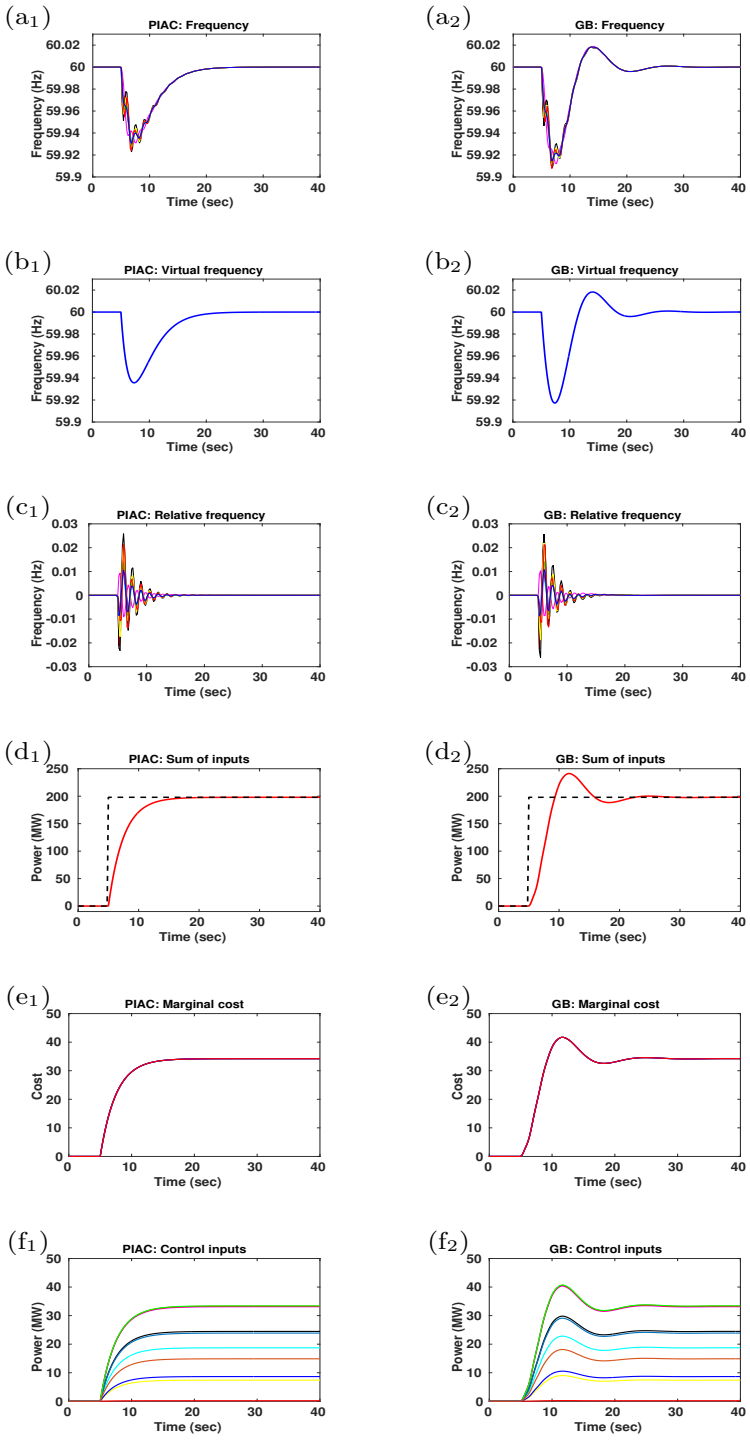


Figure 3.5: Part1: Comparison of PIAC with GB, DAI and DecI (single area implementation). In ($d_1$-$d_2$), the black dashed lines denote the power imbalance of the network.

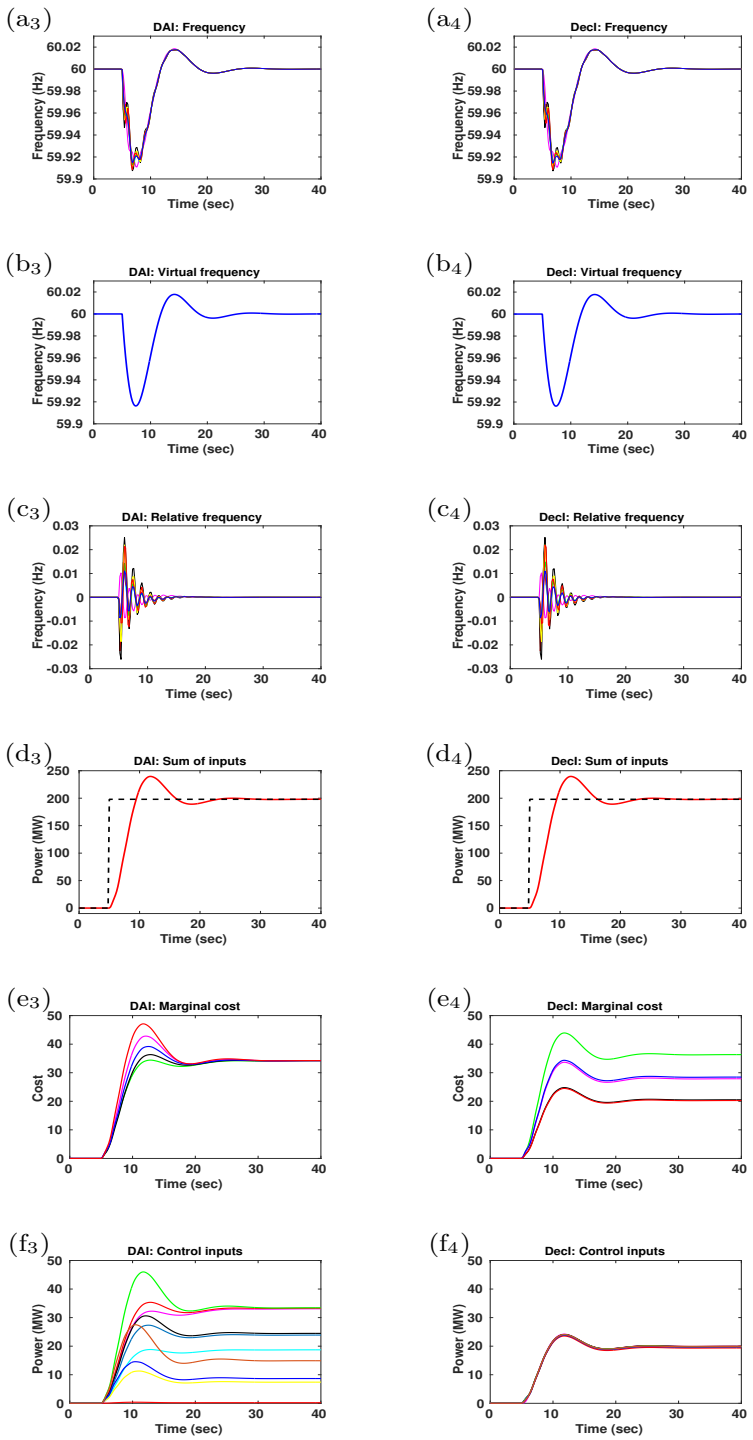


Figure 3.5: Part2: Comparison of PIAC with GB, DAI and DecI (single area implementation). In ($d_1$-$d_2$), the black dashed lines denote the power imbalance of the network.

As in Subsection 3.5.1, we also observe the dynamics of the frequency $\overline{\omega}_i + f^*$, abstract frequency $\overline{\omega}_s = \omega_s + f^*$, relative frequency $\omega_i - \omega_s$, total control input $u_s$, marginal cost $\frac{u_i}{a_i}$ and control inputs $u_i$. Fig. 3.5 shows the comparison of PIAC with GB, DAI and DecI control laws, which demonstrates a similar advantage of PIAC over the integral control laws as in Fig. 3.2. With the inclusion of the proportional input into secondary frequency control, the transient performance can be improved such that the convergence of the system state is accelerated without overshoot problems.



### 3.6.2. MULTI-AREA IMPLEMENTATION OF PIAC

In this subsection, with all the settings of the parameters being the same as in Subsection 3.6.1, we implement PIAC in multi-area control. The network separation into two areas are shown by the red dashed line in Fig. 3.1. The boundary lines are $(1,39),(3,4),(17,16)$. The sets of the generators in area $A_1$ and $A_2$ are $V_{M_1} = \{30,37,38\}$ and $V_{M_1} = \{31,32,33,34,35,36,39\}$ respectively. The step-wise increase of loads also occur at buses 4, 12 and 20 with total amount of 198 MW. We remark that compared with the case study in Subsection 3.5.2, the differences are the setting of $M_i$, $D_i$ and the size of the step-wise increase as buses 4, 12 and 20.

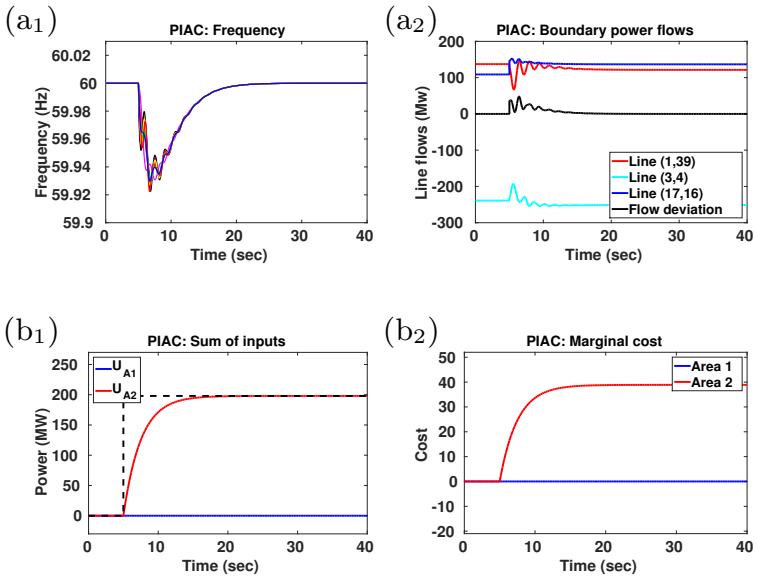


Figure 3.6: Multi-area control implementation of PIAC.

Fig. 3.6 illustrates the performance of PIAC when implemented in multi-area control. As in the case study in Subsection 3.5.2, this case study demonstrated that PIAC decouples the control actions of the two areas, i.e., the controllers in area $A_1$ are independent on the disturbance of area $A_2$.

## 3.7. CHAPTER CONCLUSION

In this chapter, we proposed a secondary frequency control approach, called PIAC, to restore the nominal frequency of power systems with a minimized control cost. A main feature of PIAC is that the estimated power imbalance converges exponentially with a speed that only depends on a gain coefficient which can be tuned according to the sensitivity of the control devices. Hence PIAC eliminates the drawback of the traditional integral control based secondary frequency control approach, in which large control gain coefficients lead to an overshoot problem of the control inputs and small ones result in a large frequency deviation of the power systems. When implemented in a network with multiple areas, PIAC decouples the control actions of the areas such that the power supply and demand of an area can be balanced locally in the area without any influences to the neighbors. For the power systems with a large amount of integrated renewable energy, the large transient frequency deviation can be reduced by PIAC with advanced control devices and communication networks. Furthermore, a frequency bound of the system with a Lipschitz-continuous power-imbalance has been derived, which shows that besides a better transient performance compared to the traditional integral control based methods, PIAC can steer the synchronized frequency to any desired range by tuning a control gain coefficient.



However, in practice, there usually is some noise from the measurement of frequency and time delays and even information losses in the communication. In addition, the resistance of the transmission lines cannot be neglected in some power networks, e.g., distribution grids of power systems or Micro-Grids. Hence, further investigation on the performance of PIAC on such a lossy power network with noisy measurements and time delays is needed.

# 4

# Multi-level Power-Imbalance Allocation Control

*A centralized control law, PIAC, is proposed in Chapter 3. In this chapter, we propose a multi-level control law, named* Multi-Level Power-Imbalance Allocation Control *(MLPIAC) for large-scale power systems partitioned into several cooperative areas, each of which possesses a central controller. In MLPIAC, a centralized control law and a consensus based distributed control law are applied within each area and over all the areas respectively. Besides restoring nominal frequency with a minimized control cost, MLPIAC also considers the transient behavior of the system after a disturbance. As in PIAC, the total control input of MLPIAC converges to the power-imbalance without any oscillations. Thus the transient performance of the power system can also be improved through an accelerated convergence without overshoot problems. Because the number of nodes in each area is smaller than the total number of nodes in the network, the communications overhead and computation complexity of the central controller of each area can be decreased. Because the number of areas is smaller than that of nodes in the entire network, MLPIAC is more efficient in minimizing control cost than the purely distributed control law. The asymptotic stability of MLPIAC is proven using the Lyapunov method and the performance is evaluated through simulations. This chapter is currently revised based on comments of reviewers for the corresponding journal paper.*

---

Parts of this chapter are based on:
K. Xi, H. X. Lin, Chen Shen, J. H. van Schuppen. Multi-Level Power-Imbalance Allocation Control for Secondary Frequency of Power Systems. under review (2018).

## 4.1. INTRODUCTION

Power systems are often geographically extended and supply power to tens of millions of inhabitants and many companies over a large domain. A major objective of the power companies is to provide alternating current at the standard frequency, 60 Hz in the USA, and 50 HZ in the main parts of Europe and in Asia. The power demand fluctuates continuously due to switching on or off loads. Consequently, the frequency of the power systems also fluctuates continuously. So the power grids must be controlled to maintain the frequency as close as possible to the agreed reference value.

For load frequency control there are three forms of control: primary, secondary, and tertiary frequency control with control operations distinguished from fast to slow timescales. Primary frequency control synchronizes the frequencies of the synchronous machines and balances the power supply and demand of the power system at a small time-scale. However, the synchronized frequency may deviate from its nominal value. Secondary frequency control restores the nominal frequency at a medium time-scale. With a prediction of power demand, tertiary control calculates the operating point stabilized by primary and secondary control at a large time-scale, which concerns the security and economy optimality of the power system.



The focus of this chapter is on secondary frequency control. The initial approach to control synthesis of secondary frequency control is to apply centralized control [10, 68, 69]. In the centralized control architecture, a central controller collects state information via communication network and computes control inputs for local actuators. *In practice today's power systems are becoming so large that they cannot be effectively controlled by a central controller. The communication overhead and the control computations carried out at the central controller take so much time that the control objectives cannot be satisfactorily achieved.*

Therefore, a form of distributed control is implemented for control of power systems [12, 13, 15, 16, 27, 28, 34–36, 41, 70]. In distributed control, each node is equipped with a controller, which aims to achieve the control objective of the entire network via coordinations and cooperations. However, *the distributed control usually suffers a slow convergence to the optimal steady state because of the large scale of the power system.*

In this chapter, we aim to synthesize a multi-level control law for secondary frequency control of large-scale power systems, which is able to balance the advantages and disadvantages of the centralized and distributed control. We consider a large-scale power system consisting of several areas, each of which has a central controller. The control objectives can be described as: restore the frequency to its nominal value, prevent oscillations and overshoots caused by the controllers, and minimize the economic cost in the operation of the power system. The control law is to be implemented in the form of centralized control within each area and in the form of distributed control over all the areas of the network.

We first present a centralized and a distributed secondary frequency control approach, called *Gather-Broadcast Power-Imbalance Allocation Control* (GBPIAC) and *Distributed Power-Imbalance Allocation Control* (DPIAC). Both approaches have the nice transient behavior such as in PIAC through an accelerated convergence of the control inputs without any extra oscillations. Then a multi-level control, *Multi-Level Power-Imbalance Allocation Control* (MLPIAC), which comprises the GBPIAC and DPIAC method for large-scale power systems is proposed. In MLPIAC for the large-scale power system consisting of a

number of areas, there are two control levels in MLPIAC, i.e., control within each area and control over the areas. GBPIAC is implemented within each area and DPIAC over the areas. Within each area, the local control inputs are calculated by solving an economic power dispatch problem. Over the areas, the marginal costs of areas are exchanged via a communication network based on the consensus control principle, thus a consensus marginal cost is achieved at the steady state. So the control cost of the system is minimized at the steady state. As in PIAC, the overshoot of the control inputs caused by oscillations are eliminated and the transient behavior of the system can be improved through an accelerated convergence of the control inputs in MLPIAC. Since the scale of the network in the distributed control on the control level over the areas becomes smaller, the marginal cost usually achieves the consensus faster. Furthermore, the consensus speed of the marginal cost can also be accelerated by increasing a single control gain coefficient, which results in a smaller control cost.



To simplify the description of MLPIAC, the two special cases of MLPIAC, the GBPIAC and DPIAC method are introduced before the MLPIAC method. This chapter is organized as follows. We formulate the control objective in Section 4.2, and propose the GBPIAC and DPIAC method in Section 4.3. We synthesize the MLPIAC method in Section 4.4 and analyze the asymptotic stability in Section 4.5. Finally, we provide case study to evaluate the performance of MLPIAC in section 4.6. Concluding remarks are given in Section 4.7.

## 4.2. MULTILEVEL CONTROL

The aim of this chapter is to synthesize a multi-level control law for system (2.4) to solve Problem (2.4.1) and (2.6.1). In this section, we define a multi-level architecture for system (2.4) and formulate the problem caused by the disadvantages of centralized and distributed control.

Multi-Level control systems have been defined before for several classes of systems [71, 72]. In the past the term *hierarchical system* was used to describe a system with at the highest-level one subsystem, at the next lower level two or more subsystems and the second lower level even more subsystems. The relations of a subsystem with its parent at the next-higher level and its children at the next-lower level have then to be defined. Because we focus on the hierarchy over the network of the power system rather than the one for frequency control with primary, secondary and tertiary control as in [11, 73], the term *multi-level system* will be used in this chapter.

**Definition 4.2.1** *Define a* multi-level architecture *for a large-scale power system (2.4) as level 1 of the entire network partitioned into several areas, level 2 of areas consisting of more than one nodes and level 3 of nodes.*

Besides Problem (2.4.1) for the steady state, Problem (2.6.1) concerning the transient phase, the shortcomings of centralized and distributed control are also considered in this chapter as follows.

**Problem 4.2.2** *Design a secondary frequency control law for* $\{u_i,\ i \in \mathcal{V}_K\}$ *of a multi-level power system as defined in (4.2.1) such that the shortcomings of centralized and distributed control can be well addressed.*

We consider quadratic cost functions in the economic power dispatch problem (2.10), which is rewritten as

$$\min_{\{u_i\in\mathbb{R}, i\in\mathcal{V}_K\}} \sum_{i\in\mathcal{V}_K} J_i(u_i) = \sum_{i\in\mathcal{V}_K} \frac{1}{2}\alpha_i u_i^2, \tag{4.1a}$$

$$s.t. \quad P_s + \sum_{i\in\mathcal{V}_K} u_i = 0, \tag{4.1b}$$

Where $\alpha_i > 0$ is the control price at node $i$, and $P_s = \sum_{i\in\mathcal{V}} P_i$ denotes the power imbalance of the system. We assume the constraints $u_i \in [\underline{u}_i, \overline{u}_i]$ for all $i \in \mathcal{V}_K$ are satisfied.

A communication network is required for the control law to solve the economic power dispatch problem (4.1), for which we make the following assumption.



**Assumption 4.2.3** *Consider the system (2.4) with secondary controllers, assume all the nodes in $\mathcal{V}_M \cup \mathcal{V}_F$ are connected by a communication network.*

With Assumption (4.2.3), the power system can be viewed as a machine, in which all the state information can be collected and all the disturbances can be estimated accurately via the state information. Furthermore, the central controller of each area can communicate its control commands to the central controllers in the neighboring areas and to the local controllers in its area. There usually are time-delays and noises in the measurement of the frequency and communications which are neglected in this chapter.

With the optimization problem (4.1), the PIAC method is defined as follows.

**Definition 4.2.4 (PIAC)** *Consider the power system described by (2.4) with Assumption (2.4.3) and (4.2.3), and with the optimization problem (4.1), the PIAC control law is defined as the dynamic controller*

$$\dot{\eta}(t) = \sum_{i\in\mathcal{V}_M\cup\mathcal{V}_F} D_i\omega_i(t), \tag{4.2a}$$

$$u_s(t) = -k\Big(\eta(t) + \sum_{j\in\mathcal{V}_M} M_j\omega_j(t)\Big), \tag{4.2b}$$

$$u_i(t) = \frac{\alpha_s}{\alpha_i}u_s(t), \tag{4.2c}$$

$$\frac{1}{\alpha_s} = \sum_{i\in\mathcal{V}_K}\frac{1}{\alpha_i}, \tag{4.2d}$$

where $k \in (0,\infty)$ is a parameter of the control law and $\alpha_s$ is a constant.

The *total control input* $u_s(t)$ is computed by (4.2b) and then economically dispatched to every local node $i \in \mathcal{V}$ according to (4.2c). Because $u_s(t)$ converges to the power imbalance $-P_s$ exponentially, the convergence of the frequency to the steady state can be accelerated. Hence, PIAC solves Problem (2.4.1) and (2.6.1). However, PIAC is a centralized control in which the main control procedure is implemented by a central controller. In order to solve Problem (2.4.1), (2.6.1) and (4.2.2), we need to synthesize a control law in which the total control input $u_s$ also converges to the power imbalance directly without oscillations.

In the following sections, we present the GBPIAC and DPIAC methods both of which solve Problem (2.4.1) and (2.6.1) as the PIAC method, followed by MLPIAC which combines GBPIAC and DPIAC to further solve Problem (4.2.2).

## 4.3. GATHER-BROADCAST AND DISTRIBUTED PIAC

In this section, we introduce the GBPIAC and DPIAC method respectively as a preparation for the multi-level control approach. To simplify the exposition, we first define an abstract frequency deviation for the system in Subsection 4.3.1, then introduce the GBPIAC method, which inherits the main characteristics of PIAC in Subsection 4.3.2, and introduce the DPIAC method in Subsection 4.3.3.

### 4.3.1. CONTROL OF THE ABSTRACT FREQUENCY DEVIATION

As explained in Chapter 3, the overshoot of $u_s$ usually causes extra frequency oscillations mentioned in Problem (2.6.1). *We remark that this overshoot of $u_s$ is caused by the oscillation of $u_s$ around $-P_s$.* In order to clearly illustrate the principle to avoid this overshoot problem, we focus on the abstract frequency defined in (3.2) in Chapter 3, which is rewritten as follows.



$$M_s\dot{\omega}_s = P_s - D_s\omega_s + u_s, \tag{4.3}$$

where $M_s = \sum_{i\in\mathcal{V}_M} M_i$, $P_s = \sum_{i\in\mathcal{V}} P_i$, $D_s = \sum_{i\in\mathcal{V}} D_i$, and $u_s = \sum_{i\in\mathcal{V}_K} u_i$.

In order to let $u_s$ converge to $-P_s$ without any oscillations, we construct the following dynamic control law for system (4.3),

$$\dot{\eta}_s = D_s\omega_s, \tag{4.4a}$$
$$\dot{\xi}_s = -k_1(M_s\omega_s + \eta_s) - k_2\xi_s, \tag{4.4b}$$
$$u_s = k_2\xi_s. \tag{4.4c}$$

With the control law (4.4), the closed-loop system of the system (4.3) is as follows,

$$M_s\dot{\omega}_s = P_s - D_s\omega_s + k_2\xi_s, \tag{4.5a}$$
$$\dot{\eta}_s = D_s\omega_s, \tag{4.5b}$$
$$\dot{\xi}_s = -k_1(M_s\omega_s + \eta_s) - k_2\xi_s. \tag{4.5c}$$

Let $v_s = (M_s\omega_s + \eta_s)$, from (4.5), it yields

$$\dot{v}_s = P_s + k_2\xi_s, \tag{4.6a}$$
$$\dot{\xi}_s = -k_1 v_s - k_2\xi_s, \tag{4.6b}$$

from which we derive the dynamics of the control input $u_s$,

$$\dot{v}_s = P_s + u_s, \tag{4.7a}$$
$$\dot{u}_s = -k_2\big(k_1 v_s - u_s\big), \tag{4.7b}$$

where $P_s$ is a constant value. The eigenvalues of the linear system (4.7) are

$$\mu = \frac{-k_2 \pm \sqrt{k_2^2 - 4k_1k_2}}{2}. \tag{4.8}$$

To avoid the sinusoid oscillations of $u_s$, which causes overshoots of $u_s$, the imaginary part of the eigenvalues in (4.8) should be zero, which leads to $k_2 \geq 4k_1$. Hence if $k_2 \geq 4k_1$, $u_s$

converges to $-P_s$ without any oscillations and subsequently the abstract frequency deviation $\omega_s(t)$ converges to zero without any extra oscillations, thus $\omega_{syn} = 0$. Furthermore, the convergence of $u_s$ to $-P_s$ is determined by $k_1$.

**Remark 4.3.1** *We use $u_s$ to estimate the power-imbalance $-P_s$ in system (4.7) which can be seen as an observer of $-P_s$. Similar to the high gain observer [74], there may be overshoot in the initialization of the controller due to the initial condition of the state. To the best of our knowledge, there do not seem general sufficient conditions on the system which guarantee that for all initial conditions the behavior of every state component is free of zero crossings and further eliminate this kind of overshoot. In this chapter, we mention the oscillation as the one where the trajectory fluctuates periodically and mention the overshoot of $u_s$ as the one caused by this oscillation.*



If $u_s$ is known, the control inputs during the transient phase can be computed by solving the optimization problem (3.6) which is rewritten as

$$\begin{aligned} &\min_{\{u_i\in\mathbb{R}, i\in\mathcal{V}_K\}} \sum_{i\in\mathcal{V}_K} J_i(u_i) = \sum_{i\in\mathcal{V}_K} \frac{1}{2}\alpha_i u_i^2, \\ &s.t. \ \ -u_s(t) + \sum_{i\in\mathcal{V}_K} u_i(t) = 0. \end{aligned} \tag{4.9}$$

which is solved by (4.2c,4.2d). It follows from (4.2c,4.2d) that as $u_s(t)$ converges to $-P_s$ without any oscillations, $u_i(t)$ also converges to the desired value without any oscillations, thus the extra oscillation of the frequency is avoided. However, $u_s$ cannot be directly calculated as in (4.4) since $\omega_s$ is a virtual frequency deviation and cannot be measured in practice. For the power system (2.4), the dynamics of the total control input $u_s$ as in (4.7) is desired to avoid oscillations in this chapter. This is different from the PIAC method with dynamics of $u_s$ as in (3.5), which will be explained in Remark (4.3.5) in Subsection 4.3.3. In the following two subsections, we will introduce the GBPIAC and DPIAC method where the total control input $u_s$ also satisfies (4.7).

### 4.3.2. GATHER-BROADCAST PIAC

With the idea of the control law (4.4) for system (4.3), we return to the power system (2.4) and synthesize a control law in which $u_s$ converges to the power imbalance $-P_s$ without any oscillations as in (4.7). The GBPIAC method is defined as a dynamic control law as follows.

**Definition 4.3.2 (GBPIAC)** *Consider the power system (2.4) of a single area with Assumption (2.4.3) and (4.2.3), and with the optimization problem (4.1), the* Gather-Broadcast

Power-Imbalance Allocation Control *method is defined as the dynamic controller,*

$$\dot{\eta}_s = \sum_{i\in\mathcal{V}_F} D_i\omega_i, \tag{4.10a}$$

$$\dot{\xi}_s = -k_1\Big(\sum_{i\in\mathcal{V}_M} M_i\omega_i + \eta_s\Big) - k_2\xi_s, \tag{4.10b}$$

$$u_i = \frac{\alpha_s}{\alpha_i}k_2\xi_s,\ i\in\mathcal{V}_K, \tag{4.10c}$$

$$\frac{1}{\alpha_s} = \sum_{i\in\mathcal{V}_K}\frac{1}{\alpha_i}, \tag{4.10d}$$

*where $\eta_s$, $\xi_s$ are state variables of the controller, $k_1$, $k_2$ are positive parameters and $\alpha_s$ is a constant.*



It can be easily obtained for GBPIAC that $k_2\xi_s$ provides the total control input at any time $t\in T$, i.e., $k_2\xi_s(t) = u_s(t)$. The procedure of the centralized control approach (4.10) is similar to that of the PIAC method. A central controller first collects the frequency deviations $\{\omega_i,\ i\in\mathcal{V}_M\cup\mathcal{V}_F\}$, then calculates the total control input $k_2\xi_s$ by (4.10a,4.10b) and local inputs $\{u_i,\ i\in\mathcal{V}_K\}$ by (4.10c,4.10d), finally allocates the control input $u_i$ to the local controller at node $i$ via the communication network.

It will be shown in the next section that GBPIAC is a special case of MLPIAC, in which the power system is controlled as a single area. The properties of GBPIAC directly follows Theorem 4.4.2 which will be present in the next section. As illustrated in Theorem 4.4.2, the total control input $u_s$ satisfies (4.7), the control gain coefficients should be such that $k_2\geq 4k_1$ to eliminate the overshoot problem. Because the objective of Problem (2.6.1) is to avoid the extra oscillation of the frequency caused by the overshoot of $u_s$, we set $k_2\geq 4k_1$ in the remaining of this chapter,

Similar to the PIAC method, the dynamics of the power system can also be decomposed into three sub-processes,

(i) the convergence process of $u_s(t)$ to $-P_s$ as in (4.7) with a speed determined by $k_1$.

(ii) the convergence process of the global frequency deviation $\omega_s(t)$ to zero as in (4.3) with a speed determined by $u_s(t)$ and $D_s$.

(iii) the synchronization process of the local frequency deviation $\omega_i(t)$ to $\omega_s(t)$ which is described by (2.4), and the synchronization speed is determined by $\{u_i(t),\ i\in\mathcal{V}_K\}$ and $\{D_i, i\in\mathcal{V}_M\cup\mathcal{V}_F\}$. Here, $u_i(t)$ is the solution of the optimization problem (4.9).

The transient performance of the power system can be improved with GBPIAC by tuning the control parameters $k_1$, $\{D_i,\ i\in\mathcal{V}_M\cup\mathcal{V}_F\}$ for the three subprocesses. Similar to PIAC, GBPIAC also focuses on the first two-subprocess in which the convergence of $u_s$ and $\omega_s$ can be accelerated with a large $k_1$. Primary control focuses on the synchronization of $\omega_i$ to $\omega_s$ which can be improved by tuning $\{D_i,\ i\in\mathcal{V}_M\cup\mathcal{V}_F\}$ as in [9, 59].

Theorem 4.4.2 indicates that the performance of GBPIAC is quite similar to that of PIAC, in which the optimization problem (4.9) is solve during the transient phase, the overshoot problem is avoided and the convergence can be accelerated. Hence Problem (2.4.1)

and (2.6.1) are solved by GBPIAC. However, GBPIAC also suffers from the overhead communications and complicated computations of the central controller. In the next section, we present a distributed control method for system (2.4) which eliminates this drawback.

### 4.3.3. DISTRIBUTED PIAC

In this subsection, we introduce the DPIAC method where the total control input $u_s$ also has the dynamics (4.7).

**Definition 4.3.3 (DPIAC)** *Consider the power system (2.4) where each node is controlled as an area with Assumption (2.4.3) and (4.2.3), and with the optimization problem (4.1). Define the* Distributed Power-Imbalance Allocation Control *method as a dynamic controller of the form: for each node $i \in \mathcal{V}_K$,*

$$\dot{\eta}_i = D_i\omega_i + k_3 \sum_{j\in\mathcal{V}} l_{ij}(k_2\alpha_i\xi_i - k_2\alpha_j\xi_j), \tag{4.11a}$$

$$\dot{\xi}_i = -k_1(M_i\omega_i + \eta_i) - k_2\xi_i, \tag{4.11b}$$

$$u_i = k_2\xi_i, \tag{4.11c}$$

*where $\eta_i, \xi_i$ are state variables of the controller, $k_1, k_2$ and $k_3$ are positive gain coefficients, $l_{ij} \in [0,\infty)$ is the weight of the communication line connecting node $i$ and node $j$. $l_{ij}$ defines a weighted undirected communication network with Laplacian matrix $(L_{ij})$*

$$L_{ij} = \begin{cases} -l_{ij}, & i \neq j, \\ \sum_{k\neq i} l_{ik}, & i = j, \end{cases} \tag{4.12}$$

In DPIAC, the local controller at node $i$ needs to calculate the control input $u_i$ with locally measured data of $\omega_i$, marginal costs $\alpha_i\xi_i$ and the marginal costs $k_2\alpha_j\xi_j$ of its neighboring areas connected by communication lines. Hence no central controller as in the PIAC and GBPIAC methods is needed. However, with the coordination on the marginal costs by the local controllers, the control cost still can be minimized at the steady state as the marginal costs achieve a consensus.

It will be shown in the next section that DPIAC is actually a special case of the MLPIAC method, in which each node is controlled as an area. So the properties of DPIAC also follows Theorem 4.4.2 directly. In particular, the dynamics of $u_s$ and $\omega_s$ satisfy (4.7) and (4.3) respectively, where $k_1$ determines the convergence speed of $u_s(t)$, and $k_1$ and $D_s$ determine the convergence speed of $\omega_s(t)$. In this case, DPIAC also eliminates the overshoot of the control input as in GBPIAC.

Unlike GBPIAC, DPIAC involves in the consensus process of the marginal cost $k_2\alpha_i\xi_i$ with a consensus speed determined by the coefficient $k_3$ and matrix $(L_{ij})$. The decomposition of the dynamics of the power system controlled by DPIAC is summarized as follows.

(i) the convergence process of $u_s(t)$ to $-P_s$ as in (4.7) with a convergence speed determined by $k_1$.

(ii) the convergence process of the global frequency deviation $\omega_s(t)$ to zero as in (4.3) with a convergence speed determined by $u_s(t)$ and $D_s$.

(iii) the synchronization process of the local frequency deviation $\omega_i(t)$ to $\omega_s(t)$ which is described by (2.4), and the synchronization speed is determined by $u_i(t)$ and $\{D_i, i \in \mathcal{V}_M \cup \mathcal{V}_F\}$.

(iv) the consensus process of the marginal cost $k_2\alpha_i u_i(t)$ with a consensus speed determined by $k_3$ and $(L_{ij})$.

We remark that the control input $u_i$ in DPIAC cannot converge directly to its optimal solution as in GBPIAC, which may have oscillations. This type of oscillations can be effectively suppressed by increasing the consensus speed of the marginal cost with a larger $k_3$. This can be observed in Fig.4.3$e_2$ and Fig. 4.3$e_3$ and will be further analyzed in Chapter 5. In addition, with the same values of $k_1$ and $D_s$, the control cost of DPIAC is larger than that of GBPIAC since the optimization problem (4.9) is not solved simultaneously in the transient phase as in GBPIAC.



**Remark 4.3.4** *Without the coordination on the marginal costs of nodes, DPIAC reduces to a decentralized control method as follows*

$$\dot{\eta}_i = D_i\omega_i, \tag{4.13a}$$

$$\dot{\xi}_i = -k_1(M_i\omega_i + \eta_i) - k_2\xi_i, \tag{4.13b}$$

$$u_i = k_2\xi_i \tag{4.13c}$$

*in which the abstract standard frequency deviation $\omega_s$ behaves identically as that of DPIAC and of GBPIAC even though the economic dispatch problem is not solved.*

The following remark explains the motivation of the introduction of $\xi_s$ and dynamics of $u_s$ in (4.4).

**Remark 4.3.5** *To utilize the consensus principle, the state variable $\xi_i$ is introduced in DPIAC. This is practical since $\xi_i$ can be used to describe the dynamics of the generator turbine which is neglected in (2.4)[6, 75]. In this case, it is natural to introduce $\xi_s$ in (4.10) in order to evaluate the global performance of DPIAC on the abstract standard frequency deviation $\omega_s$. On the other hand, without introducing $\xi_i$, as in the DAPI method [15], the variable $\eta_i$ for the integral control can be exchanged between the nodes in the distributed control with the form*

$$\dot{\eta}_i = D_i\omega_i + k_3\sum_{j\in\mathcal{V}} l_{ij}(\alpha_i\eta_i - \alpha_j\eta_j) \tag{4.14a}$$

$$u_i = -kM_i\omega_i - k\eta_i. \tag{4.14b}$$

*where the term $-kM_i\omega_i$ is added to the secondary control input $u_i(t)$ such that $u_s$ converges to $-P_s$ exponentially without an overshoot as in (3.5). Hence the behavior of the abstract frequency deviation $\omega_s$ is similar as in GBPIAC and DPIAC. However, $-\sum_{i\in\mathcal{V}_K} k\eta_i$ does not estimate the power imbalance $P_s$ during the transient phase, thus the control cost cannot be decreased by increasing the gain coefficient $k_3$.*

As GBPIAC, DPIAC solves Problem (2.4.1) and (2.6.1), and decreases the overhead communications and complexity computations for each local controllers. However, the consensus speed of the marginal costs becomes slow as the number of nodes in the network increases, which further decreases the convergence of the control inputs to the optimal state.

## 4.4. MULTILEVEL PIAC

In this section, we introduce the MLPIAC method for secondary frequency control of large-scale power systems, which addresses Problem (4.2.2).

For a large-scale power system $A$, we partition the network into $m$ areas such that

$$A = A_1 \cup \cdots \cup A_r \cup \cdots \cup A_m,\ Z_m = \{1, 2, \cdots, m\}, \tag{4.15a}$$

$$A_r \cap A_q = \emptyset,\ \forall\ r \neq q,\ r,\ q \in Z_m. \tag{4.15b}$$

Denote the set of the nodes in area $A_r$ by $\mathcal{V}_{A_r}$, the nodes of the synchronous machines by $\mathcal{V}_{M_r}$, the nodes of the frequency dependent power sources by $\mathcal{V}_{F_r}$ and the nodes with secondary controllers by $\mathcal{V}_{K_r}$. Denote the marginal cost of area $A_r$ by $\lambda_r$. Denote $Z_{m_r}$ as the set of the neighboring areas of area $A_r$ connected by communication lines.

As in Definition (4.2.1), we refer the control over the areas to as level 1 and the control within the area as level 2 and the primary control at a node in an area as level 3. The diagram in Fig. 4.1 illustrates the control architecture of MLPIAC. MLPIAC focuses on secondary frequency control at level 1 and 2.

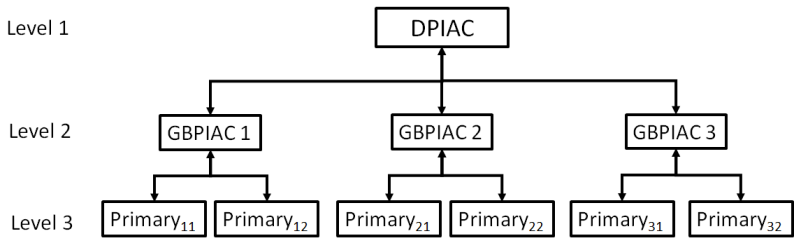


Figure 4.1: Diagram of the multi-level control of power systems.

The MLPIAC method is defined as follows.

**Definition 4.4.1 (MLPIAC)** *Consider a large-scale power system (2.4) partitioned as in (4.15) with Assumption (2.4.3) and (4.2.3) and with the optimization problem (4.1). At level 2, the dynamic control law in area $A_r$ is described by the equations*

$$\dot{\eta}_r = \sum_{i \in \mathcal{V}_{M_r} \cup \mathcal{V}_{F_r}} D_i \omega_i + k_3 v_r, \tag{4.16a}$$

$$\dot{\xi}_r = -k_1 \Big( \sum_{i \in \mathcal{V}_{M_r}} M_i \omega_i + \eta_r \Big) - k_2 \xi_r, \tag{4.16b}$$

$$0 = \frac{\lambda_r}{\alpha_r} - k_2 \xi_r, \tag{4.16c}$$

$$u_i = \frac{\lambda_r}{\alpha_i},\ i \in \mathcal{V}_{K_r}, \tag{4.16d}$$

$$\frac{1}{\alpha_r} = \sum_{i \in \mathcal{V}_{K_r}} \frac{1}{\alpha_i} \tag{4.16e}$$

*where $\eta_r, \xi_r$ are state variables of the controller, $v_r$ is an algebraic variable, $k_1, k_2, k_3 \in (0,\infty)$ are parameters, $\alpha_r$ is a constant defined as the control price of area $A_r$. At level 1, the coordination between area $A_r$ and its neighboring areas is described by the following algebraic equation*

$$v_r = \sum_{A_q \subset A} l_{rq}(\lambda_r(t) - \lambda_q(t)) \tag{4.17a}$$

*where $\{\lambda_r(t), r \in Z_m\}$ and $l_{rq} \in [0,\infty)$ is the weight of the communication line connecting area $A_r$ and node $A_q$. $l_{rq}$ defines a weighted undirected communication network with Laplacian matrix $(L_{rq}) \in \mathbb{R}^{m\times m}$*

$$L_{rq} = \begin{cases} -l_{rq}, & r \neq q, \\ \sum_{k\neq q} l_{rk}, & r = q, \end{cases} \tag{4.18}$$



In MLPIAC, at level 2, within an area $A_r$, a central controller collects the local frequency deviation $\{\omega_i,\ i \in \mathcal{V}_M \cup \mathcal{V}_F\}$ and calculates the area control input $k_2\xi_r = \sum_{i\in\mathcal{V}_{K_r}} u_i$ by (4.16a, 4.16b), the marginal cost of $\lambda_r$ area $A_r$ by (4.16c) and the local control inputs $\{u_i,\ i \in \mathcal{V}_{K_r}\}$ by (4.16d). In the remaining of this chapter, we denote the total control input of area $A_r$ by $u_r = k_2\xi_r$.

In MLPIAC, at level 1, the central controllers of the areas exchange the marginal cost in order to achieve a consensus marginal cost which is a necessary condition for the global economic power dispatch as stated in (2.12). The weight $l_{rq}$ of the communication lines can be chosen to accelerate the consensus speed.

For the large-scale power system, the multi-level control approach (4.16) reduces to the DPIAC method (4.11) if each area consists of a single node, while it reduces to the GBPIAC method (4.10) if the entire network is controlled as a single area. Hence the DPIAC and GBPIAC methods are two special cases of MLPIAC.

In the following we focus on the properties of MLPIAC at the transient phase and steady state, which is described in Theorem (4.4.2)

**Theorem 4.4.2** *Consider a large-scale power system partitioned as in (4.15), the MLPIAC method has the following properties,*

*(a) at any time $t \in T$, the total control input $u_s$ of the system satisfies (4.7), thus it converges to $-P_s$ without any oscillations if $k_2 \geq 4k_1$;*

*(b) at any time $t \in T$, within an area $A_r$, the input values $\{u_i,\ i \in \mathcal{V}_{K_r}\}$ are computed by solving the optimization problem*

$$\begin{aligned} &\min_{\{u_i\in\mathbb{R}, i\in\mathcal{V}_{K_r}\}} \sum_{i\in\mathcal{V}_{K_r}} \frac{1}{2}\alpha_i u_i^2 \\ &s.t.\ \ -u_r(t) + \sum_{i\in\mathcal{V}_{K_r}} u_i = 0. \end{aligned} \tag{4.19}$$

*So the total control input $u_r$ is dispatched to the local controllers economically;*

*(c) if there exists a steady state as in (2.5) for the system, Problem (2.4.1) is solved, i.e., $\{\omega_i^* = 0,\ i \in \mathcal{V}_M \cup \mathcal{V}_F\}$ and the optimization problem (4.1) is solved.*

*Proof:* (a) By definition of the Laplacian matrix $(L_{rq}) \in \mathbb{R}^{m\times m}$ in (4.18), we derive that

$$\sum_{r,q\in Z_m} L_{rq}(\lambda_r - \lambda_q) = 0. \tag{4.20}$$

By summing all the equations in (2.4), it is obtained that

$$\sum_{i\in\mathcal{V}_M} M_i\dot{\omega}_i \quad = P_s - \textstyle\sum_{i\in\mathcal{V}_M\cup\mathcal{V}_F} D_i\omega_i + u_s. \tag{4.21}$$

Summing all the control inputs $\{u_r,\ r \in Z_m\}$ with $u_r = k_2\xi_r$, we derive the total control input of the system as $u_s = \sum_{r\in Z_m} k_2\xi_r$. It follows from (4.20) and (4.16b) that

$$\dot{u}_s(t) = -k_2\Big(k_1(\sum_{i\in\mathcal{V}_M} M_i\omega_i + \eta_s) + u_s(t)\Big), \tag{4.22}$$

where $\eta_s = \sum_{r\in Z_m}\eta_r$ and following (4.16a) with derivative

$$\dot{\eta}_s = \sum_{i\in\mathcal{V}_M\cup\mathcal{V}_F} D_i\omega_i \tag{4.23}$$

Let $v_s(t) = \sum_{i\in\mathcal{V}_M} M_i\omega_i + \eta_s$, we derive (4.7a) from (4.21) and (4.23), and (4.7b) from (4.22). Hence $u_s$ satisfies (4.7). Following the formula (4.8) of the eigenvalues, we derive that $u_s$ converges to $-P_s$ directly without any overshoots if $k_2 \geq 4k_1$.
(b) Following (4.16d), we derive that at any time $t \in T$,

$$\alpha_i u_i = \alpha_j u_j = \alpha_r k_2\xi_r, \forall i, j \in \mathcal{V}_{K_r}.$$

Thus the necessary condition (2.12) for the optimization problem (4.19) is satisfied. Since $\sum_{i\in\mathcal{V}_{K_r}} u_i(t) = u_r(t)$. Hence the optimization problem (4.19) is solved at any time $t$.
(c) This follows Proposition 4.4.4 directly. ■

With MLPIAC (4.16), the dynamics of the power system can also be decomposed into 4 subprocesses as that of DPIAC (4.11). However, the consensus process concerns the areas' marginal costs $\{\lambda_r, A_r \subset A\}$ with consensus speed determined by $k_3$ and $(L_{rq})$. In this case, as in DPIAC, the transient behavior of the power system controlled by MLPIAC can also be greatly improved by tuning the related coefficients of the 4 subprocesses, i.e., the primary control focuses on the synchronization of the frequencies, in which the transient behavior can be improved by tunning the parameters $\{D_i,\ i \in \mathcal{V}_M \cup \mathcal{V}_F\}$ as in [9, 59], the secondary control focuses on recovering the nominal frequency, in which the convergence of the total control input can be accelerated by a large $k_1$ eliminating the extra oscillation of the frequency, the consensus control focuses on the consensus of the marginal costs, which can be accelerated by a larger $k_3$. Note that because the optimization problem (4.1) is not solved simultaneously as in GBPIAC, the control input $u_r$ in MLPIAC may have oscillations. These oscillations can be also suppressed by a large $k_3$ as in DPIAC, which will be further analyzed in Chapter 5. Hence, Problem (2.6.1) is solved by MLPIAC. Furthermore, for a system with several areas, the number of areas is smaller than that of the nodes, the speed of achieving a consensus marginal cost of the areas is much faster than in DPIAC, and within each area, the number of nodes is smaller than the total number of nodes, the

communications and computation complexity for the area controller is decreased. Hence Problem (4.2.2) is solved by MLPIAC.

In the optimal control framework (A.3) in Appendix A.2, the control objective actually is a trade-off between the control cost and frequency deviations, which is determined by $R_1$ and $R_2$ in (A.3). In MLPIAC, because the transient performance of the frequency can be improved by tuning corresponding control gain coefficients, a trade-off between the control cost and the frequency deviation is also established, which can be determined by $k_1$ and $k_3$. This will be further discussed in Chapter 5.

Before illustrating the properties of the steady state of the power system controlled by MLPIAC, we introduce the closed-loop system as follows.

$$\dot{\theta}_i = \omega_i, i \in \mathcal{V}_M \cup \mathcal{V}_F, \tag{4.24a}$$

$$M_i\dot{\omega}_i = P_i - D_i\omega_i - \sum_{j\in\mathcal{V}} B_{ij}\sin\theta_{ij} + \frac{\alpha_r}{\alpha_i}k_2\xi_r, i \in \mathcal{V}_{M_r} \subset \mathcal{V}_M, \tag{4.24b}$$

$$0 = P_i - D_i\omega_i - \sum_{j\in\mathcal{V}} B_{ij}\sin\theta_{ij} + \frac{\alpha_r}{\alpha_i}k_2\xi_r, i \in \mathcal{V}_{Fr} \subset \mathcal{V}_F, \tag{4.24c}$$

$$0 = P_i - \sum_{j\in\mathcal{V}} B_{ij}\sin\theta_{ij}, i \in \mathcal{V}_P, \tag{4.24d}$$

$$\dot{\eta}_r = \sum_{i\in\mathcal{V}_{M_r}\cup\mathcal{V}_{F_r}} D_i\omega_i + k_2k_3\sum_{q\in Z_m} l_{rq}(\alpha_r\xi_r - \alpha_q\xi_q), r \in Z_m, \tag{4.24e}$$

$$\dot{\xi}_r = -k_1(\sum_{i\in\mathcal{V}_{M_r}} M_i\omega_i + \eta_r) - k_2\xi_r,\ r \in Z_m \tag{4.24f}$$

where $\theta_{ij} = \theta_i - \theta_j$ for $(i,j) \in \mathcal{E}$, $r$ is the index for areas defined in (4.15).

As in the Kuramoto model [19], the closed-loop system (4.24) may not have a synchronous state if the power injections $\{P_i,\ \in \mathcal{V}\}$ are much larger that the line capacity $\{B_{ij},\ (i,j) \in \mathcal{E}\}$. For more details of the synchronous state of the power systems and Kuramoto model, we refer to [9] and [62]. So we make an assumption for the power system to ensure there exists a synchronous state, which can be satisfied by reserving margins in the line capacity in tertiary control which calculates the operating point of the primary and secondary frequency control.

**Assumption 4.4.3** *For the closed-loop system (4.24), there exists a synchronous state such that $\omega_i^* = \omega_{syn}$ and*

$$\theta^* \in \Theta = \left\{\theta_i \in \mathbb{R},\ \forall i \in \mathcal{V} \middle| |\theta_i - \theta_j| < \frac{\pi}{2}, \forall (i,j) \in \mathcal{E}\right\}$$

*where the condition $\theta_i^* \in \Theta$ is commonly referred to as a security constraint [14] and restricts the space of the equilibrium to desired power flows.*

Note that the equilibria with $\theta$ out of $\Theta$ usually leads to undesired power flows which either have cyclic power flows or be unstable [62].

For the synchronous state of the closed-loop system, we have the following proposition.

**Proposition 4.4.4** *If the assumptions (2.4.3), (4.2.3) and (4.4.3) hold, then there exists at most one synchronous state for the closed-loop system (4.24) such that*

$$\theta_i^* \in \Theta,\ i \in \mathcal{V} \tag{4.25a}$$
$$\omega_i^* = 0, \mathcal{V}_M \cup \mathcal{V}_F, \tag{4.25b}$$
$$P_s + k_2 \sum_{r \in Z_m} \xi_r^* = 0, \tag{4.25c}$$
$$k_1 \eta_r^* + k_2 \xi_r^* = 0,\ r \in Z_m, \tag{4.25d}$$
$$\alpha_r \xi_r^* - \alpha_q \xi_q^* = 0,\ \forall\ r, q \in Z_m, \tag{4.25e}$$
$$\alpha_i u_i^* - k_2 \alpha_r \xi_r^* = 0,\ i \in \mathcal{V}_{K_r} \subset \mathcal{V}_K. \tag{4.25f}$$

*Proof:* If follows Theorem 4.4.2 that the dynamics of $u_s$ satisfies (4.7), which yields that $u_s^* = -P_s$ at the synchronous state. Thus (4.25c) is derived with $u_s(t) = \sum_{r \in Z_m} k_2 \xi_r(t)$. Following (2.8), we further derive that $\omega_{syn} = 0$, which yields (4.25b) with the definition of the synchronous state (2.5). By (4.24f), $\omega_i^* = 0$ and $\dot{\xi}_i^* = 0$ for all $i \in \mathcal{V}_K$, we derive (4.25d). By (4.24e) and $\omega_i^* = 0$, we obtain (4.25e). By (4.16c) and (4.16d), we arrive at (4.25f). From (4.25e,4.25f) it follows that $\alpha_i u_i^* = \alpha_j u_j^*$ for all $i, j \in \mathcal{V}_K$, thus the necessary condition (2.12) is satisfied. Following (4.25c), it yields $P + \sum_{i \in \mathcal{V}_K} u_i^* = 0$ and the economic dispatch problem (4.1) is solved subsequently. If follows [64, 65] that there exists at most one synchronous state such that $\theta_i^* \in \Theta$. ■

In the following, we focus on the asymptotic stability of MLPIAC. The power flows $\{B_{ij} \sin(\theta_{ij}),\ (i, j) \in \mathcal{E}\}$ only depend on the angle differences. As in [57], we choose a reference angle $\theta_1 \in \mathcal{V}_M$ and transform the system into a new coordinate such that

$$\varphi_i = \theta_i - \theta_1,\ i \in \mathcal{V}.$$

which yields $\dot{\varphi}_i = \omega_i - \omega_1$ for all $i$ in $\mathcal{V}_M \cup \mathcal{V}_F$. In the new coordinate, the closed-loop system (4.24) becomes

$$\dot{\varphi}_i = \omega_i - \omega_1, i \in \mathcal{V}_M \cup \mathcal{V}_F, \tag{4.26a}$$
$$M_i \dot{\omega}_i = P_i - D_i \omega_i - \sum_{j \in \mathcal{V}} B_{ij} \sin \varphi_{ij} + \frac{\alpha_r}{\alpha_i} k_2 \xi_r,\ i \in \mathcal{V}_M, \tag{4.26b}$$
$$D_i \dot{\varphi}_i = P_i - D_i \omega_1 - \sum_{j \in \mathcal{V}} B_{ij} \sin \varphi_{ij} + \frac{\alpha_r}{\alpha_i} k_2 \xi_r,\ i \in \mathcal{V}_F, \tag{4.26c}$$
$$0 = P_i - \sum_{j \in \mathcal{V}} B_{ij} \sin \varphi_{ij},\ i \in \mathcal{V}_P, \tag{4.26d}$$
$$\dot{\eta}_r = \sum_{i \in \mathcal{V}_{M_r} \cup \mathcal{V}_{F_r}} D_i \omega_i + k_2 k_3 \sum_{q \in Z_m} l_{rq} (\alpha_r \xi_r - \alpha_q \xi_q),\ r \in Z_m, \tag{4.26e}$$
$$\dot{\xi}_r = -k_1 \Big( \sum_{i \in \mathcal{V}_{M_r}} M_i \omega_i + \eta_r \Big) - k_2 \xi_r,\ r \in Z_m \tag{4.26f}$$

which is in the form of DAEs (A.1) in Appendix A.1, i.e., the algebraic equations are (4.26d) and algebraic variables are $\varphi_i, i \in \mathcal{V}_P$. Following Assumption (4.4.3), $\varphi_i$ satisfies

$$\varphi \in \Phi = \Big\{ \varphi_i \in \mathbb{R}, i \in \mathcal{V} \,||\varphi_i - \varphi_j| \le \frac{\pi}{2}, \forall (i, j) \in \mathcal{E},\ \varphi_1 = 0 \Big\}.$$

We make the following assumption on the control gain coefficients $k_1, k_2, k_3$, which will be proven as a sufficient condition of the asymptotic stability of MLPIAC in subsection 4.5.2.

**Assumption 4.4.5** *Assume the control gain coefficients, $k_1, k_2, k_3$, satisfy that*

$$\frac{k_2}{k_1} > \frac{2(\alpha D)_{\max}}{(\alpha D)_{\min}(1+2k_3\lambda_{\min})}$$

where $(\alpha D)_{\min} = \min\{\alpha_i D_i,\ i \in \mathcal{V}_K\}$, $(\alpha D)_{\max} = \max\{\alpha_i D_i,\ i \in \mathcal{V}_K\}$ and $\lambda_{\min}$ is the smallest nonzero eigenvalue of matrix $L\alpha_R$ where $L = (L_{rq}) \in \mathbb{R}^{m\times m}$ is defined in (4.18) and $\alpha_R = \mathrm{diag}(\alpha_r) \in \mathbb{R}^{m\times m}$.

We rewrite the state and algebraic variables into a vector form, $(\varphi, \omega, \eta, \xi) \in \mathbb{R}^{n_t} \times \mathbb{R}^n \times \mathbb{R}^m \times \mathbb{R}^m$. The following theorem illustrates the asymptotic stability of the equilibrium of MLPIAC.

**Theorem 4.4.6** *If assumptions (2.4.3,4.2.3,4.4.3) and (4.4.5) hold, then for the closed-loop system (4.24),*

*(a) there exists an unique equilibrium state $z^* = (\varphi^*, \omega^*, \eta^*, \xi^*) \in \Psi$ where $\Psi = \Phi \times \mathbb{R}^n \times \mathbb{R}^m \times \mathbb{R}^m$.*

*(b) there exists a domain $\Psi^d \subset \Psi$ such that for any initial state $z^0 \in \Psi^d$ that satisfies the algebraic equations (4.26d), the state trajectory converges to the unique equilibrium state $z^* \in \Psi$.*

The proof of Theorem (4.4.6) is provided in Subsection 4.5.2.

**Remark 4.4.7** *In MLPIAC, Assumptions (2.4.3, 4.2.3, 4.4.3) and (4.4.5) are both necessary and realistic at the same time. Assumptions (2.4.3) and (4.2.3) are necessary for the implementation of MLPIAC to solve Problem 2.4.1. Assumptions (4.4.3) and (4.4.5) are general sufficient conditions for the stability of MLPIAC. Assumption (2.4.3) and (4.4.3) can be guaranteed by tertiary control and Assumption (4.2.3) by an effective communication infrastructure. Regarding Assumption (4.4.5), we refer to Remark (4.4.8).*

**Remark 4.4.8** *The inverse of damping coefficient, $\frac{1}{D_i}$, can be viewed as the control cost of primary control [9]. When $\alpha = \gamma D^{-1}$, $\gamma \in \mathbb{R}$ is a positive number, which indicates the secondary frequency control prices are proportional to the primary control price and leads to $(\alpha D)_{\min} = (\alpha D)_{\max}$, DPIAC is asymptotically stable if $k_2 > 2k_1$. Specially, Assumption (4.4.5) is relaxed in the GBPIAC method in the theoretical analysis as will be explained in Remark (4.5.5) in Subsection 4.5.2. For DPIAC and MLPIAC, our initial numerical simulations and numerical eigenvalue analysis of the linearized system of (4.24) have shown that the control law is asymptotically stable even though Assumption (4.4.5) is not satisfied. This will be shown in Section 4.6.*

**Remark 4.4.9** *The principle in PIAC and DPIAC to eliminate the extra frequency oscillations caused by the controllers is to let the $u_s$ converge to $-P_s$ directly. Because the total control input $u_s$ satisfies (3.5), which is different from (4.7) in DPIAC, PIAC is not compatible with DPIAC in the multi-level control where the areas cooperate with each other*

*to minimize the control cost of the whole network. However, they are compatible for the power system with multi areas which is controlled in a non-cooperative way as the multi-area control method in [69]. In that case, the controllers in an area only respond to the disturbances occurring in the area.*

**Remark 4.4.10** *MLPIAC actually includes proportional and integral control input, which are the terms $k_1 \sum_{i\in\mathcal{V}_{M_r}} M_i\omega_i$ and $k_1\eta_r$ respectively in (4.16b). In order to get a desired performance, the parameters $M_i$ and $D_i$ should be known. In practice, they are known for traditional synchronous machines [6]. However, they may not be known for the frequency dependent nodes. In that case, the uncertainties from these parameter can be added to the power-imbalance, which becomes a time-varying value and can be compensated by the controllers at the steady state because of the included integral control input. Theoretical analysis on the robustness of MLPIAC with these uncertainties needs to be further studied.*

4

## 4.5. ASYMPTOTIC STABILITY OF MLPIAC

In this section, we provide the proof of Theorem 4.4.6 in Section 4.4. For simplicity of expression, we introduce the notations in Subsection 4.5.1 for the analysis in Subsection 4.5.2.

### 4.5.1. NOTATIONS & SYMMETRIZABLE MATRIX

Denote the number of nodes in the sets $\mathcal{V}_M, \mathcal{V}_F, \mathcal{V}_P$ and $\mathcal{V}_K$ by $n_m, n_f, n_p, n$ respectively, the total number of buses in the power system by $n_t$. So $n = n_m + n_f$ and $n_t = n_m + n_f + n_p$.

To express simply, we write a diagonal matrix $\beta = \mathrm{diag}(\{\beta_i, i\cdots n\}) \in \mathbb{R}^{n\times n}$ with $\beta_i \in \mathbb{R}$ as $\mathrm{diag}(\beta_i)$. It is convenient to introduce the matrices $D = \mathrm{diag}(D_i) \in \mathbb{R}^{n\times n}$, $M = \mathrm{diag}(M_i) \in \mathbb{R}^{n\times n}$, $\alpha = \mathrm{diag}(\alpha_i) \in \mathbb{R}^{n\times n}$. Denote the identity matrix by $I_n \in \mathbb{R}^{n\times n}$. Note that $M_i = 0$ for $i \in \mathcal{V}_F$ and $M_i > 0$ for $i \in \mathcal{V}_M$. Denote the $n$ dimension vector with all elements equal to one by $1_n$. Denote $\theta = \mathrm{col}(\theta_i) \in \mathbb{R}^{n_t}$, $\omega = \mathrm{col}(\omega_i) \in \mathbb{R}^n$, $P = \mathrm{col}(P_i) \in \mathbb{R}^{n_t}$ and $\varphi = \mathrm{col}(\varphi_i) \in \mathbb{R}^{n_t}$ where $\varphi_i = \theta_i - \theta_1$ for all $i \in \mathcal{V}$. Denote $\eta = \mathrm{col}(\eta_i) \in \mathbb{R}^n, \xi = \mathrm{col}(\xi_i) \in \mathbb{R}^n$.

The number of areas is denoted by $m$, the control price of area $r$ is $\alpha_r$. Denote $\alpha_R = \mathrm{diag}(\alpha_r) \in \mathbb{R}^{m\times m}$. Define matrix $R = (r_{ir}) \in \mathbb{R}^{n\times m}$ with $r_{ir} = 1$ if node $i$ belongs to area $r$, otherwise $r_{ir} = 0$. Note that $\alpha, \alpha_R, R$ satisfy

$$R^T\alpha^{-1}R = \alpha_R^{-1}, \tag{4.27a}$$

$$1_n = R1_m. \tag{4.27b}$$

Denote $L \in \mathbb{R}^{m\times m}$ as the Laplacian matrix of the communication network as defined in (4.18).

For symmetric matrices $A$ and $B$, we say $A > 0$ (or $A \geq 0$ if $A$ is positive-definite (or semi-positive-definite), and say $A > B$ (or $A \geq B$) if $(A - B)$ is positive-definite (or semi-positive-definite).

The following inequality is used frequently in the following stability analysis of the control laws. For any $x \in \mathbb{R}^m, y \in \mathbb{R}^m$, the following inequality holds

$$x^T y \leq \frac{1}{2}x^T\varepsilon x + \frac{1}{2}y^T\varepsilon^{-1}y,$$

where $\varepsilon \in \mathbb{R}^{m\times m}$ is an invertible positive-definite diagonal matrix. The inequality follows from

$$\begin{bmatrix} x \\ y \end{bmatrix}^T \begin{bmatrix} \varepsilon & -I_m \\ -I_m & \varepsilon^{-1} \end{bmatrix} \begin{bmatrix} x \\ y \end{bmatrix} \geq 0.$$

For the asymptotic stability analysis of MLPIAC, we introduce the properties of a *symmetrizable matrix* defined as follows.

**Definition 4.5.1** *A matrix $B \in \mathbb{R}^{m\times m}$ is* symmetrizable *if there exists a positive-definite invertible diagonal matrix $A \in \mathbb{R}^{m\times m}$ and a symmetric matrix $L \in \mathbb{R}^{m\times m}$ such that $B = LA$.*

**Theorem 4.5.2** *Consider the Laplaciam matrix $L \in \mathbb{R}^{m\times m}$ as defined in (4.18) and the positive-definite diagonal matrix $\alpha_R \in \mathbb{R}^{m\times m}$ as defined in Subsection (4.5.1). The matrix $L\alpha_R$ is a symmetrizable matrix and there exists an invertible matrix $Q$ such that*

$$Q^{-1}L\alpha_R Q = \Lambda, \tag{4.28}$$

*where $\Lambda = diag(\lambda_i) \in \mathbb{R}^{m\times m}$, $\lambda_i$ is the eigenvalue of $L\alpha$ and $\lambda_1 = 0$.*

*Denote $Q^{-1} = [Q_{v1}, Q_{v2}, \cdots, Q_{vm}]^T$ and $Q = [Q_1, Q_2, \cdots, Q_m]$, we have*

$$Q_{v1} = 1_m, \tag{4.29a}$$
$$\alpha_R Q_1 = 1_m, \tag{4.29b}$$
$$Q^T \alpha_R Q = I_m, \tag{4.29c}$$
$$Q^{-1}\alpha_R^{-1}(Q^{-1})^T = I_m, \tag{4.29d}$$
$$Q^{-1} = Q^T \alpha_R. \tag{4.29e}$$

*Furthermore, the new matrix $W = [Q_{v2}, \cdots, Q_{vm}] \in \mathbb{R}^{n\times(m-1)}$ and $S = [Q_2, \cdots, Q_m] \in \mathbb{R}^{m\times(m-1)}$ satisfy that*

$$W^T S = I_{(m-1)}, \tag{4.30a}$$
$$W^T \alpha_R^{-1} W = I_{(m-1)}, \tag{4.30b}$$
$$S^T \alpha_R S = I_{(m-1)}, \tag{4.30c}$$
$$Q_{vi} = \alpha_R Q_i, \tag{4.30d}$$
$$W = \alpha_R S. \tag{4.30e}$$

*Proof*: Let $T = \sqrt{\alpha_R}$ which is a diagonal matrix, then

$$TL\alpha_R T^{-1} = \sqrt{\alpha_R} L \sqrt{\alpha_R}.$$

Hence, there exists an invertible matrix $\Gamma^{-1} = \Gamma^T$ such that

$$\Gamma^{-1} T L \alpha_R T^{-1} \Gamma = \Gamma^{-1} \sqrt{\alpha_R} L \sqrt{\alpha_R} \Gamma = \Lambda.$$

Let $Q = T^{-1}\Gamma$, we derive $Q^{-1}L\alpha_R Q = \Lambda$. Since $L$ is a Laplacian matrix as defined in (4.18), we have $1_m^T L\alpha_R = 0$, then there is a zero eigenvalue, i.e., $\lambda_1 = 0$. Denote $\Gamma = [\Gamma_1, \Gamma_2, \cdots, \Gamma_m]$, then $\Gamma^{-1} = \Gamma^T = [\Gamma_1, \Gamma_2, \cdots, \Gamma_m]^T$.

Since $\Gamma_1$ is the eigenvector corresponding to $\lambda_1 = 0$ of $\sqrt{\alpha_R}L\sqrt{\alpha_R}$ such that $L\sqrt{\alpha_R}\Gamma_1 = 0$, from which we derive $\sqrt{\alpha_R}\Gamma_1 = 1_m$. Hence by $Q = T^{-1}\Gamma$, we obtain $Q_1 = (\sqrt{\alpha_R})^{-1}\Gamma_1 = \alpha_R^{-1}1_m$. Similarly we derive $Q_{v1} = \Gamma_1^T T = \Gamma^T\sqrt{\alpha_R} = \sqrt{\alpha_R}\Gamma_1 = 1_m$.

By $Q = T^{-1}\Gamma$, we derive $\Gamma^T\alpha_R Q = \Gamma^T T^{-1}\alpha_R T^{-1}\Gamma = I_m$. $Q^{-1}\alpha_R^{-1}(Q^{-1})^T = R^T R = I_m$ can be obtained similarly.

(4.30a) is yielded directly from $Q^{-1}Q = I_m$. (4.29c) and (4.29d) yields ( 4.30b) and (4.30c). ■

### 4.5.2. ASYMPTOTIC STABILITY ANALYSIS

In this subsection, we provide the proof of Theorem (4.4.6) for MLPIAC. The closed-loop system (4.26) is rewritten in a vector form as follows,

$$\dot{\tilde{\varphi}} = \omega - \omega_1 1_n, \tag{4.31a}$$

$$M\dot{\omega} = P - D\omega - P^t + k_2\alpha^{-1}R\alpha_R\xi, \tag{4.31b}$$

$$0 = \tilde{P} - \tilde{P}^t, \tag{4.31c}$$

$$\dot{\eta} = R^T D\omega + k_2 k_3 L\alpha_R\xi, \tag{4.31d}$$

$$\dot{\xi} = -k_1(R^T M\omega + \eta) - k_2\xi, \tag{4.31e}$$

where $\tilde{\varphi} = \mathrm{col}(\varphi_i)$ with $i \in \mathcal{V}_M \cup \mathcal{V}_F$, $P = \mathrm{col}(P_i) \in \mathbb{R}^n$ for $i \in \mathcal{V}_M \cup \mathcal{V}_F$, $\tilde{P} = \mathrm{col}(P_j) \in \mathbb{R}^{n_p}$ for $j \in \mathcal{V}_P$, $P^t = \mathrm{col}(P_i^t) \in \mathbb{R}^n$ with $P_i^t = \sum_{j\in\mathcal{V}} B_{ij}\sin\varphi_{ij}$ for $i \in \mathcal{V}_M \cup \mathcal{V}_F$, $\tilde{P}^t = \mathrm{col}(\tilde{P}_i^t) \in \mathbb{R}^{n_p}$ with $\tilde{P}_i^t = \sum_{j\in\mathcal{V}} B_{ij}\sin\varphi_{ij}$ for $i \in \mathcal{V}_P$. Note that $\tilde{\varphi}$ only includes the variables $\{\varphi_i, i \in \mathcal{V}_M \cup \mathcal{V}_F\}$ while $\varphi$ defined in Subsection 4.5.1 includes $\{\varphi_i, i \in \mathcal{V}\}$. For the definitions of $M, D, R, \alpha_R$, we refer to Subsection 4.5.1.

We transform the control law (4.31d,4.31e) to a new coordinate as a preparation for the stability analysis of DPIAC. Following Theorem 4.5.2, let $\rho = Q^{-1}\eta$ and $\sigma = Q^{-1}\xi$. The vector form (4.31d,4.31e) becomes

$$\dot{\rho} = Q^{-1}R^T D\omega + k_2 k_3\Lambda\sigma,$$
$$\dot{\sigma} = -k_1 Q^{-1}R^T M\omega - k_1\rho - k_2\sigma,$$

where all the components $(\rho_i,\ \sigma_i)$ of $(\rho,\ \sigma)$ are decoupled from each other. When writing the dynamics of $(\rho_i,\ \sigma_i)$ separately, we derive

$$\dot{\rho}_i = Q_{vi}^T R^T D\omega + k_2 k_3\lambda_i\sigma_i, \tag{4.33a}$$

$$\dot{\sigma}_i = -k_1 Q_{vi}^T R^T M\omega - k_1\rho_i - k_2\sigma_i, \tag{4.33b}$$

where $Q^{-1}$ is decomposed into vectors, i.e., $Q^{-1} = (Q_{v1}, Q_{v2}, \cdots, Q_{vn})$. In (4.33), the controller of component $i$ calculates the output $\sigma_i$ with the input $\omega$ for the power system. In the following, we investigate the dynamic behavior of the component $(\rho_1, \sigma_1)$ and $\{(\rho_i, \sigma_i),\ i = 2, \cdots, n\}$ of $(\rho, \sigma)$ respectively.

For the first component $(\rho_1, \sigma_1)$ of $(\rho, \sigma)$, we have the following lemma.

**Lemma 4.5.3** *The dynamics of $(\rho_1, \sigma_1)$ described by (4.33) is identical to that of $(\eta_s, \xi_s)$ in (4.10) if they have the same initial values.*

*Proof:* By (4.33) and (4.27b), $\lambda_1 = 0$ and $Q_{vi} = 1_m$ from (4.30a), we derive the dynamics of $(\rho_1, \sigma_1)$ as follows

$$\dot{\rho}_1 = 1_m R^T D\omega = \sum_{i \in \mathcal{V}_M \cup \mathcal{V}_F} D_i \omega_i, \tag{4.34a}$$

$$\dot{\sigma}_1 = -k_1(1_m R^T M\omega + \rho_1) - k_2\sigma_1 \tag{4.34b}$$

$$= -k_1(\sum_{i \in \mathcal{V}_M} M_i\omega_i + \rho_1) - k_2\sigma_1. \tag{4.34c}$$

In addition, by summing all the equations in (4.31b), (4.31b) for all $i \in \mathcal{V}$, we derive

$$\begin{aligned}\sum_{i \in \mathcal{V}_M} M_i\dot{\omega}_i &= P_s - \sum_{i \in \mathcal{V}_M \cup \mathcal{V}_F} D_i\omega_i + k_2 1_n^T \alpha^{-1} R \alpha_R \xi \\ &\quad \text{by (4.27)} \\ &= P_s - \sum_{i \in \mathcal{V}_M \cup \mathcal{V}_F} D_i\omega_i + k_2 1_m^T \xi \\ &\quad \text{by (4.29a)} \\ &= P_s - \sum_{i \in \mathcal{V}_M \cup \mathcal{V}_F} D_i\omega_i + k_2\sigma_1. \end{aligned} \tag{4.35}$$

So $k_2\sigma_1$ is the control input for the power system (2.4) as $k_2\xi_s$. Furthermore, the initial values of $(\rho_1, \sigma_1)$ and $(\eta_s, \xi_s)$ are identical, which are both computed from $\{\omega_i(0), i \in \mathcal{V}_K\}$, so the dynamics of $(\rho_1, \sigma_1)$ is identical to that of $(\eta_s, \xi_s)$ in (4.10) if they have the same initial values. ■

As described in Remark 4.4.10, MLPIAC includes proportional and integral control input. With the superposition principle, we decompose the dynamics of $(\rho_i, \sigma_i)$ for $i = 2, \cdots, m$ for the proportional and the integral input into the following two independent dynamics.

$$\begin{aligned}\dot{\rho}_{mi} &= k_2 k_3 \lambda_i \sigma_{mi}, \\ \dot{\sigma}_{mi} &= -k_1 Q_{vi}^T R^T M\omega - k_1\rho_{mi} - k_2\sigma_{mi},\end{aligned}$$

and

$$\begin{aligned}\dot{\rho}_{di} &= Q_{vi}^T R^T D\omega + k_2 k_3 \lambda_i \sigma_{di}, \\ \dot{\sigma}_{di} &= -k_1\rho_{di} - k_2\sigma_{di},\end{aligned}$$

from which it can be easily derived that $\rho_i = \rho_{mi} + \rho_{di}$ and $\sigma_i = \sigma_{mi} + \sigma_{di}$.

In the coordinate of $(\varphi, \omega, \rho_1, \sigma_1, \rho_m, \sigma_m, \rho_d, \sigma_d)$, the closed-loop system (4.31) be-

comes

$$\dot{\tilde{\varphi}} = \omega - \omega_1 1_n, \tag{4.38a}$$
$$M\dot{\omega} = P - D\omega - P^t + k_2\alpha^{-1}R\alpha_R Q\sigma, \tag{4.38b}$$
$$0 = \tilde{P} - \tilde{P}^t, \tag{4.38c}$$
$$\dot{\rho}_1 = 1_m^T R^T D\omega, \tag{4.38d}$$
$$\dot{\sigma}_1 = -k_1 1_m^T R^T M\omega - k_1\rho_1 - k_2\sigma_1, \tag{4.38e}$$
$$\dot{\rho}_m = k_2 k_3 \Lambda\sigma_m, \tag{4.38f}$$
$$\dot{\sigma}_m = -k_1 W^T R^T M\omega - k_1\rho_m - k_2\sigma_m, \tag{4.38g}$$
$$\dot{\rho}_d = W^T R^T D\omega + k_2 k_3 \Lambda\sigma_d, \tag{4.38h}$$
$$\dot{\sigma}_d = -k_1\rho_d - k_2\sigma_d, \tag{4.38i}$$

where $\sigma = \mathrm{col}(\rho_i)$, $\rho_i = \rho_{mi} + \rho_{di}$ for $i = 2, \cdots, m$, $W$ is defined as in Theorem (4.5.2). Note that $\Lambda \in \mathbb{R}^{(m-1)\times(m-1)}$ only includes the nonzero eigenvalues of $L\alpha_R$, which is different from the one in Subsection 4.5.1.

Following Proposition (4.4.4), for the closed-loop system (4.38) we have the following Lemma on the equilibrium state.

**Lemma 4.5.4** *In the coordinate of* $(\varphi, \omega, \rho_1, \sigma_1, \rho_m, \sigma_m, \rho_d, \sigma_d)$*, the unique equilibrium state* $(\theta^*, \omega^*, \eta^*, \xi^*)$ *of the closed-loop system (4.24) proposed in Proposition (4.4.4) is equivalent to* $(\varphi^*, \omega^*, \rho_1^*, \sigma_1^*, \rho_m^*, \sigma_m^*, \rho_d^*, \sigma_d^*) \in \Phi \times \mathbb{R}^n \times \mathbb{R} \times \mathbb{R} \times \mathbb{R}^{m-1} \times \mathbb{R}^{m-1} \times \mathbb{R}^{m-1} \times \mathbb{R}^{m-1}$ *such that*

$$\varphi^* \in \Phi = \left\{\varphi \in \mathbb{R}^{n_t} \middle| |\varphi_i - \varphi_j| < \frac{\pi}{2},\ \forall (i,j) \in \mathscr{E}, \varphi_1 = 0\right\}, \tag{4.39a}$$
$$\omega_i^* = 0,\ i \in \mathcal{V}_M \cup \mathcal{V}_F, \tag{4.39b}$$
$$k_1\rho_1^* + k_2\sigma_1^* = 0, \tag{4.39c}$$
$$k_2\sigma_1^* + P_s = 0, \tag{4.39d}$$
$$\rho_{mi}^* = 0,\ i = 2, \cdots, n, \tag{4.39e}$$
$$\sigma_{mi}^* = 0,\ i = 2, \cdots, n, \tag{4.39f}$$
$$\rho_{di}^* = 0,\ i = 2, \cdots, n, \tag{4.39g}$$
$$\sigma_{di}^* = 0,\ i = 2, \cdots, n, \tag{4.39h}$$

*Proof:* When mapping $\theta$ to $\varphi$, we can easily obtain $\varphi \in \Phi = \left\{\varphi \in \mathbb{R}^{n_t} \middle| |\varphi_i - \varphi_j| < \frac{\pi}{2},\ \forall (i,j) \in \mathscr{E}, \varphi_1 = 0\right\}$, $\omega^* = 0$ can be directly derived from Proposition (4.4.4).

By Lemma (4.5.3), we have $(\rho_1^*, \sigma_1^*) = (\eta_s^*, \sigma_s^*)$ at the steady state, which yields (4.39c) and (4.39d).

By the dynamics (4.33) of $(\rho_{mi}, \sigma_{mi})$ and that of $(\rho_{di}, \sigma_{di})$, we derive that $(\rho_{mi}^*, \sigma_{mi}^*) = (0,0)$ and $(\rho_{di}^*, \sigma_{di}^*) = (0,0)$ for all $i = 2, \cdots, n$, at the steady state, which lead to (4.39e)-(4.39h). ■

In order to prove the asymptotic stability of the equilibrium $(\theta^*, \omega^*, \eta^*, \xi^*)$, we only need to prove the asymptotic stability of the equilibrium $(\varphi^*, \omega^*, \rho_1^*, \sigma_1^*, \rho_m^*, \sigma_m^*, \rho_d^*, \sigma_d^*)$.

We define function

$$U(\varphi) = \sum_{(i,j)\in\mathcal{E}} B_{ij}(1-\cos(\varphi_i - \varphi_j)) \tag{4.40}$$

and variable $v_s = \sum_{i\in\mathcal{V}_M} M_i\omega_i + \rho_1$. By (4.35) and (4.34), we obtain dynamics of $(v_s, \sigma_1)$,

$$\dot{v}_s = P_s + k_2\sigma_1, \tag{4.41a}$$
$$\dot{\sigma}_1 = -k_1 v_s - k_2\sigma_1, \tag{4.41b}$$

with equilibrium state $(v_s^*, \sigma_1^*) = (\frac{1}{k_1}P_s, -\frac{1}{k_2}P_s)$.

In the following, we prove the equilibrium $(\theta^*, \omega^*, \rho_1^*, \sigma_1^*, \rho_m^*, \sigma_m^*, \rho_d^*, \sigma_d^*)$. is locally asymptotically stable following Lyapunov method.

*Proof of Theorem (4.4.6):* Since the closed-loop system (4.24) is equivalent to (4.38), we prove the equilibrium $(\varphi^*, \omega^*, \rho_1^*, \sigma_1^*, \rho_m^*, \sigma_m^*, \rho_d^*, \sigma_d^*)$ of (4.38) is locally asymptotically stable. The proof follows Theorem (A.1.3). It follows [57, Lemma 5.2] that the algebraic equations (4.26d) are regular. In addition, there exists an unique equilibrium for the closed-loop system (4.38) following Lemma (4.5.4), we only need to find a Lyapunov function $V(x, y)$ as in Theorem (A.1.3).

Before introducing the Lyapunov function candidate, we define the following functions.

$$\begin{aligned}
V_0 &= U(\varphi) - U(\varphi^*) - \nabla_\varphi U(\varphi^*)(\varphi - \varphi^*) + \frac{1}{2}\omega^T M\omega,\\
V_1 &= (c_1+1)\Big(\frac{1}{2k_1}(k_1 v_s - k_1 v_s^*)^2 + \frac{1}{2k_2}(k_2\sigma_1 - k_2\sigma_1^*)^2\Big)\\
&\quad + \frac{1}{2k_2}(k_2\sigma_1 - k_2\sigma_1^*)^2 + \frac{1}{2k_1}(k_1 v_s + k_2\sigma_1)^2,
\end{aligned}$$

where $c_1 \in \mathbb{R}$ and $k_1 v_s^* + k_2\sigma_1^* = 0$ has been used. Denote $x_m = k_1\rho_m$, $y_m = k_2\sigma_m$, $z_m = k_1\rho_m + k_2\sigma_m$, $x_d = k_1\rho_d$, $y_d = k_2\sigma_d$, $z_d = k_1\rho_d + k_2\sigma_d$ and define

$$\begin{aligned}
V_m &= \frac{\beta_m}{2}x_m^T C_m x_m + \frac{(1+\beta_m)k_1k_3}{2k_2}y_m^T C_m\Lambda y_m + \frac{1}{2}z_m^T C_m z_m,\\
V_d &= \frac{\beta_d c_d}{2}x_d^T x_d + \frac{(1+\beta_d)c_d k_1 k_3}{2k_2}y_d^T\Lambda y_d + \frac{c_d}{2}z_d^T z_d,
\end{aligned}$$

where $\beta_m \in \mathbb{R}$, $\beta_d \in \mathbb{R}$, $c_d \in \mathbb{R}$ are positive and $C_m = \mathrm{diag}(c_{mi}) \in \mathbb{R}^{(m-1)\times(m-1)}$ with all the diagonal elements $c_{mi} > 0$, and $\Lambda \in \mathbb{R}^{(m-1)\times(m-1)}$ is a diagonal matrix with diagonal elements being the nonzero eigenvalues of $L\alpha_R$.

In the following, we focus on the derivatives of the functions $V_0, V_1, V_m, V_d$. The deriva-

tive of $V_0$ is

$$\begin{aligned}
\dot{V}_0 &= -\omega^T D\omega + (k_2\sigma - k_2\sigma^*)^T Q^T \alpha_R R^T \alpha^{-1}\omega \\
&\quad \text{by } Q = [Q_1, Q_2, \cdots, Q_n] \text{ and } S = [Q_2, \cdots, Q_n]. \\
&= -\omega^T D\omega + (k_2\sigma_1 - k_2\sigma_1^*)Q_1^T \alpha_R R^T \alpha^{-1}\omega + (k_2\sigma - k_2\sigma^*)^T S^T \alpha_R R^T \alpha^{-1}\omega \\
&= -\omega^T D\omega + (k_2\sigma_1 - k_2\sigma_1^*)Q_1^T \alpha_R R^T \alpha^{-1}\omega + (k_2\sigma_m - k_2\sigma_m^*)^T S^T \alpha_R R^T \alpha^{-1}\omega \\
&\quad + (k_2\sigma_d - k_2\sigma_d^*)^T S^T \alpha_R R^T \alpha^{-1}\omega, \\
&\quad \text{by } S^T\alpha_R = W^T,\ Q_1^T\alpha_R = Q_{v_1}^T,\ \sigma_m^* = 0 \\
&= -\omega^T D\omega + (k_2\sigma_1 - k_2\sigma_1^*)Q_{v_1}^T R^T \alpha^{-1}\omega + (k_2\sigma_m)^T W^T R^T \alpha^{-1}\omega + (k_2\sigma_d)^T W^T R^T \alpha^{-1}\omega \\
&= -\omega^T D\omega + (k_2\sigma_1 - k_2\sigma_1^*)Q_{v_1}^T R^T \alpha^{-1}\omega + y_m^T W^T R^T \alpha^{-1}\omega + y_d^T W^T R^T \alpha^{-1}\omega.
\end{aligned}$$

The derivative of $V_1$ is

$$\begin{aligned}
\dot{V}_1 &= -(c_1+1)(k_2\sigma_1 - k_2\sigma_1^*)^2 - \frac{k_2}{k_1}(k_1 v + k_2\sigma_1)^2 \\
&\quad \text{plus a term and minus it} \\
&= -(k_2\sigma_1 - k_2\sigma_1^*)Q_{v1}^T R^T \alpha^{-1}\omega + (k_2\sigma_1 - k_2\sigma_1^*)Q_{v1}^T R^T \alpha^{-1}\omega \\
&\quad - (c_1+1)(k_2\sigma_1 - k_2\sigma_1^*)^2 - \frac{k_2}{k_1}(k_1 v + k_2\sigma_1)^2.
\end{aligned}$$

By inequalities

$$(k_2\sigma_1 - k_2\sigma_1^*)Q_{v1}^T R^T \alpha^{-1}\omega \le \frac{1}{8}\omega^T \epsilon D\omega + 2(k_2\sigma_1 - k_2\sigma_1^*)^2 Q_{v1}^T R^T \alpha^{-2}(\epsilon D)^{-1} R Q_{v1},$$

we obtain

$$\begin{aligned}
\dot{V}_1 &\le -(k_2\sigma_1 - k_2\sigma_1^*)Q_{v1}^T R^T \alpha^{-1}\omega + \frac{1}{8}\omega^T \epsilon D\omega + 2(k_2\sigma_1 - k_2\sigma_1^*)^2 Q_{v1}^T R^T \alpha^{-2}(\epsilon D)^{-1} R Q_{v1} \\
&\quad - (c_1+1)(k_2\sigma_1 - k_2\sigma_1^*)^2 - \frac{k_2}{k_1}(k_1 v_s + k_2\sigma_1)^2 \\
&\quad \text{let } c_1 = 2Q_{v1}^T R^T \alpha^{-2}(\epsilon D)^{-1} R Q_{v1} \\
&= -(k_2\sigma_1 - k_2\sigma_1^*)Q_{v1}^T R^T \alpha^{-1}\omega + \frac{1}{8}\omega^T \epsilon D\omega - (k_2\sigma_1 - k_2\sigma_1^*)^2 - \frac{k_2}{k_1}(k_1 v + k_2\sigma_1)^2.
\end{aligned}$$

The derivative of $V_m$ is

$$\begin{aligned}
\dot{V}_m &= -k_2 z_m^T C_m z_m - \beta_m k_1 k_3 y_m^T C_m \Lambda y_m - k_1 k_2 z_m^T C_m W^T R^T M\omega \\
&\quad - (1+\beta_m) k_1^2 k_3 y_m^T C_m \Lambda W^T R^T M\omega \\
&= -y_m^T W^T R^T \alpha^{-1}\omega + y_m^T W^T R^T \alpha^{-1}\omega - k_2 z_m^T C_m z_m - \beta_m k_1 k_3 y_m^T C_m \Lambda y_m \\
&\quad - k_1 k_2 z_m^T C_m W^T R^T M\omega - (1+\beta_m) k_1^2 k_3 y_m^T C_m \Lambda W^T R^T M\omega \\
&= -y_m^T W^T R^T \alpha^{-1}\omega + \sum_{i=2}^{n} y_{mi} Q_{vi}^T R^T \alpha^{-1}\omega - k_2 \sum_{i=2}^{n} c_{mi} z_{mi}^2 - \beta_m k_1 k_3 \sum_{i=2}^{n} c_{mi}\lambda_i y_{mi}^2 \\
&\quad - k_1 k_2 \sum_{i=2}^{n} c_{mi} z_{mi} Q_{vi}^T R^T M\omega - (1+\beta_m) k_1^2 k_3 \sum_{i=2}^{n} \left( c_{mi}\lambda_i y_{mi} Q_{vi}^T R^T M\omega \right) \\
&= -y_m^T W^T R^T \alpha^{-1}\omega - k_2 \sum_{i=2}^{n} c_{mi} z_{mi}^2 - \beta_m k_1 k_3 \sum_{i=2}^{n} c_{mi}\lambda_i y_m^2 \\
&\quad - k_1 k_2 \sum_{i=2}^{n} \left( c_{mi} z_{mi} Q_{vi}^T R^T M\omega \right) + \sum_{i=2}^{n} y_{mi} \left( Q_{vi}^T R^T \alpha^{-1} - Q_{vi}^T (1+\beta_m) k_1^2 k_3 c_{mi}\lambda_i R^T M \right)\omega.
\end{aligned}$$

By the following inequalities

$$k_1 k_2 c_{mi} z_{mi} Q_{vi}^T R^T M\omega \le \frac{\omega^T \epsilon D \omega}{8(n-1)} + r_m z_{mi}^2,$$

where $r_z = 2(n-1)(k_1 k_2 c_{mi})^2 Q_{vi}^T R^T (D\epsilon)^{-1} M^2 R Q_{vi}$, and

$$y_{mi} Q_{vi}^T R^T \left( \alpha^{-1} - (1+\beta_m) k_1^2 k_3 c_{mi}\lambda_i M \right)\omega \le \frac{\omega^T \epsilon D \omega}{8(n-1)} + r_z y_{mi}^2,$$

where

$$r_y = 2(n-1) Q_{vi}^T R^T \left( (\alpha^{-1} - (1+\beta_m) k_1^2 k_3 c_{mi}\lambda_i M \right)^2 (\epsilon D)^{-1} R Q_{vi},$$

we obtain

$$\dot{V}_m \le -y_m^T W^T R^T \alpha^{-1}\omega + \frac{1}{4}\omega^T \epsilon D \omega - \sum_{i=2}^{n} z_{mi}^2 (k_2 c_{mi} - r_z) - \sum_{i=2}^{n} y_{mi}^2 (\beta_m k_1 k_3 c_{mi}\lambda_i - r_y).$$

The derivative of $V_d$ is

$$\begin{aligned}
\dot{V}_d &= -c_d k_2 z_d^T z_d - y_d^T (c_d \beta_d k_1 k_3 \Lambda) y_d + z_d^T ((1+\beta_d) c_d k_1) W^T R^T D\omega \\
&\quad - y_d^T (\beta_d c_d k_1 I_{n-1}) W^T R^T D\omega \\
&= -y_d^T W^T R^T \alpha^{-1}\omega + y_d^T W^T R^T \alpha^{-1}\omega - c_d k_2 z_d^T z_d \\
&\quad - y_d^T (c_d \beta_d k_1 k_3 \Lambda) y_d + z_d^T ((1+\beta_d) c_d k_1) W^T R^T D\omega - y_d^T (\beta_d c_d k_1) W^T R^T D\omega \\
&= -y_d^T W^T R^T \alpha^{-1}\omega - c_d k_2 z_d^T z_d - y_d^T (c_d \beta_d k_1 k_3 \Lambda) y_d \\
&\quad + z_d^T ((1+\beta_d) c_d k_1) W^T R^T D\omega + y_d^T W^T R^T (\alpha^{-1} - \beta_d c_d k_1 D)\omega.
\end{aligned}$$

By $\lambda_{\min} \le \lambda_i$ for all $i = 2, \cdots, n$, and inequalities

$$z_d^T W^T R^T ((1+\beta_d) c_d k_1) D\omega \le \frac{1}{2}\omega^T D\omega^T + \frac{1}{2} z_d^T X_z z_d,$$

where $X_z = W^T R^T ((1+\beta_d) c_d k_1 \alpha D)^2 D^{-1} RW$, and

$$y_d^T W^T R^T (\alpha^{-1} - \beta_d c_d k_1 D)\omega \le \frac{1}{2}\omega^T (D - \epsilon D)\omega + \frac{1}{2} y_d^T X_y y_d,$$

where $X_y = W^T R^T (\alpha^{-1} - \beta_d c_d k_1 D)^2 (D - \epsilon D)^{-1} RW$, we derive

$$\begin{aligned}
\dot{V}_d \le & -y_d^T W^T R^T \alpha^{-1}\omega - c_d k_2 z_d^T z_d - c_d \beta_d k_1 k_3 \lambda_{\min} y_d^T y_d \\
& + z_d^T W^T R^T ((1+\beta_d) c_d k_1) D\omega + y_d^T W^T R^T (\alpha^{-1} - \beta_d c_d k_1 D)\omega \\
\le & -y_d^T W^T R^T \omega + \omega^T D\omega - \frac{1}{2}\omega^T \epsilon D\omega \\
& - z_d^T \big(c_d k_2 - \frac{1}{2} X_z\big) z_d - y_d^T \big(c_d \beta_d k_1 k_3 \lambda_{\min} - \frac{1}{2} X_y\big) y_d.
\end{aligned}$$

We consider the following Lyapunov function candidate,

$$V = V_0 + V_1 + V_m + V_d.$$

In the following, we prove that (i) $\dot{V} \le 0$, (ii) equilibrium $z^* = (\varphi^*, \omega^*, \rho_1^*, \sigma_1^*, \rho_m^*, \sigma_m^*, \rho_d^*, \sigma_d^*)$ is a strict minimum of $V(\cdot)$ such that $\nabla V|_{z^*} = 0$ and $\nabla^2 V|_{z^*} > 0$, and (iii) $z^*$ is the only isolated equilibrium in the invariant set $\{z \in \Phi \times \mathbb{R}^n \times \mathbb{R} \times \mathbb{R} \times \mathbb{R}^{m-1} \times \mathbb{R}^{m-1} \times \mathbb{R}^{m-1} \times \mathbb{R}^{m-1} | \dot{V}(z) = 0\}$ step by step according to Theorem (A.1.3).

(i). $V$ has derivative

$$\dot{V} \le G_0 + G_1 + G_m + G_d, \tag{4.57}$$

where the terms $y_m^T W^T R^T \alpha^{-1}\omega$, $y_d^T W^T R^T \alpha^{-1}\omega$ have vanished and the terms $G_0, G_1, G_m, G_d$ are mainly from $\dot{V}_0, \dot{V}_1, \dot{V}_m, \dot{V}_d$ respectively with the following form,

$$\begin{aligned}
G_0 &= -\frac{1}{8}\omega^T \epsilon D\omega, \\
G_1 &= -(k_2\sigma_1 - k_2\sigma_1^*)^2 - \frac{k_2}{k_1}(k_1 \upsilon + k_2\sigma_1)^2, \\
G_m &= -\sum_{i=2}^{n} z_{mi}^2 (c_{mi} k_2 - r_z) - \sum_{i=2}^{n} y_{mi}^2 (\beta_m k_1 k_3 c_{mi} \lambda_i - r_y), \\
G_d &= -z_d^T (c_d k_2 - \frac{1}{2} X_z) z_d - y_d^T (c_d \beta_d k_1 k_3 \lambda_{\min} - \frac{1}{2} X_y) y_d.
\end{aligned}$$

It is obvious that $G_0 \le 0$ and $G_1 \le 0$. In the following, we first focus on $G_m$ and then on $G_d$. If there exist $c_{mi}$ and $\beta_m$ such that $c_{mi} k_2 - r_z > 0$ and $\beta_m k_1 k_3 c_{mi} \lambda_i - r_y > 0$, we have $G_m \le 0$ for all $z_m$ and $y_m$. We verify that such $c_{mi}$ and $\beta_m$ do exist. By (4.27a) and (4.30b), we have

$$Q_{vi}^T R^T \alpha^{-1} R Q_{vi} = Q_{vi}^T \alpha_R^{-1} Q_{vi} = 1.$$

So we only need to prove there exist $c_{mi}$ and $\beta_m$ such that

$$Q_{vi}^T R^T (c_{mi} k_2 \alpha^{-1}) R Q_{vi} - r_z > 0,$$
$$Q_{vi}^T R^T (\beta_m k_1 k_3 c_{mi} \lambda_i \alpha^{-1}) R Q_{vi} - r_y > 0.$$

which yields

$$c_{mi} k_2 \alpha^{-1} > 2(n-1)(c_{mi} k_1 k_2 M)^2 (\epsilon D)^{-1}, \tag{4.61a}$$
$$(\beta_m k_1 k_3 c_{mi} \lambda_i \alpha^{-1}) > 2(n-1)(\alpha^{-1} - c_{mi}(1+\beta_m) k_1 k_3 \lambda_i M)^2 (\epsilon D)^{-1}, \tag{4.61b}$$

From (4.61), we derive

$$c_{mi} I_{m-1} < \frac{\epsilon D}{2(n-1) k_1^2 k_2 M^2 \alpha},$$
$$\frac{I_{m-1}}{2a+b+\sqrt{4ab+b^2}} < c_{mi} I_{m-1} < \frac{2a+b+\sqrt{4ab+b^2}}{2a^2},$$

where $a = (1+\beta_m) k_1^2 k_3 \lambda_i M \alpha)$, $b = \frac{\beta_m k_1 k_3 \alpha \lambda_i \epsilon D}{2(n-1)}$. There exists $c_{mi} > 0$ satisfying (4.61) if

$$\Big(\frac{I_{n-1}}{2a+b+\sqrt{4ab+b^2}}\Big)_{\max} < \Big(\frac{\epsilon D}{2(n-1) k_1^2 k_2 M^2 \alpha}\Big)_{\min}$$

which can be satisfied by choosing a large $\beta_m$. This is because

$$\lim_{\beta_m \to \infty} \Big(\frac{1}{2a+b+\sqrt{4ab+b^2}}\Big)_{\max} = 0,$$

while the term $\Big(\frac{\epsilon D}{2(n-1) k_1^2 k_2 M^2 \alpha}\Big)_{\min}$ does not depend on $\beta_m$. Hence there exist $c_{mi} > 0$ and $\beta_m > 0$ satisfying (4.61) and $G_m \le 0$ has been proven. Here $(\cdot)_{\max}$ and $(\cdot)_{\min}$ are as defined in Assumption (4.4.5).

In the following, we focus on $G_d$. If there exist $c_d$ and $\beta_d$ such that

$$c_d k_2 I_{m-1} - \frac{1}{2} X_z > 0,$$
$$c_d \beta_d k_1 k_3 \lambda_{\min} I_{m-1} - \frac{1}{2} X_y > 0,$$

we have $G_d \le 0$. We prove such $c_d$ and $\beta_d$ do exist with Assumption (4.4.5). By (4.27a) and (4.30b), we derive

$$W^T R^T \alpha^{-1} R W = W^T \alpha_R^{-1} W = I_{m-1}.$$

So we only need to prove there exist $c_d$ and $\beta_d$ such that

$$W^T R^T (c_d k_2 \alpha^{-1}) R W - \frac{1}{2} X_z > 0,$$
$$W^T R^T (c_d \beta_d k_1 k_3 \lambda_{\min}) R W - \frac{1}{2} X_y > 0,$$

which yields

$$c_d k_2 \alpha^{-1} > \frac{1}{2}(1+\beta_d)^2 (c_d k_1 D)^2 D^{-1}, \tag{4.68a}$$

$$c_d \beta_d k_1 k_3 \lambda_{\min} \alpha^{-1} > \frac{1}{2}(\alpha^{-1} - \beta_d c_d k_1 D)^2 (D - \epsilon D)^{-1}, \tag{4.68b}$$

In the following, we prove that with assumption (4.4.5), there exist $c_d$ and $\beta_d$ satisfying the above two inequalities (4.68). We derive from (4.68) that

$$c_d I_{m-1} < \frac{2k_2}{(1+\beta_d)^2 k_1^2 \alpha D},$$

$$\frac{1}{\beta_d k_1 \alpha D b_d} < c_d I_{m-1} < \frac{b_d}{\beta_d k_1 \alpha D},$$

where

$$b_d = 1 + k_3 \lambda_{\min}(1-\epsilon) + \sqrt{k_3^2 \lambda_{\min}^2 (1-\epsilon)^2 + 2k_3 \lambda_{\min}(1-\epsilon)}.$$

There exists a $c_d$ satisfying the two inequalities (4.68) if there exists a $\beta_d$ such that

$$\frac{1}{\beta_d k_1 (\alpha D)_{\min} b_d} < \frac{2k_2}{(1+\beta_d)^2 k_1^2 (\alpha D)_{\max}}. \tag{4.70}$$

Since

$$\lim_{\epsilon \to 0} b_d(\epsilon) = 1 + k_3 \lambda_{\min} + \sqrt{k_3^2 \lambda_{\min}^2 + 2k_3 \lambda_{\min}} > 1 + 2k_3 \lambda_{\min},$$

there exists a small $\epsilon > 0$ such that $b_d(\epsilon) > 1 + 2k_3 \lambda_{\min}$. Subsequently (4.70) can be satisfied if

$$\frac{1}{\beta_d k_1 (\alpha D)_{\min} (1 + 2k_3 \lambda_{\min})} < \frac{2k_2}{(1+\beta_d)^2 k_1^2 (\alpha D)_{\max}}. \tag{4.72}$$

With assumption (4.4.5), we can obtain that there exist $\beta_d > 0$ satisfying (4.72). Hence $G_d < 0$ is proven and $\dot{V} \le 0$ subsequently.

(ii). We prove that the equilibrium $z^*$ is a strict minimum of $V(\cdot)$. It can be easily verified that $V|_{z^*} = 0$ and

$$\nabla V|_{z^*} = \mathrm{col}(\nabla_\varphi V, \nabla_{\tilde{z}} V)|_{z^*} = 0,$$

where $\tilde{z} = (\omega, \rho_1 - \rho_1^*, \sigma_1 - \sigma_1^*, \rho_m, \sigma_m, \rho_d, \sigma_d)$. Here, we have used $(\omega^*, \rho_m^*, \sigma_m^*, \rho_d^*, \sigma_d^*) = 0$. The Hessian matrix of $V$ at $z^*$ is

$$\nabla^2 V|_{z^*} = \mathrm{blkdiag}(L_p, H),$$

where $L_p$ is Hessian matrix of $V$ respect to $\varphi$ with $\varphi_1 = 0$ and $H$ is the Hessian matrix of $V$ respect to $\tilde{z}$. It follows [57, Lemma 5.3] that $L$ is positive definite. Since the components in $V$ related to $\tilde{z}$ are all quadratic and positive definite, $H$ is positive definite. Thus $\nabla^2 V|_{z^*} > 0$.

(iii). The equilibrium is the only isolated one in the invariant set $\{(\varphi,\omega,\eta_m,\xi_m,\eta_d,\xi_d)|\dot{V}=0\}$. Since $\dot{V}=0$, it yields from (4.57) that $\tilde{z}=0$. Hence $\varphi_i$ are all constant. By Proposition (4.4.4), we prove that $z^*$ is the only isolated equilibrium in the invariant set.

In this case, $z^*$ is the only one equilibrium in the neighborhood of $z^*$ , i.e., $\Psi^d = \{(\varphi,\tilde{z})|V(\varphi,\tilde{z}) \le c, \varphi \in \Phi\}$ for some $c>0$. Hence with any initial state $z^0$ that satisfies the algebraic equations (4.26d), the trajectory converges to the equilibrium state $z^*$. ■

**Remark 4.5.5** *Note that when the power system is controlled as a single area, MLPIAC reduces to GBPIAC. The dynamics of $(\rho_m,\sigma_m,\rho_d,\sigma_d)$ vanish and the one of $(\rho_1,\sigma_1)$ is left only. In the Lyapunov function $V(\cdot)$, with $V_m=0$ and $V_d=0$, we can prove the equilibrium of GBPIAC is locally asymptotically stable without Assumption (4.4.5).*

**Remark 4.5.6** *The asymptotic stability analysis is only valid for quadratic cost functions. Whether MLPIAC is still stable when the cost functions are general convex functions needs a further study.*



## 4.6. CASE STUDY

In this section, we evaluate the performance of the multi-level control approach, MLPIAC, on the IEEE-39 buses system as shown in Fig. 4.2. The GBPIAC and DPIAC method are two special cases of the MLPIAC method, so we compare GBPIAC, DPIAC and MLPIAC by observing the sub-processes identified in Section 4.3 respectively. The data of the test system are from [67]. The system consists of 10 generators, 39 buses, which serves a total load of about 6 GW. The voltage at each bus is a constant which is derived by power flow calculation with PSAT [22]. There are 49 nodes in the network including 10 nodes of generators and 39 nodes of buses. In order to involve the frequency dependent power sources, we change the buses which are not connected to synchronous machines into frequency dependent loads. Hence $\mathcal{V}_M = \{G1,G2,G3,G4,G5,G6,G7,G8,G9,G10\}$, $\mathcal{V}_P = \{30,31,32,33,34,35,36,37,38,39\}$ and the other nodes are in set $\mathcal{V}_F$. The nodes in $\mathcal{V}_M \cup \mathcal{V}_F$ are all equipped with secondary frequency controllers such that $\mathcal{V}_K = \mathcal{V}_M \cup \mathcal{V}_F$. We remark that each synchronous machine is connected to a bus and its phase angle is rigidly tied to the rotor angle of the bus if the voltages of the system are constants, e.g., the classical model of synchronous machine [11]. Thus the angles of the synchronous machine and the bus have the same dynamics. The droop control coefficients are set to be $D_i = 70$ (p.u./p.u. frequency deviation) for all $i \in \mathcal{V}_M$ and $D_i = 1$ (p.u./p.u. frequency deviation) for all $i \in \mathcal{V}_F$ under the power base 100 MVA and frequency base 60 Hz. As in Subsection 3.6, these setting of $D_i$ leads to a frequency response factor $-1.2$ p.u which equals to that of Quebec power grid connected by bus 1 [61]. The economic power dispatch coefficient $\alpha_i = 1/\beta_i$ where $\beta_i$ is generated randomly with a uniform distribution on $(0,1)$. In the simulations, the setting of $\{D_i,\ i \in \mathcal{V}_K\}$ and randomly generated coefficients $\{\alpha_i,\ i \in \mathcal{V}_K\}$ yield that $(\alpha D)_{\min} = 7.0$ and $(\alpha D)_{\max} = 42560$. The communication network is assumed to be a spanning tree network as shown by the red dashed lines in Fig. 4.2 and the requirement on the communication network in Assumption (4.2.3) is satisfied with the spanning tree network. For the GBPIAC method, the entire network is controlled as a single area. For the DPIAC method, each node $i \in \mathcal{V}_K$ is controlled as a single area. For the MLPIAC method, the network is divided into three areas by the dash-dotted black lines as shown in Fig. 4.2.

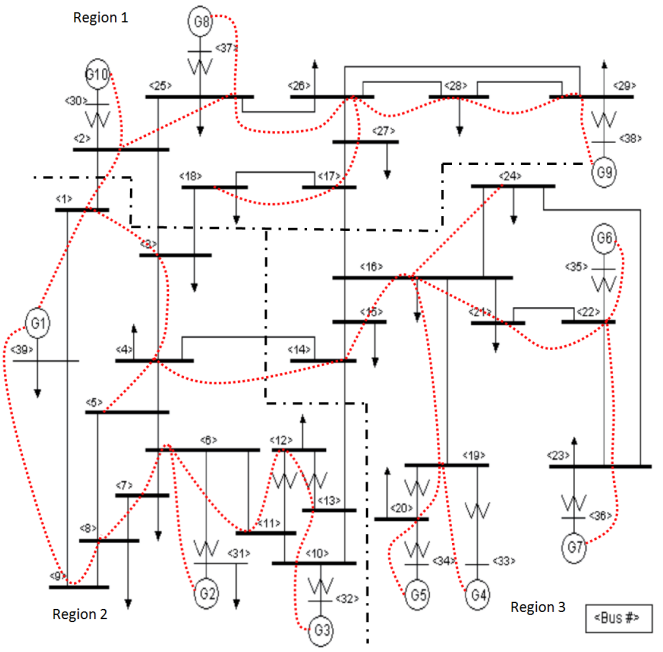


Figure 4.2: IEEE New England test power system.

We set $l_{ij} = 1$ if node $i$ and $j$ are connected by a communication line in DPIAC (4.11) and set $l_{rq} = 1$ if area $r$ and $q$ are connected by a communication line in MLPIAC (4.16). Note that area 1 and 2 are connected by communication line $(1,2)$ and area 1 and 3 are connected by $(4,14)$. However, area 1 and 3 are not connected by a communication line directly. So the marginal cost cannot be exchanged between area 1 and 3. With the control prices $\alpha$ and the Laplacian matrix of the communication network, it can be computed that $\lambda_{\min} = 0.0365$ for DPIAC and $\lambda_{\min} = 0.1933$ for MLPIAC.

At the beginning of the simulations, the power generation and loads are balanced with nominal frequency $f^* = 60$ Hz. At time $t = 5$ second, a step-wise increase of 66 MW of the loads at each of the buses 4, 12 and 20, amounting to a total power imbalance of 198 MW, causes the frequency to drop below the nominal frequency.

In the following, we evaluate the performance of the control approaches on restoring the nominal frequency with a minimized control cost. Besides the three sub-processes shared with GBPIAC, i.e., the convergence processes of $u_s(t)$ to $-P_s$, $\omega_s(t)$ to zero, and the synchronization process of $\omega_i$ to $\omega_s(t)$, DPIAC considers the consensus process of the marginal costs of all the local nodes and MLPIAC considers the consensus process of the marginal costs of all the areas. On the dynamics of the frequency, we focus on the dynamics of the frequency $\overline{\omega}_i(t) = \omega_i(t) + f^*$ and abstract frequency $\overline{\omega}_s(t) = \omega_s(t) + f^*$ instead of $\omega_i(t)$ and $\omega_s(t)$ respectively. Here, the response of $\omega_s$ are obtained from (4.3) with $u_s$ as the total control input of the three methods respectively. For illustrations of the

extra oscillation of frequency caused by the overshoot of $u_s$, we refer to the simulations in, e.g., [9, 13, 16, 27, 69].

The results are shown in Fig. 4.3 where there are 20 plots in 5 rows and 4 columns. The plots in the rows from top to bottom illustrate the dynamics of the frequency $\overline{\omega}_i(t) \in \mathcal{V}_M$, control input $u_s(t)$, abstract standard frequency $\overline{\omega}_s(t)$, relative frequency $\omega_i(t) - \omega_s(t)$ for all $i \in \mathcal{V}_M$, and marginal costs of the controllers at the nodes of the synchronous machines in DPIAC and of the areas in MLPIAC, and the plots in the column from left to right illustrate the results of GBPIAC, DPIAC with $k_3 = 10$, DPIAC with $k_3 = 20$, and MLPIAC control with $k_3 = 10$ respectively. In these four simulations, $k_1 = 0.4, k_2 = 1.6$. Note that Assumption (4.4.5) is not satisfied in the simulations of DPIAC and MLPIAC, i.e., $\frac{k_2}{k_1} = 4$ while the values of $\frac{2(\alpha D)_{\max}}{(\alpha D)_{\min}+2k_3\lambda_{\min}}$ are about 1203 and 1152 for DPIAC and MLPIAC with $k_3 = 10$ respectively. We remark that the relative frequency describes the synchronization process of $\omega_i(t)$ to $\omega_s(t)$, which is the main concern of primary control.



Let us first focus on the performance of GBPIAC in the plots in the first column. It can be observed from the plots from top to bottom that the frequencies are restored to the nominal frequency without any extra oscillations, the control input converges to the power imbalance without an overshoot, the abstract standard frequency converges to the nominal frequency without an overshoot, the frequencies synchronize to the abstract frequency $\omega_s$, the marginal costs are identical at the nodes of the synchronous machines. Hence the performance of GBPIAC is similar to that of PIAC method [57]. So GBPIAC solves Problem 2.4.1 and 2.6.1.

Second, we turn to the performance of DPIAC method in the plots in the second and third columns. Compared with the GBPIAC method by observing the plots from top to bottom, the dynamics of $\overline{\omega}_i$ are similar as in GBPIAC, the control input $u_s(t)$ and $\overline{\omega}_s(t)$ are identical to that in GBPIAC, the synchronization of $\omega_i$ to $\omega_s$ is similar as in GBPIAC with a little bit smaller magnitude of oscillations, the marginal costs are identical at the steady state. However, the marginal costs are not identical in the transient phase, which is different from that in GBPIAC. By comparing result of DPIAC method with $k_3 = 10$ and $k_3 = 20$ in the second and third column, it can be found that the consensus speed of the marginal cost is accelerated and the control cost in the transient phase is decreased by a large $k_3$. However, the coefficient $k_3$t influences the synchronization of $\omega_i$ little by comparing the subprocess of the synchronization of $\omega_i(t)$ to $\omega_s(t)$.

Third, we observe the performance of the MLPIAC method. It can be seen from Fig. 4.3a$_4$, Fig. 4.3b$_4$, Fig. 4.3c$_4$ and Fig. 4.3d$_4$ that, the subprocesses of $u_s(t)$, $\omega_s(t)$ and $\omega_i - \omega_s$ are similar as in GBPIAC and DPIAC. However, the marginal costs of the three areas shown in Fig. 4.3e$_4$ achieve consensus much faster than in the DPIAC method even though the control gain $k_3$ for the consensus process equals to the one in DPIAC method. Hence, for a large-scale network, *the multi-level control is more effective in decreasing the control cost than the distributed method.*

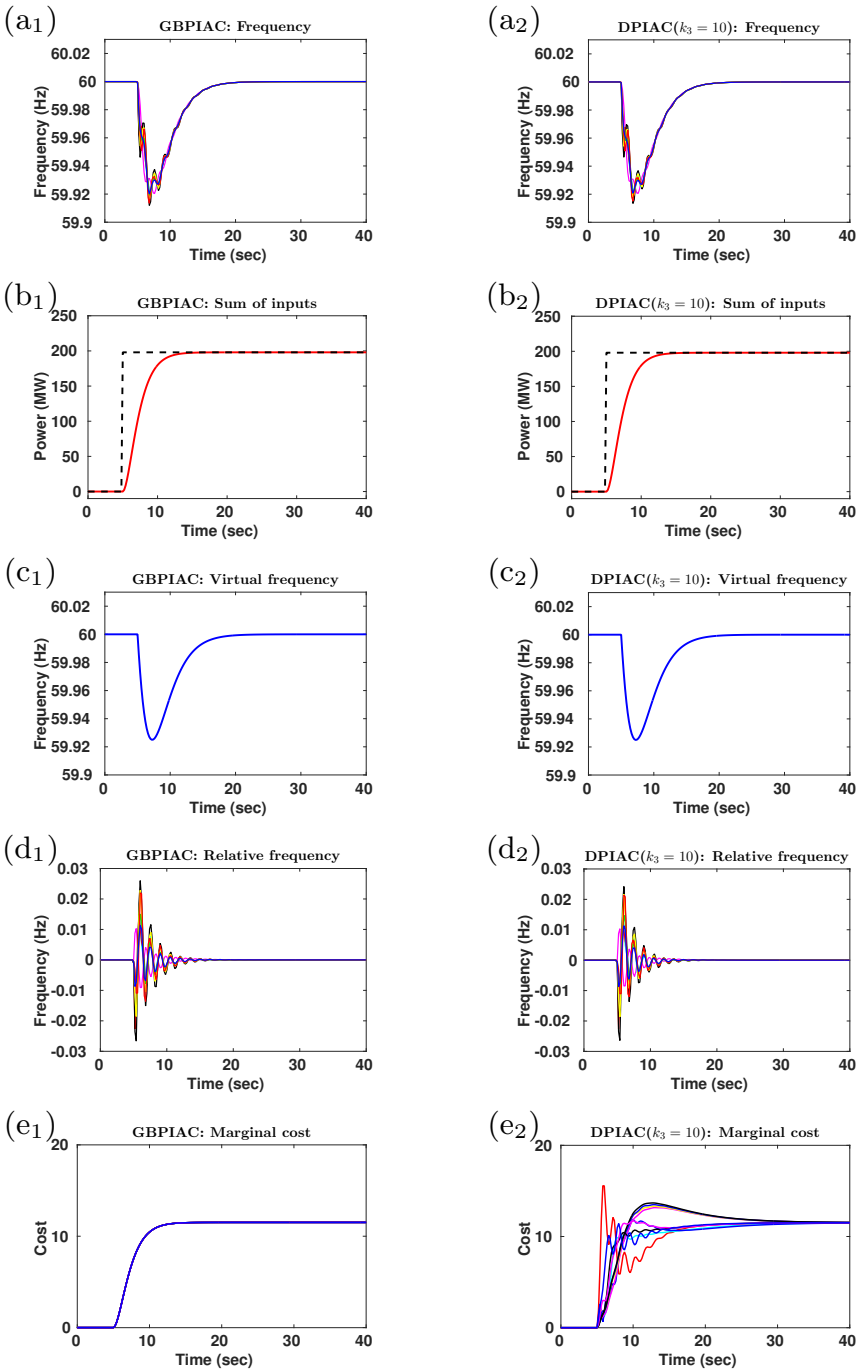


Figure 4.3: part 1: The simulation results of the GBPIAC, DPIAC and MLPIAC method with $k_1 = 0.4, k_2 = 1.6$ on IEEE 39-bus test system. The black dashed lines in $b_1$-$b_4$, denote the power imbalance of the network.

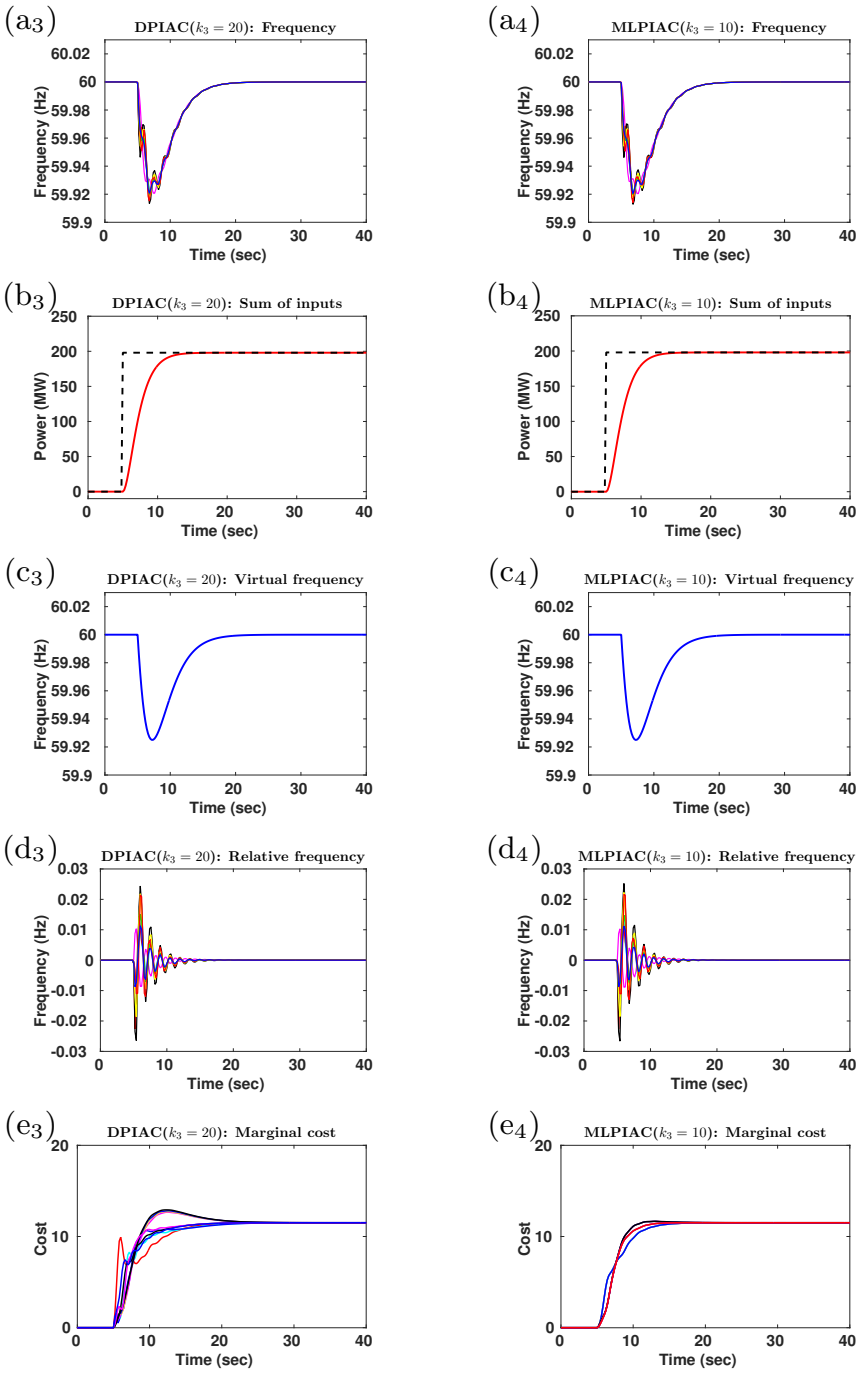


Figure 4.3: part 2: The simulation results of the GBPIAC, DPIAC and MLPIAC method with $k_1 = 0.4, k_2 = 1.6$ on IEEE 39-bus test system. The black dashed lines in $b_1$-$b_4$, denote the power imbalance of the network.

## 4.7. CHAPTER CONCLUSION

In this chapter, we proposed a multi-level secondary frequency control, named *Multi-Level Power-Imbalance Allocation control* (MLPIAC), for a large-scale power system consisting of synchronous machines, frequency dependent power sources and passive nodes. For a power system partitioned into several areas, a centralized control approach, GBPIAC, is implemented within each area and a consensus control based distributed control approach, DPIAC, is implemented over the areas. At the steady state, the nominal frequency is restored with a minimized control cost and at the transient phase, the transient behavior of the system can be improved by tuning the control gain coefficients. Because the convergence of the total control input of the system can be accelerated without an overshoot by increasing the gain coefficient $k_1$, the extra oscillations of the frequency caused by the overshoot is eliminated, thus as in PIAC [69] the transient behavior of the frequency is improved. Because the consensus of the marginal costs of the areas can be accelerated by increasing the gain coefficient $k_3$, the minimized control cost can be obtained faster. Furthermore, the large-scale network can be controlled with a minimized cost more effectively than the purely distributed control due to the number of areas is smaller that that of nodes in the system.



However, Assumption (4.4.5) is still required in the theoretical analysis of asymptotic stability of MLPIAC even though it is not required in the numerical simulations. How to relax Assumption (4.4.5) theoretically still needs further consideration. Furthermore, there usually are time-delays in the measurement of the frequency, inertias and damping coefficients and communications in practice, in which case the robustness of MLPIAC needs to be evaluated.

# 5

# TRANSIENT PERFORMANCE ANALYSIS

*In this chapter, for the proposed control laws, PIAC, GBPIAC and DPIAC, we investigate the influence of the control parameters on the transient performance of the power systems. The disturbance of power loads (variable power generation) are modelled by Gaussian white noise and the $\mathscr{H}_2$ norm is used to measure the transient performance. It is hard to analytically calculate the $\mathscr{H}_2$ norm for the power systems with heterogeneous parameters, instead we analyze the $\mathscr{H}_2$ norms for the power systems with homogeneous parameters which can provide us insights on the performance of these control laws. The analytical result shows that in these control laws a trade-off between frequency deviation and control cost is established, which is also demonstrated by case studies. This trade-off needs to be resolved by determining the control gain coefficients. Comparison of these methods shows that with the same control cost, PIAC is more efficient on suppressing the frequency deviation than GBPIAC, and the performance of the distributed control law, DPIAC, converges to that of GBPIAC as a control gain coefficient increases.*

Parts of this chapter is based on:
K.Xi, H. X. Lin and J. H. van Schuppen. Transient Performance of Power Systems with Distributed Power-Imbalance Allocation Control, to be submitted, 2018.

## 5.1. INTRODUCTION

Concerning the transient performance of power systems, we have proposed a centralized control method, *Power-Imbalance Allocation Control* (PIAC) in Chapter 3 and a multi-level control law, *Multi-Level Power-Imbalance Allocation Control* (MLPIAC) in Chapter 4 for secondary frequency control of power systems. In this chaper, we analyze the impact of the control parameters of these control laws on the transient performance of the frequency deviation and the control cost after a disturbance.

We model the disturbances at power loads (or generation) as Gaussian white noises, and use the $\mathscr{H}_2$ norm for a linearization of the closed-loop systems to measure the transient performance. This $\mathscr{H}_2$ norm has been widely used to investigate the transient performance of linear systems and of power systems [42, 76–79].

Because of the heterogeneity of the parameters in the power system, e.g., inertias of the synchronous machines and network topology, it is hard to calculate the corresponding $\mathscr{H}_2$ norms analytically for MLPIAC. Instead, we investigate the transient performance of the power system controlled by PIAC and by the two special cases of MLPIAC, namely *Gather-Broadcast Power-Imbalance Allocation Control* (GBPIAC) and *Distributed Power-Imbalance Allocation Control* (DPIAC). We calculate the $\mathscr{H}_2$ norms of the frequency deviation and control cost for the closed-loop systems of PIAC, GBPIAC and DPIAC with homogeneous parameters. Through the analytical form of these norms, we find in these control laws that a trade-off between the frequency deviation and control cost is established, which is determined by the control parameters. The frequency deviation can be controlled to a small range at the expense of control cost. We also compare the performance of these three control laws. With the same control cost, PIAC is more efficient on suppressing the frequency fluctuations than GBPIAC. As a control parameter of DPIAC goes to infinity, the performance of DPIAC converges to that of GBPIAC.

This chapter is organized as follows. We first introduce notations and the $\mathscr{H}_2$ norm for a linear input/output system with Gaussian white noise in Section 5.2, then calculate the $\mathscr{H}_2$ norms for the closed-loop systems of PIAC, GBPIAC and DPIAC and analyze the impact of the control parameters on the transient performance of the frequency deviation, control cost and the coherence of the marginal cost in Section 5.3, and finally conclude with remarks in Section 5.5.

## 5.2. NOTATIONS & THE $\mathscr{H}^2$ NORM

In this section, we introduce the notations for the power system (2.4) and the definition of the $\mathscr{H}_2$ norm of a linear input/output system.

Denote the number of nodes in the sets $\mathcal{V}_M, \mathcal{V}_F, \mathcal{V}_P$ and $\mathcal{V}_K$ by $n_m, n_f, n_p, n$ respectively, the total number of buses in the power system by $n_t$. So $n = n_m + n_f$ and $n_t = n_m + n_f + n_p$. We write a diagonal matrix $\beta = \mathrm{diag}(\{\beta_i, i \cdots n\}) \in \mathbb{R}^{n\times n}$ with $\beta_i \in \mathbb{R}$ as $\mathrm{diag}(\beta_i)$. It is convenient to introduce the matrices $D = \mathrm{diag}(D_i) \in \mathbb{R}^{n\times n}$, $M = \mathrm{diag}(M_i) \in \mathbb{R}^{n\times n}$, $\alpha = \mathrm{diag}(\alpha_i) \in \mathbb{R}^{n\times n}$. Denote the identity matrix by $I_n \in \mathbb{R}^{n\times n}$. Note that $M_i = 0$ for $i \in \mathcal{V}_F$ and $M_i > 0$ for $i \in \mathcal{V}_M$. Denote the $n$ dimension vector with all elements equal to one by $1_n$. Denote $\theta = \mathrm{col}(\theta_i) \in \mathbb{R}^{n_t}$, $\omega = \mathrm{col}(\omega_i) \in \mathbb{R}^n$, $P = \mathrm{col}(P_i) \in \mathbb{R}^{n_t}$, $\eta = \mathrm{col}(\eta_i) \in \mathbb{R}^n, \xi = \mathrm{col}(\xi_i) \in \mathbb{R}^n$. Here, $\mathrm{col}(\cdot)$ denotes a column vector.

The $\mathscr{H}_2$ norm of the transfer matrix of a linear system is defined as follows.

**Definition 5.2.1** *Consider a linear time-invariant system,*

$$\dot{x} = Ax + Bw, \tag{5.1a}$$
$$y = Cx, \tag{5.1b}$$

*where $x \in \mathbb{R}^n$, $A \in \mathbb{R}^{n\times n}$ is Hurwitz, $B \in \mathbb{R}^{n\times m}$, $C \in \mathbb{R}^{z\times n}$, the input is denoted by $w \in \mathbb{R}^m$ and the output of the system is denoted by $y \in \mathbb{R}^z$. The squared $\mathscr{H}_2$ norm of the transfer matrix $H$ of the linear plant model $(A, B, C)$ from the input $w$ to the output $y$ is defined as*

$$||H||_2^2 = tr(B^T Q_o B) = tr(CQ_c C^T), \tag{5.2a}$$
$$Q_o A + A^T Q_o + C^T C = 0, \tag{5.2b}$$
$$AQ_c + Q_c A^T + BB^T = 0, \tag{5.2c}$$

*where $tr(\cdot)$ is the trace of a matrix, $Q_o, Q_c \in \mathbb{R}^{n\times n}$ are the* observability Gramian *of $(C, A)$ and* controllability Gramian *of $(A, B)$ respectively [76],[77, chapter 2].*

There are several interpretations of the $\mathscr{H}_2$ norm. When the input $w$ is modeled as the Gaussian white noise such that $w_i \sim N(0, 1)$ for all $i = 1, \cdots, m$, the matrix $Q_v = CQ_c C^T$ is the variance matrix of the output at the steady state, i.e.,

$$Q_v = \lim_{t\to\infty} E[y(t)y^T(t)]$$

where $E[\cdot]$ denotes the expectation. Thus

$$||H||_2^2 = \mathrm{tr}(Q_v) = \lim_{t\to\infty} E[y(t)^T y(t)]. \tag{5.3}$$

When the input $w$ is modelled as Dirac impulse with $w(t) = e_i\delta(t)$ where $e_i \in \mathbb{R}^m$ is a vector with the $i$th component being one and others zero, and $\delta(t)$ is a Dirac impulse. The corresponding output to $e_i\delta(t)$ is denoted by $y_i \in \mathbb{R}^z$ for $i = 1, \cdots, m$. Then the squared $\mathscr{H}_2$ norm satisfies [80]

$$||H||_2^2 = \sum_{i=1}^{m} \int_0^\infty y_i(t)^T y_i(t) dt. \tag{5.4}$$

which measures the sum of the $\mathscr{L}_2$ norm of the outputs.

The $\mathscr{H}_2$ norm can also be interpreted as the expected $\mathscr{L}_2$ norm of the output $y$ with $w = 0$ and a random initial condition $x_0$ such that $E[x_0 x_0^T] = BB^T$, or equivalently,

$$||H||_2^2 = \int_0^\infty E[y^T(t)y(t)]dt. \tag{5.5}$$

The $\mathscr{H}_2$ norm has been often used to investigate the performance of secondary frequency control methods , e.g., [42, 78, 79], to study the optimal virtual inertia placement in Micro-Grids [81] and the synchrony level of power systems [80].

Since the phase angle difference $\theta_{ij}$ are usually small in practice, $\sin\theta_{ij}$ can be approximated by $\theta_{ij}$, e.g., [16, 27]. Rewriting (2.4) into a vector form by replacing $\sin\theta_{ij}$ by $\theta_{ij}$, we obtain

$$\dot{\theta} = \omega \tag{5.6a}$$
$$M\dot{\omega} = -B\theta - D\omega + P + u. \tag{5.6b}$$

where $B = (B_{ij})$ is a Laplacian matrix with $B_{ij}$ being the effective susceptance of the line connecting node $i$ and $j$. When $P_i$ is modeled as a constant with a disturbance, we can obtain the same linear system as (5.6) by linearizing the system (2.4) at an equilibrium point. So we model $P_i$ as a disturbance directly such that $P_i \sim N(0,1)$ for $i = 1, \cdots, n$, in this paper.

For the system (5.6), denote the squared $\mathscr{H}_2$ norm of the transfer matrix of (5.6) with output $y = \omega$ by $||H(\omega)||_2^2$, thus following (5.3), the expected value of $\omega^T(t)\omega(t)$ at the steady state is

$$||H(\omega)||_2^2 = \lim_{t\to\infty} E[\omega(t)^T \omega(t)],$$

and denote the squared $\mathscr{H}_2$ norm of the transfer matrix of (5.6) with output $y = u$ by $||H(u)||_2^2$, thus the expected value of $u(t)^T u(t)$ at the steady state is

$$||H(u)||_2^2 = \lim_{t\to\infty} E[u(t)^T u(t)].$$

These two norms are used to measure the transient performance of the frequency deviation $\omega(t)$ and control cost $u(t)$ respectively.



## 5.3. THE TRANSIENT PERFORMANCE ANALYSIS

In this section, we calculate the $\mathscr{H}_2$ norms for the closed-loop systems of the PIAC, GBPIAC and DPIAC control laws and analyze the transient performance of the system under these control laws. First, we begin with recalling these three control laws. We consider the optimization problem (2.10) with quadratic cost functions, which is rewritten as follows

$$\min_{\{u_i\in\mathbb{R}, i\in\mathcal{V}_K\}} \sum_{i\in\mathcal{V}_K} \frac{1}{2}\alpha_i u_i^2, \tag{5.7a}$$

$$s.t. \sum_{i\in\mathcal{V}} P_i + \sum_{i\in\mathcal{V}_K} u_i = 0, \tag{5.7b}$$

where $\alpha_i > 0$ is a constant.

**Definition 5.3.1 (PIAC)** *Consider the power system (2.4) with the economic power dispatch problem (5.7), the* Power-Imbalance Allocation Control *(PIAC) law is defined as [69]*

$$\dot{\eta}_s = \sum_{i\in\mathcal{V}_M\cup\mathcal{V}_F} D_i\omega_i, \tag{5.8a}$$

$$u_s = -k(\sum_{i\in\mathcal{V}_M} M_i\omega_i + \eta_s), \tag{5.8b}$$

$$u_i = \frac{\alpha_s}{\alpha_i} u_s,\ i\in\mathcal{V}_K, \tag{5.8c}$$

$$\frac{1}{\alpha_s} = \sum_{i\in\mathcal{V}_K} \frac{1}{\alpha_i}. \tag{5.8d}$$

*where $\eta_s \in \mathbb{R}$ is a state variable of the central controller, $k$ is a positive control gain coefficient, $\alpha_s$ is a constant calculated from $\alpha_i$, $i = 1, \cdots, n$.*

The GBPIAC is defined as a centralized dynamic control law as follows.

**Definition 5.3.2 (GBPIAC)** *Consider the power system (2.4) with the economic power dispatch problem (5.7), the* Gather-Broadcast Power-Imbalance Allocation Control *(GBPIAC) is defined as [82]*

$$\dot{\eta}_s = \sum_{i\in\mathcal{V}_M\cup\mathcal{V}_F} D_i\omega_i, \tag{5.9a}$$

$$\dot{\xi}_s = -k_1\Big(\sum_{i\in\mathcal{V}_M} M_i\omega_i + \eta_s\Big) - k_2\xi_s, \tag{5.9b}$$

$$u_i = \frac{\alpha_s}{\alpha_i}k_2\xi_s,\ i\in\mathcal{V}_K, \tag{5.9c}$$

$$\frac{1}{\alpha_s} = \sum_{i\in\mathcal{V}_K}\frac{1}{\alpha_i}. \tag{5.9d}$$

*where $\eta_s\in\mathbb{R}$, $\xi_s\in\mathbb{R}$ are state variables of the central controller, $k_1, k_2$ are positive control gain coefficients, $\alpha_i$, $\alpha_s$ are similar as in PIAC.*

In order to compensate the power-imbalance quickly, $k_2$ should be such that $k_2\geq 4k_1$ [82]. In this chapter, we set $k_2 = 4k_1$.

The DPIAC is defined as a distributed dynamic control law as follows.

**Definition 5.3.3 (DPIAC)** *Consider the power system (2.4) with the economic power dispatch problem (5.7), define the* Distributed Power-Imbalance Allocation Control *(DPIAC) as a dynamic controller of the form for node $i\in\mathcal{V}_K$ [82],*

$$\dot{\eta}_i = D_i\omega_i + k_3\sum_{j\in\mathcal{V}_K} l_{ij}(k_2\alpha_i\xi_i - k_2\alpha_j\xi_j), \tag{5.10a}$$

$$\dot{\xi}_i = -k_1(M_i\omega_i + \eta_i) - k_2\xi_i, \tag{5.10b}$$

$$u_i = k_2\xi_i, \tag{5.10c}$$

*where $\eta_i\in\mathbb{R}$, $\xi_i\in\mathbb{R}$ are state variables of the local controller at node $i$, $k_1, k_2$ and $k_3$ are positive gain coefficients, $(l_{ij})$ defines a weighted undirected communication network with Laplacian matrix $(L_{ij})$*

$$L_{ij} = \begin{cases} -l_{ij}, & i\neq j,\\ \sum_{k\neq i} l_{ik}, & i = j,\end{cases}$$

*and $l_{ij}\in[0,\infty)$ is the weight of the communication line connecting node $i$ and node $j$. The marginal cost at node $i$ is $\alpha_i u_i = k_2\alpha_i\xi_i$.*

To simplify the calculation of the $\mathscr{H}_2$ norms, we make the following assumption.

**Assumption 5.3.4** *For PIAC, GBPIAC and DPIAC, assume that $M_i = m$, $D_i = d$, $\alpha_i = 1$, $\mathcal{V}_F = \emptyset$, $\mathcal{V}_P = \emptyset$. For DPIAC, assume that the topology of the communication network is the same as the one of the power system such that $L = B$ or equivalently,*

$$L_{ij} = \begin{cases} -B_{ij}, & i\neq j,\\ \sum_{k\neq i} B_{ik}, & i = j,\end{cases}$$

*and set $k_2 = 4k_1$.*

Assumption 5.3.4 restricts our analysis for the power system with homogeneous parameters. From the practical point of view, the analysis with Assumption (5.3.4) is valuable, which provides us insights on how to improve the transient behavior of the power system by tuning the parameters. With Assumption (5.3.4), we have $n_t = n_m = n$ and $n_f = n_p = 0$, and following the stability analysis [69, 82], the closed-loop systems of the PIAC, GBPIAC, DPIAC control laws are all asymptotically stable. For the power systems with heterogeneous parameters, it is hard to calculate the norms analytically.

For the symmetric matrix $L$, we have the following lemma which will be used in the following calculations.

**Lemma 5.3.5** *For the symmetric Laplacian matrix $L \in \mathbb{R}^{n\times n}$, there exist an invertible matrix $Q \in \mathbb{R}^{n\times n}$ such that*

$$Q^{-1} = Q^T, \tag{5.11a}$$

$$Q^{-1}LQ = \Lambda, \tag{5.11b}$$

$$Q_1 = \frac{1}{\sqrt{n}}1_n, \tag{5.11c}$$

*where $Q = [Q_1, \cdots, Q_n]$, $\Lambda = diag(\lambda_i) \in \mathbb{R}^n$, $Q_i \in \mathbb{R}^n$ is the unit eigenvector of $L$ corresponding with eigenvalue $\lambda_i$, thus $Q_i^T Q_j = 0$ for $i \neq j$. Because $L1_n = 0$, $\lambda_1 = 0$ is one of the eigenvalues with unit eigenvector $Q_1$.*

In Subsection 5.3.1-5.3.3, we calculate the $\mathscr{H}_2$ norms of the frequency deviation and control cost for PIAC, GBPIAC and DPIAC, and analyze the impact of the control parameters. The performance of PIAC, GBPIAC and DPIAC will be compared in subsection 5.3.4.

### 5.3.1. TRANSIENT PERFORMANCE ANALYSIS FOR PIAC

With Assumption (5.3.4), $\alpha_i = 1$ for all $i \in \mathcal{V}$, the control input at node $i$ is $u_i = \frac{u_s}{n}$. We obtain the closed-loop system of PIAC from (5.6) and (5.8) as follows

$$\dot{\theta} = \omega, \tag{5.12a}$$

$$mI_n\dot{\omega} = -L\theta - dI_n\omega - \frac{k}{n}(m1_n^T\omega + \eta_s)1_n + P, \tag{5.12b}$$

$$\dot{\eta}_s = d1_n^T\omega. \tag{5.12c}$$

for which we have the following theorem for the $\mathscr{H}_2$ norms of the frequency deviation and control cost.

**Theorem 5.3.6** *Consider the closed-loop system (5.12). The power loads (or generation) $P = col(P_i)$ are modeled as Gaussian noise such that $P_i \sim N(0,1)$, the squared $\mathscr{H}_2$ norm of the frequency deviation $\omega$ and control cost $u$ are*

$$||H_P(\omega)||_2^2 = \frac{n-1}{2md} + \frac{1}{2m(km+d)}, \tag{5.13a}$$

$$||H_P(u)||_2^2 = \frac{k}{2}. \tag{5.13b}$$

*Proof:* Let $Q \in \mathbb{R}^{n\times n}$ be defined as in Lemma (5.3.5) and let $x_1 = Q^{-1}\theta,\ x_2 = Q^{-1}\omega$, the closed-loop system (5.12) becomes

$$\begin{aligned}
\dot{x}_1 &= x_2,\\
\dot{x}_2 &= -\frac{1}{m}\Lambda x_1 - \frac{d}{m}I_n x_2 - \frac{k(m1_n^T Q x_2 + \eta_s)}{nm}Q^T 1_n + \frac{1}{m}Q^T P,\\
\dot{\eta}_s &= d1_n^T Q x_2,
\end{aligned}$$

where $\Lambda$ is the diagonal matrix as defined in Lemma (5.3.5). Following Lemma (5.3.5), $1_n$ is an eigenvector of $L$ corresponding to eigenvalue $\lambda_1 = 0$, thus $Q^{-1}1_n = [\sqrt{n}, 0, \cdots, 0]^T$. Hence, the dynamics of $x_1$ and $x_2$ can be decoupled as for $i = 1$,

$$\dot{x}_{11} = x_{21}, \tag{5.15a}$$

$$\dot{x}_{21} = -(\frac{d}{m} + k)x_{21} - \frac{k}{m\sqrt{n}}\eta_s + \frac{1}{m}Q^T P, \tag{5.15b}$$

$$\dot{\eta}_s = d\sqrt{n}x_{21}, \tag{5.15c}$$

and for $i = 2, \cdots, n$,

$$\dot{x}_{1i} = x_{2i}, \tag{5.16a}$$

$$\dot{x}_{2i} = -\frac{\lambda_i}{m}x_{1i} - \frac{d}{m}x_{2i} + \frac{1}{m}Q_i^T P, \tag{5.16b}$$

The decoupled systems (5.15) and (5.16) are rewritten in a general form as (5.1) with

$$x = \begin{bmatrix} x_1 \\ x_2 \\ \eta_s \end{bmatrix}, A = \begin{bmatrix} 0 & I & 0 \\ -\frac{1}{m}\Lambda & -\frac{d}{m}I_n - kV & -\frac{k}{m\sqrt{n}}v \\ 0 & d\sqrt{n}v^T & 0 \end{bmatrix}, B = \begin{bmatrix} 0 \\ \frac{1}{m}Q^{-1} \\ 0 \end{bmatrix},$$

where $v^T = [1, 0, \cdots, 0] \in \mathbb{R}^n,\ V = \mathrm{diag}(v_i) \in \mathbb{R}^{n\times n}$ with $v_1 = 1,\ v_2 = \cdots = v_n = 0$. The input $P$ is a vector with all its components being Gaussian white noise as in (5.1). Since the closed-loop system (5.12) is asymptotically stable, it can be easily obtained that $A$ is Hurwitz regardless the rotations of the phase angle $\theta$.

For the transient performance of $\omega(t)$, we set $y = \omega = Qx_2$ and $C = [0, Q, 0, 0]$, the observability Gramian of $(C, A)$ is in the form

$$Q_o = \begin{bmatrix} Q_{o11} & Q_{o12} & Q_{o13} \\ Q_{o21} & Q_{o22} & Q_{o24} \\ Q_{o31} & Q_{o32} & Q_{o33} \end{bmatrix}.$$

Then, we obtain the squared norm of $\omega(t)$ in PIAC as

$$||H_P(\omega)||^2 = \mathrm{tr}(B^T Q_o B) = \frac{\mathrm{tr}(QQ_{o22}Q^T)}{m^2} = \frac{\mathrm{tr}(Q_{o22})}{m^2}, \tag{5.17}$$

So we only need to calculate the trace of $Q_{o22} \in \mathbb{R}^{n\times n}$. Since

$$C^T C = \begin{bmatrix} 0 & 0 & 0 \\ 0 & I_n & 0 \\ 0 & 0 & 0 \end{bmatrix},$$

only includes an identity matrix, the diagonal elements $Q_{o22}(i,i)$ of $Q_{o22}$ can be calculated by solving the observability Gramian $\tilde{Q}_i$ of $(C_i, A_i)$ such that

$$\tilde{Q}_1 A_1 + A_1^T \tilde{Q}_1 + C_1^T C_1 = 0,$$

where

$$A_1 = \begin{bmatrix} 0 & 1 & 0 \\ 0 & -\frac{d}{m} - k & -\frac{k}{m\sqrt{n}} \\ 0 & d\sqrt{n} & 0 \end{bmatrix}, C_1^T = \begin{bmatrix} 0 \\ 1 \\ 0 \end{bmatrix},$$

and

$$\tilde{Q}_i A_i + A_i^T \tilde{Q}_i + C_i^T C_i = 0,\ i = 2, \cdots, n,$$

where

$$A_i = \begin{bmatrix} 0 & 1 \\ -\frac{\lambda_i}{m} & -\frac{d}{m} \end{bmatrix}, C_i^T = \begin{bmatrix} 0 \\ 1 \end{bmatrix}.$$

The diagonal elements of $Q_{o22}$ satisfies that $Q_{o22}(i,i) = \tilde{Q}_i(2,2)$ for $i = 1, \cdots, n$. By solving the observability Gramian of $(C_i, A_i)$ for $i = 1, \cdots, n$, we obtain

$$\mathrm{tr}(B^T Q_o B) = \frac{n-1}{2md} + \frac{1}{2m(km+d)} \tag{5.18}$$

which results in (5.13a) subsequently. With the same procedure, we set $y = u_s(t) = -k(m1_n^T\omega + \eta_s) = -k(m\sqrt{n}x_{21} + \eta_s)$ and $C = [0, km\sqrt{n}v^T, k] \in \mathbb{R}^{2n+1}$, we derive

$$||H_P(u_s)||_2^2 = \frac{kn}{2}.$$

Because $u_i = \frac{u_s}{n}$ for $i = 1, \cdots, n$ and $u(t)^T u(t) = \sum_{i=1}^n u_i^2$, we obtain (5.13b). ■

Theorem (5.3.6) indicates that as $k$ increases, the frequency deviations decrease while the control cost increases. Thus, a trade-off between the frequency deviation and control cost must be resolved by selecting a control law coefficient $k$. In the right hand side of (5.13a), the first term depends on the primary control and the second one depends on the secondary control, which verifies that the decomposition of the dynamics of the power system into three sub-processes is reasonable [69]. It follows from (5.13a) that

$$\lim_{k\to\infty} ||H_P(\omega)||_2^2) = \frac{n-1}{2md},$$

which indicates that the frequency deviation cannot be arbitrarily small even though $k$ is sufficiently large at the expense of the control cost.

### 5.3.2. TRANSIENT PERFORMANCE ANALYSIS FOR GBPIAC

By Assumption (5.3.4), we derive the control input at node $i$ as $u_i = \frac{1}{n}k_1\xi_s$ in (5.9). With the notations in Section 5.2 and Assumption (5.3.4), and the setting $k_2 = 4k_1$, we obtain

from (5.6) and (5.9) the closed-loop system of GBPIAC written in a vector form as follows.

$$\dot{\theta} = \omega, \tag{5.19a}$$

$$mI_n\dot{\omega} = -L\theta - dI_n\omega + \frac{4k_1\xi_s}{n}1_n + P, \tag{5.19b}$$

$$\dot{\eta}_s = d1_n^T\omega, \tag{5.19c}$$

$$\dot{\xi}_s = -k_1 m1_n^T\omega - k_1\eta_s - 4k_1\xi_s. \tag{5.19d}$$

For the transient performance of the frequency deviation $\omega(t)$ and the control cost $u(t)$ in GBPIAC, the following theorem can be proved.

**Theorem 5.3.7** *Consider the closed-loop system (5.19), where power generation (or loads) $P = col(P_i)$ are modeled as Gaussian white noise such that $P_i \sim N(0,1)$, the squared $\mathscr{H}_2$ norm of the frequency deviation $\omega$ and control inputs $u$ are*

$$||H_G(\omega)||_2^2 = \frac{n-1}{2md} + \frac{d+5mk_1}{2m(2k_1m+d)^2}, \tag{5.20a}$$

$$||H_G(u)||_2^2 = \frac{k_1}{2}. \tag{5.20b}$$

*Proof:* This proof is similar to the one of Theorem (5.3.6). With the linear transform $x_1 = Q^{-1}\theta, x_2 = Q^{-1}\omega$ where $Q$ is defined in Lemma (5.3.5), we derive from (5.19) that

$$\begin{aligned}
\dot{x}_1 &= x_2,\\
\dot{x}_2 &= -\frac{1}{m}\Lambda x_1 - \frac{d}{m}I_n x_2 + \frac{4k_1\xi_s}{mn}Q^{-1}1_n + \frac{1}{m}Q^{-1}P,\\
\dot{\eta}_s &= d1_n^T Q x_2,\\
\dot{\xi}_s &= -k_1 m1_n^T Q x_2 - k_1\eta_s - 4k_1\xi_s.
\end{aligned}$$

where $\Lambda$ is the diagonal matrix defined in Lemma (5.3.5). Since $1_n$ is an eigenvector of $L$ corresponding to $\lambda_1 = 0$, we obtain $Q^{-1}1_n = [\sqrt{n}, 0, \cdots, 0]^T$. Thus the components of $x_1$ and $x_2$ can be decoupled as for $i = 1$,

$$\dot{x}_{11} = x_{21}, \tag{5.22a}$$

$$\dot{x}_{21} = -\frac{d}{m}x_{21} + \frac{4k_1}{m\sqrt{n}}\xi_s + \frac{1}{m}Q_1^T P, \tag{5.22b}$$

$$\dot{\eta}_s = d\sqrt{n}x_{21}, \tag{5.22c}$$

$$\dot{\xi}_s = -k_1 m\sqrt{n}x_{21} - k_1\eta_s - 4k_1\xi_s \tag{5.22d}$$

and for $i = 2, \cdots, n$,

$$\dot{x}_{1i} = x_{2i}, \tag{5.23a}$$

$$\dot{x}_{2i} = -\frac{\lambda_i}{m}x_{1i} - \frac{d}{m}x_{2i} + \frac{1}{m}Q_i^T P, \tag{5.23b}$$

We rewrite the decoupled systems of (5.22) and (5.23) in the general form as (5.1) with

$$x = \begin{bmatrix} x_1 \\ x_2 \\ \eta_s \\ \xi_s \end{bmatrix}, A = \begin{bmatrix} 0 & I & 0 & 0 \\ -\frac{\Lambda}{m} & -\frac{d}{m} I_n & 0 & \frac{4k_1}{m\sqrt{n}} v \\ 0 & d\sqrt{n} v^T & 0 & 0 \\ 0 & -k_1 m\sqrt{n} v^T & -k_1 & -4k_1 \end{bmatrix}, B = \begin{bmatrix} 0 \\ \frac{Q^{-1}}{m} \\ 0 \\ 0 \end{bmatrix},$$

where $v^T = [1, 0, \cdots, 0] \in \mathbb{R}^n$. The $\mathscr{H}_2$ norm of a state variable e.g., the frequency deviation and the control cost, can be determined by setting the output $y$ equal to that state variable. Because the closed-loop system (5.19) is asymptotically stable, $A$ is Hurwitz regardless the rotations of the phase angle $\theta$.

For the transient performance of $\omega(t)$, setting $y = \omega = Qx_2$ and $C = [0, Q, 0, 0]$ and following (5.2), we obtain the observability Gramian $Q_o$ of $(C, A)$ (5.2b) in the form,

$$Q_o = \begin{bmatrix} Q_{o11} & Q_{o12} & Q_{o13} & Q_{o14} \\ Q_{o21} & Q_{o22} & Q_{o24} & Q_{o25} \\ Q_{o31} & Q_{o32} & Q_{o33} & Q_{o34} \\ Q_{o41} & Q_{o42} & Q_{o43} & Q_{o44} \end{bmatrix}.$$



Thus,

$$||H_G(\omega)||_2^2 = \mathrm{tr}(B^T Q_o B) = \frac{\mathrm{tr}(Q Q_{o22} Q^T)}{m^2} = \frac{\mathrm{tr}(Q_{o22})}{m^2}. \tag{5.24}$$

Because

$$C^T C = \begin{bmatrix} 0 & 0 & 0 & 0 \\ 0 & I_n & 0 & 0 \\ 0 & 0 & 0 & 0 \\ 0 & 0 & 0 & 0 \end{bmatrix},$$

the diagonal elements $Q_{o22}(i, i)$ of $Q_{o22}$ can be calculated by solving the observability Gramian $\tilde{Q}_i$ of $(C_i, A_i)$ which satisfies

$$\tilde{Q}_1 A_1 + A_1^T \tilde{Q}_1 + C_1^T C_1 = 0$$

where

$$A_1 = \begin{bmatrix} 0 & 1 & 0 & 0 \\ 0 & -\frac{d}{m} & 0 & \frac{4k_1}{m\sqrt{n}} \\ 0 & d\sqrt{n} & 0 & 0 \\ 0 & -k_1 m\sqrt{n} & -k_1 & -4k_1 \end{bmatrix}, C_1^T = \begin{bmatrix} 0 \\ 1 \\ 0 \\ 0 \end{bmatrix}$$

and

$$\tilde{Q}_i A_i + A_i^T \tilde{Q}_i + C_i^T C_i = 0, \ i = 2, \cdots, n,$$

where

$$A_i = \begin{bmatrix} 0 & 1 \\ -\frac{\lambda_i}{m} & -\frac{d}{m} \end{bmatrix}, C_i^T = \begin{bmatrix} 0 \\ 1 \end{bmatrix}.$$

In this case, the diagonal elements of $Q_{o22}$ satisfies $Q_{o22}(i,i) = \tilde{Q}_i(2,2)$ for $i = 1, \cdots, n$. We thus derive from the observability Gramian $\tilde{Q}_i$ that

$$\mathrm{tr}(B^T Q_o B) = \frac{n-1}{2md} + \frac{d+5mk_1}{2m(2k_1m+d)^2}, \tag{5.25}$$

which yields (5.20a) directly. Similarly by setting $y = u_s(t) = 4k_1\xi_s(t)$ and $C = [0,0,0,4k_1]$, we derive the norm of $u_s(t)$ as

$$||H_G(u_s)||_2^2 = \frac{k_1 n}{2}, \tag{5.26}$$

Because $u_i = \frac{u_s}{n}$ for $i = 1, \cdots, n$ and $||u(t)||^2 = u(t)^T u(t) = \sum_i^n u_i^2(t)$, we further derive the norm (5.20b) of the control cost $u(t)$. ■

It can be observed from Theorem (5.3.7) that the influence of $k_1$ on the transient performance of the system in GBPIAC is quite similar to that of $k$ in PIAC. The frequency deviation decrease as $k_1$ increase which however increase the control cost. Thus, a trade-off between the frequency deviation and control cost can also be determined by $k_1$ in GBPIAC. As in Theorem (5.3.6), the norm of the frequency deviation $\omega(t)$ in (5.20a) also includes two terms, the first term on the right-hand side describes the relative oscillations and the second one describes the abstract frequency deviation. Since the relative oscillations described by the first term on the right-hand side of (5.20a) cannot be influenced by the secondary controllers, the frequency deviation cannot be controlled within an arbitrarily small range.

**Remark 5.3.8** *As $k_1$ goes to infinity, the norm of the control cost also goes to infinity. However, for a deterministic disturbance, the control cost will converge to a value that depends on the disturbance which will be demonstrated in the simulations in Section 5.4.*

### 5.3.3. TRANSIENT PERFORMANCE ANALYSIS FOR DPIAC

With Assumption (5.3.4), we derive the closed-loop system of DPIAC from (5.6) and (5.10) as

$$\dot{\theta} = \omega, \tag{5.27a}$$
$$M\dot{\omega} = -L\theta - D\omega + 4k_1\xi + P \tag{5.27b}$$
$$\dot{\eta} = D\omega + 4k_1k_3L\xi, \tag{5.27c}$$
$$\dot{\xi} = -k_1M\omega - k_1\eta - 4k_1\xi. \tag{5.27d}$$

Note that $L = (L_{ij}) \in \mathbb{R}^{n\times n}$ is the Laplacian matrix of the power network and also of the communication network. Because the differences of the marginal cost can be fully represented by $4k_1L\xi(t)$, we use the squared norm of $(4k_1L\xi(t))$ to measure the coherence of the marginal cost in DPIAC. Denote the squared $\mathscr{H}_2$ norm of the transfer matrix of (5.27) with output $y = 4k_1L\xi$ by $||H(4k_1L\xi)||^2$, thus the expected value of $(4k_1\xi)^T(4k_1\xi)$ at the steady state is

$$||H(4k_1L\xi)||_2^2 = \lim_{t\to\infty} E[(4k_1L\xi)^T(4k_1L\xi)]. \tag{5.28}$$

In this subsection, we also calculate the squared $\mathscr{H}_2$ norm of $4k_1L\xi$ as an additional metric of the influence of $k_3$ on the control cost.

The following theorem states the properties of the $\mathscr{H}_2$ norm of the frequency deviation, control cost and the coherence of the marginal cost in DPIAC.

**Theorem 5.3.9** *Consider the closed-loop system (5.27) where power generation (or loads) $P = col(P_i)$ are modeled as the Gaussian white noise with $P_i \sim N(0,1)$ for $i = 1, \cdots, n$, the squared $\mathscr{H}_2$ norm of the frequency deviation $\omega(t)$, control inputs $u(t)$ and $4k_1L\xi$ are*

$$||H_D(\omega)||_2^2 = \frac{d+5mk_1}{2m(2k_1m+d)^2} + \frac{1}{2m}\sum_{i=2}^{n}\frac{b_{1i}}{e_i}, \tag{5.29a}$$

$$||H_D(u)||_2^2 = \frac{k_1}{2} + \sum_{i=2}^{n}\frac{b_{2i}}{e_i}, \tag{5.29b}$$

$$||H_D(4k_1L\xi)||_2^2 = \sum_{i=2}^{n}\frac{\lambda_i^2 b_{2i}}{m^2 e_i}, \tag{5.29c}$$

*where*

$$b_{1i} = \lambda_i^2(4k_1^2k_3m-1)^2 + 4dmk_1^3 + k_1(d+4k_1m)(4d\lambda_ik_1k_3+5\lambda_i+4dk_1),$$
$$b_{2i} = 2dk_1^3(d+2k_1m)^2 + 2\lambda_ik_1^4m^2(4k_1k_3d+4),$$
$$e_i = d\lambda_i^2(4k_1^2k_3m-1)^2 + 16d\lambda_ik_1^4k_3m^2 + d^2\lambda_ik_1 + 4k_1(d+2k_1m)^2(dk_1+\lambda_i+d\lambda_ik_1k_3).$$

*Proof:* Let $Q \in \mathbb{R}^{n\times n}$ be defined as in Lemma (5.3.5) and let $x_1 = Q^{-1}\theta, x_2 = Q^{-1}\omega, x_3 = Q^{-1}\eta, x_4 = Q^{-1}\xi$, we obtain the closed-loop system in the general form as (5.1) with

$$x = \begin{bmatrix} x_1 \\ x_2 \\ x_3 \\ x_4 \end{bmatrix}, A = \begin{bmatrix} 0 & I & 0 & 0 \\ -\frac{1}{m}\Lambda & -\frac{d}{m}I_n & 0 & \frac{4k_1}{m}I_n \\ 0 & dI_n & 0 & 4k_1k_3\Lambda \\ 0 & -k_1mI_n & -k_1I_n & -4k_1I_n \end{bmatrix}, B = \begin{bmatrix} 0 \\ \frac{Q^{-1}}{M} \\ 0 \\ 0 \end{bmatrix}.$$

where $\Lambda$ is the diagonal matrix defined in Lemma (5.3.5). The block matrices in $A$ are either zero matrix or diagonal matrix, so the components of the vector $x_1 \in \mathbb{R}^n$, $x_2 \in \mathbb{R}^n$, $x_3 \in \mathbb{R}^n$, $x_4 \in \mathbb{R}^n$ can be decoupled.

With the same method for obtaining (5.25) in the proof of Theorem (5.3.7), for the norm of the frequency deviation $\omega(t)$, setting $y = \omega = Qx_2$, $C = [0, Q, 0, 0]$ and with the same method for obtaining (5.25), we derive (5.29a). For the norm of the control cost $u(t)$, setting $y(t) = u(t) = 4k_1\xi(t)$ and $C = [0, 0, 0, 4k_1Q]$, we derive (5.29b). For the coherence measurement of the marginal cost, $||4k_1L\xi(t)||^2$, setting $y = 4k_1L\xi$ and $C = [0, 0, 0, 4k_1LQ]$, we derive (5.29c). ■

In the following part of this subsection, we analyze the impact of $k_1$ and $k_3$ on the transient performance of the frequency deviation, control cost and marginal cost coherence in DPIAC based on Theorem (5.3.9),

#### THE FREQUENCY DEVIATION

Let us focus on the influences of $k_1$ and $k_3$ on the frequency deviation respectively. When $k_3$ is fixed, we derive from (5.29a) that

$$\lim_{k_1\to\infty} ||H_D(\omega)||_2^2 = \frac{1}{2m}\sum_{i=2}^{n}\frac{\lambda_i^2k_3^2}{d\lambda_i^2k_3^2 + d(1+2\lambda_ik_3)},$$

which indicates that when $k_3$ is a nonzero constant, even with a large gain coefficient $k_1$, the frequency deviations cannot be decreased anymore. This is consistent with PIAC and GBPIAC. However, when $k_3 = 0$, we derive

$$||H_D(\omega)||_2^2 \sim O(k_1^{-1}), \tag{5.32}$$

which states that with a sufficiently large $k_1$ in the decentralized control without coordination, the frequency deviation can be controlled within an arbitrarily small range. But this sacrifices the control cost of the entire network, which will be further explained later. *So similar to the PIAC and GBPIAC control laws, if the economic power dispatch is considered, the frequency deviation cannot be controlled to an arbitrarily small range in DPIAC.*

**Remark 5.3.10** *(5.32) indicates that if all the nodes in the network are equipped with the secondary frequency controllers, the frequency deviation can be controlled to any prespecified range even without communications. However, as k in PIAC, $k_1$ cannot be arbitrarily large, which depends on the response time of the control devices [6].*

**Remark 5.3.11** *This analysis is based on Assumption (5.3.4) which requires that each node in the network is equipped with a secondary frequency controller. However, for the power systems without all the nodes equipped with the secondary frequency controllers, the disturbance from the node without a controller must be compensated by some other nodes with controllers. In that case, the equilibrium of the system is changed and oscillation can never be avoided even though the controllers of the other nodes are sufficiently sensitive to the disturbances.*



It can be easily observed from (5.29a) that when $k_1$ is fixed, the order of $k_3$ in the term $b_{1i}$ is two which is the same as in the term $e_i$, so $k_3$ has little influences on the frequency deviation.

#### THE CONTROL COST

We first analyze the influence of $k_1$ on the cost and then that of $k_3$.

For any $k_3 \geq 0$, we derive from (5.29b) that

$$||H_D(u)||_2^2 \sim O(k_1).$$

which indicates that the control cost goes to infinity as $k_1$ increases. Further with Remark (5.3.10), we conclude that the control cost always conflicts with the frequency deviation. Hence, a trade-off should also be determined to obtain the desired frequency deviation with an acceptable control cost.

From (5.29b), we obtain that

$$||H_D(u)||_2^2 \sim \frac{k_1}{2} + O(k_1 k_3^{-1}),$$

where the second term in the right hand side is positive. It shows that as $k_3$ increases, the control cost decreases. This is because as $k_3$ increases, the consensus speed of the marginal cost is accelerated which deceases the control cost. Because $k_3$ has little influence on the frequency deviation, the control cost can be decreased by $k_3$ without sacrificing the frequency deviation much.

#### THE COHERENCE OF THE MARGINAL COSTS

The coherence of the marginal cost which is measured by the norm of $||H_D(4k_1L\xi)||^2$. From (5.29c), we obtain

$$||H_D(4k_1L\xi)||_2^2 = O(k_3^{-1})$$

which confirms that the consensus speed can be increased by increasing $k_3$.

**Remark 5.3.12** *In practice, similar to $k_1$, the coefficient $k_3$ depends on the communication devices and cannot be arbitrarily large. In addition, the communication delay also influences the transient performance of the marginal cost, which still needs further investigation.*

So we have confirmed, for the power system controlled by DPIAC with Assumption (5.3.4), that:

(i) as $k_1$ increases, the frequency deviation decreases while the control cost increases.

(ii) as $k_3$ increases, the consensus speed of the marginal cost is accelerated and the control cost is decreased, which however does not influence so much to the frequency deviation.

Hence, the trade-off between the frequency deviation and the control cost can be determined by $k_1$ and $k_3$ in DPIAC.

### 5.3.4. COMPARISON OF PIAC, GBPIAC AND DPIAC

In this subsection, we compare the performance of the PIAC, GBPIAC and DPIAC control laws. As will be shown, the performance of DPIAC converges to that of GBPIAC, so we only investigate the differences between PIAC and GBPIAC, and between GBPIAC and DPIAC.

#### THE PIAC AND GBPIAC CONTROL LAWS

These two control laws are both centralized control. From Theorem (5.3.6) and (5.3.7), when the control cost for them are identical, i.e.,

$$||H_P(u)||_2 = ||H_G(u)||_2,$$

we derive $k_1 = k$ which results in

$$||H_P(\omega)||_2 < ||H_G(\omega)||_2.$$

So with the same control cost, the expected frequency deviation of PIAC is smaller than GBPIAC. This shows that PIAC is more efficient on suppressing the frequency deviation than GBPIAC.

**Remark 5.3.13** *As introduced in [82], the GBPIAC and DPIAC control laws can be applied in the MLPIAC control law which takes the advantages of the centralized and distributed control architectures. However, in contrast to GBPIAC, the PIAC method cannot be implemented together with DPIAC to minimize the control cost of the entire network.*

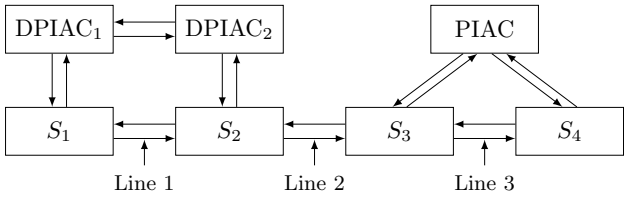


Figure 5.1: Implementation of PIAC and DPIAC in a power system.

*This is because the combination of PIAC and DPIAC cannot improve the transient performance of the marginal costs. But PIAC is compatible with DPIAC in such a way that DPIAC is implemented over the regions with cooperations while PIAC is implemented in the other regions without cooperations. As shown in Fig. (5.1), the four subsystems are coupled by line 1, line 2 and line 3. With a scheduled power flow in line 2, the control cost of the region consisting of $S_1$ and $S_2$ can be minimized by DPIAC and the one of the region consisting of $S_3$ and $S_4$ can be minimized by PIAC, while the control cost of the entire system including $S_i$, $i = 1, \cdots, 4$, cannot be minimized due to the scheduled power flow in line 2. Note that each line coupling the subsystems in Fig. (5.1) may be a set of lines connecting the buses between the subsystems.*

5

#### THE GBPIAC AND DPIAC

These two methods can be combined to form the MLPIAC method [82]. With a positive $k_1$, we can easily obtain from (5.20b) and (5.29b) that

$$||H_G(u)|| < ||H_D(u)||. \tag{5.35}$$

which is due to the differences of the marginal cost at the transient phase. The difference of the control cost between these two control laws can be decreased by accelerating the consensus speed of the marginal cost as explained in the previous subsection. In fact, from (5.29a) and (5.29b) we derive that

$$\lim_{k_3 \to \infty} ||H_D(\omega)||_2^2 = \frac{n-1}{2md} + \frac{d + 5mk_1}{2m(2k_1 m + d)^2} = ||H_G(\omega)||^2,$$
$$\lim_{k_3 \to \infty} ||H_D(u)||_2^2 = \frac{k_1}{2} = ||H_G(u)||^2.$$

Hence, as $k_3$ goes to infinity, the transient performance of the frequency deviation in DPIAC converges to the one in GBPIAC.

## 5.4. CASE STUDY

In this section, we evaluate the impact of the control parameters on the transient behavior of the frequency and marginal cost for GBPIAC and DPIAC through simulations on the IEEE 39-bus test system as in Fig. (5.2). The trade-off between the frequency deviation and control cost determined by the control parameters will be demonstrated. Because PIAC and GBPIAC are both centralized control, the role of $k_1$ and $k_1$ are similar, the trade-off in

PIAC is similar as in GBPIAC, which will not be studied in this section. The data of the test system are from [67]. All the setting of parameters for GBPIAC and DPIAC are the same as in Section 4.6 of Chapter 4 as follows. In the system, Assumption 5.3.4 is not satisfied, where $M_i$, $\alpha_i$ are heterogeneous.

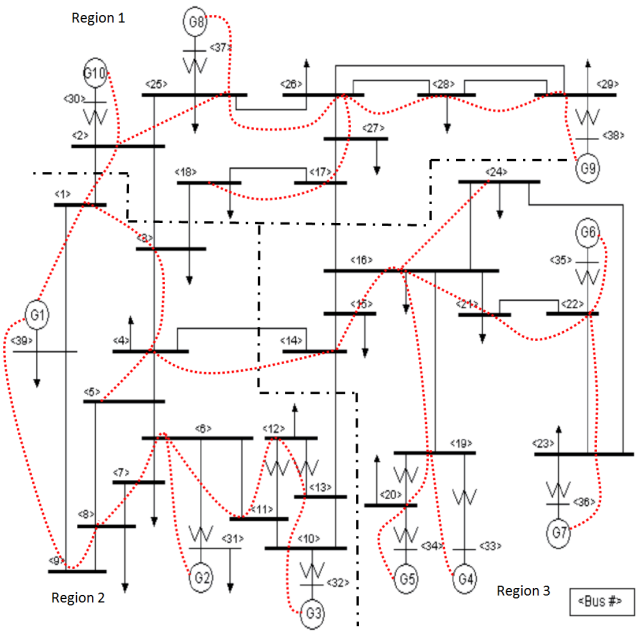


Figure 5.2: IEEE New England test power system

The system consists of 10 generators, 39 buses, which serves a total load of about 6 GW. The voltage at each bus is a constant which is derived by power flow calculation with PSAT [22]. There are 49 nodes in the network including 10 nodes of generators and 39 nodes of buses. In order to involve the frequency dependent power sources, we change the buses which are not connected to synchronous machines into frequency dependent loads. Hence $\mathcal{V}_M = \{G1, G2, G3, G4, G5, G6, G7, G8, G9, G10\}$, $\mathcal{V}_P = \{30, 31, 32, 33, 34, 35, 36, 37, 38, 39\}$ and the other nodes are in set $\mathcal{V}_F$. The nodes in $\mathcal{V}_M \cup \mathcal{V}_F$ are all equipped with secondary frequency controllers such that $\mathcal{V}_K = \mathcal{V}_M \cup \mathcal{V}_F$. We remark that each synchronous machine is connected to a bus and its phase angle is rigidly tied to the rotor angle of the bus if the voltages of the system are constants, e.g., the classical model of synchronous machine [11]. Thus the angles of the synchronous machine and the bus have the same dynamics. The droop control coefficients are set to be $D_i = 70$ (p.u./p.u. frequency deviation) for all $i \in \mathcal{V}_M$ and $D_i = 1$ p.u for all $i \in \cup\mathcal{V}_F$ under the power base 100 MVA and frequency base 60 Hz. The economic power dispatch coefficient $\alpha_i = 1/\beta_i$ where $\beta_i$ is generated randomly with a uniform distribution on $(0, 1)$. The communication network is assumed to be a spanning tree network as shown by the red lines in Fig. 5.2 and the requirement on the communication network in Assumption (4.2.3) is satisfied with the spanning tree network. For the

GBPIAC method, the entire network is controlled as a single region. We set $l_{ij} = 1$ if node $i$ and $j$ are connected by a communication line in DPIAC (4.11). Note that the topology of the communication network and the weight $l_{ij}$ also influence the transient behaviors, which however is not the main concern of this chapter. In the simulations, the system is initially in a supply-demand balanced state at the nominal frequency $f^* = 60$ Hz. At time $t = 5$ second, a step-wise increase of 66 MW of the loads at each of the buses 4, 12 and 20, amounting to a total power imbalance of 198 MW, causes the frequency to drop below the nominal frequency. We study the $\mathscr{L}_2$ norm of the frequency deviation and control cost, which reflect the $\mathscr{H}_2$ norm as integrated in (5.5).

In the following, we explain how the trade-off between the frequency deviation and the control cost can be determined by the control coefficient $k_1$ and $k_3$.

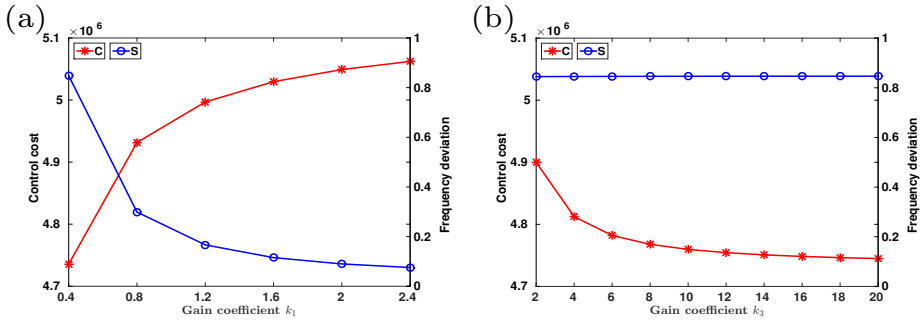


Figure 5.3: (a). The cost $S$ of frequency deviations and the cost $C$ of the control input as functions of $k_1$ (see (5.37) and (5.38). The results are of the GBPIAC method. (b). $S$ and $C$ as functions of $k_3$. The results are of the DPIAC method.

Following the objective of the optimal control in Appendix A.2, which is actually a trade-off between the frequency deviation and control cost, we calculate the frequency deviation of the nodes in $\mathcal{V}_M \cup \mathcal{V}_F$ during the transient by

$$S = \sum_{i \in \mathcal{V}_M \cup \mathcal{V}_F} \int_0^{T_0} \omega_i^2(t) dt \tag{5.37}$$

and the control cost by

$$C = \sum_{i \in \mathcal{V}_M \cup \mathcal{V}_F} \int_0^{T_0} \frac{1}{2} \alpha_i u_i^2(t) dt \tag{5.38}$$

where the simulation time $T_0$ is taken to be 50 seconds in our case. Because the role of $k_1$ in GBPIAC is the same as that in DPIAC, we only study the impact of $k_1$ on the transient performance in GBPIAC.

Fig. 5.3a shows the control cost $C$ and the frequency deviation $S$ as functions of $k_1$. It can be observed in Fig. 5.3a that as $k_1$ increases, the control cost over the transient phase also increases while the frequency deviations $S$ decreases. In an extreme case where the frequency deviation is required to be arbitrarily small, the $k_1$ must be arbitrarily large. On the contrast, if the control cost is required to be small, $k_1$ should be close to zero where

the frequency deviation will be very large. This verifies the analysis of the influences of $k_1$ on the transient performance in Section 5.3. Fig. 5.3b indicates that $k_3$ does not have as much influence to the frequency deviation $S$ as to the control cost $C$. As $k_3$ increases, the consensus speed increases leading to a small control cost. Hence, the trade-off can be resolved by the control gain coefficients.

In this case study, we conclude that the influences of the control parameters in the power systems with heterogeneous parameters are similar as in the power system with homogeneous parameter, which still needs further theoretical analysis.

## 5.5. CHAPTER CONCLUSION

In this chapter, we investigated the influence of the control parameters of the PIAC, DPIAC and GBPIAC control laws on the transient behavior of the power systems. The $\mathscr{H}_2$ norm is used to measure the transient performance. We have found that a trade-off between the frequency deviation and control cost has been established in these methods. The convergence of the total control input can be accelerated by increasing a control gain coefficient, which leads to a small frequency deviation without overshoot problem. However, this requires a high control cost. Specially, in DPIAC, the consensus of the marginal cost can also be accelerated by increasing another gain coefficient, which decreases the control cost. Hence, as in optimal control of power systems, a trade-off between the the control cost and frequency deviations can be determined by the parameters.

The calculation of the $\mathscr{H}_2$ norms are valid for the power systems with homogeneous parameters. To generalize our findings for power systems with heterogeneous parameters and for MLPIAC, the influences of these control gain coefficients on the transient performance still need further investigation. In addition, there usually are noises and delays in the measurement of the frequency and communications in practice, which are neglected in this chapter. How these factors influence the transient behaviors of the frequency and marginal cost will be studied further.

# 6

# SYNCHRONIZATION OF CYCLIC POWER GRIDS

*Synchronization is essential for the proper functioning of power grids, we investigate the synchronous states and their stability for cyclic power grids. We calculate the number of stable equilibria and investigate both linear and nonlinear stability of the synchronous state. The linear stability analysis shows that the stability of the state, determined by the smallest nonzero eigenvalue, is inversely proportional to the size of the network. We use the energy barrier to measure the nonlinear stability and calculate it by comparing the potential energy of the type-1 saddles with that of the stable synchronous state. We find that the energy barrier depends on the network size (N) in a more complicated fashion compared to the linear stability. In particular, when the generators and consumers are evenly distributed in an alternating way, the energy barrier decreases to a constant when N approaches infinity. For a heterogeneous distribution of generators and consumers, the energy barrier decreases with N. The more heterogeneous the distribution is, the stronger the energy barrier depends on N. Finally, we find that by comparing situations with equal line loads in cyclic and tree networks, tree networks exhibit reduced stability. This difference disappears in the limit of $N \to \infty$. This finding corroborates previous results reported in the literature and suggests that cyclic (sub)networks may be applied to enhance power transfer while maintaining stable synchronous operation.*

Parts of this chapter have been published in:
K. Xi, J. L. A. Dubbeldam and H. X. Lin. Synchronization of Cyclic Power Grids: Equilibria and Stability of the Synchronous State. Chaos **27**, 013109 (2017).

## 6.1. INTRODUCTION

The electrical power grid is a fundamental infrastructure in today's society and synchronization is essential for the proper functioning of the power grid. The current transition to a more distributed generation of energy by renewable sources, which are inherently more prone to fluctuations, poses even greater challenges to the functioning of the power grid. As the contribution of renewable energy to the total power being generated is surging, it becomes more challenging to keep the synchronization against large disturbances.

In power grids, the topology of the network and the distribution of power generation and consumption play important roles on the synchronization [19, 51, 59, 83–87]. The linear stability of the synchronized state against small size disturbances has been widely studied using the master stability formalism of Pecora and Carroll [88], e.g., [51, 59, 84, 87]. Complementary work on large disturbances was described by Menck *et al.* [51] with the concept of *basin stability* which was applied to estimate the basin of attraction of the synchronous state. In practice, the significance of stable operation of the power grid was acknowledged long ago and has led to general stability studies for the power grid using *direct methods* [53, 54, 89], which focus on the potential energy landscape of nonlinear power systems.

The primary interest of this chapter is to study the influence of cycles and of the distribution of generators and consumers on the synchronization. In particular, we study cyclic power grids to analyze the impact of the size of the cycle and of the heterogeneity of the power distribution on the synchronization.



We focus on the potential energy landscape of the nonlinear systems and use the *energy barrier* to measure the nonlinear stability. The energy barrier prevents loss of synchronization and is defined as the potential energy difference between the type-1 equilibria and the corresponding stable equilibrium. Starting from the commonly used second-order swing equations, we reduce our model to a system of first-order differential equations using the techniques developed by Varaiya and Chiang [23, 54] to find stability regions for synchronous operation of electric grids after a contingency. After this reduction we are left with a first-order Kuramoto model with nearest neighbor coupling.

For the case of a cyclic power grid with a homogeneous distribution of power generation and consumption, we derive analytical expressions for the stable equilibria and for their number, which generalize earlier work of DeVille [90]. Furthermore, we investigate the more general case with random distributions of generators and consumers numerically. To this end we develop a novel algorithm that allows fast determination of the stable equilibria, as well as the saddle points in the system.

Subsequently, the stability of the equilibria is studied both using linearization techniques for linear stability and direct (energy) methods for determining the nonlinear stability. By comparing our stability results for different network sizes we show that the linear stability properties differ greatly from the energy barrier obtained by direct methods when the system size increases. More specifically, the linear stability, measured by the first nonzero eigenvalue approximately scales with the number of nodes ($N$) as $1/N$. This is consistent with the findings by Lu *et al.* [91] on the linear stability of a chain or cyclic network. However, this is in contrast to the nonlinear stability result in this study, which shows that the potential energy barrier decreases to a nonzero value for $N \to \infty$. For large size cyclic power grids, small perturbations of the power supply or consumption may

lead to desynchronization. Moreover, comparison of a ring topology with a tree topology reveals enhanced stability for the ring configuration. This result suggests that the finding that dead-ends or dead-trees diminish stability by Menck *et al.* [51] can be interpreted as a special case of the more general fact that tree-like connection desynchronizes easier than ring-like connection. This confirms the earlier result in [92, 93] that forming small cycles can increase the stability of the synchronous state. However, it does not mean stability can be increased by arbitrary adding more cycles in the network because of the well-known *Braess' paradox* which has also been found in power systems [86, 87]. In this situation, the stability of the synchronous state decreases after the introduction of additional lines to the network. Hence when a cycle is added to the network to improve the stability, the Braess's paradox should be avoided.

The chapter is organized as follows. We define the model in section II and calculate the (number of) stable equilibria of cyclic networks in section III. We next analyze the linear stability of the synchronous states in section IV and the nonlinear stability in section V. Finally we conclude with a summary of our results in section VI.

## 6.2. THE MODEL

We consider the second order Kuramoto model defined by the following differential equations

$$\frac{d^2\delta_i}{dt^2} + \alpha\frac{d\delta_i}{dt} + K\sum_j A_{ij}\sin(\delta_i - \delta_j) = P_i, \tag{6.1}$$



where the summation is over all $N$ nodes in the network. In Eq. (6.1) $\delta_i$ is the phase of the $i-$th generator/load and $P_i$ is the power that is generated ($P_i > 0$) or consumed ($P_i < 0$) at node $i$ and $\alpha > 0$ is the damping parameter that we take equal for all nodes. The link or coupling strength is denoted by $K$ and $A_{ij}$ is the coefficient in the adjacency matrix of the network. The model also is called second-order Kuramoto model, see e.g., [51, 84, 94–96].

When we consider the case of a ring network, Eq. (6.1) reduce to

$$\frac{d^2\delta_i}{dt^2} + \alpha\frac{d\delta_i}{dt} + K[\sin(\delta_i - \delta_{i+1}) + \sin(\delta_i - \delta_{i-1})] = P_i, \tag{6.2}$$

with $i = 1, 2, \ldots, N$. In writing Eq. (6.2) we assumed that $\delta_{N+i} = \delta_i$. We usually rewrite the second-order differential equations as the first-order system

$$\begin{aligned} \dot{\delta}_i &= \omega_i, \\ \dot{\omega}_i &= P_i - \alpha\omega_i - K[\sin(\delta_i - \delta_{i+1}) + \sin(\delta_i - \delta_{i-1})]. \end{aligned} \tag{6.3}$$

Note that in an equilibrium, the total consumption equals to the total amount of generation, i.e., $\sum_{i=1}^{N} P_i = 0$.

The *line load* of a line is defined as follows

$$\mathscr{L}_{i,j} = K|\sin(\delta_i - \delta_j)|, \tag{6.4}$$

which measures the power transmitted by the line connecting node $i$ and node $j$.

In this chapter, we focus on the power distribution with the form

$$P_i = (-1)^{i+1}P + \xi_i, \qquad i = 1,2,\dots N-1.$$
$$\xi_i \in N(0,\sigma), \text{ and } \sum_{i=1}^{N} P_i = 0, \tag{6.5}$$

where $N(0,\sigma)$ is the normal distribution with standard deviation $\sigma \geq 0$ and mean 0, and $(\xi_1,\dots,\xi_{N-1})$ are independent and that $\xi_N = -\sum_{j=1}^{N-1}\xi_j$. We refer the model with $\sigma = 0$ as the *homogeneous model* in which power $P$ is generated at the odd nodes and $-P$ is consumed at the even nodes, i.e.,

$$P_i = (-1)^{i+1}P. \tag{6.6}$$

Further, we refer the model with $\sigma > 0$ as the *heterogeneous model* which is obtained by a Gaussian perturbation of the homogeneous model. The degree of heterogeneity of $P_i$ in the heterogeneous model is measured by $\sigma$.

To investigate the linear stability of the synchronous (equilibrium) state, Eqs. (6.3) are linearized around an equilibrium state $(\delta_i^s, 0), \quad i = 1,\dots,N$. Using vector notation $\boldsymbol{\delta} = (\delta_1,\dots,\delta_N)^T$ and $\boldsymbol{\omega} = (\omega_1,\dots,\omega_N)^T$, the linearized dynamics is given by the matrix differential equation

$$\begin{pmatrix} \dot{\boldsymbol{\delta}} \\ \dot{\boldsymbol{\omega}} \end{pmatrix} = \begin{pmatrix} 0 & I_N \\ L & -\alpha \end{pmatrix} \begin{pmatrix} \boldsymbol{\delta} \\ \boldsymbol{\omega} \end{pmatrix} = J \begin{pmatrix} \boldsymbol{\delta} \\ \boldsymbol{\omega} \end{pmatrix}, \tag{6.7}$$

with $L$ the (negative) Laplacian matrix defined by

$$\begin{aligned} L_{i,i-1} &= K\cos(\delta_i - \delta_{i-1}), \\ L_{i,i+1} &= K\cos(\delta_i - \delta_{i+1}), \\ L_{i,i} &= -K[\cos(\delta_i - \delta_{i-1}) + \cos(\delta_i - \delta_{i+1})]. \end{aligned} \tag{6.8}$$

The eigenvalues of $L$, denoted by $\lambda_i$, are related to the eigenvalues of $J$, denoted by $\mu_i$, according to the following equation

$$\mu_{i\pm} = -\frac{\alpha}{2} \pm \frac{1}{2}\sqrt{\alpha^2 + 4\lambda_i}, \quad i = 1,2,\dots,N-1. \tag{6.9}$$

These $2N-2$ eigenvalues are supplemented by two eigenvalues 0; one corresponding to a uniform frequency shift, the other to a uniform phase shift. For $\alpha > 0$, the real part of $\mu_{i\pm}$ is negative if $\lambda_i < 0$. The *type-$j$ equilibria* are defined as the ones whose Jacobian matrix $J$ have $j$ eigenvalues with a positive real part.

## 6.3. THE EQUILIBRIA OF RING NETWORKS

In this section, we study a ring network consisting of an even number of nodes ($N$) with $N/2$ generators and $N/2$ consumers, e.g., as shown in Fig. 6.1. The phase differences between neighbors are

$$\theta_1 \equiv \delta_1 - \delta_N (\text{mod } 2\pi),\ \theta_{i+1} \equiv \delta_{i+1} - \delta_i (\text{mod } 2\pi).$$

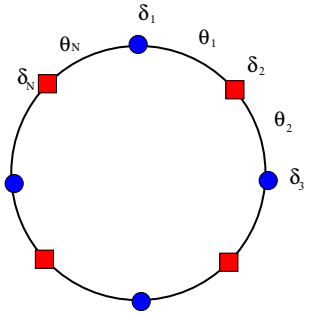


Figure 6.1: A ring network with alternating consumer and generator nodes. Circle nodes are generators and square nodes are consumers.

To find the equilibrium points we set $(\delta_i, \dot{\delta}_i) = (\delta^s, 0)$ in Eqs. (6.3) from which we find the following equations for $\theta_i$,

$$\sin\theta_i - \sin\theta_{i+1} = P_i/K, \qquad i = 1, \cdots, N \tag{6.10}$$

which is the power flow equation for this ring network.

Because all phase differences $\theta_i$ are restricted to one period of $\theta_i$, the following additional requirement holds

$$\sum_{i=1}^{N} \theta_i = 2m\pi, \quad m \in \{-\lfloor N/2 \rfloor, \ldots, -1, 0, 1, \ldots, \lfloor N/2 \rfloor\}, \tag{6.11}$$

where $\lfloor N/2 \rfloor$ denotes the floor value of $N/2$, that is, the largest integer value which is smaller than or equal to $N/2$. Each equilibrium corresponds to a synchronous state whose stability we wish to determine. We first calculate the number of stable equilibria of the homogeneous model. Note that these equilibria correspond to phase-locked solutions of a first-order Kuramoto model that was explored by DeVille [90] for the case $P = 0$. In the following three subsections, we first present an algorithm for finding all type-j equilibria of the power system, then we derive an analytical formula of the equilibria of the homogeneous model. Finally, we investigate the effect of the distribution of $P_i$ on the equilibria of the heterogeneous model.

### 6.3.1. AN ALGORITHM FOR FINDING ALL TYPE-$j$ EQUILIBRIA

The equilibria of the cyclic power grids without any power generated and consumed, i.e., $P_1 = P_2 = \cdots = P_N = 0$, have been derived by DeVille [90]. Here, we determine all the type-$j$ equilibria of general cyclic power grids with some power generated at some nodes, e.g., $P_i \neq 0$. As described in Theorem (6.4.1) which will be present in Section 6.4.1, if all the phase differences have positive cosine values, the related equilibria are stable and can be obtained directly by solving the following equations

$$\sum_{i}^{N} \theta_i = 2m\pi, \tag{6.12}$$

$$P_i - K\sin\theta_i + K\sin\theta_{i+1} = 0, \quad i = 1, \cdots, N-1, \tag{6.13}$$

with limiting $\theta_i$ into $[-\pi/2, \pi/2]$ for $i = 1, \cdots, N$ and $m$ into $(-N/4, N/4)$. Note that for heterogeneous distribution of $P_i$ with $\sigma > 0$, not all the stable equilibria can be found by solving the above equations.

In the following, we turn to the case with some phase differences having negative cosine values, i.e, phase differences exceeding $\pi/2 \pmod{2\pi}$.

If the phase difference $\theta_i$ has a negative cosine value, the line load is $s_i = K \sin\theta_i$. There must be a $\theta_i^* = \arcsin(s_i/K)$ such that $\theta_i = -\pi - \theta_i^*$ which can be plugged in Eq. (6.12) directly, the sign of the coefficient of $\theta_i$ is changed and the right hand side of Eq. (6.12) is added by $\pi$. Assume the first $i$ edges have negative cosine values. The problem is then reduced to solving the equations

$$-\theta_1 - \cdots - \theta_i + \theta_{i+1} + \cdots + \theta_N = m\pi, \tag{6.14}$$

$$P_i - K\sin\theta_i + K\sin\theta_{i+1} = 0, \quad i = 1, \cdots, N-1, \tag{6.15}$$

where $\theta_i \in [-\pi/2, \pi/2]$, and $m \in (-N/2, N/2)$ is an even integer for even $i$ and is an odd integer for odd $i$.

Assuming that $\beta = \sin\theta_N$ in Eqs. (6.14, 6.15) is known, we derive all other variables as follows.

$$\theta_i = \arcsin\Big(\frac{\sum_{j=1}^{i} P_j}{K} + \beta\Big), i = 1, \cdots, N-1. \tag{6.16}$$



By substituting the values for $\theta_i$ from Eq. (6.14), we arrive at a one-dimensional nonlinear equation for $\beta = \sin\theta_N$

$$\sum_{i=1}^{N} a_i \arcsin\Big(\frac{\sum_{j=1}^{i} P_j}{K} + \beta\Big) - m\pi = 0. \tag{6.17}$$

Where the coefficient $a_i = 1$ if edge $i$ has phase difference $\theta_i$ with a positive cosine value otherwise $a_i = -1$. All solutions to Eq. (6.17) can easily be found using the interval method [97].

We denote the number of phase differences leading to negative cosine values by $N_n$. Following the result on the spectral of weighted graph in Ref. [98], to find all the type-$j$ equilibria, it only need to solve the equilibria with $N_n = j-1, j, j+1$.

We construct the following algorithm to find all the type-$j$ equilibria of the cyclic power grids.

**Algorithm 6.1** *Finding all the type-$j$ equilibria of cyclic power grids*

1: **for** $N_n = j-1, j, j+1$ **do**
2: Collect all the combinations with $N_n$ lines whose phase difference have negative cosine values and determine the coefficient $a_i$ in Eq. (6.17). Store all the combinations and corresponding $a_i$ in a set $\mathscr{C}$.
3: **if** $N_n$ is an odd integer **then**
4: Collect odd numbers of $m$ in $(-\frac{N}{2}, \frac{N}{2})$ and store in a set $\mathscr{S}_m$,
5: **else**
6: Collect even numbers of $m$ in $(-\frac{N}{2}, \frac{N}{2})$ and store in a set $\mathscr{S}_m$.
7: **end if**
8: **for** all the combinations in $\mathscr{C}$ **do**

```
      for all m in S_m do
        Solve the one dimensional Eq. (6.17) by interval method;
        if the solution β exists then
          Calculate all the phase difference θ_i by Eq.(6.16). The ones with negative cosine
          values are π − θ_i.
          Adjust θ_N such that Σ_{i=1}^{N} θ_i = 0.
          if the equilibrium is type-j then
            Save the equilibrium.
          end if
        end if
      end for
    end for
  end for
```

Note that the computation complexity for finding all the equilibria will definitely increase at least exponentially with the number of nodes $N$. However, on finding all the type-1 equilibria, we have $N_n \leq 2$. The computational cost on solving all the type-1 equilibria is therefore $O(N^3)$. We remark that this algorithm can be extended to networks without so many cycles.

### 6.3.2. THE EQUILIBRIA OF THE HOMOGENEOUS MODEL

In this subsection, the number of stable equilibria is determined by solving the nonlinear system analytically. Our approach is similar to that of Ochab and Góra [99]. Note that for general ring networks, an upper bound of the number of stable equilibria has been derived by Delabays *et al.* [100], which is a linear function of the size $N$. Here, we focus on the special case with the homogeneous model as described in Eq. (6.6), we have the following proposition.



**Proposition 6.3.1** *Assume $P \leq 2K$, the equilibria of the ring network with homogeneous distribution of generation and consumption as in Eq.(6.6) are given by $\theta_i = \theta_1$ for odd $i$, and $\theta_i = \theta_2$ for even $i$, where*

$$\theta_1 = \arcsin\left[\frac{P}{2K\cos\frac{2m\pi}{N}}\right] + \frac{2\pi m}{N}, \tag{6.18a}$$

$$\theta_2 = -\arcsin\left[\frac{P}{2K\cos\frac{2m\pi}{N}}\right] + \frac{2\pi m}{N}, \tag{6.18b}$$

*and $m$ is an integer such that*

$$|m| \leq \lfloor \frac{N}{2\pi} \arccos\left(\sqrt{\frac{P}{2K}}\right) \rfloor.$$

*The total number of stable equilibria is given by*

$$N_s = 1 + 2\lfloor \frac{N}{2\pi} \arccos\left(\sqrt{\frac{P}{2K}}\right) \rfloor. \tag{6.19}$$

***Proof:*** In the homogeneous model as described in Eq. (6.6), it can easily be shown that the relative phase differences $\theta_i$ for all even values are either the same, that is $\theta_{2i} = \theta_2$, or satisfy $\theta_{2i} = \pi - \theta_2$ for all $i = 1, 2, \cdots N/2$. Similarly, for odd values of $i$ the $\theta_i$ are all equal to $\theta_1$ or to $\pi - \theta_1$. By Theorem (6.4.1) which will be provided in Section 6.4, the stable equilibria is with $\theta_i \in [-\pi/2, \pi/2]$, which yields $\theta_i = \theta_1$ for all odd $i$ and $\theta_i = \theta_2$ for all even $i$. So we need only consider Eq. (6.10) for a single value of $i$, which we take to be $i = 1$. The equations for homogeneous model read

$$\sin\theta_1 - \sin\theta_2 = P/K, \tag{6.20a}$$

$$\theta_1 + \theta_2 = \frac{4\pi m}{N}, \tag{6.20b}$$

We substitute the value for $\theta_2 = \frac{4\pi m}{N} - \theta_1$ in Eq. (6.20a) and solve for $\theta_1$, which is given by Eqs. (6.18). Imposing the requirement $\theta_1, \theta_2 \in [-\pi/2, \pi/2]$, we obtain the following inequality

$$\arcsin\left(\frac{P}{2K\cos(2\pi m/N)}\right) \leq \frac{\pi}{2} - \frac{2m\pi}{N}.$$

As $\sin x$ is a monotonic and positive function for $x \in [0, \pi/2]$, the inequality holds true when taking sin on both sides. Using some trigonometry we arrive at the bound of $m$, and after counting the possible values of $m$, we derive the total number of stable equilibria. ■

It follows from Proposition (6.3.1) that when $P = 0$, $N_s$ reaches the upper bound derived by Delabays *et al.* [100].

In the following we denote the stable equilibra as $\boldsymbol{\theta}_S^m = (\theta_1^m, \theta_2^m, \ldots, \theta_1^m, \theta_2^m)$ where $\theta_1^m, \theta_2^m$ can be calculated by Eqs. (6.18).

In Fig. 6.2(a), we show the total number of stable equilibria $N_S$ as a function of $P/K$. It can be clearly seen from this figure that the total number of stable equilibria decreases with $P/K$ and reaches 0 when $P/K = 2$. In the remaining of this chapter, when analysing the properties of the equilibria, we assume the capacities of the lines are large enough where there exist equilibria.

### 6.3.3. THE EQUILIBRIA OF THE HETEROGENEOUS MODEL

To investigate the effect of the distribution of $P_i$, we performed Monte Carlo (MC) simulations of the system (6.3) with the distribution of $P_i$ given by Eq. (6.5).

All the equilibria of small size power systems can be found using a software package Bertini [101–103]. However, we perform numerical calculations using Algorithm (6.1) since the size of the networks is relatively large. The algorithm amounts to finding all solutions for $\beta$ of

$$\sum_{i=1}^{N} a_i \arcsin\left(\sum_{j=1}^{i} P_j/K + \beta\right) = m\pi,$$

where $a_i = 1$ when the phase difference $\theta_i \in [-\pi/2, \pi/2]$ and $a_i = -1$ if $\theta_i \in (\pi/2, 3\pi/2]$. The bounds on the values of $m$ can be found in subsection 6.3.1. Since the number of equilibria is known to increase exponentially with $N$ as in [104, 105], it is not feasible to find all equilibria for large networks. Therefore, we developed an algorithm based on a recent theoretical paper of Bronski and DeVille [98] for finding all equilibria of type-$j$. We are particularly interested in type-1 equilibria, as a union of the stable manifolds of these

equilibria can be used to approximate the basin of stability of the stable equilibria. The algorithm is capable to find type-1 equilibria at a computational cost of $O(N^3)$ and hence can be applied to rather large networks. We remark that this algorithm might be extended to more general networks. Employing this algorithm, the number of stable equilibria are investigated as follows.

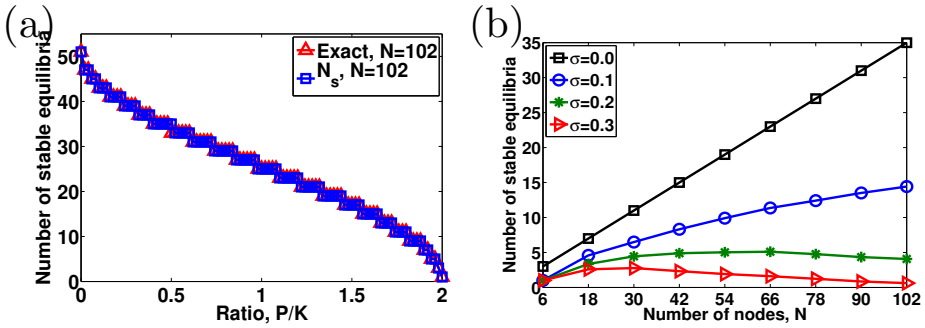


Figure 6.2: (a) The number of stable equilibria according to Eq. (6.19) compared to the numerically calculated number of stable equilibria. (b) The number of stable equilibria as a function of $N$, $P/K = 0.5$. With a larger $\sigma$, it becomes more difficult for the power system to synchronize to a stable state.



Algorithm 6.1 was applied to networks with $P/K = 0.5$ described by the heterogeneous model. In the simulations we average over 1000 independent runs for each value of $\sigma$. In Fig. 6.2(b) the number of stable equilibria is plotted as a function of the number of nodes that we vary from $N = 6$ to $N = 102$, for 4 different values of $\sigma = 0$, 0.1, 0.2, 0.3. It can clearly be seen that for $\sigma = 0.2$ or $\sigma = 0.3$ the number of stable equilibria attains a maximum value and then decreases. The same behavior is also expected for $\sigma = 0.1$. However, the decrease is expected to set in at larger values of $N$, hence such behavior cannot be observed from Fig. 6.2(b). The occurrence of a maximum for nonzero $\sigma$ can be understood as follows. If the number of nodes increases, the probability that a phase difference between two nodes exceeds $\pi/2$ also increases. Even though for moderately large $N$ ($1 < N < 50$) the fact that more equilibria can be found increases linearly with $N$, as was shown in Eq. (6.19), this increase is much smaller than the decrease caused by the arising probability of phase differences beyond $\pi/2$. This may be explained by the fact that in larger networks the probability to form clusters in which neighboring nodes $i$ and $i+1$ have large $\Delta P = |P_i - P_{i+1}|$ increases more rapidly than linearly with $N$. As a larger $\Delta P$ is associated with larger phase differences, such clusters with large fluctuations in $\Delta P$ between its members are likely to result in asynchronous behavior. This finding is in agreement with the well-known result that no synchronous states exist for an infinite Kuramoto network; see also [106].

Note that for a certain distribution of $P_i$, equilibria can be found with at least one phase difference exceeding $\frac{\pi}{2}$, but nevertheless being stable. This is in accordance with the graph theoretical result of [98] and numerical findings of Mehta *et al.* [101].

## 6.4. LINEAR STABILITY OF EQUILIBRIA

To determine the stability of the equilibria, the eigenvalues of the matrix corresponding to the system of second-order differential equations are required. These can be calculated analytically for single generator coupled to an infinite bus system for any value of damping parameter $\alpha$, in which case the system is described by a single second-order differential equation. Such an approach was also taken by Rohden *et al.* [84, 95].

The eigenvalues of the linearized system Eq. (6.7) can be explained in forms of the eigenvalues of $L$ as shown in Eq. (6.9). Thus, the stability of equilibrium is determined by the eigenvalues of $L$, i.e., a positive eigenvalue $\lambda_i$ of $L$ results in a corresponding eigenvalue $\mu_i$ with positive real part [50].

We focus on the stable equilibrium with all eigenvalues of $L$ negative and all $N-1$ pairs of eigenvalue in Eq. (6.9) are complex valued with negative real part. The most stable situation arises when the damping coefficient $\alpha$ is tuned to the optimal value $\alpha_{\text{opt}}$ described by Motter *et al.* [59]: $\alpha_{\text{opt}} = 2\sqrt{-\lambda_1}$, where $\lambda_1$ is the least negative eigenvalue of $L$, in that case $\mu_1 = -\sqrt{-\lambda_1}$. So the linear stability of the power grid is governed by the eigenvalues of $L$, which is further investigated in this section.

The entries of the matrix $L$ that arises after linearization around the synchronized state $(\boldsymbol{\delta}^s, \mathbf{0})$ are easily calculated and from that we find that $L$ is the following Laplacian matrix

$$L = \begin{pmatrix} -c_2 - c_1 & c_2 & 0 & \cdots & 0 & c_1 \\ c_2 & -c_2 - c_3 & c_3 & 0 & \cdots & 0 \\ 0 & \ddots & \ddots & \ddots & \ddots & 0 \\ 0 & \cdots & 0 & c_{N-2} & -c_{N-2} - c_{N-1} & c_{N-1} \\ c_1 & 0 & \cdots & 0 & c_{N-1} & -c_1 - c_{N-1} \end{pmatrix}, \tag{6.21}$$

where $c_i = K\cos(\delta_i - \delta_{i-1}) = K\cos\theta_i$. As matrix $L$ is a (symmetric) Laplacian matrix with zero-sum rows, $\lambda = 0$ is an eigenvalue. This reflects a symmetry in the system: if all phases are shifted by the same amount $\beta$, the system of differential equations remains invariant. It is well known that when all entries $c_i > 0$, $L$ is negative definite, hence all eigenvalues are non-positive which implies stable equilibria with the phase differences $|\delta_i - \delta_{i-1}| \leq \pi/2 \pmod{2\pi}$, for all $i = 1, \ldots, N$.

### 6.4.1. THE LINEAR STABILITY OF THE HOMOGENEOUS MODEL

For the homogeneous model, we derive a theorem which shows that type-1 equilibria appear if a single phase difference between two nodes has negative cosine value and type-$j$ equilibria with $j > 1$ appear if more than one phase differences have negative cosine value. In the following, we write a phase difference exceeds $\pi/2 \pmod{2\pi}$ if it has negative cosine value. We summarize our findings in the following theorem which slightly generalizes similar results obtained in [90, 107].

**Theorem 6.4.1** *All stable equilibria of a power grid with ring topology and homogeneous distribution of power consumption and generation as described in Eq. (6.6) are given by Eq. (6.18). Stability of the synchronous states in the network, corresponding to negative eigenvalues of the matrix J, is guaranteed as long as* $|\delta_i - \delta_{i-1}| \leq \pi/2 \pmod{2\pi}$. *If a single phase difference exceeds* $\pi/2 \pmod{2\pi}$ *this synchronous state turns unstable and*

*the corresponding equilibrium is type-1. Moreover, synchronized states with more than one absolute phase difference exceeding* $\pi/2 \pmod{2\pi}$ *correspond to equilibria with at least two unstable directions, that is, to type-*$j$ *equilibria with* $j > 1$.

***Proof:*** Since one positive eigenvalue of $J$ corresponds to one eigenvalue with positive real part of $L$, we only need to analyze the eigenvalues of $L$. The proof follows after Theorem (6.4.2). ■

**Theorem 6.4.2** *The matrix L has non-positive eigenvalues if and only if* $|\delta_i - \delta_{i-1}| \leq \frac{\pi}{2} \pmod{2\pi}$ *for* $i = 1, \ldots, N$. *A single phase difference* $|\delta_i - \delta_{i-1}| \geq \pi/2 \pmod{2\pi}$ *will result in one positive eigenvalue. If there are more than one phase differences* $|\delta_i - \delta_{i-1}| \geq \pi/2 \pmod{2\pi}$, *the number of positive eigenvalues of L is larger than 1.*

***Proof:*** The proof that all eigenvalues of $L$, are non-positive can easily be established from Gershgorin's circle theorem.

We now prove that each phase difference exceeding $\pi/2 \pmod{2\pi}$ leads to a positive eigenvalue. We will use matrix theory and Weyl's inequality to prove this, which is in the same spirit as the proof of DeVille [90] in the case of a single frequency Kuramoto network. We use the notation $\boldsymbol{\theta}_S^m$ to denote an *stable* equilibrium with a fixed value for $m$, chosen such that $\theta_1^m$, $\theta_2^m$ in the interval $[-\pi/2, \pi/2]$. The vector $\boldsymbol{\theta}_S^m$ reads in components $(\theta_1^m, \theta_2^m, \ldots, \theta_1^m, \theta_2^m)$. An equilibrium which has a single phase difference, say between node $j$ and $j-1$, exceeding $\pi/2 \pmod{2\pi}$ will be denoted by $\mathbf{T}_j^m = (\theta_1^m, \theta_2^m, \ldots, \pi - \theta_1^m, \ldots \theta_1^m, \theta_2^m)$. Depending on the $j$ being odd or even, a $\theta_1^m$ or a $\theta_2^m$ is replaced by $\pi - \theta_1^m$ or $\pi - \theta_2^m$, respectively. As the system is rotationally symmetric we might as well choose the first phase difference to be larger than $\pi/2$.

When all the phase differences are restricted to $[-\pi/2, \pi/2]$ for $\boldsymbol{\theta}_S^m$ , the Laplacian matrix $L$ takes the following form

$$L = \begin{pmatrix} -a-b & a & 0 & \ldots & 0 & b \\ a & -a-b & b & 0 & \ldots & 0 \\ 0 & b & -a-b & a & 0 & \vdots \\ \vdots & \ddots & a & -a-b & b & \vdots \\ 0 & \ddots & 0 & b & -a-b & a \\ b & 0 & \ldots & 0 & a & -a-b \end{pmatrix}, \tag{6.22}$$

with $a = K\cos(\theta_1^m) > 0$ and $b = K\cos(\theta_2^m) > 0$. It will be transformed to the Laplacian matrix $L'$:

$$L' = \begin{pmatrix} a-b & -a & 0 & \ldots & 0 & b \\ -a & a-b & b & 0 & \ldots & 0 \\ 0 & b & -a-b & a & 0 & \vdots \\ \vdots & \ddots & a & -a-b & b & \vdots \\ 0 & \ddots & 0 & b & -a-b & a \\ b & 0 & \ldots & 0 & a & -a-b \end{pmatrix}, \tag{6.23}$$

when going from the equilibrium state $\boldsymbol{\theta}_S^m$ to the equilibrium state $\mathbf{T}_j^m$. Both matrix $L$ and $L'$ have an eigenvalue $\lambda = \lambda' = 0$, with eigenvector $\mathbf{1}$. Furthermore, all other eigenvalues of $L$, which are real due to symmetry of $L$ are negative, and therefore we can order the eigenvalues of $L$ as $\lambda_0 = 0 \geq \lambda_1 \geq \lambda_2 \ldots$. As matrix $L' = L + \mathbf{x}^T\mathbf{x}$, with $\mathbf{x} = a/\sqrt{2}[1\ -1\ 0\ \ldots\ 0]$, we can use Weyl's matrix inequality to relate the eigenvalues of $L'$: $\{\lambda'\}$ to that of $L$ as follows:

$$\lambda'_0 \geq \lambda_0 = 0 \geq \lambda'_1 \geq \lambda_1. \tag{6.24}$$

Hence, at most one eigenvalue of $L'$ is negative. We can prove that one of the $\lambda'$ is negative by calculating the determinant of the reduced $(N-1)\times(N-1)$ matrix that results after removing the eigenvalue 0. $L'$ and $L'_{\text{red}}$ have the same spectrum apart from $\lambda = 0$.

$$L'_{\text{red}} = \begin{pmatrix} 2a-b & a+b & & \ldots & & \\ b & -a-b & b & 0 & \ldots & 0 \\ 0 & b & -a-b & a & 0 & \vdots \\ \vdots & \ddots & a & -a-b & b & \vdots \\ 0 & \ddots & 0 & b & -a-b & a \\ -b & -b & \ldots & -b & a-b & -a-2b \end{pmatrix}, \tag{6.25}$$

We find, using recurrence relations, that the determinant of reduced $L'$ for general values of $N > 4$ (even) is given by

$$det(L'_{\text{red}}) = a^{N/2}a^{-1}b^{-1}b^{N/2}\times \left[\frac{3}{2}bN^2 + 20bN + 56b + 14aN + 40a + aN^2\right].$$

Since the term in square brackets is always positive and $N$ is even in our case, this implies that the determinant of the reduced matrix with dimensions $(N-1)\times(N-1)$ is positive and hence there will indeed be exactly one positive eigenvalue. For the case $N \leq 4$ direct calculation of the determinant gives the result.

For the case when there are two phase differences exceeding $\pi/2 \pmod{2\pi}$, the same argument can be applied, now starting from the matrix $L'$ and defining a new matrix $L''$ in a similar fashion as above. Both the case that two neighboring phase differences exceed $\pi/2 \pmod{2\pi}$ and the case that the two non-neighboring phase differences exceed $\pi/2 \pmod{2\pi}$ must be treated. Here we shall present the case for two non neighboring phase differences exceeding $\pi/2 \pmod{2\pi}$. More precisely the equilibrium is $(\pi-\theta_1, \theta_2, \pi-\theta_1, \theta_2, \cdots, \theta_2)$. The matrix $L''$ is in this case

$$L'' = \begin{pmatrix} a-b & -a & 0 & \ldots & 0 & b \\ -a & a-b & b & 0 & \ldots & 0 \\ 0 & b & a-b & -a & 0 & \vdots \\ \vdots & \ddots & -a & a-b & b & \vdots \\ 0 & \ddots & 0 & b & -a-b & a \\ b & 0 & \ldots & 0 & a & -a-b \end{pmatrix}, \tag{6.26}$$

We remark again that the matrices $L'$ and $L''$ are related by $L'' = L' + \mathbf{x}^T\mathbf{x}$, where $\mathbf{x} = a/\sqrt{2}[0\ 0\ 1\ -1\ 0\ \ldots\ 0]$. Using Weyl's matrix inequality we can provef that $L''$ will have 2 positive eigenvalues, when the reduced $L''_{\text{red}}$ matrix, which is constructed analogous to $L'_{\text{red}}$, has a negative determinant. Using again recurrence relations, we can find $det(L''_{\text{red}})$ and hence the product of the eigenvalues of $L''$ (with $\lambda = 0$ removed)

$$det\ L''_{\text{red}} = -a^{N/2}b^{N/2}a^{-1}b^{-2}\left[(16a^2+52ab-12b^2)\right. \\ \left. + (-\frac{13}{2}a^2-20ab+3b^2)N+\frac{3}{4}(a^2+3ba)N^2\right]. \tag{6.27}$$

This expression is valid for even $N$ and $N \geq 4$, and is negative. Thus there will be two positive eigenvalues for $L''$ in this case. For $N < 4$, we can easily check our result by direct calculation. The case with two neighboring nodes having phase differences exceeding $\pi/2 \pmod{2\pi}$ can be treated in a similar fashion. In addition, it can be proven directly by Weyl's matrix inequality that $L$ has more than one positive eigenvalue if there are more than two phase differences exceeding $\pi/2 \pmod{2\pi}$. ■

A elegant proof using graph theory can be constructed as well, using the very general approach in [98]. However, here we prefer direct calculation of the reduced determinant to show that a direct calculation is feasible in this case.

Theorem (6.4.1) confirms that Eqs. (6.18) indeed capture all the stable equilibria of the homogeneous model, on which we make two remarks on the homogeneous model.

**Remark I** We notice that for the case $N \equiv 0 \pmod 4$ an infinite number of equilibria exist for the homogeneous model. We will not consider this non-generic case here, but refer to the work of DeVille [90] for more details about this case.

**Remark II** The stable equilibria depend on $m$. For practical purposes the case $m = 0$ is most desirable for transport of electricity, as in this case direct transport of power from the generator to the consumer is realized. Direct transport from generator to consumer minimizes energy losses that always accompany the transport of electrical power. The power is transported clockwise if $m < 0$ and counterclockwise if $m > 0$ as shown in Fig. 6.3(a). Note that the loop flows of the equilibria with $m \neq 0$ may exist in general networks with cycles, see [100, 108] for more details.

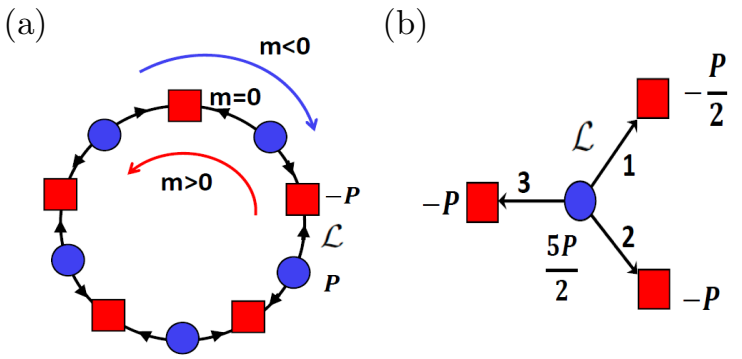


Figure 6.3: (a). A cyclic power grid with alternating consumers and generators, which may have stable equilibria with the power transported around the cycle clockwise with $m < 0$ and counterclockwise with $m > 0$. The practical synchronization state is the one with $m = 0$, in which the line load $\mathscr{L} = P/2$. (b). A tree power grid with 3 nodes. The line load of line 1 $\mathscr{L} = P/2$.

For the case $m = 0$, the stable equilibrium is $\boldsymbol{\theta}_S = (\theta_1, \theta_2, \cdots, \theta_N)$ with $\theta_1 = -\theta_2 = \arcsin\left[\frac{P}{2K}\right]$ as follows from Eqs.(6.18). It is interesting to explore the ramifications of our results for the eigenvalues of $L$ of the second-order model. We write the eigenvalues of the matrix $L$ that result after linearizing around the stable state (6.18) with $m = 0$, which can easily be determined:

$$\lambda_n = -2\sqrt{4K^2 - P^2}\sin^2\left(\frac{\pi n}{N}\right), \quad n = 0, 1, \cdots, N-1 \tag{6.28}$$

The first nonzero eigenvalue, $\lambda_1 = -2\sqrt{4K^2 - P^2}\sin^2(\pi/N)$, gives rise to an associated eigenvalue pair for matrix $J$

$$\begin{aligned} \mu_{1,+} &= \frac{-\alpha}{2} + \frac{\sqrt{\alpha^2 - 8\sin^2(\pi/N)\sqrt{4K^2 - P^2}}}{2}, \\ \mu_{1,-} &= \frac{-\alpha}{2} - \frac{\sqrt{\alpha^2 - 8\sin^2(\pi/N)\sqrt{4K^2 - P^2}}}{2}, \end{aligned} \tag{6.29}$$

whose optimal value with the largest absolute value of the real part is obtained if $\alpha$ is tuned to the value which makes the square root vanish [59]. For this value of $\alpha$, $\mu_{1,+}$=$\mu_{1,-}$=$\mu_{\text{opt}}$, which equals

$$\mu_{\text{opt}} = -\sqrt{-\lambda_1} = -\left(4K^2 - P^2\right)^{1/4}\sqrt{2}\sin(\pi/N). \tag{6.30}$$

From Eq. (6.30) we easily observe that $\mu_{\text{opt}}$ increases to 0 with a rate of $1/N$ for $N$ sufficiently large. This suggests that networks with many nodes are much more susceptible to perturbations, hence it is more difficult for the power grid to remain synchronized.

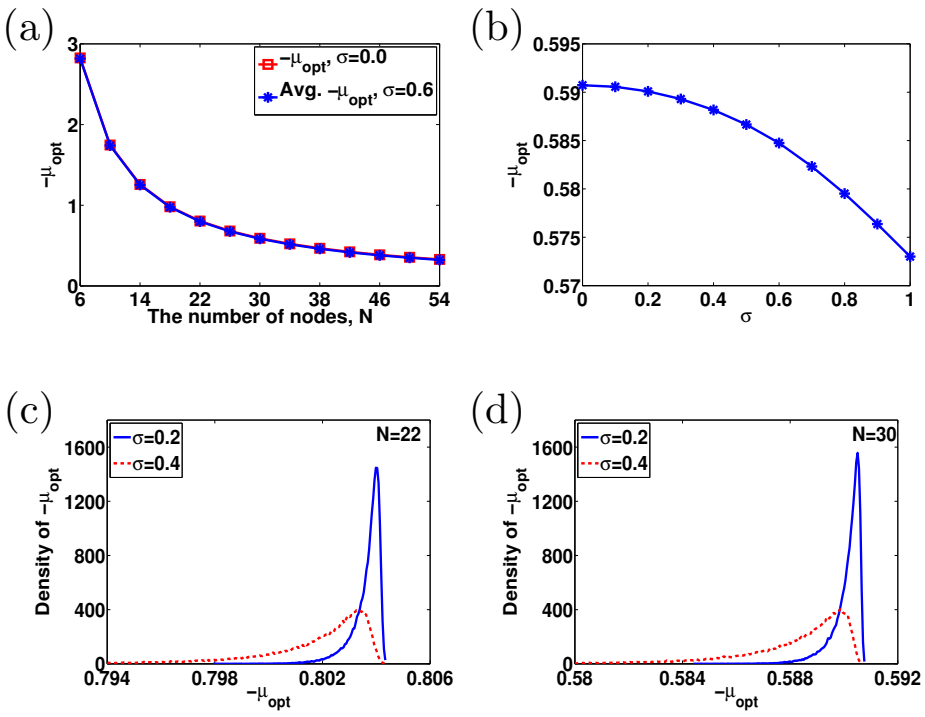


Figure 6.4: (a). $-\mu_{\text{opt}}$ as a function of $N$ for $\sigma = 0$ and $\sigma = 0.6$. (b). $-\mu_{\text{opt}}$ as a function of $\sigma$ with $N = 30$. (c). The distribution of $-\mu_{\text{opt}}$ for $\sigma = 0.2$ and $\sigma = 0.4$ and $N = 22$. (d). The density of $-\mu_{\text{opt}}$ for $\sigma = 0.2$ and $\sigma = 0.4$ where $N = 30$. $P/K = 0.125$ is kept fixed in all panels.

### 6.4.2. THE LINEAR STABILITY OF THE HETEROGENEOUS MODEL

To investigate the effect of more heterogeneous distribution of power generation and consumption, we determine the linear stability of the stable equilibria found using Algorithm 6.1. We perform MC simulations to generate heterogeneous distributions of power generation and consumption using the method given in Eq. (6.5), and average over 1000 runs. In all runs we set $P = 1$ and $K = 8$, so $P/K = 0.125$. In Fig. 6.4(a) we plotted the value of $-\mu_{\text{opt}}$ for two values of $\sigma$ as a function of $N$. Indeed the dependence on $N$ is as predicted, and the two curves almost coincide, which means the eigenvalue is not so sensitive to the heterogeneity of power distribution for the setting of $P$ and $K$. In Fig. 6.4(b) we explore the dependence on $\sigma$. Here we see as the heterogeneity of $P_i$ increases, the expected linear stability decreases. However only a very mild dependence on $\sigma$ can be seen, so the heterogeneity does not seem to be very important for this value of $P/K$. To better understand how each configuration of consumers and generators rather than the averaged configuration changes its stability with increasing heterogeneity, we plotted the distribution of $-\mu_{\text{opt}}$ in Fig. 6.4(c) and (d). These show that besides a small shift of the maximum toward smaller values of $-\mu_{\text{opt}}$ the distribution is also broader, which indicates that certain configuration will be less stable than others. We remark that the value of $y$ axis is relatively large, which

means that the $-\mu_{\text{opt}}$ is very close to the average value.

## 6.5. NONLINEAR STABILITY OF EQUILIBRIA

We next discuss the stability of synchronous operation when the system is subject to perturbations of such a degree that render the linear stability analysis of the previous section inappropriate. A measure for the stability of the stationary states is then provided by the basin of attraction of the equilibria. For high-dimensional systems this is a daunting task. However, it is possible to estimate the volume of the basin either by numerical techniques, such as for example, the recently introduced basin stability $S$, by Menck *et al.* [51, 52], in which the phase space is divided into small volumes. Choosing initial conditions in each of the small volumes and recording convergence to a stable equilibrium for each attempted initial condition, a number $S$ between 0 and 1 which is a measure for the size of the volume of the attracting phase space, can be obtained. Since this technique is computationally demanding and also labels solutions which make large excursions through phase space as stable [109], as they do belong to the stable manifold of the equilibrium, we will follow a different approach.

The stability region has been analyzed by Chiang [48] and independently Zaborszky [49, 50] and the direct method was developed by Varaiya [23, 54] to find a conservative approximation to the basin of stability. The approximation actually is the minimal energy barrier which prevents loss of synchronization.



Here, we measure the nonlinear stability by the energy barrier. We define an energy function $E(\boldsymbol{\delta}, \boldsymbol{\omega})$ by

$$\begin{aligned} E(\boldsymbol{\delta}, \boldsymbol{\omega}) &= \frac{1}{2}\sum_{i=1}^{N}\omega_i^2 - \sum_{i=1}^{N}P_i\delta_i - K\sum_{i=1}^{N}(\cos(\delta_{i+1}-\delta_i)) \\ &= \frac{1}{2}\sum_{i=1}^{N}\omega_i^2 + V(\boldsymbol{\delta}), \end{aligned} \tag{6.31}$$

where the potential $V(\boldsymbol{\delta})$ is

$$V(\boldsymbol{\delta}) = -K\sum_{i=1}^{N}\cos(\delta_{i+1}-\delta_i) - \sum_{i=1}^{N}P_i\delta_i. \tag{6.32}$$

It can easily be shown that

$$\frac{dE(\boldsymbol{\delta}, \boldsymbol{\omega})}{dt} = -\alpha\sum_{i=1}^{N}\omega_i^2 \leq 0.$$

The primary idea behind estimating the region of attraction of a stable equilibrium by the direct method, is that this region is bounded by a manifold $\mathscr{M}$ of the type-1 equilibria that reside on the *potential energy boundary surface* (PEBS) of the stable equilibrium. The PEBS can be viewed as the stability boundary of the associated gradient system [53, 54]

$$\frac{d\delta_i}{dt} = -\frac{\partial V(\boldsymbol{\delta})}{\partial \delta_i}. \tag{6.33}$$

The *closest equilibrium* is defined as the one with the lowest potential energy on the PEBS [55, 56]. By calculating the closest equilibrium with potential energy $V_{\text{min}}$ and equating this

to the total energy, it is guaranteed that points within the region bounded by the manifold $\mathscr{M} = \{(\delta, \omega) | E(\delta, \omega) = V_{\min}\}$, will always converge to the stable equilibrium point contained in $\mathscr{M}$.

The idea of estimating the region of stability by type-1 equilibria is probably best illustrated by considering a simple example of a three-node network depicted in Fig. 6.5(a). We choose this network only for illustration purposes as this small three-node network allows direct evaluation. For this network we set $P_1/K = 0.125, P_2 = -0.125, P_3/K = 0$ and $\alpha = 0$. Equipotential curves were plotted in Fig. 6.5(b). The type-1 equilibria (saddles) are displayed as little stars and pentagrams, numbered 1 to 6. It is clear that the type-1 equilibria indeed surround the stable equilibria which are shown as local minima in the potential $V$. Equilibrium 1 is the closest equilibrium with the smallest potential energy on the PEBS plotted by a black dash-dotted line. A small perturbation in the direction to saddle point 1, depicted by the red dashed curve leads to desynchronization, whereas a larger perturbation in a different direction (blue solid curve) eventually decays toward the stable equilibrium point and hence the system stays synchronized. This shows the conservativity of the direct method and the challenges in calculating the region of stability, as it depends on both the direction and size of the perturbation. One approach to this problem is to determine the so-called *controlling unstable equilibrium*, e.g., [48, 89]. We will not consider this method here, but rather restrict ourselves to the potential energy of all the type-1 saddles on the PEBS, to the energy barriers in special which are the potential energy differences between the type-1 saddles and the stable equilibrium. As displayed in Fig. 6.5(b), there are two type-1 saddles corresponding to the absolute value $|\theta_i|$ of a phase difference exceeding $\pi/2$. The potential energy of these two saddles are different and the one with smaller potential energy is more susceptible to perturbations. In the following study, all the type-1 equilibria are divided into two groups: (I) a group that corresponds to $|\theta_i|$ exceeding $\pi/2$ with smaller energy and (II) the other group with larger energy. In Fig. 6.5(b), direct calculation shows that the saddles (1-3) constitute group I and (4-6) constitute group II.



We remark that closest equilibrium 1 corresponds to the line connecting node 1 and 2 with the largest line load. This makes sense since the line with higher line load is easier to lose synchronization first.

In subsection 6.5.1, we derive the analytical approximation of energy barriers of the homogeneous model, for group I and group II respectively. In subsection 6.5.2, we present the numerical results for the heterogeneous model.

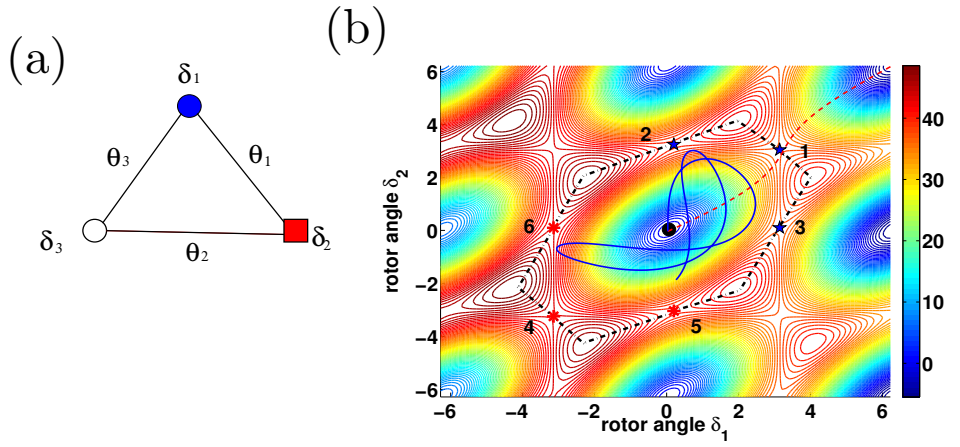


Figure 6.5: (a). A 3-node power grid with $P_1/K = 0.125, P_2/K = -0.125$ and $P_3/K = 0$, and $\theta_1 = \delta_1 - \delta_2$, $\theta_2 = \delta_2 - \delta_3$, $\theta_3 = \delta_3 - \delta_1$. (b). The potential energy as a function of $\delta_1$ and $\delta_2$, where $\delta_3 = 0$. The 6 unstable equilibria are local minima on the potential energy boundary surface (PEBS) plotted by the black dash-dotted line. The equilibria 1 and 4 correspond to the cases that $\theta_1$ exceeds $\pi/2$ and $-\pi/2$ respectively. Similarly, the equilibria 2 and 5 correspond to the cases that $\theta_2$ exceeds $-\pi/2$ and $\pi/2$ respectively, and the equilibria 3 and 6 correspond to the cases that $\theta_3$ exceeds $-\pi/2$ and $\pi/2$ respectively. Equilibrium 1 is the closest equilibrium. The trajectory plotted by the red dashed line goes through equilibrium 1 and results in desynchronization after $\theta_1$ exceeds $\pi/2$. However, the trajectory plotted by the blue solid line always stays inside the attraction of the stable equilibrium in the middle even though its energy is larger than the potential energy of equilibrium 1.



### 6.5.1. ENERGY BARRIER FOR THE HOMOGENEOUS MODEL

The potential energy of the stable state $\boldsymbol{\theta}_S^m$ derived by Eqs. (6.18) is

$$\begin{aligned} V_S^m &= -K\sum_{i=1}^{N}\cos(\theta_i^m) - \sum_{i=1}^{N} P(-1)^{i+1}\delta_i \\ &= -\frac{KN}{2}\left[\cos(\theta_1^m)+\cos(\theta_2^m)\right] + \frac{NP}{4}\left[\theta_2^m - \theta_1^m\right]. \end{aligned} \tag{6.34}$$

We next consider the potential energy of the type-1 saddle points. According to Theorem (6.4.1), a type-1 saddle point corresponds to a link with absolute phase difference exceeding $\pi/2 \pmod{2\pi}$ in the network. We denote the type-1 saddle points corresponding to the stable state $\boldsymbol{\theta}_S^m$ by

$$\boldsymbol{T}_j^m = (\hat{\theta}_1^m, \hat{\theta}_2^m, \ldots, \pi - \hat{\theta}_1^m, \hat{\theta}_2^m, \ldots, \hat{\theta}_1^m, \hat{\theta}_2^m), \tag{6.35}$$

and

$$\tilde{\boldsymbol{T}}_j^m = (\hat{\theta}_1^m, \hat{\theta}_2^m, \ldots, -\pi - \hat{\theta}_1^m, \hat{\theta}_2^m, \ldots, \hat{\theta}_1^m, \hat{\theta}_2^m) \tag{6.36}$$

where the phase difference $\theta_j$ exceeds $\pi/2 \pmod{2\pi}$ and $j$ is odd. These two equilibria belong to group I and group II respectively.

In the following, we only focus on the type-1 saddle $\boldsymbol{T}_j^m$, the same results can be obtained for $\tilde{\boldsymbol{T}}_j^m$.

The equations that determine the values of $\hat{\theta}_1^m$ and $\hat{\theta}_2^m$ are now (6.18a) (with $\hat{\theta}_i^m$ substituted for $\theta_i^m$) combined with

$$\left(\frac{N}{2}-2\right)\hat{\theta}_1^m+\frac{N}{2}\hat{\theta}_2^m=(2m-1)\pi. \tag{6.37}$$

Hence we find that the type-1 saddles are implicitly given as solutions of the following equation

$$\sin\left(\hat{\theta}_1^m-\frac{(2m-1)\pi}{N}-\frac{2\hat{\theta}_1^m}{N}\right)=\frac{P}{2K\cos\left(\frac{(2m-1)\pi}{N}+\frac{2\hat{\theta}_1^m}{N}\right)}, \tag{6.38}$$

which admits a solution $\hat{\theta}_1^m\in[0,\frac{\pi}{2}]$ when

$$\frac{P}{2K}<\cos\left((2m-1)\frac{\pi}{N}+\frac{2m+2\pi}{N(N-2)}\right).$$

Next we demonstrate that when $P=0$, the type-1 saddles found in Eq. (6.38) lie on the PEBS which surrounds the stable equilibrium $\boldsymbol{\theta}_S^m$ in the following proposition.

**Proposition 6.5.1** *If $P=0$, the type-1 saddles $\boldsymbol{T}_j^m$ and $\bar{\boldsymbol{T}}_j^m$ with $\hat{\theta}_1^m$ and $\hat{\theta}_2^m$ calculated by (6.38) and (6.37) respectively lie on the PEBS of the stable equilibrium $\boldsymbol{\theta}_S^m=(\theta_1^m,\theta_1^m,\cdots,\theta_1^m)$ with $\theta_1^m=\frac{2\pi m}{N}$.*

***Proof:*** By setting $P=0$ in Eq. (6.33) and using $\theta_i=\delta_i-\delta_{i-1}$, we obtain the dynamics of $\theta_i$ as

$$\dot{\theta}_i=-2K\sin\theta_i+K\sin\theta_{i-1}+K\sin\theta_{i+1}. \tag{6.39}$$

which coincides with the over-damped limit of Eq. (6.3). In the case of $P=0$, there are $2N$ nearby saddles with coordinates given by $\boldsymbol{T}_j^m=(\hat{\theta}_1^m,\hat{\theta}_1^m,\cdots,\pi-\hat{\theta}_1^m,\cdots,\hat{\theta}_1^m,\hat{\theta}_1^m)$ with $\hat{\theta}_1^m=\frac{(2m-1)\pi}{N-2}$ and $\bar{\boldsymbol{T}}_j^m=(\hat{\theta}_1^m,\hat{\theta}_1^m,\cdots,-\pi-\hat{\theta}_1^m,\cdots,\hat{\theta}_1^m,\hat{\theta}_1^m)$ with $\hat{\theta}_1^m=\frac{(2m+1)\pi}{N-2}$, which coincides with $\boldsymbol{T}_j^{m+1}$. We only prove $\boldsymbol{T}_j^m$ is on the PEBS of $\boldsymbol{\theta}_S^m$ and the proof of $\bar{\boldsymbol{T}}_j^m$ is analogous.

We define the region

$$I \quad = \quad \left\{(\theta_1^m,\cdots,\theta_N^m)|\sum_{i=1}^N\theta_i^m=2\pi m,\theta_i^m\in\left[\hat{\theta}_1^m,\pi-\hat{\theta}_1^m\right],i=1,\cdots N,\right\}$$

and show that $I$ is invariant under the dynamics of Eq. (6.39). It can be easily verified that the stable equilibrium $\boldsymbol{\theta}_S^m$ and the saddles $\boldsymbol{T}_j^m$ are in the region $I$.

We show that a trajectory $\boldsymbol{T}^m(t)=(\theta_1^m(t),\theta_2^m(t),\cdots,\theta_N^m(t))$ that starts in region $I$ must remain in it. As in Eq. (6.11), equation $\sum_{i=1}^N\theta_i^m(t)=2\pi m$ holds for $\boldsymbol{T}^m(t)$ with which if a component $\theta_k^m(t)$ goes through the upper bound with $\theta_k^m(t)\geq\pi-\hat{\theta}_1^m$, there must be at least one component crossing the lower bound. Otherwise, all the components satisfy $\theta_i^m(t)>\hat{\theta}_1^m, i\neq k$, which leads to $\sum_i^N\theta_i^m(t)>2\pi m$, subsequently a contradiction results. So it is only needed to prove each component $\theta_i^m(t)$ can never cross the lower bound.

First, the component of $\boldsymbol{T}^m(t)$ cannot cross the lower bound as a single component while two of its neighbors still remain in region $I$. In fact, assume a component $\theta_i^m(t)$ is going through its lower bound and its neighbors $\theta_{i+1}^m(t)$ and $\theta_{i-1}^m(t)$ are both in the range $(\hat{\theta}_1^m, \pi - \hat{\theta}_1^m)$. From Eq. (6.39), it yields

$$\dot{\theta}_i^m = -2K\sin\theta_i^m + K\sin\theta_{i+1}^m + K\sin\theta_{i-1}^m > -2K\sin\theta_i^m + 2K\sin\hat{\theta}_i^m, \tag{6.40}$$

which is positive for $\theta_i^m(t) = \hat{\theta}_1^m$. Therefore $\theta_i^m$ will increase and thus never go beyond the lower bound.

Second, the components of $\boldsymbol{T}^m(t)$ cannot cross the lower bound as a group of more than one neighboring component. Assume two components $\theta_i^m(t)$ and $\theta_{i+1}^m(t)$ are going through their lower bound and the neighbor $\theta_{i-1}^m(t)$ of $\theta_i^m(t)$ is in the range $(\hat{\theta}_1^m, \pi - \hat{\theta}_1^m)$, the inequality (6.40) for $\theta_i^m(t)$ must still be satisfied. It follows immediately $\theta_i^m(t)$ cannot cross its lower bound. Similarly it holds for $\theta_{i+1}^m(t)$.

So the only possibility for the trajectory arriving the boundary of $I$ is all its components arrive together. However, only the type-1 saddles are on the boundary. The trajectories starting from a point inside $I$ always remain inside $I$. Hence $I$ is an invariant set. Since $\boldsymbol{\theta}_S^m$ is the only stable equilibria in $I$, the unstable manifold of $\boldsymbol{T}_j^m$ limits $\boldsymbol{\theta}_S^m$. In particular, the unstable manifold of $\boldsymbol{T}_j^0(t)$ limits $\boldsymbol{\theta}_S^0$. In other words, the saddle $\boldsymbol{T}_j^0(t)$ is on the PEBS of $\boldsymbol{\theta}_S^0$. ■

One could use the same arguments as previously invoked by DeVille [90] for the case with $m = 0$. Proposition 6.5.1 remains valid for sufficiently small values of $P/K$ as the dynamical system Eq.(20) is structurally stable [110] and numerical simulations suggest that the result is in fact true for all $P/2K < 1$.

We set $m = 0$ for the reasons described in remark II in section 6.4 and denote $\boldsymbol{\theta}_S^0$ and $\boldsymbol{T}_j^0$ by $\boldsymbol{\theta}_S$ and $\boldsymbol{T}_j$ respectively. Note that there are $2N$ type-1 equilibria on the PEBS of $\boldsymbol{\theta}_S$ if $P/2K$ is sufficiently small, and each line load is $P/2$ for the equilibrium $\boldsymbol{\theta}_S$ as Fig. 6.3(a) shows.

In the following part of this subsection, we aim to calculate the potential energy differences between the stable state $\boldsymbol{\theta}_S$ and the saddle $\boldsymbol{T}_j$ for $j$ odd, which we call $\Delta V_I$

$$\begin{aligned}\Delta V_I = &-\frac{KN}{2}\left[\cos\hat{\theta}_1^0 - \cos\theta_1^0\right] - \frac{KN}{2}\left[\cos\hat{\theta}_2^0 - \cos\theta_2^0\right] \\ &+ 2K\cos\hat{\theta}_1^0 - \frac{NP}{4}\left[\hat{\theta}_1^0 - \theta_1^0\right] + \frac{NP}{4}\left[\hat{\theta}_2^0 - \theta_2^0\right] \\ &+ (-\pi/2 + \hat{\theta}_1^0)P.\end{aligned} \tag{6.41}$$

Denote $\theta_1^0, \theta_2^0$ by $\theta_1, \theta_2$ respectively for simplicity, (6.41) is rewritten as

$$\Delta V_I = \frac{KN}{2}[\cos\theta_1 - \cos\hat{\theta}_1] + \frac{KN}{2}[\cos\theta_2 - \cos\hat{\theta}_2] + 2K\cos\theta_1 + 2K[\cos\hat{\theta}_1 - \cos\theta_1] \tag{6.42}$$

$$-\frac{NP}{4}[\hat{\theta}_1 - \theta_1] + P\left(\theta_1 - \frac{\pi}{2}\right) + P(\hat{\theta}_1 - \theta_1) + \frac{NP}{4}[\hat{\theta}_2 - \theta_2].$$

It follows from (6.18a, 6.18b) and (6.38, 6.37) that

$$\hat{\theta}_1 < \theta_1, \quad \hat{\theta}_2 < \theta_2. \tag{6.43}$$

With the mean value theorem, we obtain

$$\begin{aligned}\cos\theta_1 - \cos\hat{\theta}_1 &= -(\theta_1 - \hat{\theta}_1)\sin\xi_1,\\ \cos\theta_2 - \cos\hat{\theta}_2 &= -(\theta_2 - \hat{\theta}_1)\sin\xi_2,\end{aligned} \tag{6.44}$$

where $\xi_1 \in [\hat{\theta}_1, \theta_1]$ and $\xi_2 \in [\hat{\theta}_2, \theta_2]$. With $\cos\theta_1 = \sqrt{1-(P/2K)^2}$, $\sin\theta_1 = P/2K$ and (6.44), for $\Delta V_I$, we derive

$$\Delta V_I = P\left(-\frac{\pi}{2} + \arcsin\frac{P}{2K}\right) + \sqrt{4K^2 - P^2} + \Delta U_I, \tag{6.45}$$

where $\Delta U_I$ is defined as

$$\begin{aligned}\Delta U_I = &-\frac{KN}{2}\left[\left(1-\frac{4}{N}\right)(\theta_1 - \hat{\theta}_1)\sin\xi_1 + (\theta_2 - \hat{\theta}_2)\sin\xi_2\right]\\ &+\frac{KN}{2}\left[\left(\frac{P}{2K}\right)\left[\left(1-\frac{4}{N}\right)(\theta_1 - \hat{\theta}_1) - (\theta_2 - \hat{\theta}_2)\right]\right].\end{aligned} \tag{6.46}$$

Assuming $N > 4$, we can use the fact that sin is an increasing function on $[-\pi/2, \pi/2]$ to show that

$$\Delta U_I \geq \frac{KN}{2}(\theta_1 - \hat{\theta}_1)\left[\sin\theta_1 - \frac{P}{2K}\right] + \frac{KN}{2}(\theta_2 - \hat{\theta}_2)\left[\sin\theta_2 + \frac{P}{2K}\right] = 0, \tag{6.47}$$

where we used in the last step that $\theta_2 = -\theta_1$ and $\theta_1 = \arcsin(\frac{P}{2K})$.

From (6.38) and (6.18a), we obtain that $\hat{\theta}_1 \to \theta_1$ as $N \to +\infty$. We therefore aim to find an approximate expression for type-1 saddles which are separated from the stable equilibrium by a distance that is of order $\frac{1}{N}$. We write $\hat{\theta}_1 = \Delta\theta_1 + \theta_1$. We can immediately read off from Eq. (6.38) that

$$\Delta\theta_1 = \frac{1}{N}\left(-\pi + 2\arcsin\frac{P}{2K}\right) + O(1/N^2). \tag{6.48}$$

Similarly we find for $\hat{\theta}_2 = \Delta\theta_2 + \theta_2$ that $\Delta\theta_2 = \Delta\theta_1$ is also in the order $\frac{1}{N}$. By substituting $\Delta\theta_1$ and $\Delta\theta_2$ in (6.46), we obtain

$$\Delta U_I = \frac{1}{N}\left(\frac{\pi}{2} - \arcsin\frac{P}{2K}\right)^2 \sqrt{4K^2 - P^2} + O\left(N^{-2}\right). \tag{6.49}$$

For $\tilde{\boldsymbol{T}}_j^0$, a similar calculation shows that the potential energy difference can be expressed as

$$\Delta V_{II} = P\left(\frac{\pi}{2} + \arcsin\frac{P}{2K}\right) + \sqrt{4K^2 - P^2} + \Delta U_{II}, \tag{6.50}$$

where $\Delta U_{II}$ can be proven positive and has the asymptotic form for large $N$

$$\Delta U_{II} = \frac{1}{N}\left(\frac{\pi}{2} + \arcsin\frac{P}{2K}\right)^2 \sqrt{4K^2 - P^2} + O\left(N^{-2}\right). \tag{6.51}$$

We remark that for the case $j$ is even, the derivation of the potential energy differences is analogous.

From the expression for the energy barriers $\Delta V_I$ and $\Delta V_{II}$, we can easily infer that as the line load $\mathscr{L} = P/2$ increases, $\Delta V_1$ decreases and $\Delta V_{II}$ increases. As mentioned before, $\Delta V_I$ is more susceptible to disturbances.

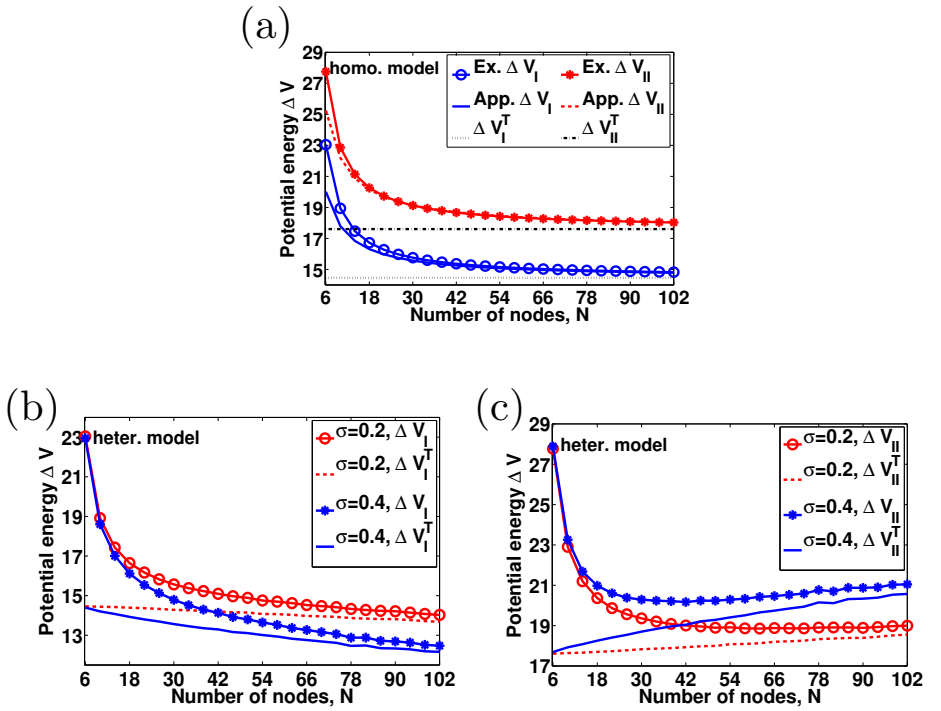


Figure 6.6: (a) The potential energy $\Delta V_I$, $\Delta V_{II}$, $\Delta V_I^T$ and $\Delta V_{II}^T$ as functions of $N$ for the homogeneous model. The approximate value of $\Delta V_I$ and $\Delta V_{II}$ are calculated neglecting the terms of $O(N^{-2})$ in Eqs. (6.49) and (6.51). (b). The average value of $\Delta V_I, \Delta V_I^T$ of heterogeneous model as functions of $N$ with $\sigma = 0.2, 0.4$. (c). The average value of $\Delta V_{II}, \Delta V_{II}^T$ of the heterogeneous model as functions of $N$ with $\sigma = 0.2, 0.4$. $P = 1$ and $K = 8$ in all panels.

Furthermore, we can immediately draw the conclusion that for large network sizes, $\Delta V_I$ and $\Delta V_{II}$ approach a limiting value that depends only on $K$ and $P$ which can be observed in Fig. 6.6(a). A direct calculation shows that the asymptotic limits correspond exactly to a potential difference found for a tree network, which is sketched in Fig. 6.3(b). Note that the line load of each line in the ring network and line 1 in the four nodes tree network are both $P/2$. Indeed, we find that for the line in a tree network with line load $P/2$, the energy leading it to desynchronization are $\Delta V_I^T$ and $\Delta V_{II}^T$ [23]

$$\begin{aligned} \Delta V_I^T &= \frac{P}{2}\left(-\pi + 2\arcsin\frac{P}{2K}\right) + \sqrt{4K^2 - P^2}, \\ \Delta V_{II}^T &= \frac{P}{2}\left(\pi + 2\arcsin\frac{P}{2K}\right) + \sqrt{4K^2 - P^2}. \end{aligned} \tag{6.52}$$

Hence the energy barrier in Eq. (6.45) and (6.50) can be explained in terms $\Delta V_I = \Delta V_I^T + \Delta U_I$ and $\Delta V_{II} = \Delta V_{II}^T + \Delta U_{II}$. As $\Delta U_I$ and $\Delta U_{II}$ are always positive, the energy needed to make a line lose synchronization (exceeding $\pi/2$ (mod $2\pi$)) is increased for the line in a ring network compared with in a tree network. In other words, the line with line load $\mathscr{L} = P/2$ in the ring network is more robust than in a tree network. This permits the line in cycles to transport more power. A ring topology results in an increased stability of the synchronous state compared to that of a tree network. This effect is larger for smaller networks. This finding corroborates the results by Menck *et al.* [51], who found decreased stability from dead-ends or, small trees in the network.

In order to examine the robustness of our results, we next perform numerically studies on the heterogeneous model as in Eq.(6.5) with $\sigma > 0$.

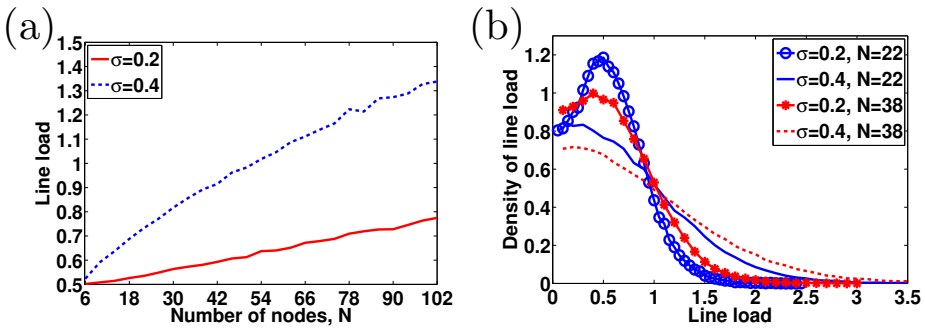


Figure 6.7: (a) The average line load, calculated by Eq. (6.4), as a function of $N$ for the heterogeneous model with $\sigma = 0.2, 0.4$. (b) The distribution of line loads of cyclic power grids with $N = 22, 38$ and $\sigma = 0.2, 0.4$. The distribution widens both for increasing values of $N$ and $\sigma$. $P = 1$ and $K = 8$ in all panels.

### 6.5.2. ENERGY BARRIER FOR THE HETEROGENEOUS MODEL

From the analysis of the nonlinear stability of cyclic power grids in homogeneous model, we know that the potential energy differences between the type-1 equilibria and the stable synchronous state with $m = 0$, is always larger than the potential energy differences for a tree like network with the same line load $\mathscr{L}$. Moreover, the potential energy barrier of the ring network approaches that of the tree network as $N$ increases. In the following, we verify whether this remains true for cyclic power grids with heterogeneous distribution of $P_i$ and study how the heterogeneity of power distribution influences the nonlinear stability.

We next focus on how the potential energy of type-1 equilibria changes as $N$ increases. As we remarked in the previous subsection, there are two groups of type-1 equilibria on the PEBS of $\boldsymbol{\theta}_S$, each having a different potential energy relative to the synchronous state, $\Delta V_I$ and $\Delta V_{II}$, respectively.

As we do not have analytical expressions for $\Delta V_I$ and $\Delta V_{II}$ in this case, we numerically compute these values for different values of $\sigma > 0$ using the same procedure for assigning values to $P_i$ as in Eq. (6.5). For different values of $N$, we perform 2000 runs to calculate $\Delta V_I$ and $\Delta V_{II}$ and compute the ensemble average. To determine which type-1 equilibria are on the PEBS of $\boldsymbol{\theta}_S$, the numerical algorithm proposed by Chiang *et al.* [48] is used.

Since $\sigma$ is nonzero, incidentally a large value of $P_i$ can be assigned to a node, which prevents the existence of a stable equilibrium. Such runs will not be considered in the average. Neither are runs in which fewer than $2N$ type-1 equilibria are found on the PEBS.

In our numerical experiments, we set again $K = 8, P = 1, P/K = 0.125$ and vary $N$ between 6 and 102 and set either $\sigma = 0.4$ or $\sigma = 0.2$.

We determine the potential differences $\Delta V_I^T$ and $\Delta V_{II}^T$ by first calculating the stable equilibria $\boldsymbol{\theta}_S$. As $\boldsymbol{\theta}_S$ determines all phase differences, it facilitates computing the line loads by Eq. (6.4) between all connected nodes. From the line loads we subsequently extract the value of $P$ which we then substitute into Eq. (6.52) to find $\Delta V_I^T$ and $\Delta V_{II}^T$, respectively.

By considering the average values of the quantities $\Delta V_I$, $\Delta V_{II}$, $\Delta V_I^T$, $\Delta V_{II}^T$, we conclude the following.

First, for the heterogeneous distribution of $P_i$, the average value of $\Delta V_I$ and $\Delta V_I^T$ decreases with $N$ as shown in Fig. 6.6(b) and Fig. 6.6(c). This is because the average line load increases with $N$ as shown in Fig. 6.7(a) and $\Delta V_I$ and $\Delta V_I^T$ are monotonously decreasing functions of the line load and $N$. However, $\Delta V_{II}$ decreases first and then increases after reaching a minimum with $N$ since it is a monotonously increasing function of line load but a decreasing function of $N$. $\Delta V_{II}^T$ always increases since it is a monotonously increasing function of the line load.

Second, for larger $\sigma$, $\Delta V_I$ decreases faster and $\Delta V_{II}$ increases faster after reaching a minimum. Since $\Delta V_I$ determines the stability more than $\Delta V_{II}$, the grid becomes less stable as $\sigma$ increases. So cyclic power grids with a homogeneous distribution of $P_i$ are more stable than ones with a heterogeneous distributed $P_i$.

Third, $\Delta V_I$ is lower bounded by $\Delta V_I^T$ and $\Delta V_{II}$ by $\Delta V_{II}^T$, and converge to the respective bound as $N \to \infty$, which is consistent with the homogeneous case. This confirms that lines in a cyclic grid can withstand larger perturbations than corresponding lines in a tree network. As the size $N$ of the cycle increases, this difference disappears gradually.

In order to get more insight in these scenarios. The distribution of $\Delta V_I, \Delta V_{II}, \Delta V_I^T$ and $\Delta V_{II}^T$ are plotted in Figs. 6.8 for different $N$ and $\sigma$.

The distribution of $\Delta V_I$ and $V_{II}$ converge to $\Delta V_I^T$ and $\Delta V_{II}^T$, respectively, which can be observed from Figs. 6.8(a-d). There is a boundary between $\Delta V_I$ and $\Delta V_{II}$ plotted by vertical black solid lines in the middle of Figs. 6.8(a-f) for different size of networks. The boundary actually is the upper bound of $\Delta V_I$ and lower bound of $\Delta V_{II}$, which is close to $2K + K\pi^2/2N$ calculated by setting $P = 0$ in Eqs. (6.45) or (6.50). This does not depend on $\sigma$, as can be verified in Figs. 6.8(e-f). For the tree connection, the boundary of $\Delta V_I^T$ and $\Delta V_{II}^T$ plotted by vertical black dashed lines in the middle of Figs. 6.8(a-d) equals $2K$ calculated by setting $P = 0$ in Eqs. (6.52).

Figs. 6.8(e-f) show that the distribution of $\Delta V_I$ and $\Delta V_{II}$ becomes broader as either $N$ or $\sigma$ increases. This is also reflected in the distribution of the line loads shown in Fig. 6.7(b). We further remark that for the heterogeneous case, the line loads are different and the lines with smaller line load becomes stronger while the ones with larger line load becomes weaker. In other words, the power grid is more resilient against some large disturbances while it is less resilient against others.

The maximum value of the density of potential energy is much smaller than that of the linear stability as shown in Figs. 6.4(c-d). This demonstrates that the potential energy is much more sensitive to the heterogeneity than the linear stability in the setting of $P$ and $K$.

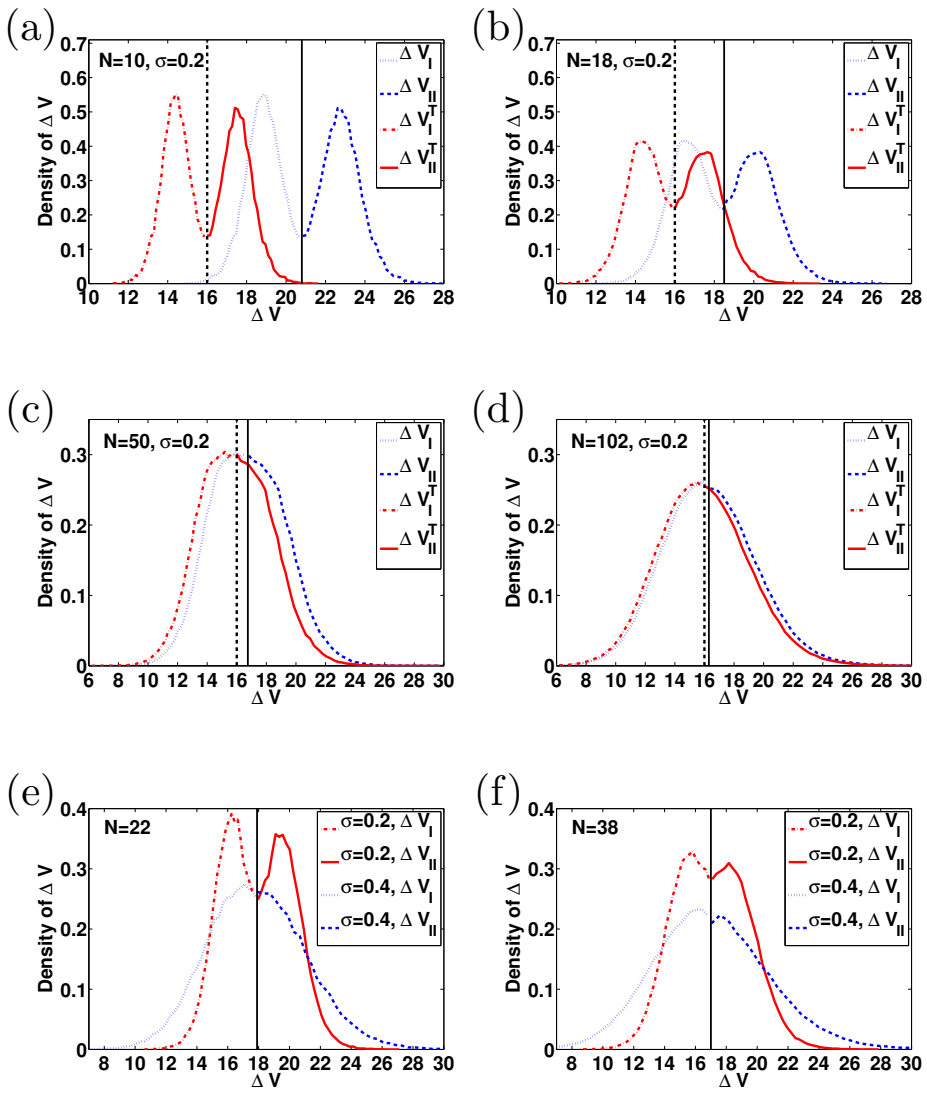


Figure 6.8: (a-d). The distribution of $\Delta V_I$, $\Delta V_{II}$, $\Delta V_I^T$ and $\Delta V_{II}^T$ for cyclic power grids for $N = 10, 18, 50, 102$. (e-f). The distribution of $\Delta V_I$ and $\Delta V_{II}$ for $\sigma = 0.2$, 0.4 with $N = 22, 38$. The vertical black dashed lines in the middle of figures (a-d) denote the boundary between $\Delta V_I^T$ and $\Delta V_{II}^T$ and the vertical black solid lines in the middle of figures (a-f) indicate the boundary between $\Delta V_I$ and $\Delta V_{II}$. $P = 1$ and $K = 8$ in all panels.

## 6.6. CHAPTER CONCLUSION

Synchronous states and their stability in cyclic power grids have been studied in this chapter. We derive analytical expressions for the stable equilibria of the cyclic power grids with homogeneous power distribution. Both linear and nonlinear stability are investigated for cyclic power grids. In particular, the nonlinear stability is measured by the energy barri-

ers, which are the potential energy differences between the type-1 equilibria and the stable equilibrium. An analytical approximation of the energy barrier is obtained for the cyclic grids with a homogeneous distributed power generation and consumption. With an efficient algorithm for all the type-1 equilibria numerical studies on the nonlinear stability have been performed for the cyclic power grids with heterogeneous distribution of power generation and consumption. For the homogeneous case, we find that adding cycles to the network increases the energy barriers. However, as the size of the cycle $N$ approaches infinity, the energy barriers decrease to constants. For the heterogeneous case, the energy barrier decreases with both the heterogeneity and the size $N$. Therefore, to benefit from the increased stability of a ring like connection, the size of the cycle should not be too large (typically $N < 10$). Furthermore, for both homogeneous and heterogeneous cases, a line connecting two nodes in a ring network is more robust than a corresponding line in a tree network carrying the same line load.

An analytical approximation of the critical clearing time [6, 111] of faults in power systems is derived by Roberts *et al.* [112] which shows that larger potential energy of the closest equilibrium may increase the critical clearing time. The energy barrier measures the energy-absorbing capability of real power grids. In further study, it is worthwhile to investigate the energy barrier of small size artificial power grids to gain insight on improving the stability of the synchronous state of general power grids. However, the challenge remains to find all the type-1 equilibria of the power systems.

# 7

# CONCLUSION

This thesis aims to investigate how to effectively suppress frequency fluctuations and improve the synchronization stability of large-scale power systems. Control laws with different control architectures have been designed, influence of the topology of the power system on the synchronization stability has been studied under the special type topology of rings. Contributions of this thesis are summarized in Section 7.1 followed by a research outlook on the control and stability analysis of power systems in Section 7.2.

## 7.1. CONCLUSIONS

We conclude this thesis by looking back at the four RQs introduced in Chapter 1.

*RQ 1. Does a stable control law exist that is able to effectively suppress the large fluctuations of the power systems integrated with a large amount of weather dependent renewable energy?*

Chapter 3 aims to answer RQ 1. In that chapter, a centralized control law named *Power-Imbalance Allocation Control* (PIAC) has been proposed to address the large frequency deviations. In the PIAC control law, a coordinator estimates the power-imbalance and dispatches the control inputs to the local controllers after solving an economic power dispatch problem. Compared to the traditional ACE based AGC control law, the proportional control input is included into secondary frequency control. With a new defined abstract frequency deviation, we decompose the dynamics of the power system into three subprocesses, i.e., the convergence of the total control input to the power-imbalance, the convergence of the abstract frequency to the nominal frequency and the synchronization of the local nodes to the abstract frequency. With this decomposition, how PIAC improves the transient performance of the power system can be explained. Because the total control input converges to the power-imbalance exponentially with a speed determined by a control coefficient only, the large frequency fluctuation problem can be effectively addressed by PIAC with a large control coefficient. In addition, when implemented in a non-cooperative multi-area control of a power network, PIAC decouples the control actions of the areas such that the control

action of one area is not influenced by the disturbances in its neighboring areas. This allows PIAC to be implemented in an asynchronous way in the areas. Lyapunov/LaSalle stability criterion based analysis shows that the PIAC control law is locally asymptotically stable for strictly convex cost functions of the economic power dispatch problem.

*RQ 2. Could the proposed control law be used in a large-scale power system? If not, how could it be reformulated for the large-scale power systems? Whether the reformulated control law for the large-scale power system is still stable?*

Because the PIAC control law is a centralized control law, it is less efficient for large-scale power systems due to the overhead of communications and complicated computations of the central coordinator. Furthermore, it is applicable only for the non-cooperative multi-area control for the power system with multi-areas where the control cost of the secondary frequency control of the entire network cannot be optimized. So PIAC is not suitable for the large-scale power systems which aim to minimize the control cost of the secondary frequency control of the entire networks. Here, the non-cooperative multi-area are not cooperative in the secondary frequency control, which however cooperate in tertiary control to negotiate on the desired power flows in the boundary lines.

Chapter 4 formulates a secondary frequency control law for large-scale power systems, which can effectively address the large frequency fluctuation problem. In that chapter, inspired by the idea of PIAC, we proposed a multi-level control law named *Multi-Level Power-Imbalance Allocation Control* (MLPIAC). In MLPIAC, the network is partitioned into two levels, at the bottom level a number of local areas consisting of nodes and at the top level a network connecting the local areas. There is a coordinator in each area. At the level of areas, a centralized control law called *Gather-Broadcast Power-Imbalance Allocation Control* (GBPIAC) is implemented. The coordinator of each area collects the frequency deviations from the nodes in the area and calculates the control inputs for these nodes by solving an economic power dispatch problem. At the top level, a distributed control law called *Distributed Power-Imbalance Allocation Control* (DPIAC) is implemented. The coordinators of the areas exchange their marginal costs based on the consensus control in order to achieve a consensus of these marginal cost. This consensus is a necessary condition to solve an economic power dispatch problem of the entire network. Besides restoring the nominal frequency, MLPIAC also solves the economic power dispatch problem of the network at the steady state. Because the total control input also converges to the power-imbalance exponentially, MLPIAC can effectively suppress the large fluctuations of the power system. The transient performance can be improved by tuning the control coefficients. With MLPIAC, there are four levels control for the load frequency control of the large-scale power system, i.e., the decentralized control of primary control at the level of nodes, centralized control GBPIAC at the level of areas which includes several nodes, distributed control DPIAC at the level of the network which consists of several areas, and tertiary control at the level of the network which guarantees the security of the system. Furthermore, the drawback of centralized control which suffers the overhead communications and complicated computations and the one of distributed control which suffers the slow convergence to the optimal steady state are well balanced in MLPIAC. Thus it is attractive to the large-scale power system with cooperative multi areas.

Asymptotic stability analysis based on the Lyapunov-LaSalle criterion is presented, which shows that if the control parameters satisfy a sufficient condition, the closed-loop system is locally asymptotically stable. However, various simulations show that MLPIAC is still stable even though this condition is not satisfied. Further investigation on finding a Lyapunov function candidate to relax this requirement is still needed.

*RQ 3. In the proposed control laws, how do the control parameters influence the transient performance of power system?*

Chapter 5 answers RQ 3. In that chapter, we investigated the transient performance of the frequency deviation and control cost of the power system controlled by PIAC, GBPIAC, DPIAC respectively. We use the $\mathscr{H}_2$ norm to measure the transient performance. It is shown in these four control laws that a trade-off is established between the frequency deviation and the control cost. The frequency deviation can be effectively suppressed at the expense of the control cost. This trade-off is determined by the control parameters of the control laws, which is illustrated by case studies. We also compared the transient performance of these three control laws. With the same control cost, PIAC is more efficient in suppressing the frequency deviation than GBPIAC. Among the GBPIAC, DPIAC control laws, with sacrificing little cost of the frequency deviations, GBPIAC is more efficient one on minimizing the control cost than DPIAC. The selection of these control laws depends on the infrastructure of the communication network, the control objectives and the cooperation of the control areas. Because MLPIAC balances the advantages and disadvantages of GBPIAC and DPIAC, the performance of MLPIAC on minimizing control cost is between GBPIAC and DPIAC.

*RQ 4. How do the rings of the power network influence the synchronization stability? How to increase the synchronization stability by controlling power generation and loads?*



In Chapter 6, we studied the synchronous (equilibrium) state of cyclic power systems. We use the energy barrier, which is the potential energy difference between the type-1 equilibria and stable equilibrium, to measure the stability of the synchronous state. The energy barrier measures the energy-absorbing capability of a power grid. Here, the energy absorbed by the system is brought by disturbances. The larger the energy barrier, the more stable the synchronization. Thus it is more difficult for the system to lose synchronization after disturbances. We find in the analysis and simulations that the energy barrier decreases as the size of the ring increases and as the power generation and loads becomes more heterogeneous. In addition, the more heterogeneous the power generation distribution is, the stronger the energy barrier depends on the size. Thus the energy barrier can be increased by adding small rings to the power network, which thus increases the synchronization stability.

By studying the energy barrier of a cyclic network and a tree network, we find that a line connecting two nodes in a cyclic network is more robust than a line in a tree network if they are transmitting the same amount of power. The smaller the ring network is, the larger the difference between them is. Thus, for the same robustness as the line in the tree network, the line in the ring network can transmit more power. Because the synchronization stability of the network is limited by the lines that are less robust, the power generation should be controlled to decrease the transmitted power by the lines with tree connections.

## 7.2. RESEARCH OUTLOOK

In the proposed control laws, the communications between the coordinator and the local controllers plays an important role on minimizing the control cost and stabilizing the system. However, there usually are noises and time-delays in the communications and in the frequency measurement, which may destroy the stability of the control laws. Hence, the robustness of the control laws needs further study.

In the model of the power system, the power losses of the transmission lines are neglected, which is realistic for traditional power system. In contrast, it is not so realistic for a micro-grid where the transmission lines are usually lossy due to large ratio of $R/X$. In addition, the voltages are assumed to be constants at all the nodes, which is also realistic for the traditional power system but not for the micro-grids because the voltage and frequency are strongly coupled when the transmission lines are lossy. So whether the proposed control laws are still stable when implemented in the micro-grid needs further investigation.

In this thesis, the overload problem of transmission lines, which is also called the *congestion problem*, is neglected. To guarantee the reliability of the power systems, the congestion problem, which may be triggered by a large disturbance, should be avoided. Otherwise, the system may lose the frequency synchronization during the transient phase, which may further lead to blackout. A sufficient condition to avoid the congestion problem is to let the phase angle differences between the nodes be in a specified range, which is considered as a constraint of the power flow in the optimal power flow calculation. However, the constraint is only valid for the steady state. In order to realize the real-time optimal control of the power flow, the congestion should be avoided on-line. How to avoid the congestion problem with improved transient performance needs further investigation.

In this thesis, the synchronization stability (transient stability) is measured by the energy barrier of the system which is related to the phase angle differences. We studied the energy barrier of ring power networks and concluded that a line in a ring should transmit more power than a comparable line in a tree. The smaller the ring, the more power can be transmitted by the lines in the ring. However the derived formula of the energy barrier is only valid for ring power network. In practice, a line may be in more than one rings. So it is valuable to study the energy barrier in general networks. In addition, the energy barrier depends on the distribution of power generation and loads. The energy barrier is usually larger if the power generation and loads are less heterogeneously distributed. Because the loads are always fluctuating, it is valuable to control the power generation to improve the energy barrier on-line in order to avoid losing the frequency synchronization. This issue also needs a further study.

# A

# APPENDIX

## A.1. STABILITY OF DAE SYSTEMS

Consider the following *Differential Algebraic Equation* (DAE) systems

$$\dot{x} = f(x, y), \tag{A.1a}$$

$$0 = g(x, y). \tag{A.1b}$$

where $x \in \mathbb{R}^n$, $y \in \mathbb{R}^m$ and $f : \mathbb{R}^n \times \mathbb{R}^m \to \mathbb{R}^n$ and $g : \mathbb{R}^n \times \mathbb{R}^m \to \mathbb{R}^m$ are twice continuously differentiable functions. $(x(x_0, y_0, t), y(x_0, y_0, t))$ is the solution with the admissible initial conditions $(x_0, y_0)$ satisfying the algebraic constraints

$$0 = g(x_0, y_0), \tag{A.2}$$

and the maximal domain of a solution of (A.1) is denoted by $\mathscr{I} \subset \mathbb{R}_{\geq 0}$ where $\mathbb{R}_{\geq 0} = \{t \in \mathbb{R} | t \geq 0\}$.

Before presenting the Lyapunove/LaSalle stability criterion of the DAE system, we make the following two assumptions.

**Assumption A.1.1** *There exists an equilibrium state $(x^*, y^*)$ for the DAEs system (A.1) such that $f(x^*, y^*) = 0,\ g(x^*, y^*) = 0$.*

**Assumption A.1.2** *Let $\Omega \subseteq \mathbb{R}^n \times \mathbb{R}^m$ be an open connected set containing $(x^*, y^*)$, assume (A.1b) is* regular *such that the Jacobian of $g$ with respect to $y$ is a full rank matrix for any $(x, y) \in \Omega$, i.e.,*

$$rank(\nabla_y g(x, y)) = m,\ \forall (x, y) \in \Omega.$$

Assumption A.1.2 ensures the existence and uniqueness of the solutions of (A.1) in $\Omega$ over the interval $\mathscr{I}$ with the initial condition $(x_0, y_0)$ satisfying (A.2).

The following theorem provides a sufficient stability criterion of the equilibrium of the DAE system (A.1).

A

**Theorem A.1.3** *(Lyapunov/LaSalle stability criterion [113, 114]): Consider the DAE system in (A.1) with assumptions A.1.1 and A.1.2, and an equilibrium* $(x^*, y^*) \in \Omega_H \subset \Omega$. *If there exists a continuously differentiable function* $H : \Omega_H \to R$, *such that* $(x^*, y^*)$ *is a strict minimum of* $H$ *i.e.,* $\nabla H|_{(x^*,y^*)} = 0$ *and* $\nabla^2 H|_{(x^*,y^*)} > 0$, *and* $\dot{H}(x, y) \leq 0,\ \forall (x, y) \in \Omega_H$, *then the following statements hold: (1).* $(x^*, y^*)$ *is a stable equilibrium with a local Lyapunov function* $V(x, y) = H(x, y) - H(x^*, y^*) \geq 0$ *for* $(x, y)$ *near* $(x^*, y^*)$, *(2). Let* $\Omega_c = \{(x, y) \in \Omega_H | H(x, y) \leq c\}$ *be a compact sub-level set for some* $c > H(x^*, y^*)$. *If no solution can stay in* $\{(x, y) \in \Omega_c | \dot{H}(x, y) = 0\}$ *other than* $(x^*, y^*)$, *then* $(x^*, y^*)$ *is asymptotically stable.*

We refer to [113] and [114] for the proof of Theorem A.1.3.

## A.2. OPTIMAL CONTROL FRAMEWORK OF DAEs

Consider the following optimal control problem of a *Differential Algebraic Equation* (DAE) system [39],

$$\min_{u_i \in \mathbb{R}} \int_0^{T_0} u^T(t) R_1 u(t) + x(t)^T R_2 x(t) dt \tag{A.3a}$$

$$s.t. \qquad \dot{x} = f(x, y, u), \tag{A.3b}$$

$$0 = g(x, y, u), \tag{A.3c}$$

with the initial condition $(x(0), y(0), u(0)) = (x_0, y_0, u_0)$ such that $g(x_0, y_0, u_0) = 0$. Here, $x \in \mathbb{R}^n, y \in \mathbb{R}^m, u \in \mathbb{R}^z$ are the state variable, algebraic variable and control input respectively, and $f : \mathbb{R}^n \times \mathbb{R}^m \times \mathbb{R}^z \to \mathbb{R}^n$ and $g : \mathbb{R}^n \times \mathbb{R}^m \times \mathbb{R}^z \to \mathbb{R}^m$. The matrix $R_1 \in \mathbb{R}^z \times \mathbb{R}^z$ and $R_2 \in \mathbb{R}^n \times \mathbb{R}^n$. $R_1 = R_1^T > 0$ and $R_2 = R_2^T > 0$ determine the trade-off between the control input and the state oscillations.

# REFERENCES


[1] WindEurope, *Report: Wind in power-2016 Europen Statistics,* (2017), https://windeurope.org/about-wind/statistics/european/wind-in-power-2016 .

[2] SolarPowerEurope, *Report: Global market outlook for solar power (2017-2021),* (2017), http://www.solarpowereurope.org/reports/global-market-outlook-2017 .

[3] E. Marris, *Energy: Upgrading the grid,* Nature News **454**, 570 (2008).

[4] J. Slootweg, *Wind power: Modelling and impact on power system dynamics*, Ph.D. thesis, TUDelft (2003).

[5] E. F. Camacho, T. Samad, M. Garcia-Sanz, and I. Hiskens, *Control for Renewable Energy and Smart Grids,* The Impact of Control Technology, Control system society , 69 (2011).

[6] P. Kundur, *Power system stability and control* (McGraw-Hill, New York, 1994).

[7] J. W. Simpson-Porco, F. Dörfler, and F. Bullo, *Voltage collapse in complex power grids,* Nat. Commun. **7**, 10790 (2016).

[8] P. Schavemaker and L. van der Sluis, *Electrical power system essentials* (John Wiley & Sons, 2008).

[9] F. Dörfler, J. W. Simpson-Porco, and F. Bullo, *Breaking the hierarchy: distributed control and economic optimality in microgrids,* IEEE Trans. Control Netw. Syst. **3**, 241 (2016), 1401.1767 .

[10] F. Dörfler and S. Grammatico, *Gather-and-broadcast frequency control in power systems,* Automatica **79**, 296 (2017).

[11] M. Ilić and J. Zaborszky, *Dynamics and control of large electric power systems* (John Wiley & Sons, 2000).

[12] C. Zhao, E. Mallada, S. Low, and J. Bialek, *A unified framework for frequency control and congestion management,* in *2016 Power Systems Computation Conference (PSCC)* (2016) pp. 1–7.

[13] S. Trip, M. Bürger, and C. D. Persis, *An internal model approach to (optimal) frequency regulation in power grids with time-varying voltages,* Automatica **64**, 240 (2016).

[14] C. D. Persis and N. Monshizadeh, *Bregman storage functions for microgrid control,* IEEE Trans. Autom. Control **63**, 53 (2018).

[15] J. Schiffer, F. Dörfler, and E. Fridman, *Robustness of distributed averaging control in power systems: Time delays & dynamic communication topology,* Automatica **80**, 261 (2017).

[16] N. Li, C. Zhao, and L. Chen, *Connecting automatic generation control and economic dispatch from an optimization view,* IEEE Trans. Control Netw. Syst. **3**, 254 (2016).

[17] J. Schiffer, R. Ortega, A. Astolfi, J. Raisch, and T. Sezi, *Conditions for stability of droop-controlled inverter-based microgrids,* Automatica **50**, 2457 (2014).

[18] J. Schiffer, D. Goldin, J. Raisch, and T. Sezi, *Synchronization of droop-controlled microgrids with distributed rotational and electronic generation,* in *52nd IEEE Conference on Decision and Control* (2013) pp. 2334–2339.

[19] F. Dörfler and F. Bullo, *Synchronization in complex networks of phase oscillators: A survey,* Automatica **50**, 1539 (2014).

[20] J. Machowski, J. W. Bialek, and J. R. Bumby, *Power system dynamics: stability and control*, 2nd ed. (Johan Wiley & Sons Ltd, 2008).

[21] A. J. Wood, B. F. Wollenberg, and G. B. Sheble, *Power Generation, Operation, and Control*, 3rd ed. (Hoboken, New Jersey : Wiley-IEEE, 2013).

[22] F. Milano, *Power systems analysis toolbox* (University of Castilla, Castilla-La Mancha, Spain, 2008).

[23] H. D. Chiang, *Direct methods for stability analysis of electric power systems* (John Wiley & Sons, Inc., New Jersey, 2010).

[24] S. Boyed and L. Vandenberghe, *Convex Optimization* (Cambridge University Press, 2009).

[25] J. Schiffer, T. Seel, J. Raisch, and T. Sezi, *Voltage stability and reactive power sharing in inverter-based microgrids with consensus-based distributed voltage control,* IEEE Trans. Control Syst. Technol. **24**, 96 (2016).

[26] M. Andreasson, D. V. Dimarogonas, H. Sandberg, and K. H. Johansson, *Distributed control of networked dynamical systems: Static feedback, integral action and consensus,* IEEE Trans. Autom. Control **59**, 1750 (2014).

[27] C. Zhao, E. Mallada, and F. Dörfler, *Distributed frequency control for stability and economic dispatch in power networks,* in *2015 American Control Conference (ACC)* (2015) pp. 2359–2364.

[28] J. W. Simpson-Porco, Q. Shafiee, F. Dörfler, J. C. Vasquez, J. M. Guerrero, and F. Bullo, *Secondary frequency and voltage control of islanded microgrids via distributed averaging,* IEEE Trans. Ind. Electron. **62**, 7025 (2015).

[29] X. Wu, C. Shen, and R. Iravani, *A distributed, cooperative frequency and voltage control for microgrids,* IEEE Trans. Smart Grid **PP**, 1 (2017).

[30] A. W. Berger and F. C. Schweppe, *Real time pricing to assist in load frequency control,* IEEE Trans. Power Syst. **4**, 920 (1989).

[31] O. I. Elgerd and C. E. Fosha, *Optimum megawatt-frequency control of multiarea electric energy systems,* IEEE Trans. Power App. Syst. **PAS-89**, 556 (1970).

[32] Ibraheem, P. Kumar, and D. P. Kothari, *Recent philosophies of automatic generation control strategies in power systems,* IEEE Trans. Power Syst. **20**, 346 (2005).

[33] S. Boyd, N. Parikh, E. Chu, B. Peleato, and J. Eckstein, *Distributed optimization and statistical learning via the alternating direction method of multipliers,* Foundations and Trends® in Machine Learning **3**, 1 (2010).

[34] Y. Liu, Z. Qu, H. Xin, and D. Gan, *Distributed real-time optimal power flow control in smart grid,* IEEE Trans. Power Syst. **32**, 3403 (2017).

[35] Z. Wang, F. Liu, S. H. Low, C. Zhao, and S. Mei, *Distributed Frequency Control with Operational Constraints, Part II: Network Power Balance,* IEEE Trans. Smart Grid **PP**, 1 (2017).

[36] D. K. Molzahn, F. Dörfler, H. Sandberg, S. H. Low, S. Chakrabarti, R. Baldick, and J. Lavaei, *A survey of distributed optimization and control algorithms for electric power systems,* IEEE Trans. Smart Grid **PP**, 1 (2017).

[37] J. Han, *From PID to active disturbance rejection control,* IEEE Trans. Ind. Electron. **56**, 900 (2009).

[38] L. Dong, Y. Zhang, and Z. Gao, *A robust decentralized load frequency controller for interconnected power systems,* ISA Trans. **51**, 410 (2012).

[39] F. Liu, Y. H. Song, J. Ma, S. Mei, and Q. Lu, *Optimal load-frequency control in restructured power systems,* IEE Proceedings - Generation, Transmission and Distribution **150**, 87 (2003).

[40] W. Fleming and R. W. Rishel, *Determistic and stochastic optimal control* (Springer-Verlag, 1975).

[41] X. Wu and C. Shen, *Distributed optimal control for stability enhancement of microgrids with multiple distributed generators,* IEEE Trans. Power Syst. **32**, 4045 (2017).

[42] X. Wu, F. Dörfler, and M. R. Jovanovic, *Input-Output analysis and decentralized optimal control of inter-area oscillations in power systems,* IEEE Trans. Power Syst. **31**, 2434 (2016), 1502.03221 .

[43] K. Vrdoljak, N. Perić, and I. Petrović, *Sliding mode based load-frequency control in power systems,* Electr. Pow. Syst. Res **80**, 514 (2010).

[44] Y. Mi, Y. Fu, C. Wang, and P. Wang, *Decentralized sliding mode load frequency control for multi-area power systems,* IEEE Trans. Power Syst. **28**, 4301 (2013).

[45] H. Bevrani, *Robust Power System Frequency Control*, 2nd ed. (Springer, 2014).

[46] D. Rerkpreedapong, A. Hasanovic, and A. Feliachi, *Robust load frequency control using genetic algorithms and linear matrix inequalities,* IEEE Trans. Power Syst. **18**, 855 (2003).

A

[47] P. Babahajiani, Q. Shafiee, and H. Bevrani, *Intelligent demand response contribution in frequency control of multi-area power systems,* IEEE Trans. Smart Grid **PP**, 1 (2016).

[48] H. D. Chiang, M. Hirsch, and F. Wu, *Stability regions of nonlinear autonomous dynamical systems,* IEEE Trans. Autom. Control **33**, 16 (1988).

[49] J. Zaborsky, G. Huang, T. C. Leung, and B. Zheng, *Stability monitoring on the large electric power system,* in *24th IEEE Conf. Decision Control*, Vol. 24 (IEEE, 1985) pp. 787–798.

[50] J. Zaborszky, G. Huang, B. Zheng, and T. C. Leung, *On the phase portrait of a class of large nonlinear dynamic systems such as the power system,* IEEE Trans. Autom. Control **33**, 4 (1988).

[51] P. J. Menck, J. Heitzig, J. Kurths, and H. Joachim Schellnhuber, *How dead ends undermine power grid stability,* Nat. Commun. **5**, 3969 (2014).

[52] P. J. Menck, J. Heitzig, N. Marwan, and J. Kurths, *How basin stability complements the linear-stability paradigm,* Nat. Phys. **9**, 89 (2013).

[53] H. D. Chiang, F. F. Wu, and P. P. Varaiya, *Foundations of the potential energy boundary surface method for power system transient stability analysis,* IEEE Trans. Circuits Syst. **35**, 712 (1988).

[54] P. P. Varaiya, F. F. Wu, and R. L. Chen, *Direct methods for transient stability analysis of power systems: Recent results,* Proc. IEEE **73**, 1703 (1985).

[55] C. W. Liu and J. S. Thorp, *A novel method to compute the closest unstable equilibrium point for transient stability region estimate in power systems,* IEEE Trans. Circuits Syst. I, Fundam. Theory Appl. **44**, 630 (1997).

[56] J. Lee and H. D. Chiang, *A singular fixed-point homotopy methodtolocate the closest unstable equilibrium point for transient stability region estimate,* IEEE Trans. Circuits Syst. II, Exp. Briefs **51**, 185 (2004).

[57] K. Xi, J. L. Dubbeldam, H. X. Lin, and J. H. van Schuppen, *Power-imbalance allocation control for secondary frequency control of power systems,* IFAC-PapersOnLine **50**, 4382 (2017), 20th IFAC World Congress.

[58] K. J. Aström and R. M. Murray, *Feedback Systems: An introduction for scientists and Engineers* (Princeton, NJ: Princeton UP, 2008).

[59] A. E. Motter, S. A. Myers, M. Anghel, and T. Nishikawa, *Spontaneous synchrony in power-grid networks,* Nat. Phys. **9**, 191 (2013).

[60] K. Xi, H. X. Lin, and J. H. van Schuppen, *Power-imbalance allocation control of frequency control of power systems-a frequency bound for time-varying loads,* in *the 36th Chinese Control Conference, Dalian, China* (2017) pp. 10528–10533.

[61] North Amertican Electric Reliablity Corporation, *Balancing and Frequency Control: A Technical Document Prepared by the NERC Resource Subcommittee,* (2011).

[62] K. Xi, J. L. A. Dubbeldam, and H. X. Lin, *Synchronization of cyclic power grids: equilibria and stability of the synchronous state,* Chaos **27**, 013109 (2017).

[63] F. Dörfler and F. Bullo, *Synchronization and transient stability in power networks and nonuniform Kuramoto oscillators,* SIAM J. Control Optim. **50**, 1616 (2012).

[64] A. Araposthatis, S. Sastry, and P. Varaiya, *Analysis of power-flow equation,* Int. J. Elec. Power **3**, 115 (1981).

[65] S. J. Skar, *Stability of multi-machine power systems with nontrivial transfer conductances,* SIAM J. Appl. Math. **39**, 475 (1980).

[66] R. A. Brualdi and H. J. Ryser, *Combinatorial matrix theory*, Vol. 39 (Cambridge University Press, 1991).

[67] T. Athay, R. Podmore, and S. Virmani, *A practical method for the direct analysis of transient stability,* IEEE Trans. Power App. Syst. **PAS-98**, 573 (1979).

[68] S. Trip and C. D. Persis, *Communication requirements in a master-slave control structure for optimal load frequency control,* IFAC-PapersOnLine **50**, 10102 (2017), 20th IFAC World Congress.

[69] K. Xi, J. L. A. Dubbeldam, H. X. Lin, and J. H. van Schuppen, *Power imbalance allocation control of power systems-secondary frequency control,* Automatica **92**, 72 (2018).

[70] Q. Shafiee, J. M. Guerrero, and J. C. Vasquez, *Distributed secondary control for islanded microgrids-a novel approach,* IEEE Trans. Power Electron. **29**, 1018 (2014).

[71] P. L. Kempker, A. C. M. Ran, and J. H. van Schuppen, *LQ control for coordinated linear systems,* IEEE Trans. Autom. Control **59**, 851 (2014).

[72] J. Komenda, T. Masopust, and J. H. van Schuppen, *Multilevel coordination control of modular des,* in *52nd IEEE Conference on Decision and Control* (2013) pp. 6323–6328.

[73] J. M. Guerrero, J. C. Vasquez, J. Matas, L. G. de Vicuna, and M. Castilla, *Hierarchical control of droop-controlled ac and dc microgrids-a general approach toward standardization,* IEEE Trans. Ind. Electron. **58**, 158 (2011).

[74] H. K. Khalil, *Nonlinear Systems*, 3rd ed. (Prentice Hall, Upper Saddle River, New Jersey 07458, 2002).

[75] S. Trip and C. De Persis, *Optimal frequency regulation in nonlinear structure preserving power networks including turbine dynamics: An incremental passivity approach,* in *2016 American Control Conference (ACC)*, Vol. 2016-July (IEEE, 2016) pp. 4132–4137.

A

[76] J. C. Doyle, K. Glover, P. P. Khargonekar, and B. A. Francis, *State-space solutions to standard H2 and H infinty control problems,* IEEE Trans. Autom. Control **34**, 831 (1989).

[77] R. Toscano, *Sturctured controllers for uncertain systems* (Springer-verlag, London, 2013).

[78] M. Andreasson, E. Tegling, H. Sandberg, and K. H. Johansson, *Coherence in synchronizing power networks with distributed integral control,* arXiv:1703.10425 (2017).

[79] J. W. Simpson-Porco, B. K. Poolla, N. Monshizadeh, and F. Dörfler, *Quadratic performance of primal-dual methods with application to secondary frequency control of power systems,* in *2016 IEEE 55th Conference on Decision and Control (CDC)* (2016) pp. 1840–1845.

[80] E. Tegling, B. Bamieh, and D. F. Gayme, *The price of synchrony: Evaluating the resistive losses in synchronizing power networks,* IEEE Trans. Control Netw. Syst. **2**, 254 (2015).

[81] B. K. Poolla, S. Bolognani, and F. Dörfler, *Optimal placement of virtual inertia in power grids,* IEEE Trans. Autom. Control **PP**, 1 (2017).

[82] K. Xi, H. X. Lin, C. Shen, and J. H. van Schuppen, *Multi-level power imbalance allocation control for secondary frequency control in power systems,* arXiv:1708.03832 (2017).

[83] S. Lozano, L. Buzna, and A. Díaz-Guilera, *Role of network topology in the synchronization of power systems,* Eur. Phys. J. B **85**, 231 (2012).

[84] M. Rohden, A. Sorge, D. Witthaut, and M. Timme, *Impact of network topology on synchrony of oscillatory power grids,* Chaos **24**, 013123 (2014).

[85] A. Arenas, A. Díaz-Guilera, J. Kurths, Y. Moreno, and C. Zhou, *Synchronization in complex networks,* Phys. Rep. **469**, 93 (2008).

[86] D. Witthaut and M. Timme, *Braess's paradox in oscillator networks, desynchronization and power outage,* New J. Phys. **14**, 083036 (2012).

[87] T. Coletta and P. Jacquod, *Linear stability and the Braess paradox in coupled-oscillator networks and electric power grids,* Phys. Rev. E **93**, 032222 (2016).

[88] L. M. Pecora and T. L. Carroll, *Master stability functions for synchronized coupled systems,* Phys. Rev. Lett. **80**, 2109 (1998).

[89] H. D. Chang, C. C. Chu, and G. Cauley, *Direct stability analysis of electric power systems using energy functions: theory, applications, and perspective,* Proc. IEEE **83**, 1497 (1995).

[90] L. DeVille, *Transitions amongst synchronous solutions in the stochastic Kuramoto model,* Nonlinearity **25**, 1473 (2012).

[91] J. A. Lu, Y. Zhang, J. Chen, and J. Lü, *Scalability analysis of the synchronizability for ring or chain networks with dense clusters,* J. Stat. Mech. Theor. Exp. **2014**, P03008 (2014).

[92] P. Schultz, T. Peron, D. Eroglu, T. Stemler, G. M. Ramírez Ávila, F. A. Rodrigues, and J. Kurths, *Tweaking synchronization by connectivity modifications,* Phys. Rev. E **93**, 062211 (2016).

[93] T. Nishikawa and A. E. Motter, *Synchronization is optimal in nondiagonalizable networks,* Phys. Rev. E **73**, 065106 (2006).

[94] G. Filatrella, A. H. Nielsen, and N. F. Pedersen, *Analysis of a power grid using a Kuramoto-like model,* Eur. Phys. J. B **61**, 485 (2008).

[95] M. Rohden, A. Sorge, M. Timme, and D. Witthaut, *Self-Organized Synchronization in Decentralized Power Grids,* Phys. Rev. Lett. **109**, 064101 (2012).

[96] A. R. Bergen and V. Vittal, *Power Systems Analysis*, 2nd ed. (Prentice-Hall Inc., New Jersey, 2000).

[97] R. E. Moore and L. Qi, *A successive interval test for nonlinear systems,* SIAM J. Numer. Anal. **19**, 845 (1982).

[98] J. C. Bronski and L. DeVille, *Spectral theory for dynamics on graphs containing attractive and repulsive interactions,* SIAM J. Appl. Math. **74**, 83 (2014).

[99] J.Ochab and P. Góra, *Synchronization of coupled oscillators in a local one-dimensional Kuramoto model,* Acta. Phys. Pol. B Proc. Suppl. **3**, 453 (2010).

[100] R. Delabays, T. Coletta, and P. Jacquod, *Multistability of phase-locking and topological winding numbers in locally coupled kuramoto models on single-loop networks,* J. Math. Phys. **57**, 032701 (2016).

[101] D. Mehta, N. S. Daleo, F. Dörfler, and J. D. Hauenstein, *Algebraic geometrization of the Kuramoto model: Equilibria and stability analysis,* Chaos **25**, 053103 (2015).

[102] D. Mehta, H. D. Nguyen, and K. Turitsyn, *Numerical polynomial homotopy continuation method to locate all the power flow solutions,* IET Gener. Transm. Distrib. **10**, 2972 (2016).

[103] D. J. Bates, J. D. Hauenstein, A. J. Sommese, and C. W. Wampler, *Bertini: Software for numerical algebraic geometry,* available at http://bertini.nd.edu .

[104] L. A. Luxemburg and G. Huang, *On the number of unstable equilibria of a class of nonlinear systems,* in *26th IEEE Conf. Decision Control*, Vol. 20 (IEEE, 1987) pp. 889–894.

[105] J. Baillieul and C. Byrnes, *Geometric critical point analysis of lossless power system models,* IEEE Trans. Circuits Syst. **29**, 724 (1982).

[106] S. H. Strogatz and R. E. Mirollo, *Collective synchronisation in lattices of nonlinear oscillators with randomness,* J. Phys. A: Math. Gen. **21**, L699 (1988).

[107] J. A. Rogge and D. Aeyels, *Stability of phase locking in a ring of unidirectionally coupled oscillators,* J. Phys. A: Math. Gen. **37**, 11135 (2004).

[108] T. Coletta, R. Delabays, I. Adagideli, and P. Jacquod, *Topologically protected loop flows in high voltage ac power grids,* New J. Phys. **18**, 103042 (2016).

[109] F. Hellmmann, P. Schutz, C. Grabow, J. Heitzig, and J. Kurths, *Survivability of deterministic dynamical systems,* Sci. Rep. **6**, 29654 (2016).

[110] J. Guckenheimer and P. J. Holmes, *Nonlinear Oscillations, Dynamical Systems, and Bifurcations of Vector Fields* (Sprinter-Verlag, 1983).

[111] P. M. Anderson and A. A. Fouad, *Power system control and stability*, 2nd ed. (Wiley-IEEE press, 2002).

[112] L. G. W. Roberts, A. R. Champneys, K. R. W. Bell, and M. di Bernardo, *Analytical approximations of critical clearing time for parametric analysis of power system transient stability,* IEEE J. Emerg Sel. Topics Circuits Syst. **5**, 465 (2015).

[113] J. Schiffer and F. Dörfler, *On stability of a distributed averaging PI frequency and active power controlled differential-algebraic power system model,* in *2016 European Control Conference (ECC)* (2016) pp. 1487–1492.

[114] D. J. Hill and I. M. Y. Mareels, *Stability theory for differential algebraic systems with applications to power systems,* IEEE Trans. Circuits Syst. **37**, 1416 (1990).

# ACKNOWLEDGEMENTS

PhD study is a challenging but enjoyable journey, which definitely broadens one's horizons and sharpens his or her research skills. Herewith, I acknowledge the China Scholarship Council for the financial support and express my gratitude to all the people who helped me make this memorable journey possible.

I would like to thank my supervisors, Prof. Hai Xiang Lin, Prof. Jan H. van Schuppen and Dr. Johan L. A. Dubbeldam. It is my honor to be your student. I could not finish my PhD project without your consistent help and support.

Hai Xiang, thank you for your confidence in me and providing me a chance to study as a PhD candidate in TUDelft. I really enjoyed your supervision which allowed me to research on what I was interested in, and your patient guidance on how to become an independent researcher. I respect your broad view on the scientific problems in the future energy supply. The discussions with you on these problems evoked my passion in my research topic. I appreciate your constant encouragement in my research specially in the second year of my PhD study when I was frustrated. You were always patient when I made mistakes, again and again. Thanks also go for your warm help in my life in the Netherlands.

Jan, thank you for bringing me into the world of control theory. You introduced me the classical courses and encouraged me to attend international conferences in this field, which built up my confidence on the research of power system control. Whenever I had questions, you either explained corresponding theory directly or suggested me possible books to find answers. This led to a rapid growth of my knowledge on system control, which provided me effective tools to solve problems from my research. I like the words " Do not worry about it" from you, which calmed my mind when I felt anxious. Thanks also go for your gifts of the classical books of control theory which definitely are great fortune for my future study.

Johan, thank you for your patient daily supervision. The word "daily" was fully illustrated by our non-appointed meetings held in your office even without knocking the door. Smiles are always on your face. This makes our meetings pleasant and efficient. I enjoyed our research topic of non-linear stability analysis of power systems though it was a hard topic in slow progress. I also appreciate your guidance on the study of non-linear systems.

I owe a great debt of gratitude to Prof. Chen Shen from the faculty of electrical engineering of Tsinghua University, who taught me the background of power systems and collaborated with me on my research topic. This collaboration was really precious to me as a mathematician. I also express my appreciation to my colleagues, Dr. J. W. van der Woude, Dr. D. Jeltsema, Dr. M. Popov and I. Tyuryukanov, for their useful discussions on my research topic.

I want to thank Prof. Arnold Heemink who helped me join the Dutch Institute of System and Control (DISC). The courses and winter school of DISC taught me the primary knowledge of system and control theory, which played a very important role in my research. I am also grateful to Kees Lemmens, Evelyn, Dorothee and Wim, who are always friendly and

A

helpful for my research and life in the Netherlands. With your help, I felt the warm of a family in which I could pay my full attention to my research.

I would like to express my gratitude to my supervisors in my master study in Shandong University, Prof. Aijie Cheng, Prof. Tongchao Lu and Prof. Hong Wang, who had all encouraged, supported and helped me to study abroad. Thank you for providing me a position of research assistant in Shandong University before I came to TUDelft. This work experience was not only memorable but also very useful for my PhD study. I also express my gratitude to Jialin Dai, Yunxin Liu, Yunxian Liu, Ning Du, Yongqiang Ren, Xuhao Zhang, Weidong Cao, Guo Chen, Daowan Song, Dai Tao and Jinbiao Yu, who all helped me a lot during this precious work experience.

I would also like to thank my friends and colleagues, with whom my life overseas becomes colorful and not so lonely. Xiaoyan, Mohit, Corine, Tugce, Nick, Yoeri, Bijan, Mahya, Adelaide, Isabel, Paulo, Xiangrong, Jianbing, Cong, Senlei, Haochuan, Yandong, Xiaohui, Renli, Jie, Xiao, Xinchao, Yuan, Jingtang, Changgong, Qian, Yunlong, Yuanhao, Zhijie, Yu, Chong and Chuanqing, I really enjoyed our lunch time, drinking time, various entertainments and pleasant talking about various topics. In particular, I want to thank my friends, Guangliang and Sha, from whom I had got many help to quickly get used to the life in the new environment.

My PhD journy could not be started without all the support from my family. I express my gratitude to my uncles, Shunqi Xi and Bo Zhu, and my aunt, Baoyan, for your useful advices on this long term study. Papa, Mama, thank you for bringing me to this colourful world and also for your unconditional support in my long term study. Kaiying, Kailan, I am so happy to have you two sisters. Without your care of our parents, I cannot spend my full energy on my PhD study. Finally, I would like to thank my wife. Yanjun, I cannot find a word to describe how lucky I am to marry you. Thank you for your understanding and warm encouragement in the past more than four years. The happiest thing in the world must be becoming a father. Thank you for bringing our daughter, Xinyue, to me. She makes my life so wonderful. I love you very much.

*Kaihua*

*Delft, May 2018*

# CURRICULUM VITÆ

Kaihua Xi was born on 20 February 1986, in Linyi, Shandong province, China. In 2003, he went to Shandong Normal University for an undergraduate study majored in computational mathematics. After obtaining his bachelor degree in 2007, he started his master study in the School of Mathematics, Shandong University, where he studied on numerical analysis of partial differential equations and multi-phase flow equations in porous media. After his master thesis defense in June 2010, he worked as a research assistant in the School of Mathematics, Shandong University, where he researched on fast numerical algorithms for oil reservoir simulations for enhanced oil recovery technology, such as alkaline, polymer and surfactant flooding.

In October 2013, he started his PhD study at Delft Institute of Applied Mathematics, Delft University of Technology, under the supervision of Prof. Hai Xiang Lin, Prof. Jan H. van Schuppen and Dr. Johan L. A. Dubbeldam. His research topic was control and stability analysis of power systems, which aimed to improve the reliability and security of the power systems with a large amount of variable renewable energy supplies.

# List of Publications

**Journal Publications:**

1. **Kaihua Xi**, Hai Xiang Lin and Jan H. van Schuppen. *Transient Performance of Power Systems with Distributed Power-Imbalance Allocation Control*, to be Submitted (2018).

2. **Kaihua Xi**, Hai Xiang Lin, Chen Shen and Jan H. van Schuppen. *Multi-Level Power-Imbalance Allocation Control for Secondary Frequency Control of Power Systems*, under review (2018).

3. **Kaihua Xi**, Johan L. A. Dubbeldam, Hai Xiang Lin and Jan H. van Schuppen. *Power-Imbalance Allocation Control of Power Systems-Secondary Frequency Control*, Automatica, 92: 72-85, (2018).

4. **Kaihua Xi**, Johan L. A. Dubbeldam and Hai Xiang Lin. *Synchronization of Cyclic Power Grids: Equilibria and Stability of the Synchronous State* , Chaos **27**(1): 013109 (2017).

**Conference Publications:**

1. Jan H. van Schuppen, **Kaihua Xi**, Jana Němcová. *A subalgebraic Procedure for System Identification of a Continuous-Time Polynomial System*, In proceedings of the 18th IFAC Symposium on System Identification (SYSID), Stockholm, Sweden (2018), to appear.

2. **Kaihua Xi**, Hai Xiang Lin and Jan H. van Schuppen. *Power-Imbalance Allocation Control of Frequency Control of Power Systems-A frequency bound for Time-Varying Loads*, In Proceedings of the 36th Chinese Control Conference, Dalian, China (2017), pp: 10528-10533.

3. **Kaihua Xi**, Johan L. A. Dubbeldam, Hai Xiang Lin and Jan H. van Schuppen. *Power-Imbalance Allocation Control of Secondary Frequency Control of Power Systems*, In Proceedings of the 20th IFAC World Congress, Toulouse, France (2017), pp: 4382-4387.